THE UNIVERSITY
of EDINBURGH

Investigating the impact of osteoblast-specific NPP1 ablation on bone and energy metabolism

Fiona Roberts

This thesis is presented for the degree of Doctor of Philosophy at The University of Edinburgh

Doctor of Philosophy – The University of Edinburgh – 2019

Declaration

I declare that this thesis has been composed entirely by the candidate, Fiona Roberts. This work has not previously been submitted for a Doctor of Philosophy, a degree or any professional qualification. I have done all the work unless acknowledged otherwise. All source of information have been acknowledged.

Fiona Roberts

December 2019

Acknowledgements

I would firstly like to thank my supervisors, Vicky MacRae, Colin Farquharson and Nik Morton. Throughout my time of research, and writing, I have received great professional supervision, guidance and support. I am particularly grateful for the personal support that Vicky has given me during challenging times. This understanding, help and comfort was invaluable.

My thanks also go to all members of the MacRae and Farquharson groups at the Roslin Institute. It has been a joy working with such great friends every day and I will cherish happy memories of long chats, silly jokes, food-filled lab meetings, too-long coffee breaks and lots of laughter together. I would also like to give thanks to the collaborators I have worked with during this project, including Professor Elspeth Milne, Norrie Russell, Dr Isabel Orriss, Dr Karla Suchacki, Dr Will Cawthorn, Professor Gerard Karsenty, Julian Berger, Professor Timothy Kendall, Professor Neil Henderson, Janna Zoll and Professor Olivia Le Saux. I would also like to give thanks to The University of Edinburgh's College of Medicine and Veterinary Medicine for funding this project.

I would like to take this chance to give my thanks to Barbara Cohen. In my early scientific career, Barbara attended a small, informal seminar at the University of Aberdeen given by Dr. Justin Rochford. Feeling enthused by a good talk, Barbara suggested that I contact Dr. Rochford, which I did. This first contact led to a successful summer internship, and Dr. Rochford later pointed me in the direction of Dr Will Cawthorn. This in turn led to an insightful 4th year undergraduate research project in the Cawthorn lab and a connection to the Roslin Institute through Karla Suchacki, who I am so grateful to have met and been mentored by. These experiences culminated in my application to complete my PhD at the Roslin Institute. Barbara, without your input all those years ago, this may not have happened. Thank you for shaping my life.

A special thank you goes to Lucy Cui. Without you, my entire PhD experience would have been very different and certainly not as fun. Similarly, I would like to give my thanks to Alisia Sim – a definite lab best friend and a certain friend for life. Without Scott Dillon, I would have been

completely lost in the lab and at times in life – I owe you more than thanks. Living and working with you has been wonderful and I will miss you dearly. Thank you to Holly Woodward – our many evenings of home-cooked dinners, movies and wine kept me sane this last year. I am so glad we became such great friends after that trip to Philadelphia. I am so grateful to have had these special friendships throughout my studies.

I cannot express enough gratitude to my immediate family who have been my biggest support and have provided unwavering encouragement. My Grandpa – thank you for always listening and for your calm life advice, which will never be forgotten. Mum – thank you for always being at the other end of the phone to give me guidance and love me through everything, always. My dear sister Claire – you are my great inspiration for life and I hope to grow up to be like you. Dad – thank you for being my biggest fan, for the constant encouragement and unwavering confidence in my abilities. Who would I be without you all?

Finally, thank you to my fiancée Greg for years of great friendship as we worked together at the Roslin Institute. Our many coffees together, walks, ridiculous chats, serious conversations, scientific partnership and fun has made my life, and PhD, all the more enjoyable. I look forward to the achievements we will make and the many years we have together. Next stop - Copenhagen!

Abstract

The skeleton is a mineralised tissue, which facilitates classical functions of locomotion, organ protection and mineral homeostasis. However, the bone has more recently been identified as an endocrine organ with the ability to regulate systemic glucose and thus energy metabolism. The acknowledgement of this previously unanticipated role of the skeleton emerged following the identification of a novel role of osteocalcin. This osteoblast-secreted hormone promotes peripheral insulin sensitivity and secretion by the pancreas. Within the bone and endocrine field, attention is now being paid to delineating further roles of proteins known to regulate mineralisation. These proteins either promote or inhibit mineralisation through various enzymatic pathways.

Ectonucleotide pyrophosphatase phosphodiesterase-1 (NPP1 in mice, ENPP1 in humans) is recognised as a mineralisation regulator. By the hydrolysis of ATP, this enzyme generates extracellular pyrophosphate (PP_i) which is a potent inhibitor of mineralisation (*e.g*. for bone and soft tissue such as the vasculature). However, NPP1 is also recognised as a pathogenic factor for insulin resistance, whereby it binds to the insulin receptor (IR) and abrogates downstream glucose mediation. This may lead to the development of insulin resistance which is a prerequisite for type 2 diabetes mellitus. Previous work has demonstrated that the global knockout of NPP1 in mice (*Enpp1*$^{-/-}$) leads to pathological mineralisation, systemically reduced serum PP_i and protection against insulin resistance and obesity following chronic high-fat diet feeding. However, the cell-specific contributions of NPP1 to the bone and metabolic phenotype remains unknown.

The data presented in this thesis has expanded on this previous work by investigating the bone and metabolic phenotype of an osteoblast-specific NPP1 knockout mouse model (*Enpp1*$^{flox/flox;}$*Ocn*-cre) compared to controls (*Enpp1*$^{flox/flox}$). Previous work has shown that global Enpp1 knockout mice present with severe joint hypermineralisation, spinal ankylosis and soft tissue mineralisation (*e.g*. the tunica media of the aorta). These mice also present with a

paradoxical hypomineralisation of the long bone diaphysis. In contrast, the work presented in this thesis includes a detailed analysis of the bone phenotype which revealed a significantly increased bone mass and bone mineral density in the *Enpp1*$^{flox/flox}$;*Ocn*-cre. This finding was supported by *in vitro* analysis of primary osteoblasts isolated from the *Enpp1*$^{flox/flox}$;*Ocn*-cre mice and grown under mineralising conditions. This *in vitro* work demonstrated that *Enpp1*$^{flox/flox}$;*Ocn*-cre isolated osteoblasts mineralise more quickly, and to a greater extent, compared to their controls. This work also revealed that systemic levels of PPi remain unchanged in the *Enpp1*$^{flox/flox}$;*Ocn*-cre mice; indeed these mice have an absence of pathological soft tissue mineralisation likely as a product of this.

The metabolic phenotype of *Enpp1*$^{flox/flox}$;*Ocn*-cre mice was assessed following both control and high-fat diet feeding. *In vivo* characterisation revealed unaltered blood glucose levels, insulin sensitivity and glucose tolerance in 16-week old control fed *Enpp1*$^{flox/flox}$;*Ocn*-cre mice. These mice did present with significantly increased uncarboxylated osteocalcin, reflecting results observed in the global *Enpp1*$^{-/-}$ mice. Following high-fat diet feeding, *Enpp1*$^{flox/flox}$;*Ocn*-cre mice did not confer protection against obesity or insulin resistance and did not demonstrate differences in osteocalcin (total or uncarboxylated). This is in contrast to the metabolic protection observed in the global *Enpp1*$^{-/-}$ mice and indicates that ablation of NPP1 within bone, one of its principal sites of action, is metabolically detrimental.

This work adds to the increasing body of evidence supporting a role for NPP1 in metabolic dysfunction. I have demonstrated that the osteoblast-specific ablation of NPP1 in mice results in an alteration of osteocalcin carboxylation status, whilst offering reduced protection against insulin resistance and obesity. The mechanisms of this action remain incompletely understood and warrants further investigation. A greater comprehension of the tissue-specific roles of NPP1 may aid in identifying potential therapeutic strategies for the management and treatment of type 2 diabetes mellitus.

Lay Summary

Insulin is a major controller of energy utilisation. The maintenance of the skeleton has a high energetic cost, and the skeleton coordinates whole body energy utilisation through its hormonal interactions with other tissues. This PhD project investigated the actions of a molecule involved in regulating bone function called ectonucleotide pyrophosphatase/phosphodiesterase-1 (NPP1) in controlling the body's response body to the normal actions of insulin and bone development.

First, the project investigated mice with the gene for NPP1 removed specifically in bone forming cells known as osteoblasts. This revealed how vital NPP1 in osteoblasts is for bone function, the regulation of insulin and the accumulation of fat tissue. Subsequent studies then examined whether NPP1 in osteoblasts promotes the development of obesity and insulin resistance. This was done by giving the transgenic mice a high-fat diet and studying their weight gain, responses to insulin and bone biology. Together, these studies helped to establish NPP1 as a key modulator of the skeleton's ability to regulate energy usage.

This project also investigated bones of mice with the gene for NPP1 removed in bone cells. This demonstrated how important NPP1 in osteoblasts is for bone formation. Through its enzyme function the NPP1 protein generates pyrophosphate which inhibits the deposition of mineral in bone. This work used multiple tools to assess bone structure, strength and content to assess bone formation.

This work expands the current understanding of the role of NPP1 in energy metabolism and bone formation. Such work may aid in contributing to the development of therapeutic tools to target bone disorders and metabolic disorders including type 2 diabetes mellitus.

Publications

Suchacki, K., **Roberts, F**., Lovdel, A., Farquharson, C., Morton, NM., MacRae, VE., Cawthorn, W., (2017), Skeletal Energy Homeostasis: A Paradigm of Endocrine Discovery, Journal of Endocrinology, [Online], Available: 10.1530/JOE-17-0147

Roberts, F., Zhu, D., Farquharson, C., Macrae, VE., (2019), ENPP1 in the regulation of mineralisation and beyond, *Trends in Biochemical Sciences,* available online: [https://doi.org/10.1016/j.tibs.2019.01.010]

Rashdan, N., Sim, A., Cui, L., **Roberts, F**., Carter, R., Ozdemir, D., Hohenstein, P., Hung, J., Kaczynski, J., Newby, D., Baker, A., Karsenty, G., Morton, NM., MacRae., VE., (2019), Osteocalcin Regulates Arterial Calcification via Altered Wnt Signalling and Glucose Metabolism, *Journal of Bone and Mineral Research,* [Online], Available: https://doi.org/10.1002/jbmr.3888

Roberts, F, .Rashdan, N., Markby, G., Dillon, S., Phadwal, K., Zoll, J., Berger, J., Milne, E., Orriss, IR., Karsenty, G., Le Saux, O., Morton, NM., Farquharson, C., MacRae, VE., (2019) Osteoblast-specific deficiency of NPP1 engenders insulin resistance in mice (in submission)

Roberts, F, Markby, G., Dillon, S., Farquharson, C., MacRae, VE., Beyond mineralisation - metabolic functions for matrix mineralisation regulators, Invited review for *Journal of Endocrinology* (in submission)

Cui, L., **Roberts, F.,** Macrae, VE., The role of the ENPP family in vascular calcification and bone biology (Manuscript in Preparation).

Awards and Grants

The International Conference on the Chemistry and Biology of Mineralized Tissues, Young Investigator Award: ($1000), 2019.

The Bone Research Society: Best Poster Pitch, 2019.

The Physiological Society Poster Award: Best Poster, (£250), 2019**.**

The Physiological Society Travel Grant, (£500), 2019.

The British Society for Developmental Biology: The Company of Biologists Travel Grant, (£600), 2019.

Birrel Gray Travel Scholarship, (£500), 2018.

Top Downloaded Author for the paper 'Skeletal energy homeostasis: A paradigm of Energy Metabolism', May 2018.

Bone Research Society New Investigator Award, (£400), 2018, 2017.

Contents

Chapter 1. Introduction. 1
1.1. Preface 2
1.2. Bone structure and function 2
1.2.1 Cortical bone 3
1.2.3. Embryonic bone formation 8
1.2.4. Intramembranous ossification 9
1.2.5. Endochondral ossification 10
1.2.6. Bone modelling and remodelling 13
1.2.7. Cells of the skeleton 16
1.2.8. Matrix mineralisation 20
1.2.9. Regulation of mineralisation 20
1.2.10. Energetic cost of the skeleton 26
1.2.11. Bone is an endocrine organ 26
1.2.12. Members of the ENPP family 30
1.2.13. Roles of ENPP1 in soft tissue mineralisation 33
1.2.14. ENPP1 pathways 34
1.3. Aims and strategy 39
Chapter 2. Materials and methods. 41
2.1. Chemicals, media and buffers 42
2.2. Cell culture 42
2.2.1 Cell culture reagents 42
2.2.2 Cell types 42
2.2.3 Maintaining and passaging cells 42
2.2.4 Freezing/thawing of MC3T3-E1 sub-clone c14 cells 43
2.2.5 Dissection and extraction of primary osteoblasts from calvariae 43
2.2.6 Plating of cells for experiments 44
2.3. RNA methods 45
2.3.1 Isolation of RNA from cells 45
2.3.2 Reverse transcription 45
2.3.3 Real-time quantitative PCR (qPCR) and quantification of gene expression 46

2.3.4. Genotyping 46
2.4. Protein methods 47
2.4.1 Protein extraction from cells for western blot analysis 47
2.4.2 Quantification of protein concentration: Bio-Rad DC assay 47
2.4.3. Western blot analysis 48
2.5. Cell-based assays and staining 49
2.5.1 *O*-cresolphthalein complexone calcium assay 49
2.5.2 Alizarin red S staining and quantification 49
2.6. *In vivo* studies 50
2.6.1 Animal welfare and generation 50
2.6.2 Maintenance of *Enpp1*$^{flox/flox}$;*Ocn*-cre and *Enpp1*$^{flox/flox}$ mice 50
2.6.3. Metabolic analysis of animals 53
2.6.4 Glucose and insulin tolerance testing 53
2.6.5. Catwalk analysis 53
2.7. *Ex vivo* bone analysis and gross analysis 55
2.7.1 Bone length and 3-point bending 55
2.7.2. Micro-computed tomography imaging 57
2.7.3 Gross analysis 59
2.7.4 Histopathological assessment 59
2.7.5. Osmium staining of marrow adipose tissue 59
2.8. Histological analysis 60
2.8.1. Preparation of tissue for microscopical analysis 60
2.8.2. Paraffin-embedded tissues 60
2.8.3. Haemotoxylin and eosin staining 61
2.8.4 Von kossa staining 62
2.8.5. Toluidine blue/fast green staining 62
2.8.6. Goldner's trichrome staining 62
2.8.7. Measurement of pancreatic islet number and size 64
2.8.8. Measurement of adipocytes in fat pads 65
2.8.9. Liver staining 65
2.8.10. Immunohistochemistry 65

2.9. Blood and further tissue analysis 66
2.9.1. Serum analysis by ELISA 66
2.9.2. Serum osteocalcin and biochemistry analysis 66
2.9.3. Serum pyrophosphate analysis 67
2.9.4. Analysis of liver triglycerides 68
2.10. Statistical analysis 68
Chapter 3. Investigating the effect of osteoblast-specific NPP1 ablation on bone phenotype. 69
3.1. Introduction 70
3.2. Hypothesis 73
3.3 Materials and methods 74
3.3.1. Generation of mice 74
3.3.2. Histopathological assessment of soft tissue and bone 74
3.3.3. Osmium staining of marrow adipose tissue 74
3.3.4. Gross analysis of bone 74
3.3.5. Three-point bending analysis 75
3.3.6. Micro-computed tomography imaging 75
3.3.7. Tissue preparation for microscopy and Bioquant histomorphometric analysis 75
3.3.8. Analysis of serum bone formation and bone resorption markers 76
3.4. Results 77
3.4.1. Gross anatomy - body mass and long bone length of juvenile mice 77
3.4.2. Serum pyrophosphate and markers of bone resorption and formation of juvenile mice 79
3.4.3. Gross histological analysis of joint and soft tissue 79
3.4.5. Analysing bone mineral density of long bones of juvenile mice 91
3.4.6. Analysing the mechanical properties of long bones in juvenile mice 91
3.4.7. Histomorphometry analysis of juvenile mice using Bioquant OSTEO software 95
3.4.8. μ-CT analysis of bone marrow adiposity of 16-week old male mice 99
3.4.9. Gross anatomy - body mass and long bone length of adult mice 101
3.4.10. Serum markers of bone resorption and formation in adult mice 103
3.4.11. μ-CT analysis of the long bones of adult mice 105

3.4.12. Analysing the mechanical properties of long bones in adult mice 113
3.4.13. Analysing bone mineral density of long bones of adult mice 113
3.5. Discussion 117
Chapter 4. Investigating the profile of *Enpp1* expression during osteoblast matrix mineralisation *in vitro* 125
4.1 Introduction 126
4.2. Hypothesis 129
4.3 Aims 129
4.4.1. MC3T3-E1 sub-clone c14 and primary cell culture 130
4.4.2. qPCR analysis of MC3T3-E1 sub-clone c14 and primary osteoblast gene expression throughout mineralisation time course 130
4.4.3. Calcium deposition 130
4.4.4. ALP activity 131
4.4.5 Bio-Rad DC assay 132
4.4.6. Seahorse metabolic analysis of primary osteoblasts 132
4.4.7. Serum PP_i Assay 133
4.4.8. Treatment with TNAP inhibitor. 133
4.5. Results 134
4.5.1. Investigating the mineralisation profile of the mouse cell Line MC3T3-E1 sub-clone c14 134
4.5.2. Investigating the matrix mineralisation profile of primary osteoblasts isolated from *Enpp1*$^{flox/flox}$;*Ocn*-cre and *Enpp1*$^{flox/flox}$ 140
4.5.3. Analysing the effect of TNAP inhibition on primary osteoblast matrix mineralisation 147
4.5.4. Analysing metabolic differences in primary osteoblast cells 149
4.6. Discussion. 151
Chapter 5. Investigating the role of osteoblast-specific NPP1 ablation on metabolism. 161
5.1. Introduction 162
5.2. Hypothesis 164
5.3. Aims 164
5.4. Materials and methods 164
5.4.1. Animal generation, food, weighing, and consumption 164

5.4.2. Gross analysis 164
5.4.3. Glucose tolerance and insulin tolerance testing 165
5.4.4. Serum OCN analysis and biochemistry 165
5.4.5. Histological analysis 165
5.4.6. Immunohistochemistry of pancreas 165
5.4.7. Analysis of liver triglyceride content 166
5.4.8. mRNA analysis of metabolic tissues 166
5.4.9. Three-point bending of long bones 166
5.4.10. μ-CT of long bones 166
5.4.11. Catwalk analysis 166
5.5. Results 167
5.5.1. *Enpp1*$^{flox/flox}$*;Ocn*-cre mice demonstrate unaltered body mass and food consumption. 167
5.5.2. *Enpp1*$^{flox/flox}$*;Ocn*-cre mice demonstrate unaltered insulin sensitivity, reduced liver mass and increased muscle mass 167
5.5.3 *Enpp1*$^{flox/flox}$*;Ocn-cre* mice exhibit altered gait 172
5.5.4. Analysis of *Enpp1*$^{flox/flox}$*;Ocn*-cre mice liver histology and triglyceride content. 172
5.5.5. *Enpp1*$^{flox/flox}$*;Ocn*-cre mice exhibit increased uncarboxylated-OCN and unaltered pancreata. 176
5.5.6. Analysis of adipocytes from the white and brown fat depots 176
5.5.7. Analysis of metabolic genes in metabolic tissues 180
5.5.8. Analysis of long bone micro-architecture, length and mechanical strength 186
5.6. Discussion 192
Chapter 6. Investigating the role of osteoblast-specific ablation of NPP1 on the metabolic phenotype of chronically high-fat diet fed mice. 199
6.1 Introduction 200
6.2. Hypothesis 203
6.3. Aims 203
6.4. Materials and methods 203
6.4.1. Animal generation, food, weighing and consumption. 203
6.4.2. Gross analysis 203
6.4.3. Glucose tolerance and insulin tolerance testing 204

6.4.4. Serum OCN analysis and biochemistry 204
6.4.5. Histological analysis 204
6.4.6. Immunohistochemistry of pancreas 204
6.4.7. Analysis of liver triglyceride content 205
6.4.8. mRNA analysis of metabolic tissues 205
6.4.9. Three-point bending of long bones 205
6.4.10. μ-CT of long bones 205
6.4.11. Catwalk analysis 205
6.5. Results 206
6.5.1. *Enpp1*$^{flox/flox}$*;Ocn*-cre do not demonstrate resistance to obesity following chronic high-fat diet challenge 206
6.5.2. *Enpp1*$^{flox/flox}$*;Ocn*-cre demonstrate glucose intolerance, insulin resistance and increased brown fat and liver mass 206
6.5.3. Analysis of *Enpp1*$^{flox/flox}$*;Ocn*-cre liver histology and triglyceride content 210
6.5.4. *Enpp1*$^{flox/flox}$*;Ocn*-cre mice exhibit unaltered OCN and pancreata 210
6.5.6. Analysis of metabolic genes in metabolic tissues from high-fat diet fed mice 216
6.5.6. Analysis of long bone micro-architecture, length and mechanical strength. 216
6.5.6. Analysis of long bone marrow adipose tissue by osmium staining 225
6.6. Discussion 228
Chapter 7. Discussion. 235
7.1. General discussion 236
7.2. Direction for future research 247
Appendix I. PCR primers. 292
Appendix II. Buffers and solutions. 294
Appendix III. Schematics of Animal Use. 296

List of Figures

FIGURE 1.1. BONE IS A COMPOSITE MATERIAL. 5
FIGURE 1.2. CORTICAL BONE 6
FIGURE 1.3. TRABECULAR BONE. 8
FIGURE 1.4. ENDOCHONDRAL OSSIFICATION. 12
FIGURE 1.5. COMPARISON OF NORMAL AND OSTEOPOROTIC BONE ARCHITECTURE. 17
FIGURE 1.6. OSTEOCLAST AND OSTEOCYTE CELLS. 18
FIGURE 1.7. REGULATION OF MINERALISATION BY BONE FACTORS. 25
FIGURE 1.8. SCHEMATIC OF NEWLY DISCOVERED ENDOCRINE FUNCTIONS OF BONE, MUSCLE AND ADIPOSE TISSUE. 29
FIGURE 1.9. REGULATION OF MINERALISATION BY BONE FACTORS.... **ERROR! BOOKMARK NOT DEFINED.**
FIGURE 2.1. REPRESENTATIVE GENOTYPING GEL 51
FIGURE 2.2. REPRESENTATIVE WESTERN BLOT ANALYSIS 52
FIGURE 2.3. SCHEMATIC OF CATWALK GAIT ANALYSIS. 54
FIGURE 2.4. THREE-POINT BENDING LOAD EXTENSION CURVE. 56
FIGURE 3.1. SCHEMATIC REPRESENTATION OF MATRIX MINERALISATION REGULATORS. ..... **ERROR! BOOKMARK NOT DEFINED.**
FIGURE 3.2. THE MASS AND LONG BONE LENGTH OF MALE AND FEMALE 6-WEEK OLD MICE 78
FIGURE 3.3. SERUM CONCENTRATION OF PP_i, CTX AND P1NP FROM MALE AND FEMALE MICE. 80
FIGURE 3.4. PART 1. HISTOLOGICAL ASSESSMENT OF H&E STAINED SOFT TISSUE. 81
FIGURE 3.5: PART 1. HISTOLOGICAL ASSESSMENT OF ALIZARIN RED S STAINED SOFT TISSUE 81
FIGURE 3.6. PART 1. H&E STAINED HISTOLOGICAL BONE SECTIONS 81
FIGURE 3.7. µ-CT ANALYSIS OF THE EPIPHYSEAL BONE FROM MALE AND FEMALE MICE 89
FIGURE 3.8. µ-CT ANALYSIS OF THE LATERAL AND MEDIAL SUBCHONDRAL BONE FROM MALE AND FEMALE MICE. 90
FIGURE 3.9. µ-CT ANALYSIS OF TIBIAE AND FEMORA CORTICAL AND TRABECULAR BONE MINERAL DENSITY FROM 6-WEEK FEMALE MICE. 92
FIGURE 3.10 PART 1. HISTOMORPHOMETRY ANALYSIS OF 6-WEEK OLD MALE AND FEMALE FEMORA 96
FIGURE 3.11. µ-CT ANALYSIS OF OSMIUM STAINED TIBIAE FOR MARROW ADIPOSITY 100
FIGURE 3.12. THE MASS AND LONG BONE LENGTH OF MALE AND FEMALE 22-WEEK OLD MICE 102
FIGURE 3.13. SERUM CONCENTRATION OF CTX AND P1NP FROM MALE AND FEMALE ADULT MICE 104
FIGURE 3.14. µ-CT ANALYSIS OF THE EPIPHYSEAL BONE FROM MALE AND FEMALE MICE 111
FIGURE 3.15. µ-CT ANALYSIS OF THE LATERAL AND MEDIAL SUBCHONDRAL BONE FROM 22-WEEK OLD MALE AND FEMALE MICE. 112
FIGURE 3.16. TIBIAE AND FEMORA CORTICAL AND TRABECULAR BONE MINERAL DENSITY OF 6-WEEK FEMALE MICE. 116
FIGURE 4.1. A SCHEMATIC REPRESENTATION OF REGULATORS INVOLVED IN MINERALISATION. 127
FIGURE 4.2. ANALYSIS OF CALCIUM DEPOSITION IN MC3T3-E1 SUB-CLONE C14 CELLS. 135
FIGURE 4.3. PART 1. ASSESSING THE RELATIVE CHANGE OF BONE-ASSOCIATED MRNA EXPRESSION IN MC3T3-E1 SUB-CLONE C14 CELLS. 137

FIGURE 4.4. INVESTIGATING ALP ACTIVITY IN MC3T3-E1 SUB-CLONE C14 CELLS..... 139
FIGURE 4.5. CALCIUM CONTENT IN PRIMARY OSTEOBLASTS BY ALIZARIN RED S STAINING..... 141
FIGURE 4.6. PRIMARY OSTEOBLAST TOTAL CALCIUM CONTENT. 142
FIGURE 4.7. PART 1. BONE-RELATED MRNA EXPRESSION IN PRIMARY OSTEOBLASTS. 144
FIGURE 4.8. EXTRACELLULAR PYROPHOSPHATE CONCENTRATIONS IN PRIMARY OSTEOBLAST CELLS. .. 146
FIGURE 4.9. ANALYSIS OF CALCIUM DEPOSITION FOLLOWING TNAP INHIBITION OF PRIMARY OSTEOBLASTS. 148
FIGURE 4.10. *ENPP1*$^{FLOX/FLOX}$*;OCN*-CRE PRIMARY OSTEOBLASTS DEMONSTRATE DECREASED AEROBIC RESPIRATION AND GLYCOLYTIC FUNCTION. 150
FIGURE 5.1. WEIGHT GAIN AND FOOD CONSUMPTION..... 169
FIGURE 5.2. ASSESSMENT OF GLUCOSE TOLERANCE AND INSULIN SENSITIVITY. 170
FIGURE 5.3. ORGAN MASS AT 16-WEEKS OF AGE..... 171
FIGURE 5.4. STRIDE LENGTH. 173
FIGURE 5.5. GAIT ANALYSIS OF MICE. 174
FIGURE 5.6. LIVER TRIGLYCERIDE QUANTIFICATION. 175
FIGURE 5.7. ANALYSIS OF SERUM OCN AND INSULIN-SECRETING PANCREATIC ISLETS..... 177
FIGURE 5.8. ANALYSIS OF THE WHITE FAT DEPOTS ADIPOCYTE NUMBER, AREA, AND SIZE-FREQUENCY DISTRIBUTION. 178
FIGURE 5.9. QUANTITATIVE ASSESSMENT OF BROWN ADIPOSE TISSUE NUCLEI. 179
FIGURE 5.10. ANALYSIS OF THE GLUT RECEPTORS OF *QUADRICEPS FEMORIS* MUSCLE. 181
FIGURE 5.11. ANALYSIS OF THE GLUT RECEPTORS OF GONADAL FAT PAD. 182
FIGURE 5.12. ANALYSIS OF LIVER METABOLIC GENES..... 184
FIGURE 5.13. ANALYSIS OF SELECTED BROWN ADIPOSE TISSUE METABOLIC GENES. 185
FIGURE 5.14. µ-CT ANALYSIS OF TIBIAE TRABECULAR BONE FROM 16-WEEK MALE MICE..... 187
FIGURE 5.15. µ-CT ANALYSIS OF TIBIAE TRABECULAR BONE FROM 16-WEEK MALE MICE. 188
FIGURE 5.16. µ-CT ANALYSIS OF FEMORA TRABECULAR BONE FROM 16-WEEK MALE MICE. 189
FIGURE 5.17. : µ-CT ANALYSIS OF FEMORA TRABECULAR BONE FROM 16-WEEK MALE MICE. 190
FIGURE 6.1. WEIGHT GAIN AND FOOD CONSUMPTION OF HIGH-FAT DIET FED MICE. 207
FIGURE 6.2. ASSESSMENT OF GLUCOSE TOLERANCE AND INSULIN SENSITIVITY. 208
FIGURE 6.3. HIGH-FAT DIET FED MICE ORGAN MASS. 209
FIGURE 6.4. LIVER TRIGLYCERIDE QUANTIFICATION..... 211
FIGURE 6.5. ANALYSIS OF SERUM OCN AND INSULIN-SECRETING PANCREATIC ISLETS..... 212
FIGURE 6.6. ANALYSIS OF THE WHITE FAT DEPOT ADIPOCYTE NUMBER, AREA AND SIZE-FREQUENCY DISTRIBUTION. 214
FIGURE 6.7. QUANTITATIVE ASSESSMENT OF BROWN ADIPOSE TISSUE NUCLEI. 215
FIGURE 6.8. ANALYSIS OF THE MRNA EXPRESSION OF GLUT RECEPTORS OF *QUADRICEPS FEMORIS* MUSCLE..... 217
FIGURE 6.9. ANALYSIS OF THE MRNA EXPRESSION OF GLUT RECEPTORS OF GONADAL FAT PAD. 218
FIGURE 6.10. ANALYSIS OF THE MRNA EXPRESSION OF LIVER TISSUE-ASSOCIATED METABOLIC GENES. 219

FIGURE 6.11. ANALYSIS OF THE MRNA EXPRESSION OF BROWN ADIPOSE TISSUE-ASSOCIATED METABOLIC GENES. 220
FIGURE 6.12. µ-CT ANALYSIS OF TIBIAE TRABECULAR BONE. 221
FIGURE 6.13. µ-CT ANALYSIS OF TIBIAE CORTICAL BONE. 222
FIGURE 6.14. µ-CT ANALYSIS OF FEMORA TRABECULAR BONE. 223
FIGURE 6.15. µ-CT ANALYSIS OF FEMORA CORTICAL BONE. 224
FIGURE 6.16. OSMIUM STAINING OF TIBIAE MARROW ADIPOSE TISSUE. 226
FIGURE 6.17. OSMIUM STAINING OF TOTAL FEMORAL MARROW ADIPOSE TISSUE. 227
FIGURE 7.1. RISK FACTORS AND DISEASE EXPERIENCED IN THE METABOLIC SYNDROME. 238
FIGURE 7.2. SCHEMATIC REPRESENTING THE PROPOSED ROLE AND DOWNSTREAM EFFECTS OF ENPP1 EXPRESSION IN THE LIVER. 243
FIGURE 7.3. SERUM ANALYTE ANALYSIS FROM FEMALE MICE. 244

List of Tables

TABLE 1.1. CHARACTERISTICS OF MODELLING AND REMODELLING....14
TABLE 2.1. GOLDNER'S TRICHROME STAINING SOLUTIONS....64
TABLE 2.2. COMPONENTS OF MASTER MIX FOR PP_i ANALYSIS. 68
TABLE 3.1. µ-CT ANALYSIS OF TIBIAE AND FEMORA TRABECULAR BONE FROM 6-WEEK MALE MICE. 83
TABLE 3.2. µ-CT ANALYSIS OF TIBIAE AND FEMORA CORTICAL BONE FROM 6-WEEK MALE MICE. 84
TABLE 3.3. µ-CT ANALYSIS OF TIBIAE AND FEMORA TRABECULAR BONE FROM 6-WEEK FEMALE MICE...86
TABLE 3.4. µ-CT ANALYSIS OF TIBIAE AND FEMORA CORTICAL BONE FROM 6-WEEK FEMALE MICE....87
TABLE 3.5. 3-POINT BENDING ANALYSIS OF FEMORA FROM 6-WEEK OLD MICE. 93
TABLE 3.6. 3-POINT BENDING ANALYSIS OF TIBIAE FROM 6-WEEK OLD MICE....94
TABLE 3.7. µ-CT ANALYSIS OF TIBIAE AND FEMORA TRABECULAR BONE FROM 22-WEEK MALE MICE. . 106
TABLE 3.8. µ-CT ANALYSIS OF TIBIAE AND FEMORA CORTICAL BONE FROM 22-WEEK MALE MICE. 107
TABLE 3.9. µ-CT ANALYSIS OF TIBIAE AND FEMORA TRABECULAR BONE FROM 22-WEEK FEMALE MICE. 108
TABLE 3.10. µ-CT ANALYSIS OF TIBIAE AND FEMORA CORTICAL BONE FROM 22-WEEK FEMALE MICE.. 109
TABLE 3.11. 3-POINT BENDING OF 22-WEEK OLD FEMORA. 114
TABLE 3.12. 3-POINT BENDING SHOWING LARGELY UNALTERED MECHANICAL STRENGTH OF 22-WEEK OLD TIBIAE. 115
TABLE 5.1. LENGTH AND MECHANICAL PROPERTIES OF LONG BONES FROM 16-WEEK OLD MALE MICE. 191

Chapter 1. Introduction.

1.1. Preface

Bone has been long regarded as an inert and structural organ, which facilitates an array of functions from locomotion to mineral homeostasis (Copp and Shim, 1963, Charles and Aliprantis, 2014, Suchacki et al., 2017). Advances in genetic manipulation of animal models have revealed that bone is not only integral as a structural biomaterial but also as a regulator of metabolic processes (Fedde et al., 1999a, Karsenty et al., 2012, Huesa et al., 2014, Bonnet et al., 2019, Roberts et al., 2019b). These discoveries indicate an endocrine function of the skeleton. This thesis will investigate the role of ectonucleotide pyrophosphatase/phosphodiesterase 1 (ENPP1) as a regulator of mineralisation and energy metabolism, pertaining particularly to its role in osteoblasts. It is imperative to widen the understanding of mechanisms involved in these processes, such that therapeutics for both mineralisation disorders (*e.g*. generalised arterial calcification of infancy) and metabolic diseases, such as diabetes, may be developed.

1.2. Bone structure and function

The skeleton is recognised as a structural scaffold for an organism, made out of a rigid tissue. This bone tissue is a composite tissue, consisting, not exclusively, of collagen and hydroxyapatite (Fig. 1.1). In keeping with this classical perception, the skeleton does indeed provide many structurally associated functions. For example, the skeleton provides the attachment site for most skeletal muscles, vital organ protection, facilitates weight-bearing motion, and provides the hematopoietic niche (Schofield, 1978, Florencio-Silva et al., 2015b). The skeleton is also recognised as highly dynamic, with the coordination of numerous cell types to facilitate skeletal functions (Gonciulea and de Beur, 2015). Furthermore, significant developments in cellular, molecular, whole-systems and animal modelling have enhanced the modern-day understanding of bone function. The recent emergence of bone as an endocrine regulatory organ has prompted a reconsideration of the role of the skeleton to encompass this new, and more complex era of bone research (Guntur and Rosen, 2012, Karsenty and Olson, 2016, Suchacki et al., 2017).

The function of bone is complemented and facilitated by its complex and highly regulated structure. The bones of the skeleton range in location, shape and size. These bones may be

divided firstly by location. The skeleton comprises the axial and the appendicular skeleton. The axial skeleton consists of the skull, vertebral column and ribcage, whereas the fore/hind-limbs and pelvis form the appendicular skeleton . Further classification of the skeleton can be based upon the structure of bones, which include; flat bones (*e.g.* skull, ribs, pelvis), long bones (*e.g.* femur), short bones (*e.g*. bones of the wrist) and irregular bones (*e.g*. scapula).

Within the bone, there is an inner 'spongy' layer of trabecular bone and an outer layer of cortical bone (Eriksen et al., 1994). Overall, the bone consists of a periosteal envelope, the trabecular (spongy) bone, endosteal envelope and the bone marrow. The periosteal envelope represents the outermost layer of the bone (Squier et al., 1990). The compact bone that lies beneath this periosteal envelope is tough and dense (Squier et al., 1990, Dwek, 2010). The medullary cavity is situated inside the endosteal envelope, within the trabecular bone (Moore and Dawson, 1990). This cavity contains red bone marrow, which is responsible for haematopoiesis, comprising of immature and mature erythrocytes and leukocytes, as well as haematopoietic stem cells and which reduces in volume with age (Moore and Dawson, 1990).

The yellow bone marrow, also present in the endosteal envelope, is made up predominantly of adipocytes (fat cells), which during times of caloric deficit, can be used as an energy reserve (Zakaria and Shafrir, 1967). Interestingly, the body may also convert this yellow marrow into red marrow in times of food deprivation or severe illness to maximise blood cell production (Maniatis et al., 1971, Bigelow and Tavassoli, 1984, Gurevitch et al., 2007, Fazeli et al., 2013).

1.2.1 Cortical bone

Cortical bone accounts for 80% of the total bone mass in an adult human (Morgan et al., 2008). This portion of bone allows survival of mechanical pressures and tensile forces experienced by bone through various physiological processes, for example, to resist bending during loading activities (Augat and Schorlemmer, 2006). The principal building blocks of cortical bone are osteons. These osteons are comprised of highly organised and concentric lamellae, organised in

Haversian systems, referred to as 'cortical osteons' (Sommerfeldt and Rubin, 2001, Clarke, 2008). With a cylindrical shape, these osteons form a branched network within the cortical cone, giving rise to a large surface area. These Haversian systems contain within them a Haversian canal. Present within the canal are blood vessels, connective tissue, nerve fibres and lymphatic vessels. Within the osteons osteocytes are visible – these are embedded cells that are supplied with lymph and nerves within the Haversian system (Fig. 1.2) (Sommerfeldt and Rubin, 2001). There is evidence to show that osteocytes behave as mechanosensors and are involved in regulating the bone remodelling process (Pead et al., 1988, Barragan-Adjemian et al., 2006, Clarke, 2008, Karsenty et al., 2009, Bonewald, 2011).

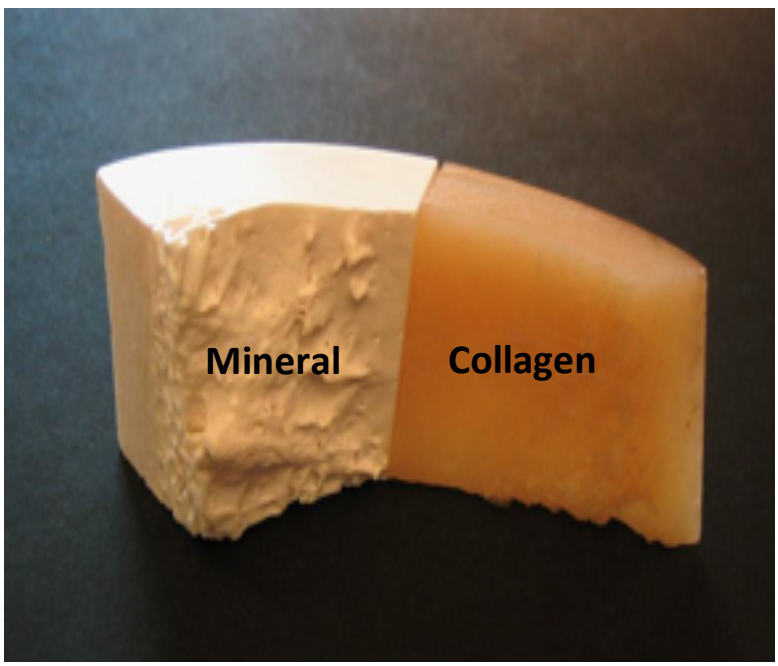

Figure 1.1. Bone is a composite material

On the left, a bone explant is treated with hypochlorite (bleach) which digests the collagen to leave the bone mineral hydroxyapatite (HA) intact. On the right, the bone explant is next treated with hydrochloric acid to dissolve the bone mineral HA and leave the collagen intact. Images provided from the Bone Research Society, by kind permission of Tim Arnett.

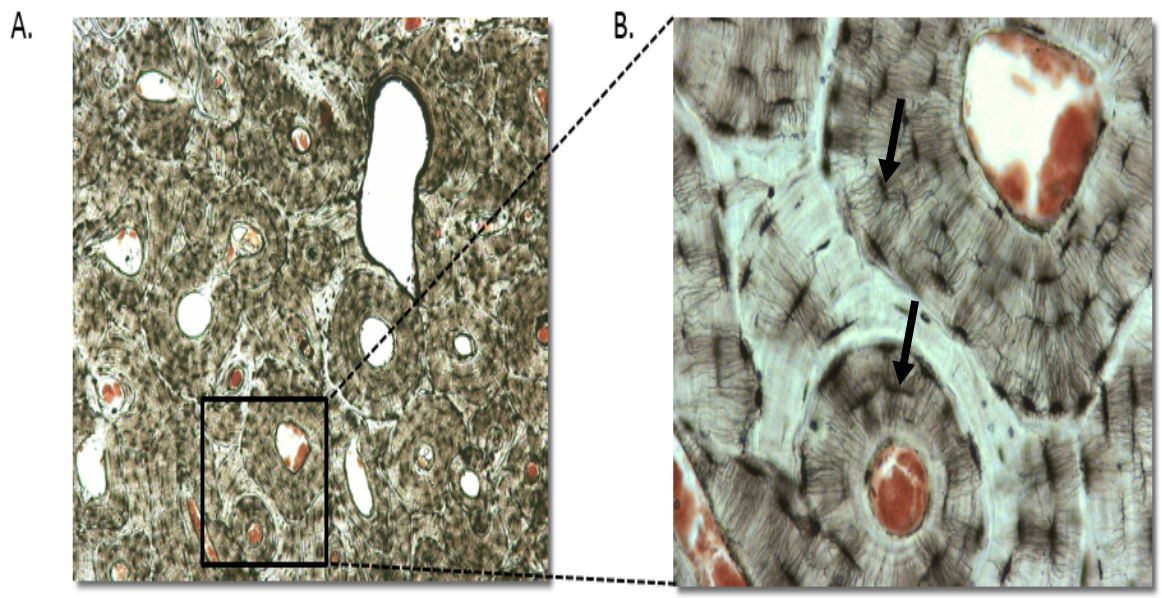

Figure 1.2. Cortical bone

Figure shows (A) Haversian (osteonal) systems in cortical bone with (B) Image demonstrating osteocytes in human cortical bone (arrows). Here osteocytes are visible within the concentric layers of bone matrix. Images provided from the Bone Research Society, by kind permission of Tim Arnett.

1.2.2. Trabecular bone

The trabecular (cancellous) bone represents the innermost portion of bone, surrounding the bone marrow. This bone type has a 'honeycomb' structure, owing to its porous nature, such that its total surface area is 10 times that of cortical bone despite contributing only 20% of the total bone mass (Singh, 1978, Sommerfeldt and Rubin, 2001). The overall effect of trabecular bone is to give a lighter total mass of the skeletal structure and to resist mechanical stresses experienced by the skeleton (Bayraktar et al., 2004, Oftadeh et al., 2015). This less dense bone material is primarily located at the ends of long bones (metaphysis) (Dyson and Whitehouse, 1968). The trabecular bone exhibits a highly porous meshwork-like appearance; this structure is comprised of trabeculae arranged in a highly organised three-dimensional structure (Fig. 1.3). This arrangement provides a lower stiffness, density, calcium content and greater elasticity to trabecular bone compared to cortical bone (Gong et al., 1964, Dyson and Whitehouse, 1968, Fritsch and Hellmich, 2007, Hart et al., 2017). These properties of trabecular bone facilitate resistance of compressive forces experienced throughout weight-bearing activities. For both the cortical and trabecular bone, there is deposition of collagen fibres in alternating orientations by the bone-forming (osteoblast) cells (Hulmes et al., 1995, Traub et al., 1989, Clarke, 2008, Orgel et al., 2006, Nudelman et al., 2010) (Fig. 1.3).

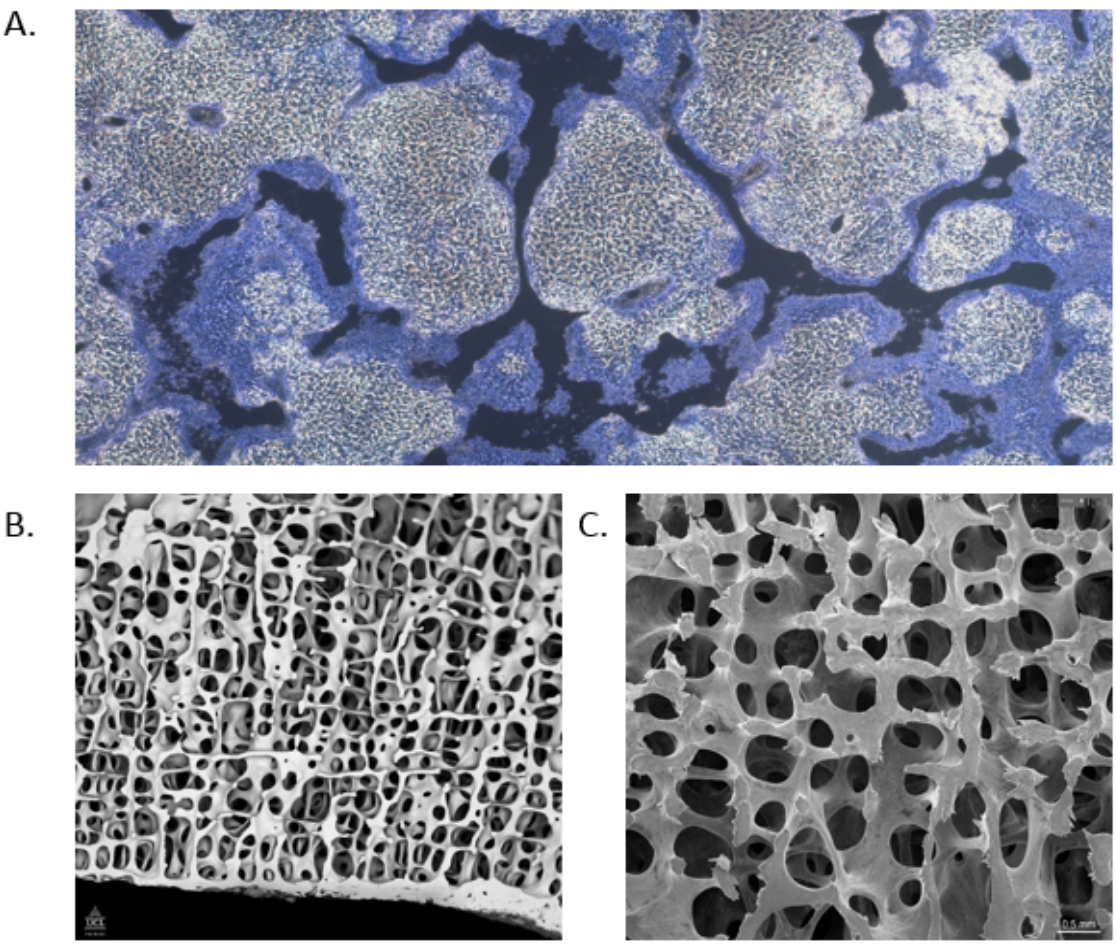

Figure 1.3. Trabecular bone.

(A) Mineralisation of osteoblast (bone-forming) cells *in vitro,* (B) very low powered scanning electron microscopy showing normal bone architecture of both cortical and trabecular bone in the fourth lumbar vertebrae of a 41-year-old male (x8), (C) low powered scanning electron microscopy showing normal trabecular bone architecture in the third lumbar vertebrae of a 30-year-old women (x20). Scanning electron microscopy images demonstrate a regular pattern of interconnected plates and rods. Images provided from the Bone Research Society, by kind permission of (A) Tim Arnett and (B, C) Alan Boyde.

1.2.3. Embryonic bone formation

Bone is composed of organic collagen proteins (principally type I collagen), non-collagenous proteins (Osteocalcin (OCN), osteonectin (ONN), osteopontin (OPN), and bone sialoprotein II (BSP II)), poorly crystalline substituted HA mineral, proteoglycans and water (Sommer et al., 1996, Morgan, 2001, Young, 2003, Shen, 2005, Roberts et al., 2007b). Within this, a large population of living cells (the osteocytes) are entombed (Parfitt, 1976, Bonewald, 2011). Bone's material properties are a function of both the relative proportions of these elementary constituents and its structure across length scales, conveying remarkable mechanical properties in a range of contexts from the ear ossicles to the load-bearing bones of the lower limb (Nalla et al., 2004, Fantner et al., 2005, Zimmermann et al., 2011). The collagen matrix is comprised of two main building blocks: the osteoid (the organic portion) and hydroxyapatite (HA) crystals (the inorganic portion, comprising 60% of bone tissue) (Morgan, 2001, Oftadeh et al., 2015, Zhu and Prince, 2015). The structural support and capabilities of the skeleton to resist load-bearing are facilitated by the calcification of the organic portion, which is made up of a crystalline HA complex of calcium and phosphate [$Ca_{10}(PO_4)_6(OH_2)$] which is embedded in the collagen matrix (Bayraktar et al., 2004). The formation of the skeleton, during foetal development, occurs via two distinct models of bone formation known as intramembranous ossification and endochondral ossification (Karsenty and Wagner, 2002, Kronenberg, 2003a, Yang et al., 2014). Both of these modes of formation give rise to the synthesis of bone from pre-existing mesenchymal tissue (Kronenberg, 2003b). For intramembranous ossification, this process occurs directly, whereas for endochondral ossification occurs via an intermediate hyaline cartilage scaffold which becomes replaced by bone (Kronenberg, 2003b, Colnot et al., 2004).

1.2.4. Intramembranous ossification

The process of intramembranous ossification involves the formation of compact and spongy bone, which develops directly from sheets of mesenchymal connective tissue. Intramembranous ossification is important for the formation of flat bones including skill, mandible and clavicle (Anon, 1940). During embryonic development, this process begins: mesenchymal stem cells undergo condensation and begin to differentiate into specialised cells (Hall and Miyake, 1992). These cells may differentiate to form capillaries, whereas others become osteogenic and later

forms osteoblasts (Hall and Miyake, 1992, Ducy et al., 1997, Gerber et al., 1999). These early osteoblasts initially form in a cluster known as the 'ossification centre'. These osteoblasts secrete osteoid which later becomes calcified and eventually, the collagen secreting osteoblast becomes embedded into the surrounding mineralised matrix (Anderson, 1984, Roach, 1990). Once this occurs, the osteoblast further differentiates and then forms the terminally differentiated osteocyte (Parfitt et al., 1987, Manolagas, 2000, Li et al., 2004). The continued formation of osteoid and its subsequent mineralisation gives rise to an arrangement of calcified bone tissue known as 'woven bone' (Moreira et al., 2000). The remodelling of woven bone gives rise to secondary bone known as lamellar bone (Clarke, 2008). This has a regular and parallel alignment of collagen into sheets and is mechanically strong and highly organised (Rho et al., 1997, Rho et al., 1998).

1.2.5. Endochondral ossification

The coordinated action of the skeletal cells is exemplified in the formation of the appendicular skeleton (long bones) through the process of endochondral ossification (Mackie et al., 2008, Cui et al., 2016) (Fig. 1.4). This process proceeds with a cartilaginous scaffold. Here, mesenchymal stem cells differentiate into chondrocytes, under the regulation of the transcription factor '(Sex determining region Y)-Box 9' (Sox-9) (Provot and Schipani, 2005). The lineage origins of these mesenchymal stem cells give rise to different locations of the resultant bone. Mesenchymal cells from somites give rise to the axial skeleton, whereas somatopleure gives rise to the appendicular skeleton (Provot and Schipani, 2005, Saito et al., 2006, Nakajima et al., 2018). The chondrocyte cell aggregates are responsible for the secretion of an extracellular matrix (ECM) consisting mostly of type II collagen and proteoglycans (Akkiraju and Nohe, 2015). Regulated by several growth factors and transcription factors, chondrocytes will progress through morphologically distinct maturation zones (Hunziker et al., 1987, Ballock and O'Keefe, 2003). In the most peripheral region of the growth plate, chondrocytes will exit the cell cycle and thereafter become hypertrophic (Ballock and O'Keefe, 2003, Mackie et al., 2008). These hypertrophic chondrocytes mineralise their ECM through the release of matrix vesicles (MVs) containing HA (Cui et al., 2016). There is a further invasion of the cartilaginous scaffold, whereby specialised bone cells (osteoclasts) resorb the chondrocyte remnants and the majority of the cartilaginous matrix

(Colnot et al., 2004, Odgren et al., 2016). Later osteoblasts are responsible for depositing bone-specific type I collagen-rich matrix onto the remnants of chondrocyte ECM, which subsequently undergoes mineralisation (Arkill and Winlove, 2008, Mackie et al., 2008). This process results in the formation of primary spongiosa, which is eventually reabsorbed by osteoclasts and true trabecular bone is formed.

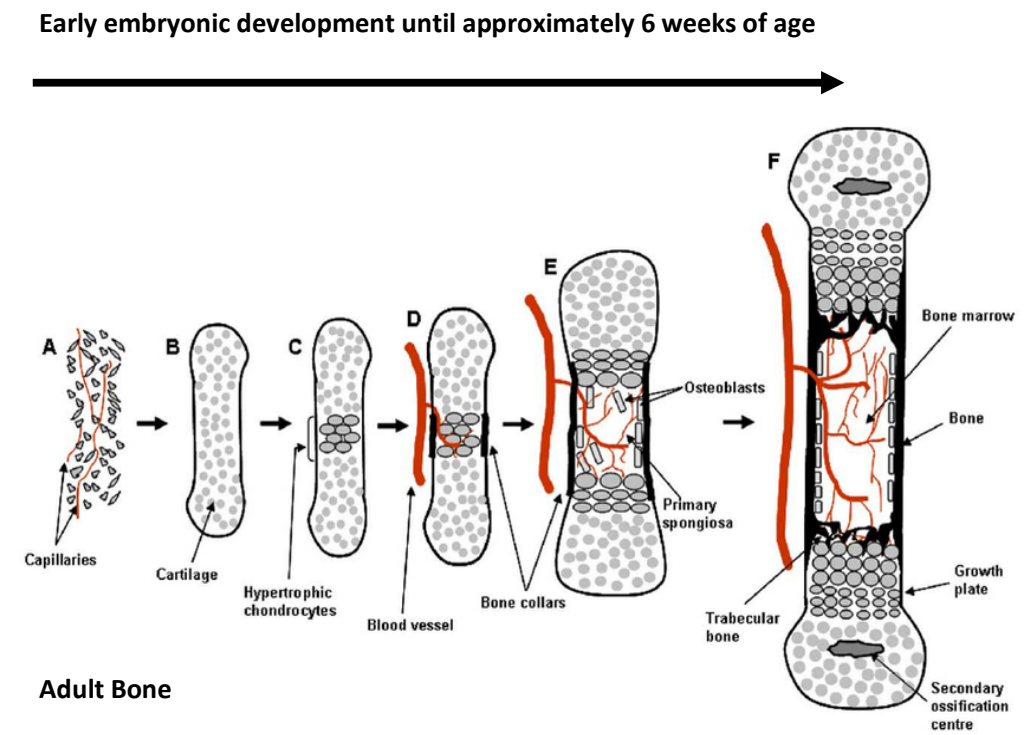

Figure 1.4. Endochondral ossification.

The process of endochondral ossification to approximately 6-weeks of age. Mesenchymal cells condense and (B) differentiate into chondrocytes forming an avascular cartilage model of the future bone. (C) At the centre of the condensation, the chondrocytes cease proliferating and become hypertrophic. (D) perichondral cells adjacent to the hypertrophic chondrocytes differentiate into osteoblasts forming a bone collar. The hypertrophic chondrocytes regulate the formation of mineralised matrix; the release of angiogenic factors to attract blood vessels and undergoes apoptosis. (E) The coordination of osteoblasts and vascular invasion form the primary spongiosa. The chondrocytes continue to proliferate with concomitant vascularisation resulting in a coordinated process that lengthens the bone. Osteoblasts of the bone collar will eventually form cortical bone; while osteoblasts precursors located in the primary spongiosa will eventually form trabecular bone. (F) At the ends of the bone, secondary ossification centres develop through cycles of chondrocyte hypertrophy, vascular invasion and osteoblast activity. Columns of proliferating chondrocytes form in the growth plate beneath the secondary ossification centre. finally, the expansion of stromal cells and hematopoietic marrow starts to take place in the marrow space (Kanczler and Oreffo, 2008).

Mineralised tissue is present within the resultant boney structure. These centres are vascularised (Mackie et al., 2011). Endochondral ossification is integral not only for the development of the majority of bones but also is an essential proponent in postnatal longitudinal bone growth and fracture healing (Ford et al., 2004, Miclau et al., 2007, Miller et al., 2015, Ghiasi et al., 2017).

The longitudinal growth of bone is highly regulated and occurs at the growth plate through the process of endochondral ossification (Nilsson et al., 2005). Proliferation and hypertrophy of the growth plate chondrocytes tightly controlled and influenced by endocrine factors (Hunziker et al., 1987, Nilsson et al., 2005, Staines et al., 2012a). For example, thyroid hormones, oestrogens/androgens, glucocorticoids and vitamin D can all regulate this process through their actions on chondrocyte maturation alone (Bohme et al., 1992, Boersma et al., 1996, Talwar et al., 2006, Bouillon et al., 2008, Idelevich et al., 2011, Wit and Camacho-Hubner, 2011, Weise et al., 2001). It is worth noting that the longitudinal growth can also be governed by the surrounding mechanical environment (Frost, 1987, Frost, 1994, Villemure and Stokes, 2009).

1.2.6. Bone modelling and remodelling

The skeleton represents a highly dynamic and adaptive organ, such that it can respond to demands placed upon it (Suchacki et al., 2017). These demands may be mechanical or centred on erythrocyte/cytokine production and calcium homeostasis (Brown, 1982, Brown and Hebert, 1997, Skerry, 2008, Wilson et al., 2008, Takizawa et al., 2012). The modification processes of the skeleton are routinely characterised into two processes known as modelling and re-modelling which have specific characteristics (Table 1.1). Together, these processes facilitate development by allowing bones to both change shape and grow whilst concomitantly maintaining proportions to allow ambulation. Under Wolff's Law, the shape, size and section modulus (i.e. bending strength) of bones is determined by the loads placed upon them (Frost, 1987). It is modelling and remodelling that are the core processes enabling bones to adapt to physical stress (Cowin, 1984, Robling and Turner, 2009).

	Modelling	Remodelling
Goal	Shape bone, increase bone mass	Renew bone
Cells	Osteoclasts or osteoblasts and precursors	Osteoclasts, osteoblasts, and precursors
Bone envelope	Periosteal, endocortical, trabecular	Periosteal, endocortical, trabecular, intracortical
Mechanism	Activation-formation or activation-resorption	Activation-resorption-formation
Timing	Primarily childhood but continues throughout life	Throughout life
Net effect on bone mass	Increase	Maintain or slight decrease

Table 1.1. Characteristics of modelling and remodelling

(Modified from (Allen and Burr, 2014).

Modelling can be either the formation of bone by osteoblasts or resorption of bone on an existing surface by osteoclasts which may occur at periosteal, endosteal or trabecular surfaces (Allen and Burr, 2014). Despite occurring predominantly in the growth and development stages of life, this process may be initiated if there is damage to bone (*e.g.* a bone break) (Schindeler et al., 2008, Odgren et al., 2016). There are two forms of remodelling, including formation whereby there is deposition of new bone, or resorption whereby there is the breaking down of existing bone (Burr, 2002, Clarke, 2008). Formation and resorption can work independently from each other, at differing anatomical locations and under different timeframes (Burr, 2002, Parfitt, 2002). The primary functions of bone modelling are to increase bone mass and to ensure that bone shape is maintained (Allen and Burr, 2014).

If an individual experiences a high degree of strain, formation modelling and resorption, modelling may act in concert. This ensures that there is the addition of bone mass and/or the re-shaping of bone such that future skeletal stresses may be better tolerated (Henriksen et al., 2009). If there are low levels of strain, only resorption modelling is activated to give a reduction of bone mass and a resultant freeing of stored minerals into the bloodstream (Henriksen et al., 2009).

Remodelling is the process of osteoclast-mediated resorption, followed by osteoblast-mediated bone formation occurring at the same location (Frost, 1990, Crockett et al., 2011). This is the major differentiator from resorption modelling and formation modelling (Table 1.1). The process of bone remodelling occurs at the periosteal, endosteal, trabecular and intracortical surfaces (Crockett et al., 2011). The process of remodelling can be subdivided into two categories: targeted and stochastic. The process of targeted remodelling ensures that the mechanical integrity of bones is maintained. It is therefore largely recognised that this process is activated when bones experience micro-damage (Seeman, 2009). Conversely, stochastic remodelling occurs randomly and is mostly hormonally driven (Poole and Reeve, 2005, Khosla et al., 2012). The current working hypothesis supports the notion that stochastic remodelling is integral to calcium homeostasis maintenance (Seeman, 2009). Therefore, to allow bone development and

to maintain skeletal architecture and composition, there is continuous homeostatic adjustment of the skeleton. Central to this adjustment is the highly regulated interplay and actions of the distinct bone cell types.

1.2.7. Cells of the skeleton

Skeletal biology plays key roles in maintaining homeostasis and in conditioning the body to better respond to future physical tasks. The process of modelling and remodelling is under constant control of both local factors (*e.g*. growth factors) and systemic factors (*e.g*. oestrogens) (Raisz, 1988, Mohan and Baylink, 1996, Vaananen and Harkonen, 1996). These factors ensure that bone is maintained at an optimal level of conditioning to respond best to future physical tasks. It is important to note that an imbalance between resorption and formation of bone may result in development of certain bone diseases (Feng and McDonald, 2011). One such example is osteoporosis, whereby the resorption rate of the osteoclast outstrips the bone-formation rate of the osteoblasts, causing decreased bone density and increased propensity for bone fracture (2001, Feng and McDonald, 2011) (Fig. 1.5). Conversely, osteopetrosis is a rare bone disease whereby there is a genetic mutation that gives decreased bone resorption, resulting in an abnormal accumulation of bone mass (Saftig et al., 1998). These permutations in normal physiology reflect the importance of the normal bone modelling process for the maintenance of bone homeostasis.

Normal Bone

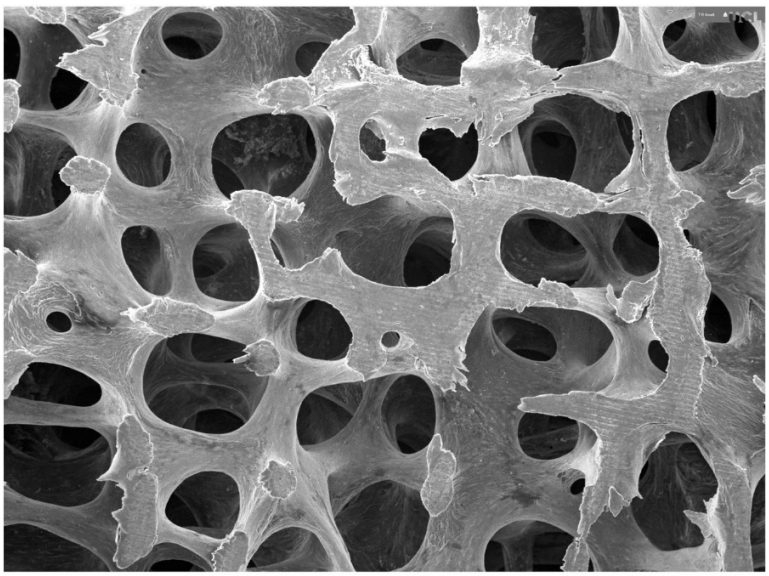

Osteoporotic Bone

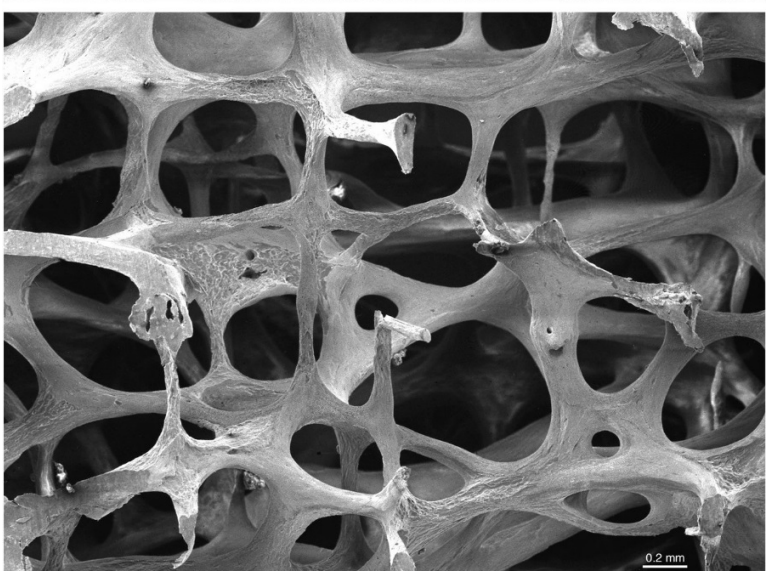

Figure 1.5. Comparison of normal and osteoporotic bone architecture.

Low powered scanning electron microscopy of trabecular bone from 3rd lumbar vertebrae (marrow and other cells have been removed). Top panel shows normal trabecular bone architecture. Bottom panel shows extensive pitting caused by osteoclasts. Images provided from the Bone Research Society, by kind permission of Tim Arnett.

This bone homeostasis is regulated by the complex interplay of specialised bone cells. There are three universally recognised bone cell types: osteoblasts, osteocytes and osteoclasts (Fig. 1.6). Osteoblasts, representing 4-6% of total bone cells, exhibit a cuboidal morphology and are located along the bone surface (Florencio-Silva et al., 2015a). With a mesenchymal stem cell origin, the lineage commitment to osteoblasts requires the expression of genes and programmed steps (Rutkovskiy et al., 2016). One example of this is the Wnt/*β*-catenin pathway (Saidak et al., 2015). For the differentiation of osteoblast specifically, the expression of transcription factors (runt-related transcription factor 2 (*Runx2)* distal-less homebox 5 (*Dlx5*), and osteoblast-specific transcription factor osterix (*Osx*)) is critical (Stein et al., 2004, Jensen et al., 2010, Rutkovskiy et al., 2016). Specifically, *Runx2* referred to as the 'master gene of osteoblast differentiation' is required to promote the up-regulation of osteoblast-specific genes (collagen type 1 alpha (*Collα1), alkaline phosphatase (ALP),* bone sialoprotein (*Bsp)* and *Ocn)* (Jensen et al., 2010, Komori, 2010, Li et al., 2012, Rutkovskiy et al., 2016).

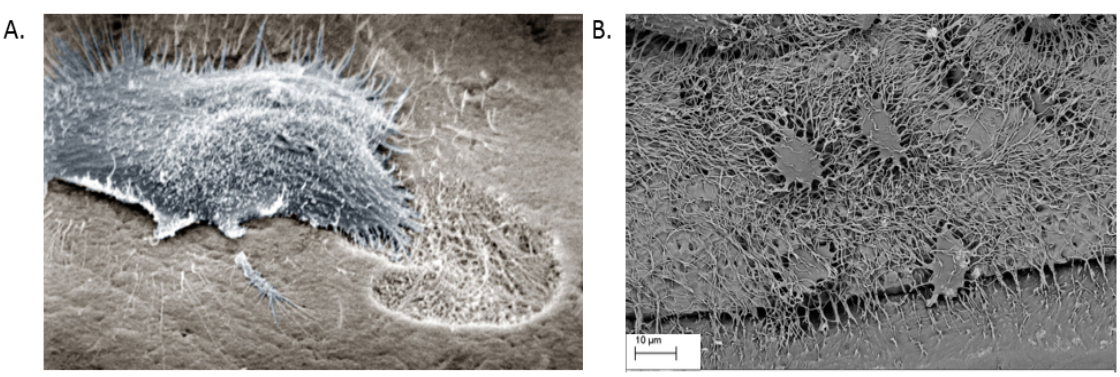

Figure 1.6. Osteoclast and osteocyte cells.

(A) Scanning electron micrograph of an osteoclast reabsorbing bone surface and (B) scanning electron microscope image of an osteocyte organised within the osteocytic lucanar-canalicular system. Images provided from the Bone Research Society with kind permission of (A) Tim Arnett and (B) Kevin Mackenzie.

Osteocytes represent the most abundant and long-lived cells within bone, comprising over 90-95% of all bone cells in the adult skeleton (Lanyon, 1993, Florencio-Silva et al., 2015a). Owing to complexities in isolating the osteocytes from bone matrix, initial studies required significant time and effort to determine their function (Stern et al., 2012). Due to this, it was hypothesised that these cells are quiescent or passive, leading to a misrepresentation, until recently, of both structure and function (Dallas et al., 2013).

The osteocytes are located within their lacunae and surrounded by mineralised matrix. This gives rise to the description of osteocytes as 'buried cells', whereby they remain embedded and persistent in the bone matrix (Franz-Odendaal et al., 2006). Originating from the site where the cell body is isolated (lacunae space), these cells exhibit cytoplasmic processes, which provide the osteocyte-lacunocannalicular system: the cytoplasmic processes of the neighbouring cells are interconnected with gap junctions, and provide a large surface area of the osteocyte population (Shapiro, 1997). Cell-cell communication and the presence of the lacunocannalicular system allow these cells to act as mechanosensors within an interconnected network which includes connection to neighbouring osteocytes and bone surface osteoblasts (Seliger, 1970, Cowin et al., 1991, Burger and Klein-Nulend, 1999, Yellowley et al., 2000). This facilitates the detection of mechanical pressure load changes and allows adaptation of bone such that structural integrity is retained and any micro-damages can be repaired (Paluch et al., 2015).

Osteoclasts are terminally differentiated multinucleated cells that originate from a hematopoietic stem cell origin (Loutit and Nisbet, 1982, Bar-Shavit, 2007). These cells, in contrast to osteoblasts, have the unique function of destroying the tissue in which they reside (Blair et al., 1989, Abu-Amer et al., 1997, Clarke, 2008). As such, these cells are responsible for the resorption of bone material. Osteoclasts polarise during the remodelling of bone (resorption) such that a ruffled border comes into contact with the bone matrix (Charles and Aliprantis, 2014). This ruffled structure has a vacuolar-type H^+-ATPase, which facilitates the acidification of the resorption lacunae and allows for the dissolution of the HA crystals (Teitelbaum, 2000, Teitelbaum, 2011). Parathyroid hormone (PTH) promotes bone resorption to release calcium, yet

this action is via the PTH1 receptor which is situated on the osteoblast (Juppner et al., 1991, Datta and Abou-Samra, 2009). Furthermore, the osteoblast (and osteocytes) secrete osteoprotegerin (OPG) and receptor activator of nuclear factors κB (NF-κB) ligand, which in turn controls osteoclast formation and activity (Udagawa et al., 2000). This cross-talk is critical in facilitating the coordinated function of the remodelling process.

1.2.8. Matrix mineralisation

Although controversial, HA formation in bone is largely accepted to involve membrane-limited specialised structures known as MVs (Bonucci, 1967, Ali, 1976, Anderson, 1967, Anderson, 1984, Anderson, 1995, Cui et al., 2016). These bodies are nano-spherical, with a diameter of 100 nm to 200 nm and a trilaminar membrane (Anderson, 1995). These MVs are derived through a 'budding process' from the plasma membrane of mineral forming cells, including chondrocytes, osteoblasts and odontoblasts (Ali, 1976, Yamada and Ozawa, 1978, Anderson, 1969, Cui et al., 2016). The mineralisation process is biphasic and is initiated by the accumulation of both calcium ions and inorganic phosphate (P_i) within the MVs (Ali, 1976, Anderson, 1984, Boyan et al., 1989, Genge et al., 1989, Anderson, 1995, Genge et al., 2007, Wuthier and Lipscomb, 2011). Once a sufficient concentration of both calcium and P_i has been reached, the calcium phosphate begins to precipitate (Traub et al., 1992, Traub et al., 1989, Wu et al., 2008, Landis and Silver, 2009). Initially, this precipitate is non-crystalline. Subsequently, a series of intermediates allow the formation of HA crystals (Nudelman et al., 2013). After this initial phase, there is a penetration of the MV membrane by HA crystals, resulting in their exposure to extracellular fluid (Nudelman et al., 2013). Following this, the crystals continue to grow and develop, forming in alignment with the collagen fibrils of the ECM (Nudelman et al., 2010, Nudelman et al., 2013, Cui et al., 2016). The MV-regulated mineralisation is coordinated by the ratio of mineralisation promoters and mineralisation inhibitors.

1.2.9. Regulation of mineralisation

For the mechanical functions of the skeleton to occur, there is a continuous homeostatic and dynamic adjustment of the skeleton whereby old bone is removed and new bone (osteoid) is laid

down (Crockett et al., 2011). The newly laid down bone becomes mineralised, whereby HA crystals containing calcium and P_i are deposited into an organic ECM (Karsenty et al., 2009). The tightly regulated mineralisation process is maintained by the actions of mineralisation inhibitors including pyrophosphate (PP_i) and mineralisation promoters (*e.g.* P_i).The ratio of P_i/PP_i is mediated by a variety of proteins: ENPP1 and progressive ankylosis protein (ANK) which work synergistically to regulate PP_i levels to inhibit HA accumulation (Hakim et al., 1984b, Yadav et al., 2011b, Staines et al., 2012b, Millán, 2013).

PP_i is recognised as a key inhibitor of both physiological and pathophysiological mineralisation relating to both bone and soft tissue (Fleisch and Bisaz, 1962, Orriss et al., 2016). The mineralisation regulators, which suppress spontaneous mineralisation, maintain the physiological PP_i levels. A disturbance to PP_i levels, for example owing to abnormal PP_i metabolism, is reported and associated with dysregulation or pathological mineralisation (Mackenzie et al., 2012). Therefore, any functional disruption to the regulatory proteins can be anticipated to result in phenotypic changes related to abnormal mineralisation of the skeleton.

The cell-surface enzyme tissue non-specific alkaline phosphatase (TNAP) is found in a variety of cells including osteoblasts, chondrocytes and the surface of these cells' MVs (Yadav et al., 2011b). TNAP is encoded by the *Akp2* or *Alpl* gene in mice and the *ALPL* gene in humans (Whyte et al., 2015). TNAP hydrolyses PP_i, thereby decreasing extracellular PP_i concentrations and facilitating HA formation. In humans, mutations of *ALPL* can result in the inherited skeletal disease of hypophosphatasia (Rathbun, 1948, Mornet, 2000, Mumm et al., 2001). This disease manifests in a hypomineralisation phenotype, which results in infant and childhood rickets, spontaneous fractures, deficiency of bone alkaline phosphatase (TNAP) activity and increased extracellular PP_i concentrations (Oikawa et al., 2014, Whyte et al., 2015). The severity of hypophosphatasia is related to the nature of the *ALPL* mutation (Whyte et al., 1988).

Mouse studies have been key in determining the importance of TNAP in regulation of mineralisation. The *Alpl* knockout mouse, a model for infantile hypophosphatasia, reflect the human disease whereby this mouse model demonstrates rachitic abnormalities and growth plate chondrocyte differentiation arrest (Fedde et al., 1999b, Liu et al., 2014). These mice also present with a disturbed bone remodelling and associated disordered matrix architecture and notable skeletal hypomineralisation with associated elevated PP_i concentration (Liu et al., 2014). Furthermore, transgenic overexpression of TNAP in mice has been shown to cause decreased PP_i concentrations further indicating the key role TNAP plays in promoting mineralisation by decreasing PP_i and thus decreasing inhibitory regulation of mineralisation (Savinov et al., 2015, Romanelli et al., 2017).

Phosphatase orphan 1 (PHOSPHO1) is also important for the regulation of mineralisation (Roberts et al., 2007a, Huesa et al., 2015a, Houston et al., 2016). PHOSPHO1 exhibits its action within osteoblast and chondrocyte-derived MV's and generates P_i (Stewart et al., 2006, Roberts et al., 2007a). The expression of *Phospho1* is approximately 100-fold higher in mineralising chondrocytes in comparison to non-skeletal tissues and has been shown to exhibit highly specific activity for phosphoethanolamine (PEA) and phosphocholine (PChol) (Roberts et al., 2007a). It is largely regarded that PHOSPHO1 is integral in the generation of P_i to facilitate skeletal mineralisation through its highly specific phosphohydrolase activity for PEA and PChol and that this occurs within the MVs derived from both osteoblasts and chondrocytes (Stewart et al., 2006). Analysis of mice deficient in PHOSPHO1 (*Phospho1*$^{-/-}$) have demonstrated that PHOSPHO1 is essential for physiological endochondral ossification and for normal bone fracture healing to occur (Morcos et al., 2018). These *Phospho1*$^{-/-}$ mice present with spontaneous fractures, hypomineralisation of the skeleton, bowed long bones and scoliosis, particularly in young age cohorts (Huesa et al., 2011, Yadav et al., 2011b, Javaheri et al., 2015). In 2001, Yadav *et al.,* demonstrated that the double knockout of TNAP and PHOSPHO1 resulted in the complete absence of a mineralised matrix. As such, it is proposed that intra-vesicular PHOSPHO1 facilitates P_i influx to the MV, which is crucial for the mineralisation and the function of TNAP, NPP1 and the extra-vesicular continuation of mineralisation to occur (Yadav et al., 2011a).

Encoded by the progressive ankylosing gene (*Ank)*, ANK is responsible for facilitating the extracellular movement of intracellular PP_i (Ho et al., 2000, Kim et al., 2010). This protein acts as a transmembrane PP_i-channelling protein and is detectable on the surface of both osteoblasts and chondrocytes (Ho et al., 2000, Harmey et al., 2004). Disruptions to this transporter are associated with significant skeletal phenotypes. Mice possessing a spontaneous loss-of-function mutation in the *Ank* gene present with a progressive form of generalised arthritis, boney outgrowths, pathological joint formation and increased mineral deposition (Sweet and Green, 1981, Gurley et al., 2006b). These *Ank/Ank* mutant mice also show a significant decrease in extracellular PP_i, with a concomitant increase in intracellular PP_i (specific to fibroblasts), compared to wild-type counterpart cells (Mitton-Fitzgerald et al., 2016). As such, ANK regulates PP_i to mediate physiological mineralisation and the incidence of arthritis, particularly in calcium pyrophosphate deposition disease (CPPD).

In concert, ENPP1, TNAP, PHOSPHO1 and ANK are key regulators for the controlled and physiological mineralisation of both the skeleton and soft tissue mineralisation (Fig. 1.7). Investigation into both rare tissue mineralising diseases and transgenic mouse models have been integral in the early research conducted to determine the role of these enzymes concerning mineralisation (Rashdan et al., 2016). The first definitive link of defective *Enpp1* and disturbed mineralisation was shown in the 'tiptoe walking' (*ttw/ttw*) mouse model, whereby there is a premature stop codon in the *Enpp1* coding sequence resultant of a homozygous GRT substitution (Okawa et al., 1998b). As a result, these mice have a truncated NPP1 protein, which leads to a loss of calcium-binding domain and putative glycosylation sites. The bone phenotype associated with such disruption includes abnormal bone hypermineralisation (progressive ankylosing intervertebral and peripheral joint hyperostosis), as well as ectopic calcification including spontaneous arterial and articular cartilage calcification (Okawa et al., 1998b).

The second mouse model to demonstrate the link of *Enpp1* mutation and abnormal bone phenotype was a transgenic strain, homozygous for disruption of Exon 9 of the *Enpp1* gene

(*Enpp1*$^{-/-}$) (Johnson et al., 2003). The resultant phenotype resembled that of *ttw/ttw* mice. In both mouse models, decreased extracellular PP_i was observed, with abnormal long bone and calvaria mineralisation, as well as pathological ectopic calcification of soft tissues, including peri-spinal and arterial calcification. This phenotype is also reflected in mutant *Enpp1*^{asj} mice. These mice harbour a missense mutation, p.V246D, in the *Enpp1* gene and develop stiffened joints accompanied by decreased systemic PP_i and extensive soft tissue and vasculature mineralisation (Jiang and Uitto, 2012, Li et al., 2013, Zhao et al., 2017).

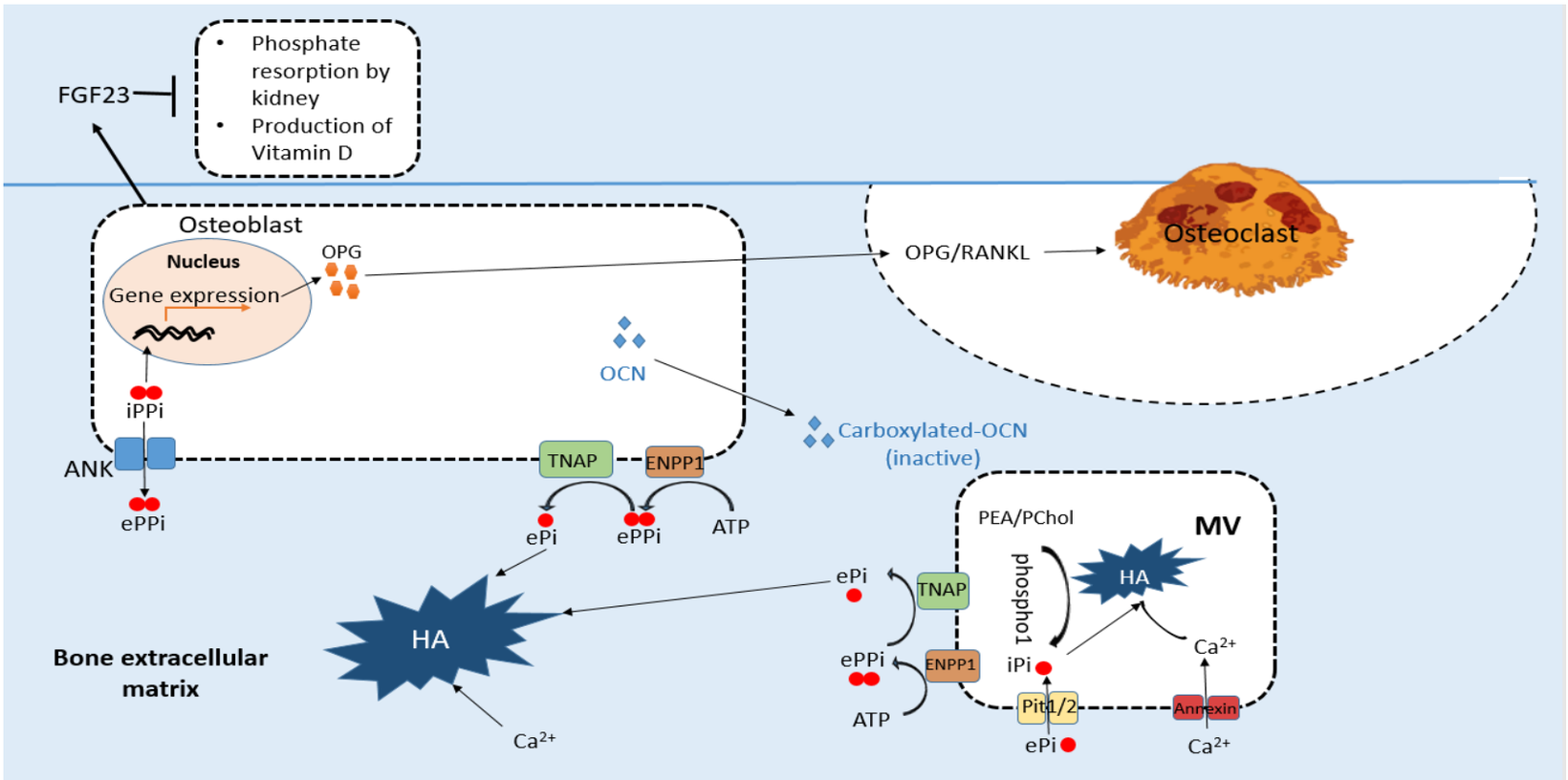

Figure 1.7. Regulation of mineralisation by bone factors.

HA crystals consist of phosphate (Pi) and calcium (Ca^{2+}). In MVs released from osteoblasts, extracellular Pi (ePi) is intracellularly channelled by Pit1/2 phosphate transporters. Additionally, ePi is generated via phosphomonoester (PEA/Pchol) hydrolysis by the phosphatase PHOSPHO1. Ca^{2+} is transported into MV via annexin channels. HA nucleates from MVs into extracellular space. Extracellular PPi (ePPi) is generated by hydrolysis of ATP by ENPP1, and also intracellular PPi is extracellularly exported by ANK at the site of osteoblast membranes. Both ePPi and OPN inhibit HA formation. The majority of ePi is generated by the actions of TNAP via ePPi hydrolysis and facilitates HA formation. OPG, produced in osteoblasts, activates the RANKL pathway to regulate osteoclast resorption activity.

1.2.10. Energetic cost of the skeleton

The regenerative process of bone, a structure which contributes a large proportion of body mass (approximately 15% in men, and 10% in women), requires a great number of proteins to be synthesised and secreted (Vaananen et al., 2000, Karsenty et al., 2012). It is possible, therefore, to consider that this comes at a high energetic cost to the organism. Bones themselves likely represent a survival factor which was strongly selected for, owing to skeletal structure providing motility such that scavenging, survival of injury and thus survival of the organism could occur (Karsenty et al., 2012). Yet, it is likely that the selection of the skeleton involved other important evolutionary components: for example, that part of the selection process for bones involves its integral role in the regulation of endocrine control of whole-body energy metabolism (Karsenty and Olson, 2016).

1.2.11. Bone is an endocrine organ

In addition to the structural roles and homeostatic roles in the regulation of calcium and P_i, the skeleton is also well recognised as an endocrine target (Guntur and Rosen, 2012). Central to the theory of homeostasis is that there is a reciprocal cross-talk between the signalling organ and the target organ (Ramsay and Woods, 2014). It is therefore important to discuss the endocrine signalling actions of the skeleton. Despite a currently vague understanding of the skeleton's recently discovered metabolic-endocrine function, there is increasing evidence to support this new paradigm. Investigation into this field was catalysed following the discovery of hormonally active OCN, which is the most abundant of the osteoblast-specific non-collagenous proteins (Ducy et al., 1996).

Released from the osteoblast and present in the general circulation, OCN exists in carboxylated, partially-carboxylated and fully under-carboxylated forms (Ferron et al., 2010b, Clemens and Karsenty, 2011, Karsenty and Olson, 2016). Of these forms, the latter represents the hormonally active variant, whereby there is promotion of pancreatic β-cell proliferation, insulin secretion, peripheral insulin sensitivity and energy expenditure (Karsenty et al., 2012). This un-carboxylated-OCN is formed when carboxylated-OCN, secreted by osteoblasts and found in the

ECM, is decarboxylated at the acidic pH (4.5) of the osteoclastic resorption lacunae (Faienza et al., 2015). This points towards the delicate interplay between the two opposing, yet related, cell types (osteoblasts and osteoclasts) and their integral role in regulating bone-specific factors related to both skeletal formation and whole-body metabolism. By utilising primary human and rat long-bone derived osteoblast-like cells, it has been revealed that a paracrine communication exists between osteoblast and endothelial cells, mediated by vascular endothelial growth factor to regulate bone vascularisation (Clarkin et al., 2008).

Further evidence supports the key role of osteoblast-associated bone factors and energy metabolism. One example of which is PHOSPHO1, a member of the large haloacid dehydrogenase superfamily of Mg^{2+} dependent hydrolases (Houston et al., 2004). This bone-factor is active whilst inside the osteoblast-derived MV: at this site, P_i is scavenged from MV membrane proteins to promote the intra-vesicular HA deposition. Yet, novel roles of PHOSPHO1 in energy homeostasis exist. Mice with *Phospho1* ablation exhibit a decreased body size and protection against both obesity and diabetes, regardless of the carboxylation status of OCN (Oldknow et al., 2014, Dillon et al., 2019). Evidence also exists to suggest that sclerostin (SOST) plays a role in a bone-metabolic phenotype regulation. Since SOST, predominantly released from osteocytes, inhibits the *Wnt*-signalling pathway, it also serves to inhibit osteoblast differentiation and bone formation, whilst promoting adipogenesis (Klangjareonchai et al., 2014). Putative investigations in human cohorts have revealed positively correlated circulating sclerostin and fat mass (abdominal and gynoid), as well as in type 2 diabetes mellitus (T2DM) patients (Klangjareonchai et al., 2014). This indicates a bone-fat interrelationship. The identification of links amongst these bone-secreted proteins will improve our understanding of the potential bone-adipose-muscle interactions, which may aid in developing a therapeutic intervention for the disease of these tissues, whilst avoiding adverse side effects on non-targeted tissues.

Indeed, the last decade has seen an increasing understanding of the skeleton's ability to act as an endocrine regulator (Fig. 1.9). Significant development of both mouse models and cellular systems have facilitated a rapid expansion of knowledge and evidence in favour of the skeleton's

endocrine function. This adds further credence to the importance of the skeleton for survival beyond its mechanical roles. It is logical to propose that the skeleton produces hormones to regulate skeletal mineralisation, and, at the same time, cooperates with other endocrine organs to regulate calcium, phosphate and wider metabolic parameters. Continued identification of bone-secreted factors and their function will aid in answering the questions of how and why bone-specific regulation of energy metabolism have arisen.

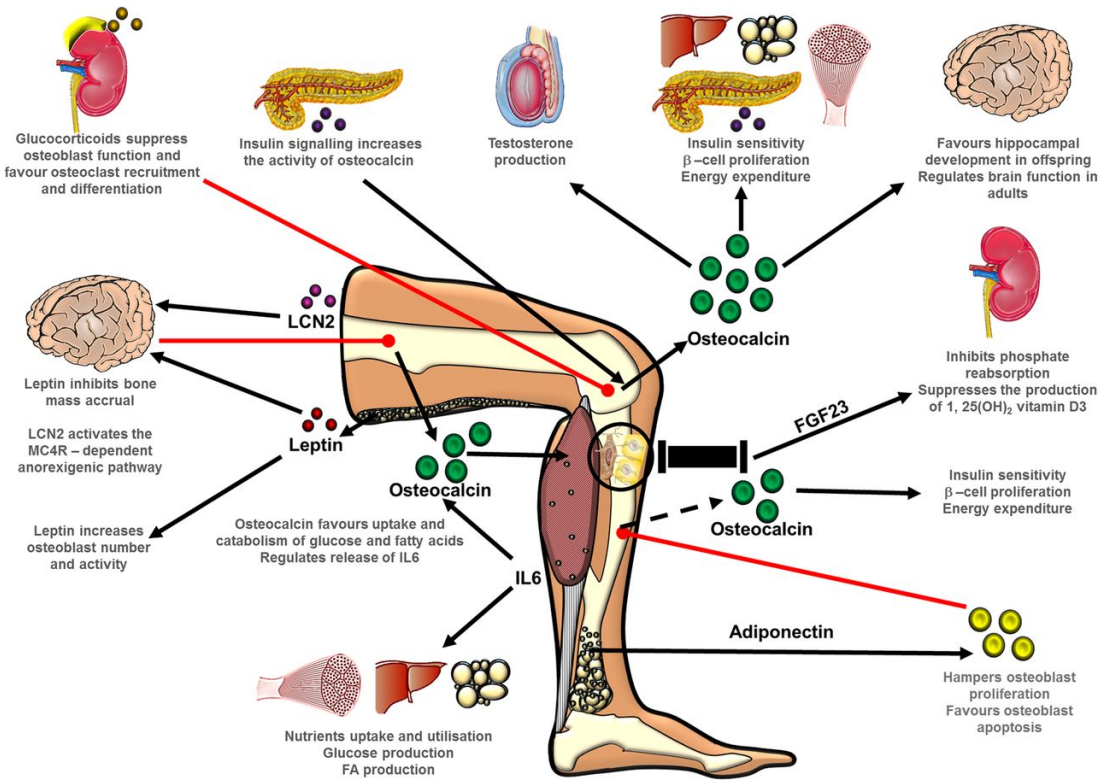

Figure 1.8. Schematic of newly discovered endocrine functions of bone, muscle and adipose tissue.

Insulin secretion from the pancreas acts upon the IR on the osteoblast, which subsequently inhibits Forkhead box protein O 1 (*FoxO1*) expression and suppresses twist basic helix-loop-helix transcription factor 2 (*Twist2*), favouring bone resorption via osteoclast activation. The adipocyte-derived hormone leptin has been shown to have two opposing roles, acting centrally to inhibit bone mass accrual and peripherally, increasing osteoblast number and activity. The acidic pH generated in the resorption lacunae decarboxylates OCN on its three glutamic acid residues (GLU13, GLU17 and GLU20), which enable it to be released from the bone matrix into the general circulation. Once circulating, OCN can regulate global energy metabolism via the stimulation of insulin secretion and β-cell proliferation in the pancreas; energy expenditure by muscle and insulin sensitivity in adipose tissue, muscle and liver. Furthermore, OCN favours hippocampal development in offspring; brain function in adults and male fertility by stimulating testosterone synthesis in Leydig cells of the testis. A bone–muscle feed-forward axis exists where systemic undercarboxylated OCN signals to myofibres favouring uptake and subsequent catabolism of glucose and fatty acids, facilitating physical adaptation to exercise and release of exercise-induced IL-6. The latter drives the production of bioactive OCN. Adiponectin release from bone marrow adipose tissue may act to indirectly increase bioactive OCN by suppressing osteoblast proliferation, potentially favouring osteoclast activity. Another possibility is that excess local OCN production is responsible, at least in part, for elevated adiponectin production from MAT; however, this remains unclear (Arrow key: black solid – accepted; black dashed – speculative; red – inhibitory.) (Suchacki et al., 2017)

1.2.12. Members of the ENPP family

The ectonucleotide pyrophosphatase/phosphodiesterase (ENPP) family is comprised of 7 structurally related members (Terkeltaub, 2006). These family members have been recognised for over 20 years and are known to have roles in nucleotide recycling, purinergic signalling, homeostasis of $PP_{i,}$ cell motility and regulation of IR activity (Terkeltaub, 2001, Robson et al., 2005, Vorhoff et al., 2005, Terkeltaub, 2006). Although the principal focus of this project is on ENPP1, this section will address the six other members of the ENPP enzymatic family. As previously discussed, all members of the ENPP family share a structurally related catalytic domain: despite this, there is diversity in the enzymatic (and non-enzymatic) functions of each family member (Goding et al., 2003). Consequently, there is variation amongst the pathology suffered from deleterious mutations or aberrant expression of each ENPP family member.

ENPP1-3 are expressed in a wide range of tissues, although specific individual isoforms are reportedly restricted in a tissue-specific nature (Harahap and Goding, 1988, Narita et al., 1994, Bollen et al., 2000). The catalytic function of ENPP1-3 has been determined, which has allowed classification of these three isozymes as the alkaline ENPP's (Narita et al., 1994, Deissler et al., 1995). There is a wide range of substrates which can be acted upon by ENPP1-3, whereby both pyrophosphatase and phosphodiesterase bonds are catalysed in a two-step fashion (Bollen et al., 2000, Gijsbers et al., 2001). It is important to note that the substrate specificity of the ENPP family is not solely restricted to nucleotides and indeed encompasses a wide variety of other substrates (Goding et al., 2003). This signifies that the ENPP family may be involved in the regulation of many different physiological processes. Indeed, abnormal expression of ENPPs has been recognised in pathologies ranging from mineralisation disorders, cell motility, angiogenesis, cancer and metabolic diseases (Goding et al., 2003, Terkeltaub, 2006). Much remains unknown about the mechanism, which govern these diverse biological processes.

Of the seven isoenzymes, ENPP1-3 have received the majority of focus regarding investigation into their modular structure and functions in normal and disease states. The remaining members of the ENPP family (ENPP 4-7) have been identified based upon sequence homology of their

catalytic site, although less detail is known of their physiological catalytic functions (Bollen et al., 2000). ENPP4-7 are predicted to be type I transmembrane orientation exhibiting shorter C-terminal domains, which are intracellular, along with a smaller extracellular domain when compared to their ENPP1-3 counterparts (Goding et al., 2003). In contrast, ENPP1-3 are type II transmembrane glycoproteins, which have a short intracellular domain, a single transmembrane domain and one large, extracellular domain (Andoh et al., 1999, Bollen et al., 2000, Kamikubo et al., 2002, Goding et al., 2003).

When considering the different isoenzymes, the most obvious structural difference is the lack of conservation of the intracellular domain, which is the N-terminal region of ENPP1-3, and the C-terminal region of ENPP4-5 (Gijsbers et al., 2001). These domain lengths range, both between isoforms and species. For example, ENPP1 has the longest of the intracellular domains; the human form is 76 amino acids long whereas the mouse 58 amino acids long (Belli et al., 1993, Frittitta et al., 1998, Banakh et al., 2002). Additionally, ENPP1-3 have been identified as having active forms of the enzyme in a soluble form, both in serum and conditioned media (Hosoda et al., 1999). This is achieved by the cleavage of the protein, which sits out-with the transmembrane region, resulting in a 125kD enzymatically active fragment, yet to date, the physiological roles of these soluble ENPPs remain undetermined (Meerson et al., 1998).

ENPP2, also referred to as autotaxin, was first identified as an autocrine motility factor and was identified during a cell culture study (Stracke et al., 1992). Here, investigators discovered the autocrine factor in the conditioned media from human melanoma cell line A2058 (Stracke et al., 1992). The main expression of ENPP2 is within the brain, placenta, ovary and small intestine in humans, with further identification in the ciliary, iris pigment epithelial cells, cartilage and cranial bone of rats (Narita et al., 1994, Fuss et al., 1997, Bachner et al., 1999). It has been determined that ENPP2 hydrolyses lypophophatidylcholine (LPC) to generate the active form of phospholipid lysophosphatidic acid (LPA), concurrently generating choline (Tokumura et al., 2002, Umezu-Goto et al., 2002). The resultant LPA is capable of influencing a range of physiological processes including cell proliferation, survival and motility, as well as activating a subset of six G-protein

coupled receptors (Moolenaar, 1995, Fukushima et al., 2001, Mills and Moolenaar, 2003). Observations of chronic hepatitis C patients have revealed that an increase in serum LPA and ENPP2 activity are associated with greater severity of liver disease (Pleli et al., 2014). Studies in rats have revealed that increased LPA leads to an activation of pro-fibrotic signals within the liver (Kaffe et al., 2017). Although these are early observations, it signifies the role of ENPP2 in liver health and potentially points towards a therapeutic approach for the treatment of fibrotic liver.

ENPP3 is also capable of hydrolysing ATP (together with ENPP1 and ENPP2) and is well recognised as an activation marker of human basophils (Buhring et al., 1999, Bühring et al., 2001). As such, ENPP3 can be used as a diagnostic marker for allergic diseases (Buhring et al., 2004). Studies of murine basophil mast cell have revealed an increase in the expression of ENPP3 when stimulated with IgE and antigen compared to unstimulated controls (Tsai et al., 2015). Little is known about ENPP3 and its activity. ENPP4 and ENPP5 are even more poorly understood, and have to date been mapped to their respective locations which include 17B2 and 17C in mice, 6p12.3 and 6p21.1-p11.2 in human and both at 9q12 on the rat genome, respectively (Goding et al., 2003).

It has been determined that ENPP6 is a choline-specific phosphodiesterase which is capable of hydrolysing a range of substrates, with a preference for lysopohlysophosphatidylcholine (LPC), sphingosylphosphorylcholine (SPC) and glycerophosphorylcholine (GPC) (Sakagami et al., 2005, Stewart et al., 2017). The exact localisation of ENPP6 within tissues/cells remains to be confirmed, although initial studies have located it within the brain and kidney proximal tubules (Stewart et al., 2017). It has also been shown that ENPP6 is present in bone, and is expressed in osteoblasts lining the bone surface (Stewart et al., 2017). The function of ENPP6 within both normal and disease physiological states remains to be determined.

ENPP7 was initially thought to be an alkaline sphingomyelinease and was discovered in 1969 (Nilsson, 1969). However, cloning studies in the early 2000's revealed that this gene actually belong to the ENPP family, and has since been identified in the intestinal tract of a variety of

species, as well as in the bile and liver exclusive to humans (Duan et al., 2003, Wu et al., 2005). This member of the family is distinct from the others, excluding ENPP6, in that it has no nucleotide activity, but instead exhibits phospholipase C activity (Duan et al., 2003). Most attention has been paid to its action in the intestinal tract, where ENPP7 digests ingested sphingomyelin, promotes cholesterol absorption and inhibits colon cancer formation (Cheng et al., 2007). Less attention has been paid to roles in the liver, an expression site of ENPP7 that is unique to humans.

Due to the wide range of actions, and many associated biological processes, a member, or members, of the ENPP family, could be targeted therapeutically. Continued efforts to comprehend this family of isoenzymes, their functions, interactions and co-dependency, effects of redundancy and the mechanisms which govern them will undoubtedly reveal prognostic and diagnostic value and warrants further investigation.

1.2.13. Roles of ENPP1 in soft tissue mineralisation

The investigation of mouse models of disease has undeniably increased our understanding of the genetic basis of skeletal-associated mineralisation defects relating to ENPP1. Additionally, observations of rare genetic diseases of mineralisation have also allowed insight to be gained. Generalised arterial calcification of infancy (GACI) is a rare autosomal recessive disease, which can be characterised by the formation of calcification in mineralisation competent tissues (Li et al., 2014b). This includes the deposition of calcium in the medium-sized arteries, which may ultimately lead to arterial stenosis due to intimal proliferation (Rashdan et al., 2016). Those individuals most severely affected by GACI will usually die within 6-months as a product of the sequelae associated with damage to the organs from myocardial infarction due to ectopic calcification (Glatz et al., 2006). A further investigation of patients presenting with GACI revealed that a subset of individuals develop aberrant calcification of the greater joints, characterised by lower than average levels of PP_i, due to defective ENPP1 enzymatic function (Nitschke et al., 2012). Resultant investigation into the genetic basis of GACI revealed that the majority of

patients with GACI suffered mutations in the ENPP1 encoding gene (predominantly with bi-allelic mutations of *ENPP1*) (Nitschke and Rutsch, 2012) (Fig. 1.9).

1.2.14. ENPP1 pathways

This research project focuses on ENPP1, also referred to as plasma-cell membrane glycoprotein 1 (PC-1) (Jansen et al., 2012). Specific to ENPP1 is the hydrolysis of ATP, yet other ENPP's hydrolyse substrates including, but not limited to, nucleoside triphosphates, lysophospholipids and choline phosphate esters (Bollen et al., 2000, Stefan et al., 2005, Zimmermann et al., 2012). ENPP1 is a glycoprotein that forms disulphide-bonded homodimers, present both in the plasma membrane and in the mineral depositing MVs of osteoblasts and chondrocytes (Jansen et al., 2012). Through the generation of PP_i as a by-product of ATP hydrolysis, ENPP1 serves to potently inhibit HA crystal formation that occurs in mineralisation-competent tissues (bone and soft tissue) (Addison et al., 2007).

Furthermore, ENPP1 regulates glucose homeostasis via suppression of the IR signalling in various tissues, including adipose, bone, and muscle (Maddux et al., 1995, Mackenzie et al., 2012). ENPP1 binds to the α-subunit of the IR, resulting in inhibition of insulin-induced IR conformational changes. The binding of ENPP1 prevents the recruitment, and binding, of tyrosine kinase to the intracellular region of the β-subunit of the IR, as such abrogating the IR β-subunit autophosphorylation (Maddux et al., 1995). Here, the Akt/P13K pathway is not activated and thus no translocation of insulin-regulated glucose transporter 4 (GLUT4) receptor from the GLUT4 receptor vesicles to the cell membrane (Zhou et al., 2009, Pan et al., 2012). As a product of this altered signalling pathway, there is a disruption to glucose homeostasis and as such, ENPP1 is considered a pathogenic factor in the development of insulin resistance (Huesa et al., 2014, Roberts et al., 2019b) (Fig. 1.9)

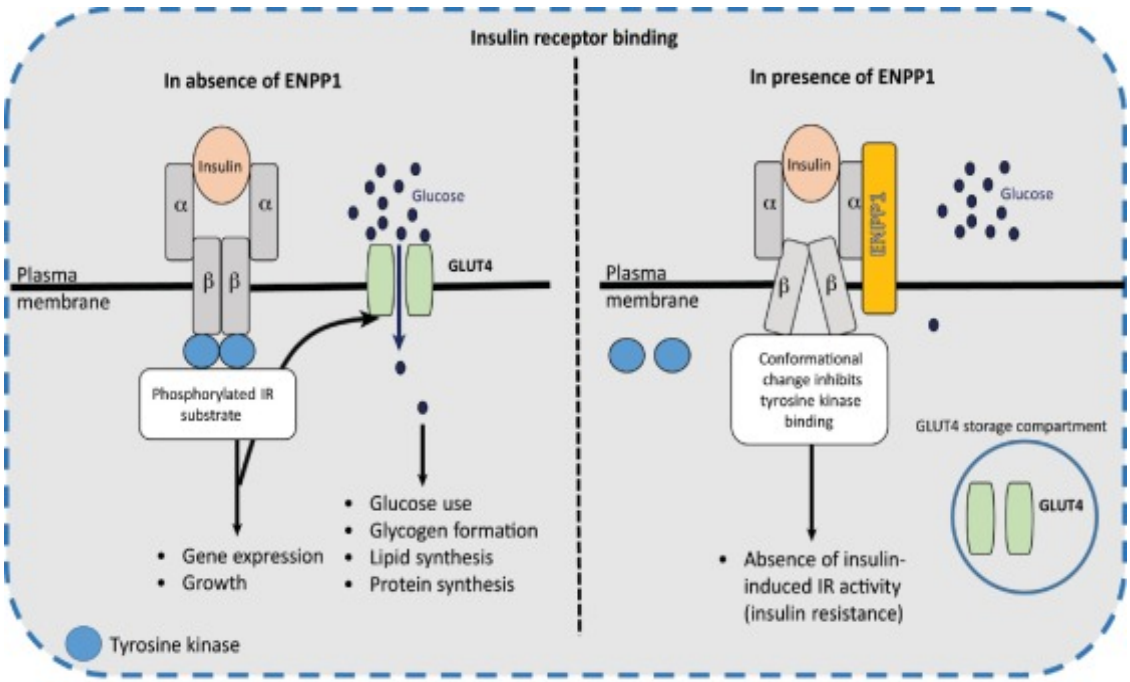

Figure 1.9. Schematic of insulin receptor binding in the absence and presence of ENPP1.

In the absence of ENPP1 (left), insulin binds to the α-subunits of the insulin receptor (IR) and stimulates a cascade of events. Notably, this binding facilitates tyrosine kinase-mediated auto-phosphorylation of the IR β-subunits, leading to the downstream mediation of glucose regulation by the subsequent activation of pathways (*e.g.* P13K and AKT activation) and resulting in altered gene expression and/or growth. Insulin binding also stimulates the translocation of the GLUT4 receptor to the plasma membrane where it regulates intracellular glucose transport to muscle and adipose tissues and, in turn, leads to pleiotropic effects such as the use of glucose, the formation of glycogen, the promotion of lipid synthesis, and protein synthesis. In the presence of ENPP1 (right), insulin binds to the α-subunit of the IR. This results in a conformational change of the β-subunit, preventing tyrosine kinase binding and thus inhibiting IR β-subunit auto-phosphorylation. As such, the downstream mediation of glucose is disturbed. There is an absence of GLUT4 translocation to the plasma membrane and dysregulation of glucose homeostasis, resulting in insulin resistance (Roberts et al., 2019b).

Insulin resistance is a widely acknowledged pathogenic risk factor for the development of both T2DM and cardiovascular disease. Amongst humans suffering from insulin resistance, levels of ENPP1 expression in metabolic tissues (e.g. muscle) have been reported as elevated (Frittitta et al., 2001, Pan et al., 2012). Furthermore, studies have shown that increased ENPP1 expression in muscle correlates with increased body mass index and decreased stimulation of muscle glucose transport by insulin (Frittitta et al., 1998, Goldfine et al., 2008). These described findings indicate that there is an important role in glucose homeostasis and insulin signalling centred on the functions of ENPP1 and that ENPP1 may link muscle and insulin resistance through its mode of action.

ENPP1 may also contribute to T2DM through its actions in the liver. A recent study by Di Paola *et al*., revealed that suppressed ENPP1 expression in the liver, skeletal muscle and pancreatic β-cells of mice results in improved insulin sensitivity (Di Paola et al., 2011). Furthermore, improved insulin sensitivity is observed following the liver-specific adenoviral knockdown of *Enpp1* expression in the *db/db* mouse model of diabetes (Zhou et al., 2009). These liver-specific *Enpp1* knockdown mice exhibited an 80% lower *Enpp1* mRNA level, with a 25% lower fasting plasma glucose (Zhou et al., 2009). Interestingly, transgenic mice which over-express ENPP1 (regulated by a cytomegalovirus promoter) demonstrated hyperglycaemia, hyperinsulinemia and impaired glucose tolerance (Zhou et al., 2009). Furthermore overexpression of human ENPP1 using recombinant adenovirus caused an increase in the expression of gluconeogenic associated genes. Further studies are required to fully elucidate the complex regulatory hepatic mechanisms of ENPP1's action, PP_i production and regulation of T2DM.

It has also been demonstrated that ENPP1 polymorphisms in humans are associated with T2DM. There are several documented genetic studies which have mapped insulin resistance associations to the ENPP1 chromosome locus. For example, the *ENPP1* K121Q polymorphism is well documented to be associated with T2DM (Leitão et al., 2008). The K121Q polymorphism (a missense mutation) demonstrates a stronger insulin receptor inhibition (Frittitta et al., 2001). Reportedly, there is a 38% increased risk for the development of T2DM in European individuals who are homozygous for the K121Q mutation, and the K121Q allele is associated with hyperglycaemia and insulin resistance (McAteer et al., 2008, Stolerman et al., 2008).

The majority of studies have focused upon the over-expression of *Enpp1* in rodent models to elucidate its mechanisms of action. Interesting work by Zhou *et al*., investigated the impact of *Enpp1* knockdown using siRNA. It reported that *Enpp1* knockdown significantly increased insulin-stimulated Akt-phosphorylation in HuH7 human hepatoma cells (Zhou et al., 2009). As such, the suppression of *Enpp1* expression may be used as a potential therapeutic approach to the treatment of T2DM. The pathways that underpin the effects of insulin resistance are currently unknown, this action may be mediated through the hormonally active form of OCN. This would result in insulin secretion through pancreatic β-cell proliferation, which augments peripheral insulin sensitivity, and thus energy expenditure (Ferron et al., 2010a, Fulzele et al., 2010).

NPP1 is capable of hydrolysing nucleotides. Nucleotides are present in the extracellular and are critical signalling molecules which are able to regulate a variety of biological affects via the purinergic cell-surface receptors (Ralevic and Burnstock, 1998). There are two main purinergic receptor families including the P1 receptors (which are activated adenosine) and P2 receptors. The P2 receptors can be divided into two families including the P2X and P2Y receptors and these are activated by nucleotides including ADP, ATP, UDP and UTP (Müller and Jacobson, 2011, Lee and Müller, 2017). Nucleotides activate these receptors and can alter processes including, but not limited to, smooth muscle contraction, hormonal secretion, immune response modulation, cell proliferation, cellular differentiation and apoptosis (Lee and Müller, 2017). Relatedly, there is a tight control of nucleotides via their hydrolysis and this includes the action of NPP1 which

accepts a range of substrates including nicotinamide adenine dinucleotide, 3'-phosphoadenosine-5'-triphosphate or diadenosine tetraphosphate and UDP-glucose, cyclic guanosine-(2'-5')-monophosphate-adenosine'(3",5")-monophosphate (2',3"-cGAMP) (Namasivayam et al., 2017, Bollen et al., 2000, Kelly et al., 1975, Zimmermann, 2001, Li et al., 2014a, Barber, 2014). There are also several synthetic substrates of NPP1 including *p*-Nitrophenyl 5'-thymidine monophosphate (*p*-Nph-5'-TMP), *p*-Nitrophenyl phenyl phosphate (*p*-NPPP) and bis(*p*-nitrophenyl) phosphate (bis(*p*-NP)P) (Henz et al., 2007, Lee et al., 2012). These actions of NPP1 on substrates other than ATP (and the subsequent generation of PP_i) and the effects on purinergic signalling remain beyond the scope of this thesis, although would be enlightening.

ENPP1 plays multifaceted roles in normal physiology, including the regulation of calcium and P_i homeostasis, the inhibition of soft tissue mineralisation by generation of PP_i, the maintenance of skeletal function, regulation of insulin signalling and energy homeostasis. Yet the exact function and mechanisms of ENPP1 within this relationship remains unclear, with many unanswered questions. For example, which cells types are responsible for the current poorly understood metabolic-related roles of ENPP1?

The rationale for further investigating cell-specific roles in metabolism lies in the knowledge that the osteoblast-derived hormones may be responsible for many of the skeleton's energy homeostatic actions. This has been demonstrated by the partial ablation of osteoblasts in mice, which resulted in profound effects in glucose metabolism, gonadal fat mass and an increased energy expenditure (Yoshikawa et al., 2011). OCN administration partly corrected the metabolic phenotype, however, it did not improve the increased energy expenditure or decrease gonadal fat (Yoshikawa et al., 2011). This suggests that osteoblasts can affect glucose metabolism through both OCN-dependent and OCN-independent mechanisms. Since the osteoblast is integral to OCN-related bone-endocrine functions, could this cell also play a key role in the actions of ENPP1? Much remains to be explored regarding specific mechanisms of actions and pathways of new candidates relating to skeletal-metabolic homeostasis. Once determined, this knowledge

may aid in identifying novel pharmacological approaches for the management and treatment of skeletal and metabolic diseases.

1.3. Aims and strategy

ENPP1 is well known as a generator of PP_i which potently inhibits mineralisation. Less well known is ENPP1's identified role as a pathogenic factor, predisposing to insulin resistance and subsequent T2DM (Bacci et al., 2007). Indeed, T2DM is an independent risk factor for further downstream metabolic diseases. Previous studies have revealed that *Enpp1*$^{-/-}$ mice have notable skeletal and metabolic phenotypes (Mackenzie et al., 2012, Huesa et al., 2014). These mice exhibit hypomineralisation of the long bones and abnormal pathological calcification of soft tissues including the vasculature. The insulin-sensitive metabolic phenotype, which is pronounced following high-fat diet challenge, results in protection against both obesity and insulin resistance (Huesa et al., 2014). ENPP1 is highly expressed in certain tissue and cell types including kidney, pancreas and muscle, as well as chondrocytes and osteoblasts. However, the organ and cell-specific contributions remain unknown.

In the present project, I hypothesised that the ablation of NPP1 in the osteoblasts of mice would recapitulate the metabolic protection observed in the *Enpp1*$^{-/-}$ mice, and would result in increased bone mineralisation as a product of reduced PP_i. To investigate this hypothesis the following aims were addressed in this thesis:

1. To determine the impact of osteoblast-specific NPP1 ablation on bone geometry and micro-architecture, matrix mineralisation and biomechanical properties in mice.

2. To investigate the profile of NPP1 during osteoblast matrix mineralisation *in vitro*. This involves the use of established cell lines and cells isolated from the novel osteoblast-specific NPP1 ablated mouse model.

3. To investigate the impact of osteoblast-specific NPP1 ablation on the metabolic phenotype of mice following control-diet feeding and chronic high-fat diet feeding.

To address the aims of this PhD both *in vitro* and *in vivo* models have been utilised. The work presented in chapter 4 demonstrates that osteoblast-specific NPP1 ablation engenders increased bone mass and bone mineral density in juvenile mice. Primary osteoblasts were isolated from the novel NPP1 conditional mouse model to investigate and confirm whether a hypermineralisation phenotype was reflected *in vitro*. These findings support the hypothesis that ablated *Enpp1* mouse models would have increased bone formation likely due to decreased PP_i levels.

Due to the concomitant role of ENPP1 in bone and insulin resistance, this project then investigated the impact of *Enpp1* ablation in osteoblasts on metabolic phenotype, including both under normal dietary conditions, and under obesogenic dietary conditions of a high-fat diet. Multiple parameters were investigated in detail including *in vitro* glucose regulation, detailed histological analysis of organs, and biochemical analysis (chapter 5 and 6). These data are essential to further understand the link between energy metabolism, bone formation and cell-specific contributions to these biological processes.

Chapter 2. Materials and methods.

2.1. Chemicals, media and buffers

Unless otherwise stated, all chemicals were purchased from Sigma-Aldrich (Dorset, UK) and tissue culture medium and buffers from Thermo Fisher (Loughborough, UK). Polymerase chain reaction (PCR) primers were purchased from Qiagen (West Sussex, UK) and Sigma (Dorset, UK). A table of primers used can be found in Appendix I. A list of buffers and solutions can be found in Appendix II.

2.2. Cell culture

2.2.1 Cell culture reagents

Cell and tissue culture reagents were prepared in a sterile category 2 hood. Cell media was supplemented with broad-spectrum antibiotic gentamicin (0.05 mg/ml), and 10% heat-inactivated foetal bovine serum (FBS) (Life Technologies), which was filter-sterilised using a 0.22 μm filter (Sigma-Aldrich, UK) before use. For minerlisation experiments, mineralisation media was used, further supplemented with 50 μg/ml ascorbic acid and 5 mM β-glycerophosphate (β-GP) disodium salt hydrate.

2.2.2 Cell types

For time-course mineralisation studies up to 21 days, the murine pre-osteoblastic cell line MC3T3-E1 sub-clone C14 (a fast mineralising variant) was selected (Wang et al., 1999a). Primary osteoblasts from *Enpp1*$^{flox/flox}$ and *Enpp1*$^{flox/flox}$;*Ocn*-cre mouse pups (2-5 days old) were isolated (Section 2.7.1) and used for time-course mineralisation studies up to 28 days.

2.2.3 Maintaining and passaging cells

Once cells reached sub-confluence (70-80%), the cells were passaged by trypsinisation. The culture medium was initially removed and the cell monolayer subsequently rinsed with wash buffer consisting of Hank's Buffered Salt Solution (HBSS; Life Technologies, Paisley, UK) containing 1% gentamicin. Cells were subsequently detached from plastic by incubation with TrypLE Express Enzyme (Life Technologies) for 5 minutes at 37°C, in a humidified incubator, in

the presence of 5% CO_2. The trypsinisation reaction was then neutralised with the addition of at least double the volume of appropriate cell culture medium containing 10% FBS. Cellular suspensions were then collected and centrifuged at 2000 *g* for 5 minutes such that a cellular pellet was obtained the supernatant was discarded and the cells were subsequently re-suspended in 1 ml of appropriate fresh culture medium (warmed to 37°C). The cells were subsequently counted using a Neubauer haemocytometer and resuspended in a known volume of required culture medium.

2.2.4 Freezing/thawing of MC3T3-E1 sub-clone c14 cells

To maintain stocks of the MC3T3-E1 sub-clone c14, cells were initially grown to 100% confluence in T175 flasks and subsequently counted (Section 2.2.3). Cells were then centrifuged at 2000 *g* for 5 minutes, and resuspended in a 1:1 culture media and freezing media containing dimethyl sulfoxide (DMSO) (Appendix 2), at a density of 4 x 10^6/ml. Cells were transferred to cryovials (Corning, U.K), and placed in a polystyrene box, and kept for 48-72 hours at -80°C. Subsequently, cryovials were moved to -150°C for long term storage. When cells were required, the cryovial was warmed in a 37°C water bath and immediately added drop by drop to 20mL of pre-warmed culture media. The cell suspension was then centrifuged at 2000 *g* for 5 minutes to remove the DMSO and any cellular debris. The cell pellet was resuspended in culture media and transferred to a T175 flask and left to propagate in a humidified atmosphere of 95% air/5% CO_2 at 37°C.

2.2.5 Dissection and extraction of primary osteoblasts from calvariae

All steps were conducted under sterile conditions. One calvariae per new-born mouse (2- to 5-days old) was dissected and collected into a universal containing 6mls of HBSS containing 1% gentamicin and washed. The HBSS was removed and calvariae digested as follows:

1. 2-3 mls collagenase type 2 (Worthington, Lakewood, NJ) was added to the universal containing calvariae at 1 mg/ml and shaken for 10 minutes in a heated and shaking incubator at 37°C.

2. The supernatant was discarded, 2-3 mls of fresh collagenase type 2 (Worthington) at 1 mg/ml was added, shaking at 37°C for 45 minutes. The supernatant (referred to as 'fraction 1') was removed and retained.

3. Calvariae were washed with 6 mls of phosphate-buffered saline (PBS), which was subsequently removed and added to fraction 1.

4. The calvariae were then treated with 2-3 mls of 4 mM ethylenediaminetetraacetic acid (EDTA) (Thermo-Fisher), shaking at 37°C for 10 minutes. The supernatant was removed and retained (referred to as 'fraction 2'). The calvariae were washed with 6 mls HBSS, which was subsequently removed and added to fraction 2.

5. Fresh 2-3 mls of collagenase was added to the calvariae, shaking at 37°C for 45 minutes. The supernatant from this final digest was collected (referred to as 'fraction 3').

From fractions 1-3, osteoblasts were isolated by centrifuging (2000 *g* for 5 minutes) and were resuspended in primary osteoblast medium before being pooled to obtain a single-cell suspension. The extracted osteoblast cells were seeded into a T75 flask in a humidified atmosphere of 95% air/5% CO_2 at 37°C. After 3 hours, media in the flask was replaced with fresh media and returned to the incubator. The flasks were left to reach 85-90% confluence and were then plated at 100,000 cells/well in 6-well plates for individual experiments. For a schematic representation of this process see Appendix III.

2.2.6 Plating of cells for experiments

The cells (either MC3T3-E1 sub-clone c14 or primary osteoblasts) were trypsinised and counted (Section 2.2.3), and then resuspended media. Of this cell suspension, 2 mls of media were added

to each well of a 6-well plate to ensure 10,000 cells/well. For 12-well experiments, cells were plated at 50,000 cells/well. Appropriate culture media was changed every 2-3 days until cells reached confluence (day 0). After this point, for mineralisation time point experiments, mineralisation media (containing 50 μg/ml ascorbic acid, and 5 mM β-GP) replaced the culture media and was changed every 2-3 days.

2.3. RNA methods

2.3.1 Isolation of RNA from cells

Before RNA extraction, cultured cells were washed with PBS and scraped from individual wells in RLT buffer containing 1% β-mercaptoethanol (Qiagen, Crawley, UK) and stored at 4°C. The RNeasy Kit (Qiagen, Crawley, UK) was used to isolate mRNA from cell lines as follows. An equal volume of 70% alcohol was added and mixed by pipetting up and down. The cell lysate solution was transferred into a Qiagen RNeasy spin column provided by the kit. The column was centrifuged at 8000 *g* and the flow-through was discarded. Next, the column was washed with RW1 buffer and then twice with RPE buffer. The RNA was eluted with 40 μl nuclease-free distilled water (dH_2O). The extracted mRNA sample concentrations were determined using a NanoDrop Spectrophotometer (Labtech, Tampa, USA), and all samples were diluted using nuclease-free water (NFW) to achieve a concentration equal to that of the least concentrated samples or 5μg/ml.

2.3.2 Reverse transcription

Complementary DNA (cDNA) was prepared from 20 μl of the diluted RNA using reverse transcription. Briefly, 4 μl of random primers (diluted 1:60, Life Technologies) was added to the 20 μl of diluted mRNA. Samples were then heated for 10 minutes at 70°C in a Hybaid polymerase chain reaction (PCR) Express Thermal Cycler (Thermo Scientific, Northumberland, UK). Samples were then incubated at 4°C to block non-specific sites. The Superscript II kit was used to obtain cDNA following manufacturer's guidelines: 15 μl of Mastermix (5 μL 5x First-Strand buffer (Life Technologies), 2 μl Dithiothreitol (DTT; 0.1M, Life Technologies, 2 μl dNTP (10mM; Life

Technologies) and 1 µl Superscript II Reverse Transcriptase (Invitrogen; Renfrewshire, UK) was added to each mRNA. Samples were then run on the following programme in the Hybaid PCR machine: 25°C for 10 minutes, 42°C for 50 minutes, 70°C for 15 minutes. The cDNA was then diluted with NFW to 5 ng/µl and stored at -20°C until use.

2.3.3 Real-time quantitative PCR (qPCR) and quantification of gene expression

For each qPCR sample, a master-mix was made consisting of: 10 µl SYBR Green PrecisionPLUS qPCR Master Mix (PrimerDesign, UK), 1 µl of the forward/reverse primer (10 µM) for the target gene and 4 µl dH_2O. Total reaction volume was 20 µl, comprising 15 µl of master-mix and 5 µl of cDNA sample. Technical duplicates of samples were used for all reactions. For the negative control, a reaction consisting of 5 µl of dH_20 and 15 µl of mastermix was used. Real-time qPCR reactions were conducted in a 96-well plate (Thermo Scientific) and cycled using a Stratagene mx300P PCR cycler (Agilent Technologies, Santa Clara, USA) with the following programme; 1 cycle of 95°C for 10 minutes, 50 cycles of 95°C for 15 seconds and 60°C for 1 minute. Results were compared to the β-Actin (ACT-B) and Glyceraldehyde 3-phosphate dehydrogenase (GAPDH) housekeeping-gene(s). To test the efficiency of primers, serial dilutions of cDNA (which express the target gene) were used to create a standard curve. Primers used had an amplification efficiency between 85-110%, and an R^2 value between 0.90 and 1.00. The primer specificity was demonstrated by the generation of a clean, single peak in the dissociation curve. The reactions were analysed using standard curves and amplification plots, which shows the fluorescence signals versus cycle numbers. The baseline for the plot is defined by Rox (reference dye). For analysis, the fold change in the expression of the gene of interest's relative to the housekeeping gene(s) was calculated using the ΔΔCt method, where an arbitrary amplification threshold (CT) is set and the relative expression levels of samples are calculated by comparison to the number of amplification samples required to cross this CT (Livak and Schmittgen, 2001).

2.3.4. Genotyping

As needed, agarose gel was made by diluting 1.5 g of agarose in 100 ml of Tris-acetateethylenediaminetetraacetic acid (TAE) buffer (Ambion, Cambridge, UK) containing 0.1

µl/ml SYBR-Safe (Thermo Fisher). The samples were loaded at a volume of 20 µL per well. As a negative control, an equal volume of dH_2O was used to replace cDNA. The gel was run in TAE buffer, in an electrophoresis tank at 100 V for 50 minutes. HyperLadder 1 kb Bioline) was used as molecular weight markers. The resulting gel was visualised under UV light using the Gel Logic 200 Imaging System and software (Kodak, Herts, UK).

2.4. Protein methods

2.4.1 Protein extraction from cells for western blot analysis

From each well, the culture media was discarded and the cellular monolayers were washed with PBS to remove excess media. An appropriate volume of RIPA buffer (Sigma-Aldrich) was added to scrape the cellular monolayer. All samples were centrifuged and the supernatant removed and stored at -20°C before quantification.

2.4.2 Quantification of protein concentration: Bio-Rad DC assay

The media from the cellular monolayer was discarded and cell monolayers were washed with PBS to remove excess media. An appropriate volume of 0.1 M NaOH 0.1% sodium dodecyl sulphate (SDS) lysis buffer was added to the cellular monolayer to denature cellular proteins and incubated at room temperature on a shaker for 1 hour. The cells were scraped and collected into Eppendorf tubes. Tubes were subsequently vortexed and centrifuged at 10,000 rpm for 10 seconds. To quantify protein concentrations, Bio-Rad DC Protein Assay (Bio-Rad Hertfordshire, UK) was used according to manufacturer's instructions, with a protein standard used to obtain a standard curve. The protein standard of bovine γ-globulin protein (0.125 – 2 mg/mL; Bio-Rad) was prepared in a solution of 0.1 M NaOH 0.1% SDS. For both protein standard and protein, 5 µl of sample was assessed in duplicate on a 96-well plate, with 25 µl alkaline copper tartrate (Reagent A) and 200 µl Folin's reagent (Reagent B) subsequently added. The 96-well plate was incubated at room temperature for 15-60 minutes before the absorbance measurement (at a wavelength of 690 nm) using the Synergy HT Multi-Mode Microplate reader (BioTek, Bedfordshire, UK). Protein concentration was determined from the standard curve.

2.4.3. Western blot analysis

Bone marrow was removed from cut humeri by centrifugation. The bones were next homogenised in cold RIPA buffer (Invitrogen) containing 'phosphatase inhibitor cocktail 2' (Sigma) and 'complete' protease inhibitor cocktail (Roche) according to the manufacturer's instruction. Western blotting was conducted with specific antibodies against ENPP1 (LI-COR Biosciences, 1:15000 dilution in Blocking buffer (Odyssey)) and β-actin (LI-COR Biosciences, 1:15000 dilution in Blocking buffer (Odyssey)). Following the determination of protein concentration (Section 2.4.2.), samples were diluted to the same concentration (between 10-30 μg) and the appropriate volume of 4x lithium dodecyl sulphate (LDS) sample buffer and reducing agent DTT was added to each sample. Diluted protein samples were denatured at 70°C for 10 minutes. The denatured protein samples and a pre-stained molecular weight marker to accurately determine protein size (All blue, Bio-RAD) were chilled on ice before being loaded onto a pre-cast 10% Bis-Tris gel (Invitrogen, Paisley, UK). Gels were run in a Novex Gel Tank (Invitrogen) containing 1x Tris Acetate or 1x MOPS running buffer, respectively. Anti-oxidant was added to the centre compartment of the tank to preserve reduced proteins (2.5 μl/ml; Invitrogen). Proteins were separated by electrophoresis for 5 minutes at 170 V followed by 55 minutes at 150 V. The gel was subsequently transferred to a methanol activated polyvinylidene difluoride (PVDF) membrane via a semi-dry transfer (Bio-Rad) for 90 minutes at 18 V. Following transfer, the membrane was washed several times in Tris-Buffered Saline and Tween 20 (TBST). The membrane was blocked in Odyssey blocking buffer (Licor). Primary antibody was applied overnight at 4°C with agitation. Membranes were next washed in TBST and incubated in a secondary antibody diluted in Oddysey blocking buffer with agitation at room temperature for 1 hour. Membranes were protected from light due to the light-sensitivity of Licor antibodies. Bound antibody was detected and imaged using the Licor Odyssey® scanner.

2.5. Cell-based assays and staining

2.5.1 *O*-cresolphthalein complexone calcium assay

Media from the cellular monolayer was discarded and the cell monolayers were washed with PBS. Next, 500 µl of 0.6 M HCl was added to the monolayer and incubated at 4°C to disrupt the cellular membrane. A Calcium Assay Kit (Randox, County Antrim, UK) was used to quantify the calcium deposition in the cells, with samples and standard run in duplicate. The working principle of this assay is based upon the binding between *o*-cresolphthalein complexone and calcium ions in an alkaline media. A negative control using the leaching solution, 0.6 M of HCl, was included, as well as a calcium standard (10.2 ng/ml) needed for calcium concentration calculation, provided by the kit. Next, 6.25 µl of standard/negative control/sample was added to a 96-well plate, in duplicate. Subsequently, 250 µl of 1:1 ratio of 2-amino-2-methyl-propan-l-ol (R1) and *o*-Cresolphthalein complexone, 8-Hydoxyquinoline, HCl (R2) were added to each well. The optical density (OD) was then read on a Synergy HT Multi-Mode Microplate reader at 570 nm. The calcium concentration of each sample was determined using the following equation:

$$\text{Concentration} = \left(\frac{\text{mmol}}{\text{L}}\right) = \left(\frac{\text{Sample OD}}{\text{Standard OD}}\right) * \text{standard concentration } \left(\frac{\text{mmol}}{\text{L}}\right)$$

Calcium concentration was then normalised to total protein concentration.

2.5.2 Alizarin red S staining and quantification

The media from each culture well was discarded and the cellular monolayer was washed with PBS. Cells were then fixed with 4% PFA for 15 minutes at room temperature. The PFA was discarded, and cellular monolayers were washed three times with PBS. Subsequently, 2% (w/v) Alizarin Red S Stain (pH 4.2) was added and incubated at room temperature for 10 minutes. Cellular monolayers were washed with water until any unbound Alizarin red S stain had been removed. The cellular monolayer was allowed to dry and was photographed. After photographing, cells were stored dry at -20°C. When required, bound Alizarin red S stain was solubilised using 10% cetylpyridinium chloride. Samples were collected and run in duplicate, using cetylpyridinium chloride as a blank, in a 96-well plate to measure the optical density at 570

nm. Optical density was determined using the Synergy HT Multi-Mode Microplate reader (BioTek, Bedfordshire, UK).

2.6. *In vivo* studies

2.6.1 Animal welfare and generation

Animal experiments were approved by the Roslin Institute's Animal Users Committee. All animals were maintained in accordance with the Home Office Guidelines for the care and use of laboratory animals. To further study NPP1 function, the osteoblast-specific *Enpp1* ablated mouse model (*Enpp1*$^{flox/flox}$;*Ocn*-cre) was generated. Here, a commercially available *Enpp1*$^{flox/flox}$ mouse (Cyagen Biosciences, California, USA) with floxing site on exon 9 was crossed with an Osteocalcin-Cre mouse (*Ocn*-cre) (Yoshikawa et al., 2011, Staines et al., 2017). The resultant mice express Cre recombinase specifically in osteoblast cells: therefore, floxed *Enpp1* in this cell type will not be expressed (Fig 2.1). Male and female mice were culled at 6-weeks (juvenile), 16-weeks, and 22-weeks (adult) of age; gender and number of mice studied are specified in each experiment. Genotyping as required was performed on genomic DNA isolated from ear clips and analysed using PCR protocols (Section 2.3.4). Confirmation of knockout status as required was performed by western blot analysis for NPP1 from protein isolates of tissues (Fig. 2.2) (Section 2.4.3). For a schematic of animals used for metabolic or bone phenotyping, associated ages and sex of mice see Appendix III.

2.6.2 Maintenance of *Enpp1*$^{flox/flox}$;*Ocn*-cre and *Enpp1*$^{flox/flox}$ mice

The generation and characterisation of *Enpp1*$^{flox/flox}$;*Ocn*-cre is described above. Genotyping of pups (aged 2-5 days) was performed using genomic DNA isolated from tail snips, whereas genomic DNA isolated from ear clips was used for all other mice. Offspring carrying the *Ocn*-cre gene were identified using Genomic DNA, which was analysed using PCR protocols (developed by Professor Thomas Clemens, USA) (Section 2.3.4). For primary osteoblast cell culture experiments, mice were culled between 2-days and 5-days of age. Mice involved in metabolic phenotyping experiments were fed either a control diet (6.2% fat; Harlan Laboratories, Indianapolis, IN, USA) or a high-fat diet (HFD) (58% from fat; Research Diets, Inc, New Brunswick,

NJ, USA) from 4-weeks of age until culling. *Ad libitum* food consumption and weight gain was monitored weekly until cull.

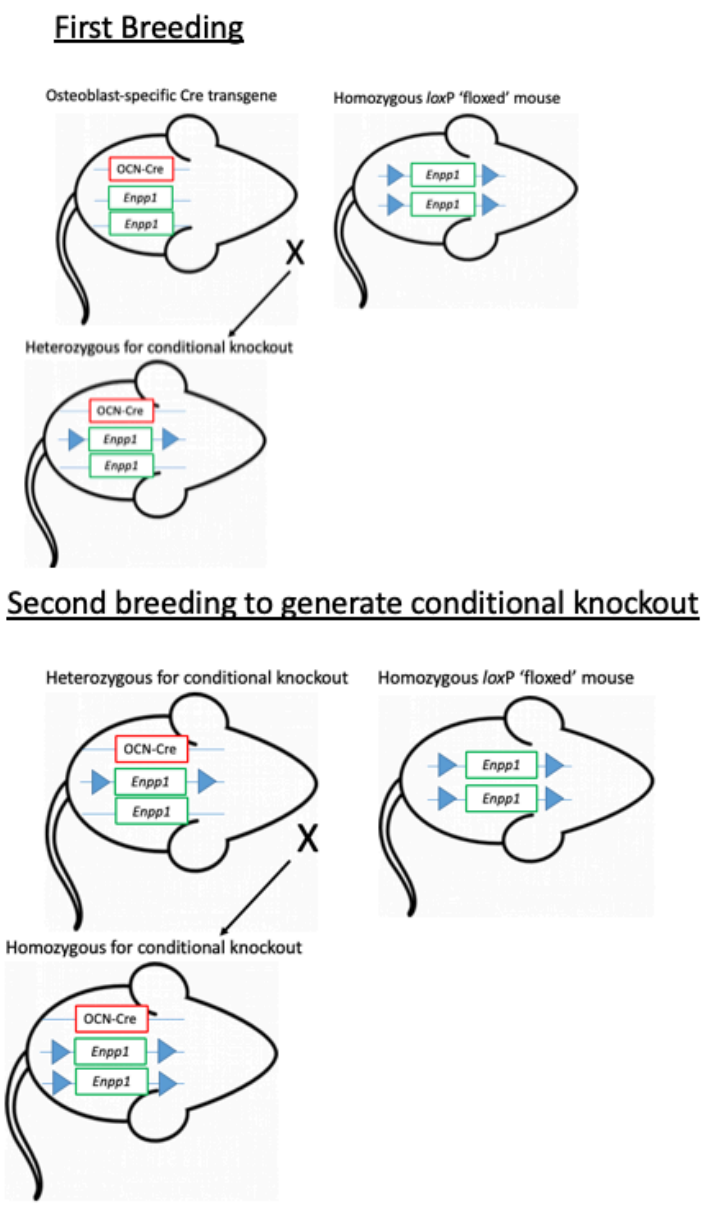

Figure 2.1. Breeding Scheme for osteoblast-specific ablated Mice.

The first breeding scheme generates mice which are heterozygous for the *LoxP*-flanked allele of *Enpp1.* These mice were selected and mated with a homozygous LoxP 'floxed' mouse in a second breeding. This generates approximately 25% of progeny which are homozygous for the *LoxP*-flanked allele and heterozygous for the *cre* transgene. These are the experimental mice. Homozygous *Enpp1*$^{flox/flox}$ mice were used as controls.

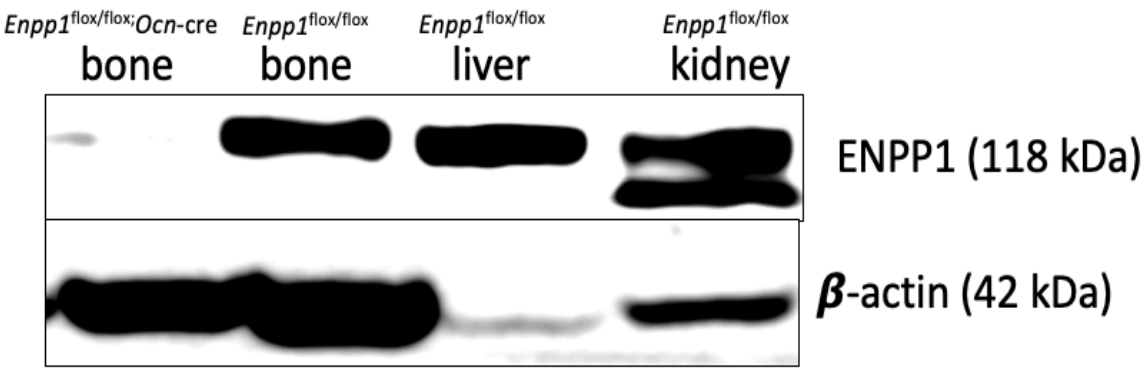

Figure 2.2. Representative western blot analysis

Assessment of NPP1 protein in bone and selected soft tissues of mice. The order on the blot is as follows: bone (humerus) of *Enpp1*$^{flox/flox}$;*Ocn*-cre moose, bone (humerus) of *Enpp1*$^{flox/flox}$ mouse, kidney of *Enpp1*$^{flox/flox}$;*Ocn*-cre and liver of *Enpp1*$^{flox/flox}$;*Ocn*-cre mouse.

2.6.3. Metabolic analysis of animals

A total of 300 g of food was provided per cage and food remaining after 7 days was recorded and average weekly food consumption per mouse calculated from 4 to 16-weeks of age. Blood was extracted from these mice via cardiac puncture and collected via a 4% EDTA laced syringe and into 4% EDTA coated tubes (Sarstedt, Numbrecht, Germany). Tubes were then centrifuged at 1000 *g* resulting in separation of plasma. This plasma was carefully collected and stored at -80°C until use.

2.6.4 Glucose and insulin tolerance testing

For glucose tolerance testing (GTT), adult *Enpp1*$^{flox/flox}$ and *Enpp1*$^{flox/flox}$;*Ocn*-cre male mice (14-weeks of age) were fasted for 4 hours and administered 2 mg of D-Glucose per g of body weight by oral gavage. For insulin tolerance testing (ITT), 16-week old mice were fasted for 4 hours and administered 0.75 mU of insulin (Actrapid, NovoNordisk, Bagsvaerd, Denmark) per g of body weight intraperitoneally (i.p). At time points of 0, 15, 30, 60 and 120 minutes post-administration, blood glucose was measured with an Accu-Check® Aviva glucose meter (Roche Diagnostics LTD, Lewes, UK) and glucose-stimulated insulin secretion (GSIS) was measured by ELISA (ChrystalChem, Chicago, IL, USA). Mice were allowed to recover before subsequent sacrifice occurring at 16-weeks of age. Tissues including pancreas, liver, *quadriceps femoris* muscle, and brown, subcutaneous, mesenteric and gonadal fat pads were collected for histological assessment, gene and protein expression analysis.

2.6.5. Catwalk analysis

Gait analysis was recorded using a CatWalk XT gait analysis system (Noldus Information Technology, the Netherlands) and previously described (Hamers, Lankhorst, Van Laar, Veldhuis, Gispen 2001; Maschocha & Parvathy, 2009). Briefly, each mouse was placed on the catwalk and moved at their own free will down a glass walkway corridor that detects their gait and locomotion (Fig. 2.3). Mice were habituated to the equipment for 2-weeks before analysis. Data were collected following three compliant runs from each mouse at an age of 14-weeks.

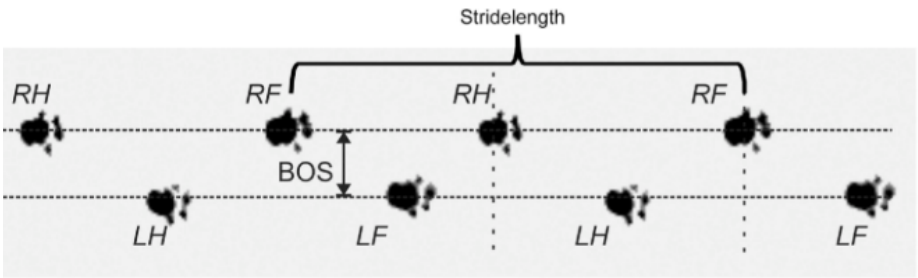

Figure 2.3. Schematic of catwalk gait analysis.

Representative walking pattern of mouse on Catwalk gait analyser. Examples of measured parameters include the base of support (BOS) and stride length (the distance between one right front (RF) and another RF footprint). Other footprints include Right hind (RH), left front (LF) and left hind (LH). Other parameters include coupling of different paws, paw print width, duration of paw print present on glass. Adapted from (Herold et al., 2016).

2.7. *Ex vivo* bone analysis and gross analysis

2.7.1 Bone length and 3-point bending

The length of tibiae and femora from male and female *Enpp1*$^{flox/flox}$ and *Enpp1*$^{flox/flox}$;*Ocn*-cre mice at ages 6-weeks, 16-weeks and 22-weeks of age were measured using DigiMax digital Vernier callipers (R. S. Components Ltd, Corby, Northants, UK). Three-point bending was also conducted on tibiae and femora using an LXR materials testing machine (Lloyds Instruments, West Sussex, U.K.) fitted with a 500 N load cell. The lowering of the crosshead was set at a speed of 1 mm/min. To ensure the same sight of the anvil head, tibiae and femurs were placed on the anvil in a pre-determined, consistent orientation. Data began recording after every 0.2 N change in load and after 0.1 mm change in deflection (Fig. 2.4). Both tibiae and femora were tested until the point of fracture. From the generated load extension curve, failure (being the point of maximum load), fracture (whereby the load rapidly decreases to 0), maximum stiffness (defined as the maximum gradient of the rising portion of the curve) and yield (70% of the maximum stiffness) were defined.

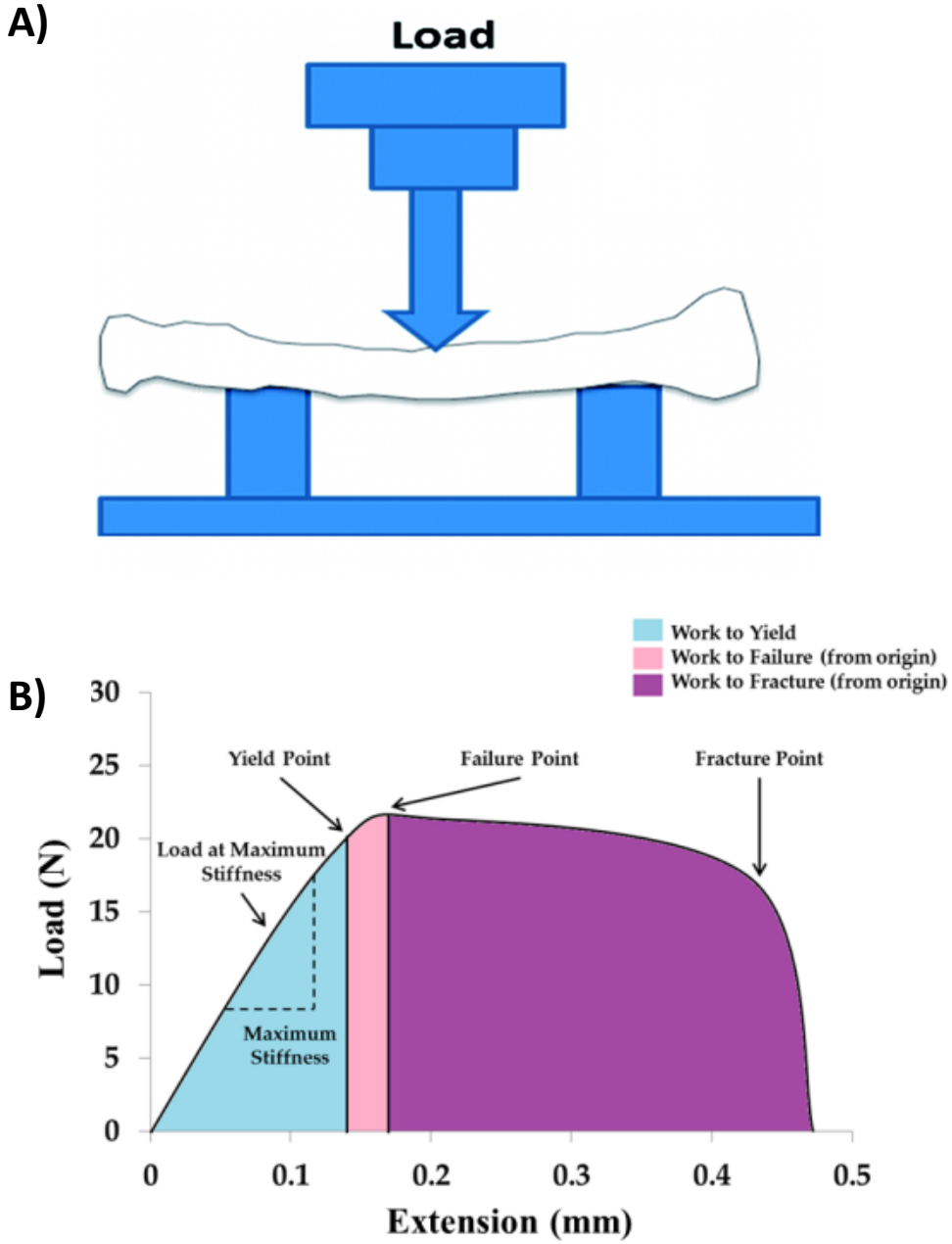

Figure 2.4. Three-point bending and load extension curve.

(A) Figure demonstrates the typical placement of a bone on the apparatus platform with load head aimed at central diaphysis. (B) A typical load extension curve that is obtained during 3-point bending analysis.

2.7.2. Micro-computed tomography imaging

Tibiae and femora were dissected from 6-week and 22-week old male and female *Enpp1*$^{flox/flox}$ *and Enpp1*$^{flox/flox}$;*Ocn*-cre, fixed in 10% NBF for 24 hours and subsequently stored in 70% ethanol. The long bones were scanned using a micro-computed tomography (µ-CT) system (Skycan 1172, Bruker, Aartselaar, Belgium) to assess trabecular architecture and cortical geometry. High-resolution scans with an isotropic voxel size of 4-5 µM were acquired (50 kV, 200 µA Al filter, 0.4° rotation step). Scan time was approximately 1 hour per bone. The scans were reconstructed using NRecon software (Skyscan, Bruker, Belgium). For each bone, the growth plate was used as a standard reference point, and a region of 1 mm in height was analysed. A 0.4 mm and 2.50 mm offset from the growth plate was used for trabecular and cortical bone respectively. All bones were corrected in DataViewer to ensure the same orientation.

Bone tissue was identified by thresh-holding, whereby the optimum threshold was determined using the image histogram, and set to exclude soft tissue whilst still including poorly mineralised bone. The thresh-hold used remained consistent throughout the analysis of all samples at values of 80 and 225. For calculation of bone mineral density, an appropriate calibration of the Skyscan CT analyser was conducted using phantoms known calcium hydroxyapatite densities of 0.25 and 0.75 g/cm^{-3}.

The following parameters were analysed using CTan software (Skyscan, Belgium); in trabecular bone.bone volume (BV/TV), trabecular number (TB.N;/mm) bone mineral density (BMD; g/cm^3), trabecular thickness (Tb.Th; mm), trabecular separation (Tb.Sp) and structural model index (SMI) were evaluated. For cortical bone, % BV/TV, BMD (g/cm^3), cortical thickness, cross-sectional area (mm^2) and percentage porosity (Po.op %) were measured.

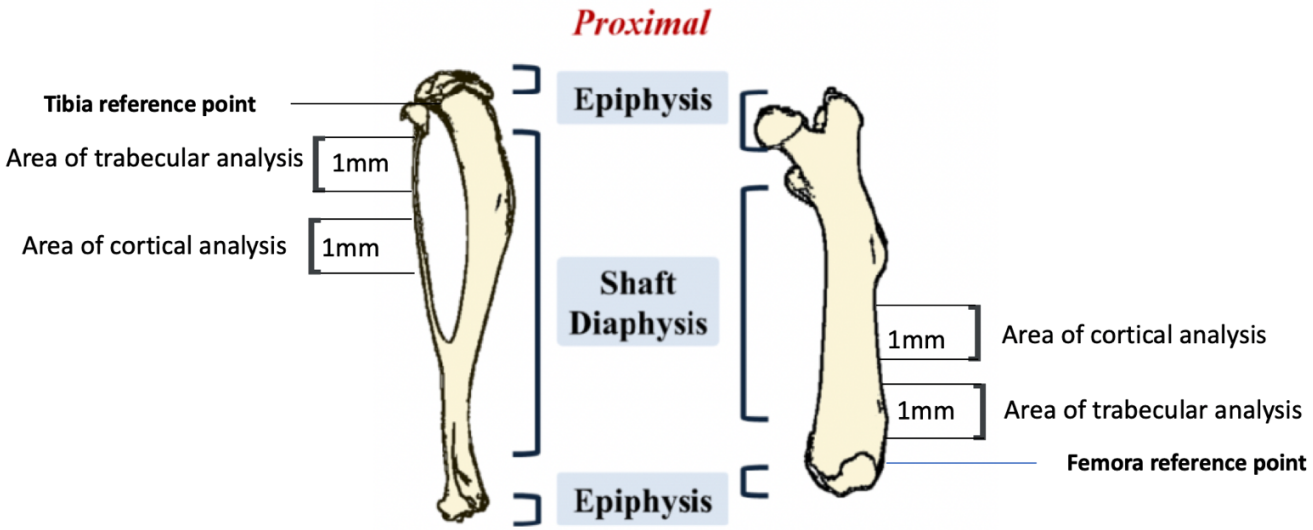

Figure 2.5. Representative Schematic of areas assessed by μ-CT. Reference point refers to the proximal growth plate tibia, and the distal growth plate of the femur. The area of trabecular analysis is 0.4 mm from the reference point. The area of cortical analysis is 2.5mm from the reference point.

2.7.3 Gross analysis

Following the euthanasia of male *Ocn*-cre*;Enpp1*$^{flox/flox}$ and *Enpp1*$^{flox/flox}$ mice for metabolic phenotyping at 16-weeks of age, the following were weighed using an analytical balance (Fisher Scientific); total body weight, brown fat, hind-body subcutaneous fat, gonadal fat, mesenteric fat, spleen, pancreas, kidney, liver, right and left quadriceps.

2.7.4 Histopathological assessment

Following euthanasia at 16-weeks of age, the following soft tissues were fixed in 10% neutral buffered formalin (NBF), embedded in paraffin wax using standard procedures. Kindly performed by Prof Elspeth Milne, the 5 µM thick sections were stained with Hematoxylin and Eosin (H&E) and Von Kossa to assess calcification status of heart, brain, kidney, liver, pancreas, *quadriceps femoris* muscle and whisker follicle.

2.7.5. Osmium staining of marrow adipose tissue

Following euthanasia of male *Enpp1*$^{flox/flox}$*;Ocn-cre* and *Enpp1*$^{flox/flox}$ mice from both control-diet fed and high-fat diet fed (Section 2.7.2) cohorts at 16-weeks of age, femora and tibiae were dissected and soft tissue was cleaned from the bone. Bones were fixed in an appropriate volume of 10% NBF for 24 hours at room temperature. Tibiae and femora were separated from each other, ensuring the tibia remained 100% intact. Bones were subsequently decalcified in 14% EDTA (pH 7.4) for a minimum of 14 days at 4°C (EDTA was changed every 3-4 days). Upon complete decalcification, bones were washed in Sorensen's buffer (3 changes, each wash for 1 hour). Bones were then stained with 1% osmium tetroxide solution (2% w/v, Agar Scientific, UK diluted 1:1 in Sorensen's Phosphate buffer) for 48 hours at room temperature, washed in Sorensen's buffer (3 changes, each wash for 1 hour) and stored in Sorensen's phosphate buffer (pH 7.4) at 4°C until use (maximum of 7 days). For µ-CT analysis of the osmium stained marrow adipose tissue, layers of 4 to 5 stained tibia were arranged in parallel in 1 % agarose in a 30 mL universal tube and mounted in a Skyscan 1172 desktop µ-CT (Bruker, Kontich, Belgium). The

samples were scanned through 360° using a step of 0.4° between exposures. A voxel resolution of 12 μm was obtained in the scans and the following control settings were used: 54 kV source voltage, 185 μA source current and an exposure time of 885 ms. A 0.5-mm aluminium filter and a two-frame averaging were used to optimise the scan. Following scanning, data were reconstructed using Skyscan software NRecon v1.6.9.4 (Bruker, Kontich, Belgium). The reconstruction thresh-holding window was optimised to encapsulate the target image. Volumetric analysis of marrow adipose tissue stained with osmium was conducted using CT Analyser v1.13.5.1 (Bruker Kontich, Belgium). This work was kindly performed by Dr Karla Suchacki and Dr Will Cawthorn of the University of Edinburgh.

2.8. Histological analysis

2.8.1. Preparation of tissue for microscopical analysis

All soft tissues were fixed in 10% NBF, embedded in wax and sections were cut to appropriate thickness for microscopical analysis using a Thermo microtome. For fat pads (brown, mesenteric, gonadal and subcutaneous) 4 μM thick sections were stained with H&E to assess adipocyte number and size distribution. For pancreas, 5 μM thick sections were stained with H&E to assess insulin-secreting β-cell number and size. For liver, 5 μM sections were H&E stained to assess tissue architecture, and 8 μM sections were stained with picrosirius red (with fast-green counterstain) to identify collagen deposition and assess fibrosis. Similarly, long bones were fixed in 10% NBF and decalcified in 10% EDTA for 14 days at 4°C and embedded in wax and 4 μM thick sections were cut using conventional means.

2.8.2. Paraffin-embedded tissues

For wax sections, tissues were fixed in either 4% PFA or 10% NBF for a minimum of 48 hours and subsequently transferred to 70% ethanol. For calcified tissues, a decalcification was performed before fixing. Here, tissues were decalcified in 10% EDTA (pH 7.4) for approximately 21 days, with gentle agitation at 4°C. Throughout the 21 days, EDTA was regularly changed. The NBF and PFA

fixed tissues were placed in cassettes and underwent the following automated protocol involving two changes of the following:

- 70% ethanol (1 hour)
- 80% ethanol (1 hour)
- 95% ethanol (1 hour)
- 100% ethanol (1 hour)
- Xylene (VWR, Leicester, UK) for 1 hour
- Overnight in paraffin wax (VWR) and 60 °C

Subsequently, cassettes were placed in fresh paraffin wax for 1 hour. The processed tissues were then embedded in paraffin wax using plastic moulds. After setting at 4°C, paraffin blocks were trimmed to size and stored at room temperature until required. For thirty minutes before sectioning, paraffin blocks were cooled on an ice block. A microtome with blades (MX35 Premier+ Microtome Blades, Thermo Scientific, Cheshire, UK) was used to section at 5 µM thickness. Sections were placed to float on water at 40°C for 1 minute before transferring to Superfrost microscope slides. Slides were placed to dry at 37°C overnight to ensure that sections adhered to the slide. Slides subsequently stored at room temperature until required.

2.8.3. Haemotoxylin and eosin staining

Paraffin-embedded tissue sections were stained with haemotoxylin and eosin (H&E). Slides were initially de-waxed in xylene and rehydrated through a series of alcohols to dH_2O and stained with H&E using a Leica Autostainer and mounted in DePeX (VWR, Lutterworth, UK). This involved submerging sections in alum haemotoxylin for 5 minutes and rinsing with running tap water for 5 minutes. Slides were then differentiated by dipping in 0.5% acid alcohol and rinsed again with running tap water for 5 minutes. Next, slides were blued with 0.2% ammonia for 30 seconds, before washing with running tap water for 5 minutes and rinsed by dipping in 95% ethanol. Lastly, the slides were counterstained with eosin for 2 minutes, dehydrated with 2x 5-minute incubations in 95% ethanol and cleared with 2x 5-minute incubations in xylene. Slides were then mounted with DePex and visualised using a Nikon CoolScan V (Nikon, Surrey, UK).

2.8.4 Von kossa staining

Von kossa staining was performed to allow an assessment of calcification in soft tissue. For tissue staining, the sections were rinsed with dH_20 and slides were placed in a Coplin jar and 5% silver nitrate. The slides were subsequently exposed to strong light for 30 minutes and rinsed with dH_20. Un-reacted silver was removed by incubation with 5% sodium thiosulfate for 4 minutes. Slides were then dehydrated with 3x changes of absolute ethanol and cleared with 3x changes of xylene. The slides were then mounted with DePex. Scott Dillon provided the protocols of this work. Staining was performed by Dr Elspeth Milne.

2.8.5. Toluidine blue/fast green staining

For toluidine blue/fast green staining of sectioned bone, sections were deparaffinised, blotted dry and rinsed with dH_2O. A sodium acetate buffer was made (13.6 g of sodium acetate diluted in 1 L of dH_2O) and titrated to pH 4 using glacial acetic acid This solution was stored at 4°C. A 0.4% toluidine blue solution was made (0.4 g of toluidine blue O in 100 mls of sodium acetate buffer), wrapped in foil and stored at 4°C and equilibrated to room temperature before staining. A 0.002% fast green solution was made (0.05 g of Fast Green dissolved in 250 mls dH_2O). The deparaffinised sections were incubated in the toluidine blue solution for 10 minutes, rinsed in three changes of dH_2O. Slides were then counterstained in 0.002% fast green for three minutes and rinsed in three changes of dH_2O. Slides were blotted dry, quick mounted using DePex and visualised using a Nikon CoolScan V (Nikon, Surrey, UK). Scott Dillon provided the protocols of this work.

2.8.6. Goldner's trichrome staining

All solutions were made according to Table 2.1. For staining of sectioned bone to assess osteoid and cartilage, sections were deparaffinised and stained in Wiegert's haematoxylin solution for 10 minutes. Sections were next differentiated in 1% acid alcohol for 15 seconds and washed well under agitation for 10 minutes in dH_2O. Slides were stained next in Red solution for 5 minutes rinsed in 1% acetic acid, stained in Orange solution for 10 minutes, rinsed in 1% acetic acid,

stained in Green solution for 5 minutes and rinsed in dH_2O. Slides were blotted dry, quick mounted and visualised using a Nikon CoolScan V (Nikon, Surrey, UK). Scott Dillon provided the protocols of this work.

Solution	*Method*
Wiegert's hematoxylin (Sigma-Aldrich)	*Mix equal parts of solutions A and B immediately before staining. Mix well*
Ponceau de Xylidine-acid fuschin stock	*Add 2 ml glacial acetic acid to 98 mls dH_2O* *Dissolve 1.5 g of Ponceau de Xylidine and 0.5 g of acid fuschin*
Azophloxine stock	*Add 0.6 mls of glacial acetic acid to 99.4 ml of dH_2O.* *Dissolve 0.5 g of axophlozine.*
Red solution	*Make up 80 mls of 0.2% acetic acid in dH_2O* *Add 12 mls of Ponceau de Xylidine acid-fuschin stock solution and 8 mls of azophloxine stock solution.*
Orange solution	*Dissolve 3 g phosphomolybdic acid and 2 g Orange G in 500 mls dH_2O*
Green solution	*Add 1 ml of glacial acetic acid to 499 mls of dH_2O* *Dissolve 1g of light green*

Table 2.1. Goldner's trichrome staining solutions

2.8.7. Measurement of pancreatic islet number and size

Sections at 4 µM were cut through each pancreas, stained with H&E and scanned using a Nikon CoolScan V (Nikon, Surrey, UK). The total area of stained pancreas section was measured, along with the number and size of the islets in that section using ImageJ Software (Wayne Rasband, National Institutes of Health, USA).

2.8.8. Measurement of adipocytes in fat pads

Sections at 4 µM were cut through each fat pad (including mesenteric, subcutaneous, brown and gonadal), stained with H&E and scanned using a Nikon CoolScan V (Nikon, Surrey, UK). The total area of fat was measured, along with the number and size of adipocytes in that section using ImageJ Software (Wayne Rasband, National Institutes of Health, USA).

2.8.9. Liver staining

Liver sections were taken at 5 µM and stained with H&E (Section 2.9.3). Liver sections were also taken at 8 µM and used for picosirius staining with Weigert's haemotoxylin and fast-green counterstaining. For tissue staining, sections were deparaffinised and the nuclei were stained with Weigert's haematoxylin for 8 minutes, followed by a 10-minute wash in running tap water. Slides were stained in picosirius red for 1 hour and washed in two changes of acidified water (5 mls of glacial acetic acid in 1 L of dH_2O). Slides were blotted dry, dehydrates in three changes of 100% ethanol, cleared in xylene and quick-mounted in DePex before being visualised using a Nikon CoolScan V (Nikon, Surrey, UK).

2.8.10. Immunohistochemistry

Pancreas sections were taken at 5 µM (Section 2.9.3). For immunohistochemistry, sections were deparaffinised and immersed in a 1% H_2O_2 solution (1% H_2O_2 in methanol) for 10 minutes. Slides were subsequently rinsed in running tap water and a sodium citrate epitope retrieval protocol was performed. Slides were placed in a sodium citrate buffer (10 mM Sodium citrate (Tri-sodium dehydrate) and 0.05% Tween 20 in 1 L of distilled water; pH to 6.0 using 1 M HCl) and autoclaved at 121°C for 15 minutes. The slides were slowly cooled using running water for 15 minutes and subsequently rinsed in cool running tap water. A Pap pen was used to draw a small section around the tissue, and slides were washed in a Wash buffer (PBS/0.1% BSA). Slides were next incubated for 20 minutes with diluted normal blocking serum (5% Normal Goat Serum in PBS). The serum was removed, excess serum tapped was gently removed from sections and the slides were incubated in a humidified chamber with an insulin primary antibody (Rabbit polyclonal

insulin antibody, Cell Signalling Technology) diluted in 5% normal goat serum at a 1:100 antibody dilution. Slides were left to incubate with primary antibody overnight in a humidified chamber at room temperature. Following incubation, slides were washed for five minutes in wash buffer (PBS/0.1% BSA) three times. Slides were incubated for 30 minutes in a humidified chamber with diluted biotinylated secondary antibody solution: A goat anti-rabbit:biotinylated antibody diluted 1:400 in 5% Normal Goat Serum. Slides were next washed in wash buffer for 5 minutes three times. Slides were incubated for 30 minutes using the ABC Elite PK6100 kit (VECTOR laboratories, Maraval LifeSciences), and next washed in wash buffer for 5 minutes three times. The slides were next stained using a DAB staining kit as according to manufacturer's protocols (Abcam) for a maximum of 8 minutes and subsequently rinsed in tap water. Slides were finally counterstained with H&E (Section 2.9.3) and coverslips applied.

2.9. Blood and further tissue analysis

2.9.1. Serum analysis by ELISA

Following euthanasia of animals, blood samples from 6-week and 22-week old male and female *Enpp1*$^{flox/flox}$;*Ocn*-cre and *Enpp1*$^{flox/flox}$ mice and 16-week old male *Enpp1*$^{flox/flox}$;*Ocn*-cre *Enpp1*$^{flox/flox}$ mice were obtained by cardiac puncture using heparin-coated needles and collected Eppendorf tubes. Samples were centrifuged at 1000 *g* for 20 minutes and serum samples were gently aspirated and placed in a clean Eppendorf tube. To analyse the difference in bone remodelling rates, bone formation and bone resorption markers were measured in serum samples were analysed. This was conducted using a Procollagen 1 N-Terminal Peptide ELISA Kit (Mouse) (AMSBIO, Abingdon, UK) and a C-terminal telopeptide of Type I Collagen ELISA Kit (Mouse) (AMSBIO, Abingdon, UK).

2.9.2. Serum osteocalcin and biochemistry analysis

Total carboxylated OCN and undercarboxylated-OCN in serum was measured as previously described (Ferron *et al.,* 2010). Julian Berger of Columbia University (USA) kindly completed this work. Colin Wood of the University of Edinburgh completed general biochemistry analysis of the serum including cholesterol, globulin, protein, and albumin quantification.

2.9.3. Serum pyrophosphate analysis

Blood was collected from *Enpp1*$^{flox/flox}$ and *Enpp1*$^{flox/flox}$;*Ocn*-cre using a 1 ml syringe with 27 G needle, pre-lubricated with heparin solution and kept cool on ice before collection. Plasma pyrophosphate analysis was performed in accordance with the previously described protocol (Pomozi et al., 2019). Samples were centrifuged for 10 minutes at 4°C and 1000 *g*. Serum was carefully separated and transferred to 300,000 molecular weight separation tubes (Sartorius, Germany) and filter-centrifuged for 25 minutes at 4°C and 2000 *g*. The supernatant was transferred to pre-cooled Eppendorf tubes and samples were frozen at -80°C until required. For the bioluminescence assay, samples and reagents were slowly thawed on ice. A mastermix for the reaction was made according to Table 2.2 and stored in a precooled Eppendorf tube on ice until use. Subsequently, 35 µl mastermix was added to each well of a 96-well PCR plate which was centrifuged at 1400 *g* for 4 minutes to ensure the absence of air bubbles. All samples and PP_i calibration curve (5, 2.5, 1.25, 0.625, 0.3126, 0.0156. 0.078 and 0 µm) were added (5 µl) and run in duplicate. The 96-well plate was briefly centrifuged and spun at 1400 *g* for 4 minutes. The 96-well plate was subsequently incubated for 30 minutes at 37°C, and heat-inactivated for 10 minutes at 90°C. Plate was spun at 1400 *g* for 4 minutes. Following this, 30 µl of sample/mastermix solution was transferred to an opaque 96 well plate, and 15 µl of BacTiter-Glo (Promega, USA), which was pre-warmed to room temperature for a minimum of 15 minutes, was added. Sample and BacTiter-Glo were mixed several times by gentle pipetting to avoid air bubbles. The opaque 96-well plate was then centrifuged at 1400 *g* for 4 minutes. The plate was subsequently covered with tinfoil, to prevent damage to the light-sensitive BacTiter-Glo reagent, and incubated at room temperature for a maximum duration of 10 minutes. Luminescence was measured using a Synergy HT Multi-Mode Microplate reader (BioTek), pre-warmed to 24°C. This protocol was developed together with Janna Zoll and Professor Olivia Le Saux of John A. Burns School of Medicine, University of Hawaii.

	Stock solution	Final conc.	Per 1 sample (µl)
$MgCl_2$	800 µM	80 µM	4
ATPS (ProSpec, Israel)	4 U/ml	32 mU/ml	0.32
APS (Santa Cruz Biotechnology, USA)	640 µM	16 µM	1
Hepes pH 7.4 (Life Technologies)	0.25 M	50 mM	8
Sample	-	-	5
MQ water	-	-	21.68

Table 2.2. Components of master mix for PP_i analysis.

2.9.4. Analysis of liver triglycerides

Following euthanasia of male mice at 16-weeks of age, livers were collected, frozen, and stored at -80° C. Tissue was prepared and total triglyceride was measured using a Triglyceride (TG) Assay (Sentinel Diagnostics, Milan, Italy).

2.10. Statistical analysis

Data were checked to be normally distributed using a Kolmogorov-Smirnov normality test using GraphPad Prism Veresion 8.11 (La Jolla California USA). For data from two experimental groups, a Student's *t*-test analysis was used. For data from more than two experimental groups, two-way analysis of variance (ANOVA) incorporating Tukey post-hoc pairwise comparisons was performed. If data were not normally distributed, a suitable non-parametric test was performed Data are presented as the mean ± standard error of the mean (S.E.M) where appropriate, with all statistical analysis performed using Minitab (Minitab Inc., Coventry, UK). Regression and correlation coefficients are given with the intervals of confidence as (*P = 0.05) and P<0.05* was considered significant. For graphing and table representations, *P* values are represented as * *P<0.05,* ** *P<0.01*, *** *P<0.001*.

Chapter 3. Investigating the effect of osteoblast-specific NPP1 ablation on bone phenotype.

3.1. Introduction

As discussed in chapter 1, mineralisation of the ECM is a tightly regulated process (Anderson, 1995). Controlled mineralisation is critical for maintaining the integrity of the skeletal structure and function, occurring during development and throughout the life-long remodelling of bone (Kenkre and Bassett, 2018). However, mineralisation may also be pathological, occurring abnormally at the site of the bone, cartilage or soft tissues such as the vasculature (Yiu et al., 2015). There are many factors involved in the phenomenon of mineralisation regulation (Harmey et al., 2004). The emergence of sophisticated technologies in cell biology, imaging of genetically altered mouse models and mineral phase chemical characterisation has progressed understanding of the fine control of matrix mineralisation during skeletal development and the pathological ramifications if mineralisation is poorly or abnormally regulated. This has led to a conceptualisation of the network and mechanisms of action of the various mineralisation regulators at play (including promotors and inhibitors) (Fig. 1.7). These regulators maintain an appropriate ratio of P_i (which facilitates the mineralisation of the skeleton and soft tissue) and PP_i (which inhibits the mineralisation of the skeleton soft tissue), a process which is regulated by feedback signalling to allow mediation of this process (Hessle et al., 2002, Murshed et al., 2004)

The enzyme ENPP1 is important in the generation of PP_i by the cleavage of ATP, which is critical for the inhibition of mineralisation (Meyer, 1984, Bollen et al., 2000, Harmey et al., 2004). The scientific community has utilised mouse models to elucidate the specific actions of ENPP1 regarding bone and soft tissue calcification. To date, there are several different mouse models of *Enpp1*-deficiency (described in chapter 1) all of which demonstrate an increase in ectopic tissue mineralisation, an expected result due to the absence of NPP1 enzymatic activity.

In addition to mouse models that target only *Enpp1*, there are double-knockout mice, which have facilitated further understanding of bone mineralisation regulation. As previously highlighted, the controlled mineralisation is mediated by the presence of mineralisation inhibitors and promoters. The protein TNAP is encoded by the gene *Akp2* which is also known as *Alpl*, generates P_i by the hydrolysis of PP_i. This P_i is a constituent part of HA, although the main role of matrix mineralisation regulation is via the hydrolysis and thus depletion of PP_i. The role of TNAP has been well studied by analysis of a mouse model with globally deleted TNAP (*Akp2*$^{-/-}$*).* This mouse presents with hypophosphatasia, which includes rickets, poorly mineralised long bones, bone fractures and increased PP_i levels (Waymire et al., 1995, Narisawa et al., 1997, Wennberg et al., 2000, Anderson et al., 2005a). Additionally, these mice die by 20-days of age as a result of severe skeletal hypomineralization and epileptic seizures (Waymire et al., 1995).

The *Akp2*$^{-/-}$ mouse has been previously crossed with the *Enpp1*$^{-/-}$ mouse, resulting in a respective correction of the bone mineralisation abnormalities of both the TNAP (*Akp2)* and NPP1 (*Enpp1) genes* (Hessle et al., 2002). This further supports the hypothesis that TNAP and NPP1 work in close concert to allow physiological mineralisation of bone by the generation and hydrolysis of PP_i, maintaining a physiologically preferential P_i/PP_i ratio.

ANK (encoded by *ANKH* gene *(Ank* in mice)), is responsible for channeling of PP_i to the extracellular space, which has been conclusively linked with ECM mineralisation regulation in humans and mice (Ho et al., 2000). Deficiency in either ENPP1 or ANK leads to a disruption of

the PP_i/P_i ratio, resulting in dysregulated pathological mineralisation in humans (Ferreira et al., 1993, Mitton-Fitzgerald et al., 2016). Mice that have a mutated *Ank* locus and subsequent non-functional ANK protein demonstrate a phenotype reflective of the *Enpp1*$^{-/-}$ mice, with joint ankylosis and concomitantly decreased PP_i levels (Gurley et al., 2006a). As such, ANK and NPP1 are functional partners in the regulation of extracellular PP_i concentration.

It is imperative to further delineate the specific mechanisms of action of ENPP1 such that therapeutic intervention options for ENPP1-related disease may be identified and developed. To date, the cell-specific contributions of NPP1 have not been elucidated despite the literature reporting relatively higher levels of expression in specific tissues such as bone and cartilage, and cell types including osteoblasts and chondrocytes (Caswell and Russell, 1988, Harahap and Goding, 1988, Huang et al., 1994, Huang et al., 2018).

The availability of mouse models with loss-of-function of specific genes *in vivo* has dramatically altered the field of bone biology in the last 20 years. The use of genetically altered animals (mainly mice) has been utilised to demonstrate the role of a specific gene (or genes) in a variety of biological processes related to bone including its development, remodelling, metastasis and repair. However, mouse models are not without their limitations, notably when considering global knockouts. A global knockout mouse model is relevant to address the question of 'what is the contribution of this gene to bone homeostasis?' However, the use of a conditional knockout (such as cell-specific knockout) allows the scientist to dissect the putative and distinctive roles of one gene within one cell type. The interpretation of such conditional (and single Cre transgenic mouse lines to delete a gene of interest) must be completed with caution, whereby control mice must be compared to Cre-negative, exon-floxed controls, from mice of the same background strain.

Given that OCN is secreted solely by osteoblast, the use of an OCN-based cre-drive is unique to the osteoblast cell type (Hauschka et al., 1989, Zhang et al., 2002). The specificity of Cre activity

in mice can be assessed by crossing with ROSA and mT/mG reporter mice. Indeed, the specificity of Ocn-cre has been demonstrated in this way (Zhong et al., 2012).

The osteoblast is key to the formation of bone: determining the roles that specific genes (and their translated proteins) play within this cell type will undoubtedly enhance understanding of bone formation and the identification of potential therapeutic routes for those suffering mineralisation related diseases. As such this thesis determined the role of osteoblast-specific NPP1 in bone formation at both juvenile (6-week old) and adult (22-weeks old) ages of mice. This work utilised the Cre-lox system to specifically ablated ENPP1 in mouse osteoblasts. To achieve an osteoblast-specific ablation, the Ocn-cre mouse, and an *Enpp1*$^{flox/flox}$ mouse was utilised. It is important to acknowledge that this Ocn-cre mouse is well characterised and does not present with a notable phenotype compared to wild-type controls (Zhang et al., 2002, Staines et al., 2017), thus addressing limitations of genetically altered mouse models as previously discussed. The overarching aim of this chapter was to characterise the skeletal phenotype of the *Enpp1*$^{flox/flox}$;*Ocn*-cre mouse model and to investigate whether potentially decreased PP_i in the osteoblast-specific ablated mouse can result in ectopic mineralisation.

3.2. Hypothesis

The decreased *Enpp1* activity and serum PP_i concentration of the *Enpp1*$^{flox/flox}$;*Ocn*-cre mouse will result in an altered bone (and soft tissue) phenotype, presenting with increased levels of mineralisation compared to age-matched control (*Enpp1*$^{flox/flox}$) mice. This hypothesis will be addressed by assessing the following aims:

I. To analyse the bone phenotype in juvenile (6-week old) mice.

II. To analyse the bone phenotype in adult (22-week old) mice.

III. To analyse serum PP_i levels.

IV. To assess soft tissue calcification in adult mice.

3.3 Materials and methods

3.3.1. Generation of mice

The *Enpp1*$^{flox/flox}$;*Ocn*-cre and age-matched *Enpp1*$^{flox/flox}$ control male and female mice were generated (Section 2.7.1). Mice were fed a control diet and were culled at 6-weeks of age and 22-weeks of age for skeletal phenotyping analysis, and 16-weeks for histopathological analysis.

3.3.2. Histopathological assessment of soft tissue and bone

Following euthanasia of adult *Enpp1*$^{flox/flox}$;*Ocn*-cre and *Enpp1*$^{flox/flox}$ mice soft tissue and bone tissue was fixed in 10% NBF, embedded in paraffin wax and 5 µM thick sections were stained with H&E. Soft tissue was also stained with Alizarin red S to assess mineralisation.

3.3.3. Osmium staining of marrow adipose tissue

Following euthanasia at 16-weeks of age, *Enpp1*$^{flox/flox}$;*Ocn*-cre and *Enpp1*$^{flox/flox}$ mice femora and tibiae were dissected and soft tissue removed. Bones were prepared by fixing in 10% NBF for at least 24 hours. Bones were next washed with Sorensen's buffer and stained with 1% osmium tetroxide. Bones were µ-CT, reconstructed and analysed to determine quantitative volumetric data of marrow adipose tissue (Section 2.6.6). Dr Karla Suchacki of The University of Edinburgh kindly performed this work.

3.3.4. Gross analysis of bone

Tibiae and femora from male and female *Enpp1*$^{flox/flox}$;*Ocn*-cre and *Enpp1*$^{flox/flox}$ mice aged 6-weeks and 22-weeks of age were dissected and soft tissue removed. The length of the long bones were measured using DigiMax digital Vernier callipers (R. S. Components Ltd, Corby, Northants, UK).

3.3.5. Three-point bending analysis

Tibiae and femora from male and female *Enpp1*$^{flox/flox}$;*Ocn*-cre and *Enpp1*$^{flox/flox}$ mice aged 6-weeks and 22-weeks of age were dissected out and soft tissue removed. Three-point bending was performed using an LXR materials testing machine (Lloyds Instruments, West Sussex, U.K.) fitted with a 500 N load cell (Section 2.6.1).

3.3.6. Micro-computed tomography imaging

Tibiae and femora were dissected from 6-week and 22-week old male and female *Enpp1*$^{flox/flox}$;*Ocn*-cre and *Enpp1*$^{flox/flox}$ mice were fixed in 10% NBF and scanned using a µ-CT scanner (Section 2.6.2). The scans were reconstructed using NRecon software and analysed. Trabecular parameters assessed included trabecular bone volume/tissue volume (BV/TV; %), trabecular pattern factor (Tr.Pf), structural model index (SMI), trabecular thickness (Tr.Th; mm), trabecular number (Tr.No) and trabecular separation (Tr/Sp; mm). Cortical parameters assessed included endosteal diameter (mm), periosteal diameter (mm), bone volume (BV; mm^3), cortical thickness (Ct.Th; mm) and per cent open porosity (Po(oP); %).

3.3.7. Tissue preparation for microscopy and Bioquant histomorphometric analysis

Femora were dissected from 6-week and 22-week old male and female *Enpp1*$^{flox/flox}$;*Ocn*-cre and *Enpp1*$^{flox/flox}$ mice and soft tissue was removed. Femora were decalcified and fixed in 10% NBF (Section 2.9.2). Tissues were subsequently processed, embedded in paraffin wax and sectioned at 5 µM (Section 2.9.2). Sectioned tissues were air-dried, dewaxed using Leica Autostainer and stained with H&E (Section 2.8.3), toluidine blue-fast green stained (Section 2.8.5) and Goldner's Trichrome stained (Section 2.8.6). Sections were imaged using a Nikon CoolScan V (Nikon, Surrey, UK) and analysed by Scott Dillon using Bioquant software to support observations of µ-CT data. The following parameters were determined; trabecular separation (mm), trabecular diameter (mm), trabecular number, tissue volume ($µm^2$), bone volume ($µm^3$), bone volume/tissue volume, bone surface (mm), bone surface/bone volume, osteoid volume ($µm^3$), osteoid volume/bone volume, osteoid surface (mm), osteoid surface/bone volume, osteoid

width (mm), adipocyte volume (μm^3), and adipocyte volume/tissue volume. The analysed area was referred to as the 'region of interest' and is a region of bone defined below the growth plate (Fig. 3.1). The same region was assessed for each different stain. Two sections were analyzed with an N=6 for each genotype and each sex.

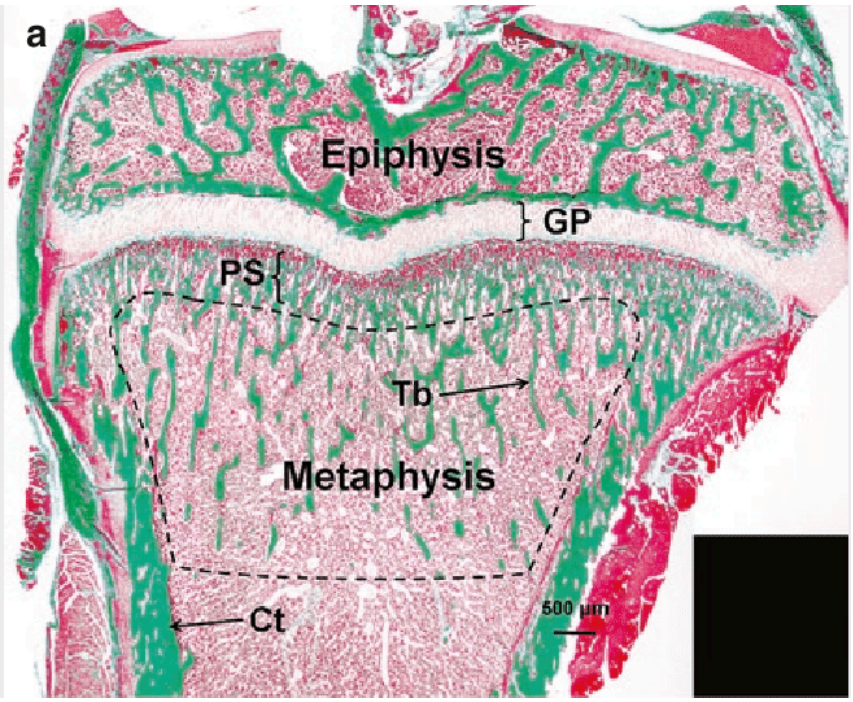

Figure 3.1. Region of Interest delimitation for Histomorphometry Analysis. Representative image of region of interest (ROI) for histomorphometry analysis in proximal femur. The dotted outline represents the region of interest to be assessed by BioQuant analysis. Tb stands for trabecular bone, Ct stands for cortical bone. GP stands for growth plate. Figure adapted from work by Dion et al. (Dion et al., 2011).

3.3.8. Analysis of serum bone formation and bone resorption markers

Serum samples were collected (Section 2.10.1). To analyse the difference in bone modelling and remodelling rates, bone formation and bone resorption markers were measured in serum samples taken from mice at 6-week and 22-week old mice. This was done using a P1NP ELISA

Kit (Mouse) (AMSBIO, Abingdon, UK) and a C-terminal telopeptide of CtX Kit (Mouse) (AMSBIO, Abingdon, UK).

3.4. Results

3.4.1. Gross anatomy - body mass and long bone length of juvenile mice

At 6-weeks of age, sex-effects were observed whereby male *Enpp1*$^{flox/flox}$ mice were significantly heavier than female *Enpp1*$^{flox/flox}$ mice (22.59 g vs. 16.05 g; $P<0.01$) (Fig. 3.2A). This was also true of male *Enpp1*$^{flox/flox}$;*Ocn*-cre mice compared to female *Enpp1*$^{flox/flox}$;*Ocn*-cre mice (21.98 g vs. 17.57 g; $P<0.001$) (Fig. 3.2A). No significant genotype effect was observed for male mice, however female *Enpp1*$^{flox/flox}$;*Ocn*-cre mice were significantly heavier than their *Enpp1*$^{flox/flox}$ controls (17.57 g vs. 16.04; $P<0.01$) (Fig. 3.2A).

The male *Enpp1*$^{flox/flox}$ mice tibiae were significantly longer than those of female *Enpp1*$^{flox/flox}$ mice (16.58 mm vs. 15.04 mm; $P<0.001$) as were those of the male *Enpp1*$^{flox/flox}$;*Ocn*-cre mice compared to female *Enpp1*$^{flox/flox}$;*Ocn*-cre mice (15.65 mm vs. 14.94 mm; $P<0.01$) (Fig. 3.2B). No differences between genotype were observed for female 6-week old mice. Male *Enpp1*$^{flox/flox}$;*Ocn*-cre mice exhibited decreased tibiae length compared to *Enpp1*$^{flox/flox}$ controls (16.48 mm vs. 14.65 mm; $P<0.01$) (Fig. 3.2B). For femora, no significant difference in bone length between genotype was observed for either male or female mice (Fig. 3.2C). Again, sex differences were observed; the tibiae of *Enpp1*$^{flox/flox}$ male mice were significantly longer than tibiae of female *Enpp1*$^{flox/flox}$ (13.76 mm vs. 12.42 mm; $P<0.001$) as were the tibiae of male *Enpp1*$^{flox/flox}$;*Ocn*-cre mice compared to the tibiae of female *Enpp1*$^{flox/flox}$;*Ocn*-cre mice (13.04 mm vs. 11.84 mm; $P<0.01$) (Fig. 3.2B).

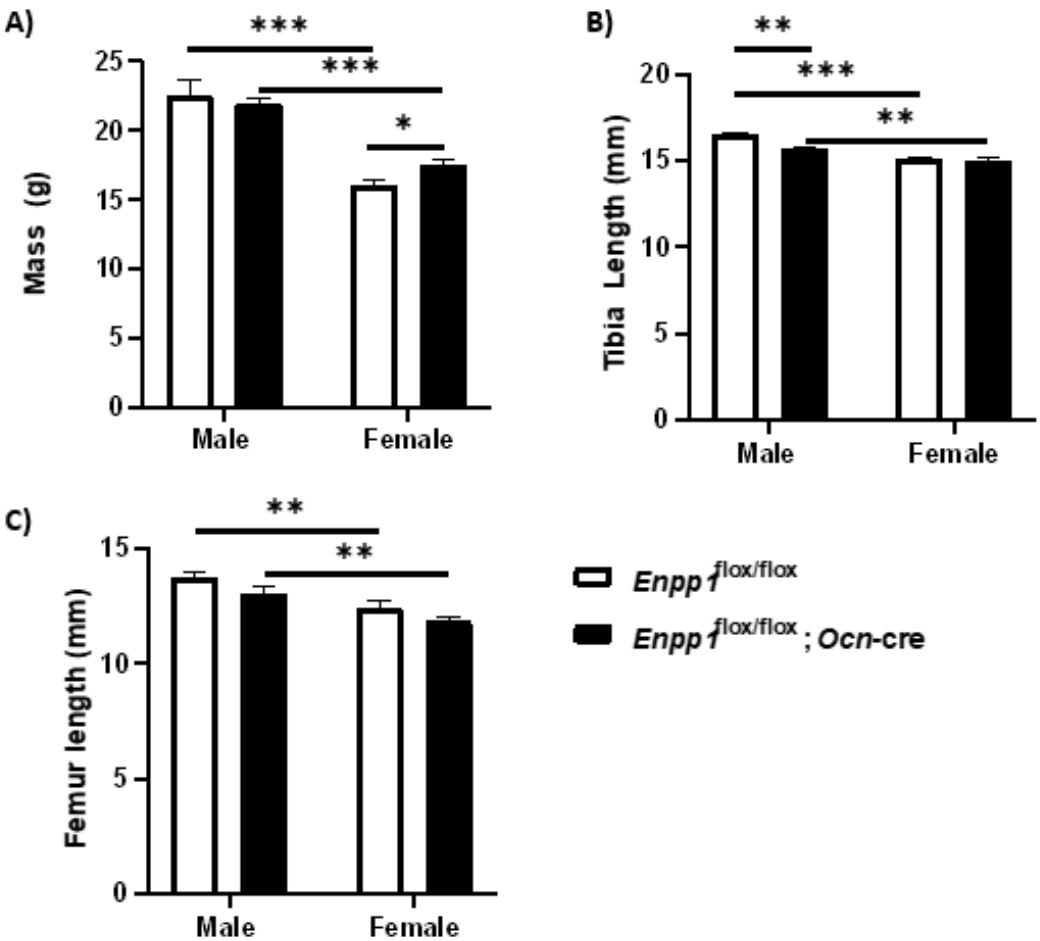

Figure 3.2. The mass and long bone length of male and female 6-week old mice show genotype and sex specific differences.

(A) The bone mass at 6-weeks of age for *Enpp1*$^{flox/flox}$;*Ocn*-cre and *Enpp1*$^{flox/flox}$ male and female mice and the (B) tibiae and (C) femora length. Data are presented as the mean ± S.E.M (n=6). Significance is denoted by **P*<0.05, ***P*<0.01, ****P*<0.001.

3.4.2. Serum pyrophosphate and markers of bone resorption and formation of juvenile mice

No significant differences in serum PP_i concentration were observed between genotypes for male or female mice (Fig. 3.3A). Additionally, no sex-effect was observed regarding PP_i concentration (Fig. 3.3A). Given the investigation into gross anatomy of long bones revealed genotype-specific significant differences in length, I next investigated whether there were increased bone resorption and formation marker concentrations. This revealed no significant difference between genotype or sex for bone formation (P1NP) or resorption (Ctx) (Fig. 3.3B, Fig. 3.3C).

3.4.3. Gross histological analysis of joint and soft tissue

A detailed histological assessment was completed by Prof Elspeth Milne to aid in understanding more fully the physiological role of osteoblast-specific NPP1 on skeletal development and pathological mineralisation. An absence of ectopic (soft tissue) pathological mineralisation as evidenced via analysis of soft tissue H&E staining and soft tissue Alizarin red S staining (Table 3.1) . Similarly, no pathological or abnormal architecture was observed amongst the analysed bone tissue in H&E stained sections (Table 3.1)

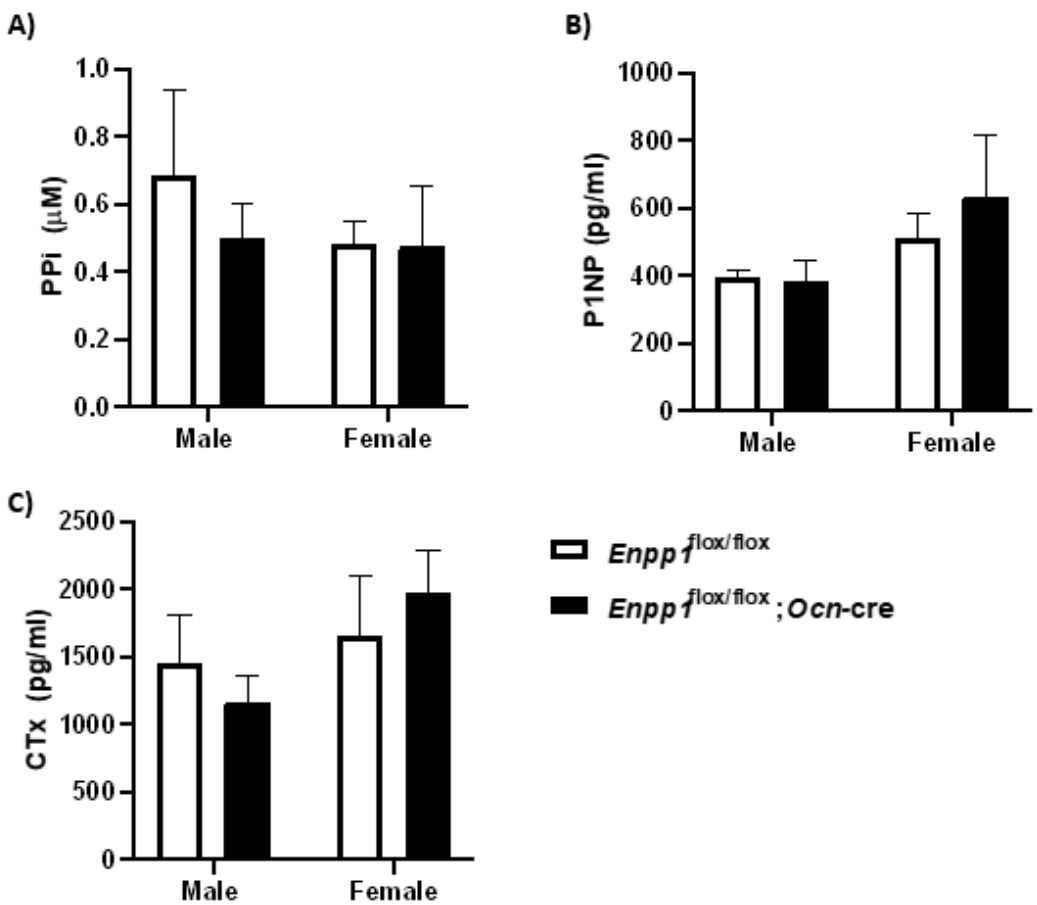

Figure 3.3. Serum concentration of PP_i, Ctx and P1NP from male and female mice are unchanged between genotype.

(A) The serum concentration of PP_i of male and female *Enpp1*$^{flox/flox}$;*Ocn*-cre and *Enpp1*$^{flox/flox}$ mice and the (B) marker of bone resorption (Ctx) and of (C) bone formation (P1NP). Data are presented as the mean ± S.E.M (n=6).

Tissue	Pathological observation of Enpp1$^{flox/flox}$ mice	Pathological observation of Enpp1$^{flox/flox}$;Ocn-Cre mice
Aorta	No reported pathology	No reported pathology
Brain	No reported pathology	No reported pathology
Heart	No reported pathology	No reported pathology
Kidney	No reported pathology	No reported pathology
Liver	No reported pathology	No reported pathology
Quadriceps Femoris	No reported pathology	No reported pathology
Whisker Follicle	No reported pathology	No reported pathology
Mid neck	No reported pathology	No reported pathology
Mid thoracic spine	No reported pathology	No reported pathology
Upper lumbar spine	No reported pathology	No reported pathology
Mid lumbar spine	No reported pathology	No reported pathology
Hock joint	No reported pathology	No reported pathology
Stifle joint	No reported pathology	No reported pathology

Table 3.1 Histopathological assessment of soft and bone tissue demonstrating no abnormal pathology.

Professor Elspeth Milne conducted assessment of 1 mouse of each genotype with Von Kossa and Alizarin red staining to assess mineralisation and tissue architecture. No reported pathology was observed in any of the anatomical regions assessed.

3.4.4. μ-CT analysis of the long bones of juvenile mice

The differences in bone architecture between genotypes are less evident at 6-weeks old in males compared to females. For both tibiae and femora, no significant differences between genotype for male 6-week old mice were observed in the measured trabecular parameters (Table 3.2). Regarding femora cortical parameters, a significantly decreased femora cortical thickness (mm) was observed in the *Enpp1*$^{flox/flox}$;*Ocn*-cre mice compared to *Enpp1*$^{flox/flox}$ control mice (0.109 mm vs. 0.117 mm; $P<0.05$). However, a significantly increased tibiae periosteal diameter was observed in the *Enpp1*$^{flox/flox}$;*Ocn*-cre mice compared to *Enpp1*$^{flox/flox}$ control mice (1.817 mm vs. 1.66 mm; $P<0.05$) (Table 3.3).

Bone	Genotype	BV/TV (%)	Tr. Pf.	SMI	Tr. Th. (mm)	Tr. No.	Tr. Sp. (mm)
Femur	*Enpp1*$^{flox/flox}$	22.239 (1.90)	7.243 (3.05)	1.052 (0.15)	0.0421 (0.00)	5.241 (0.33)	0.141 (0.01)
	Enpp1$^{flox/flox}$*;Ocn*-cre	26.960 (0.05)	4.147 (2.80)	0.928 (0.13)	0.0444 (0.00)	6.023 (0.26)	0.131 (0.00)
Tibia	*Enpp1*$^{flox/flox}$	16.552 (1.55)	22.425 (2.46)	1.772 (0.09)	0.0400 (0.00)	4.122 (0.26)	0.144 (0.01)
	Enpp1$^{flox/flox}$*;Ocn*-cre	16.678 (0.94)	21.587 (1.93)	1.7125 (0.05)	0.040 (0.00)	4.122 (0.015)	0.150 (0.00)

Table 3.2. µ-CT analysis of tibiae and femora trabecular bone from 6-week male mice shows no differences between genotype.

The following parameters were measured; per cent bone volume (BV/TV), trabecular patterning factor (Tr. Pf.), structural model index (SMI), trabecular thickness (Tr. Th.), trabecular number (Tr. No.), trabecular spacing (Tr. Sp.). Data are presented as the mean ± S.E.M (n=6).

Bone	Genotype	Peri. Di (mm)	Endo. Di (mm)	BV (mm^3)	Ct. Th (mm)	Po(op) (%)
Femur	*Enpp1*$^{flox/flox}$	2.144 (0.06)	1.773 (0.06)	0.800 (0.05)	0.117 (0.00)	2.059 (0.30)
	Enpp1$^{flox/flox}$*;Ocn*-cre	2.147 (0.04)	1.783 (0.06)	0.815 (0.02)	0.109 (0.00)*	2.828 (0.19)
Tibia	*Enpp1*$^{flox/flox}$	1.66 (0.05)*	1.277 (0.07)	0.857 (0.04)	0.101 (0.01)	3.467 (0.50)
	Enpp1$^{flox/flox}$*;Ocn*-cre	1.817 (0.02)	1.357 (0.03)	0.859 (0.02)	0.09 (0.00)	4.128 (0.29)

Table 3.3. µ-CT analysis of tibiae and femora cortical bone from 6-week male mice demonstrates largely unaltered parameters between genotype.

The following parameters were analysed; periosteal diameter (Peri. Di), endosteal diameter (Endo. Di), bone volume (BV), cortical thickness (Ct.Th) and porosity (Po(op)). Data are presented as the mean ± S.E.M (n=6). Significance between genotype is denoted by *P<0.05.

The female 6-week old *Enpp1*$^{flox/flox}$;*Ocn*-cre mice demonstrate notable significant differences both in cortical and trabecular parameters investigated, indicating an increased bone mass in these mice compared to their *Enpp1*$^{flox/flox}$ controls. For the femora trabecular parameters, female *Enpp1*$^{flox/flox}$;*Ocn*-cre mice exhibit increased bone volume/tissue volume (17.50% vs. 11.67%; $P<0.01$), decreased trabecular pattern factor (15.23 vs. 24.46; $P<0.01$), decreased structural model index (1.39 vs. 1.71; $P<0.01$), increased trabecular number (4.61 vs. 3.19; $P<0.001$) and decreased trabecular spacing (0.157 vs. 0.187; $P<0.01$) compared to *Enpp1*$^{flox/flox}$ mice (Table. 3.4). For the tibiae trabecular parameters, *Enpp1*$^{flox/flox}$;*Ocn*-cre female mice demonstrate increased bone volume/tissue volume (11.54% vs. 7.72%; $P<0.01$), increased trabecular number (3.32 vs. 2.24; $P<0.001$) and decreased trabecular spacing compared to their *Enpp1*$^{flox/flox}$ controls (0.180 mm vs. 0.230 mm; $P<0.001$) (Table 3.4). For the cortical parameters, *Enpp1*$^{flox/flox}$;*Ocn*-cre female 6-week old mice increased femora endosteal diameter (1.95 mm vs. 1.67 mm; $P<0.001$), and increased open porosity compared to their *Enpp1*$^{flox/flox}$ controls (2.46% vs. 2.04%; $P<0.05$) (Table 3.5). For the cortical tibia factors an increased endosteal diameter was also observed for the *Enpp1*$^{flox/flox}$;*Ocn*-cre mice compared to their *Enpp1*$^{flox/flox}$ controls (1.48 mm vs. 1.29 mm; $P<0.001$) (Table 3.5).

Bone	Genotype	BV/TV (%)	Tr. Pf.	SMI	Tr. Th. (mm)	Tr. No.	Tr. Sp. (mm)
Femur	*Enpp1*$^{flox/flox}$	11.67 (0.93)	24.46 (1.61)	1.71 (0.05)	0.036 (0.08)	3.19 (0.18)	0.187 (0.006)
	Enpp1$^{flox/flox}$*;Ocn*-cre	17.50 (0.58)**	15.23 (1.42)**	1.39 (0.04)**	0.038 (0.01)	4.61 (0.15)***	0.157 (0.004)**
Tibia	*Enpp1*$^{flox/flox}$	7.72 (0.55)	33.23 (1.96)	1.97 (0.05)	0.034 (0.06)	2.24 (0.13)	0.230 (0.009)
	Enpp1$^{flox/flox}$*;Ocn*-cre	11.54 (0.43)**	26.73 (1.78)	1.80 (0.03)	0.034 (0.01)	3.32 (0.08)***	0.180 (0.005)**

Table 3.4. µ-CT analysis of tibiae and femora trabecular bone from 6-week female mice show significant differences between genotype.

The following parameters were measured; per cent bone volume (BV/TV), trabecular patterning factor (Tr. Pf.), structural model index (SMI), trabecular thickness (Tr. Th.), trabecular number (Tr. No.), trabecular spacing (Tr. Sp.). Data are presented as the mean ± S.E.M (n=6). Significance between genotype is denoted by $^{**}P<0.01$, $^{***}P<0.001$.

Bone	Genotype	Peri. Di (mm)	Endo. Di (mm)	BV (mm^3)	Ct. Th (mm)	Po(op) (%)
Femur	*Enpp1*$^{flox/flox}$	1.97 (0.03)	1.67 (0.03)	0.565 (0.03)	105.73 (2.07)	2.04 (0.09)
	Enpp1$^{flox/flox}$*;Ocn*-cre	2.25 (0.03)	1.95 (0.03)***	0.64 (0.04)	98.32 (3.40)	2.46 (0.14)*
Tibia	*Enpp1*$^{flox/flox}$	1.57 (0.13)	1.29 (0.02)	0.624 (0.02)	91.15 (2.20)	3.35 (0.28)
	Enpp1$^{flox/flox}$*;Ocn*-cre	1.89 (0.04)*	1.48 (0.03)***	0.68 (0.03)	85.20 (2.58)	3.53 (0.16)

Table 3.5. µ-CT analysis of tibiae and femora cortical bone from 6-week female mice show significant differences between genotype.

The following parameters were measured; periosteal diameter (Peri. Di.), endosteal diameter (Endo. Di), bone volume (BV), cortical thickness (Tb. Th.), open porosity (%) (Po(op)). Data are presented as the mean ± S.E.M (n=6). Significance between genotype is denoted by *P<0.05, ***P<0.001.

The results from the epiphyseal trabecular bone, the lateral subchondral bone of the femorotibial joint, and the medial subchondral bone of the femorotibial joint also demonstrate genotype differences indicative of increased bone formation.

Male mice 6-week old *Enpp1*$^{flox/flox}$;*Ocn*-cre mice exhibit increased epiphyseal bone volume/tissue volume (41.35% vs. 35.12; $P<0.05$) (Fig. 3.4), unaltered trabecular number and trabecular separation (Fig. 3.4b, Fig. 3.4C) compared to *Enpp1*$^{flox/flox}$ controls. However, the male 6-week old *Enpp1*$^{flox/flox}$;*Ocn*-cre mice do show significantly increased trabecular thickness compared to their *Enpp1*$^{flox/flox}$ controls (0.06 mm vs. 0.05 mm; $P<0.05$) (Fig. 3.4D). The trabecular pattern factor (an indicator of trabecular connectedness) and structural model index (an indicator of whether the trabeculae are in a more rod or plate-like in their geometry), remained unchanged between genotypes (Fig. 3.4E, Fig. 3.4F). Female 6-week old *Enpp1*$^{flox/flox}$;*Ocn*-cre mice demonstrate, to a greater extent than the male mice, an increase in epiphyseal increased bone mass compared to their *Enpp1*$^{flox/flox}$ controls. The female mice have significantly increased epiphyseal bone volume/tissue volume (37.41% vs. 28.87%; $P<0.001$) (Fig. 3.4A), trabecular number (6.85 vs. 5.76; $P<0.001$) (Fig. 3.4B), with unaltered trabecular separation compared to their *Enpp1*$^{flox/flox}$ controls (Fig. 3.4C). The trabecular thickness of the female *Enpp1*$^{flox/flox}$;*Ocn*-cre mice was also significantly increased (0.06 mm vs 0.05 mm; $P<0.05$), as was the trabecular pattern factor (16.87 vs 8.62; $P<0.001$), indicating a greater degree of connectedness compared to their *Enpp1*$^{flox/flox}$ controls (Fig. 3.4D, 3.4E). The structural model index for female *Enpp1*$^{flox/flox}$;*Ocn*-cre was also significantly decreased, indicating that the trabecular bone is more plate-like than the *Enpp1*$^{flox/flox}$ controls (1.33 vs. 1.65; $P<0.01$) (Fig. 3.4.F).

Analysis of the medial and lateral subchondral bone parameters indicated only decreased lateral subchondral bone porosity in the *Enpp1*$^{flox/flox}$;*Ocn*-cre male 6-week old mice compared to their *Enpp1*$^{flox/flox}$ controls (0.27 mm^3 vs 0.22 mm^3; $P<0.05$) (Fig. 3.5C) and increased medial subchondral bone porosity in the *Enpp1*$^{flox/flox}$;*Ocn*-cre female 6-week old mice compared to controls (Fig. 3.85). No other significant differences were observed (Fig. 3.5A-3.5E).

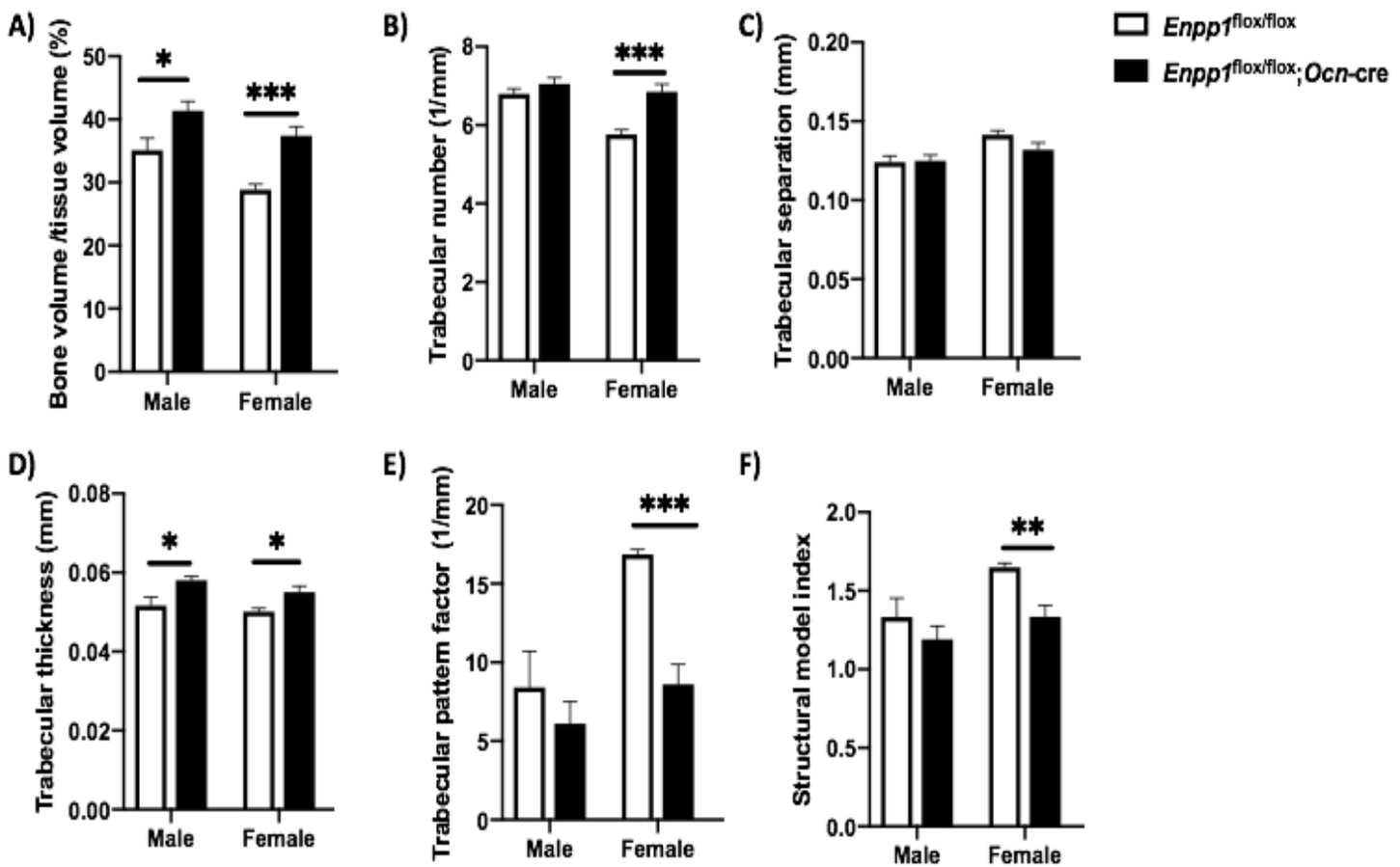

Figure 3.4. µ-CT analysis of the epiphyseal bone from male and female mice show genotype specific differences.

The parameters analysed include the trabecular (A) bone volume/tissue volume, (B) trabecular number, (C) trabecular separation, (D) trabecular thickness, (E) trabecular pattern factor and (F) structural model index. Data are presented as the mean ± S.E.M (n≥5). Significance between genotype is denoted by **P*<0.05, ***P*<0.01, ****P*<0.001.

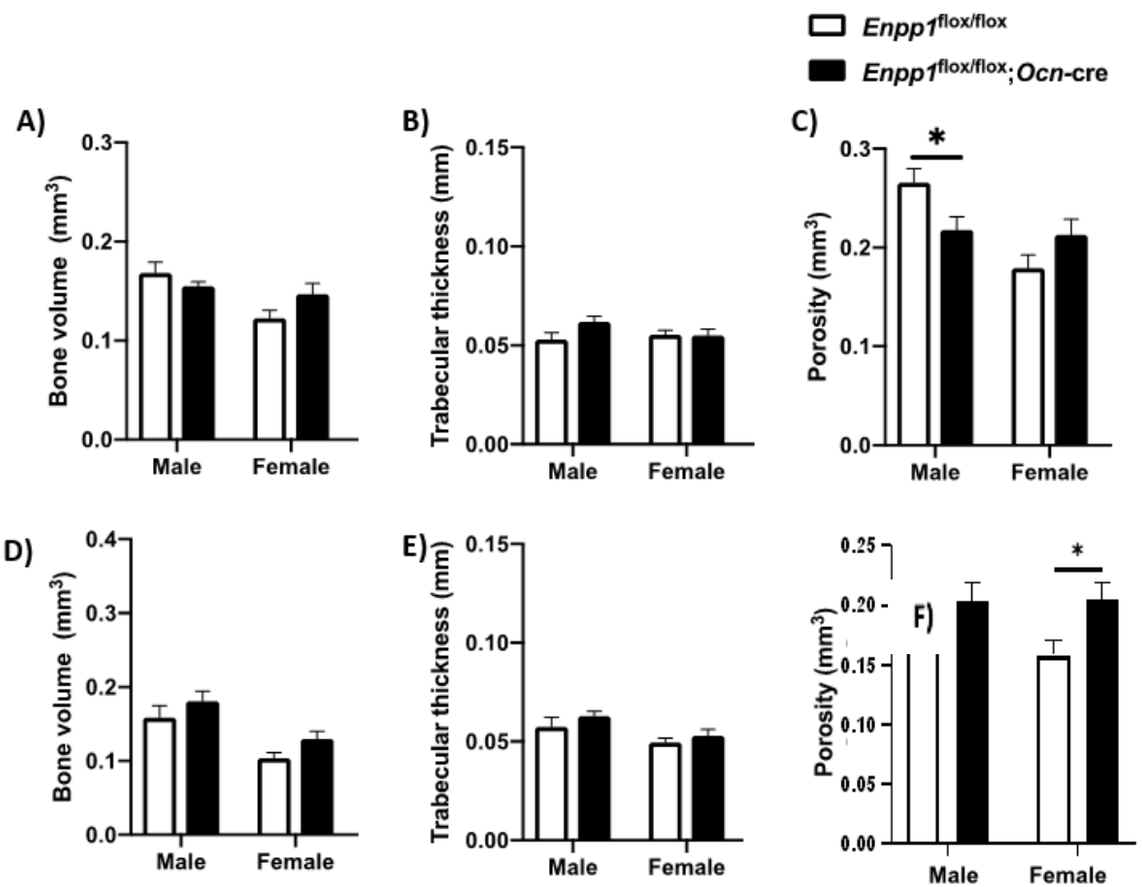

Figure 3.5. µ-CT analysis of the lateral and medial subchondral bone from male and female mice show largely unaltered differences between genotype.

The subchondral bone parameters measured include (A) lateral bone volume, (B) lateral trabecular thickness, (C) lateral porosity, (D) medial bone volume, (E) medial trabecular thickness and (F) medial trabecular porosity. Data are presented as the mean ± S.E.M (n≥5). Significance between genotype is denoted by *P<0.05.

3.4.5. Analysing bone mineral density of long bones of juvenile mice

μ-CT scanning was used to quantitatively determine whether osteoblast-specific NPP1 ablation impacts the ability of bones to form mineral at a juvenile age point. The use of bone mineral density measurements is a common surrogate assessment of the strength of bone tissue. Analysis revealed no significant difference between genotype in the cortical bone mineral density of the tibiae and the femora (Fig. 3.6A, C). A sex difference was observed whereby the female *Enpp1*$^{flox/flox}$ mice exhibit greater femora cortical bone mineral density compared to male *Enpp1*$^{flox/flox}$ mice (0.42 mg/cm^3 vs 0.37 mg/cm^3; P<0.05): this result was not reflected in the *Enpp1*$^{flox/flox}$;*Ocn*-cre male and female mice (Fig. 3.6C). Although no significant differences were observed for the trabecular bone mineral density of the femora, I observed notable alterations in the tibiae bone mineral density (Fig. 3.6B & 3.6D). A sex-specific effect was again observed, whereby the female *Enpp1*$^{flox/flox}$ mice exhibit this time significantly reduced trabecular bone mineral density compared to the *Enpp1*$^{flox/flox}$ male mice (0.20 mg/cm^3 vs. 0.26 mg/cm^3; P<0.01) (Fig. 3.6B). A significantly increased bone mineral density of the tibia trabecular bone of the female *Enpp1*$^{flox/flox}$;*Ocn*-cre 6-week old mice compared to the *Enpp1*$^{flox/flox}$ female 6-week old mice was observed (0.20 mg/cm^3 vs. 0.16 mg/cm^3; P<0.05) (Fig. 3.6B).

3.4.6. Analysing the mechanical properties of long bones in juvenile mice

To determine whether the micro-architectural changes in bone translated to altered mechanical properties, the tibiae and femora of *Enpp1*$^{flox/flox}$;*Ocn*-cre and *Enpp1*$^{flox/flox}$ control mice were subjected to 3-point bending analysis. At 6-weeks of age, two parameters showed significant differences. The female 6-week old *Enpp1*$^{flox/flox}$;*Ocn*-cre mice exhibited increased work to rupture for the femora bone (4.19x10^{-3} J vs. 2.97 4.19x10^{-3} J; P<0.01) (Table 3.6) , and the male *Enpp1*$^{flox/flox}$;*Ocn*-cre mice showed increased deflection at rupture (1.20 mm vs. 0.90 mm; P<0.05) (Table 3.7) compared to *Enpp1*$^{flox/flox}$ sex-matched controls. This indicates that there is a small increased amount of energy required to break the bones of the *Enpp1*$^{flox/flox}$;*Ocn*-cre mice compared to that of the *Enpp1*$^{flox/flox}$.

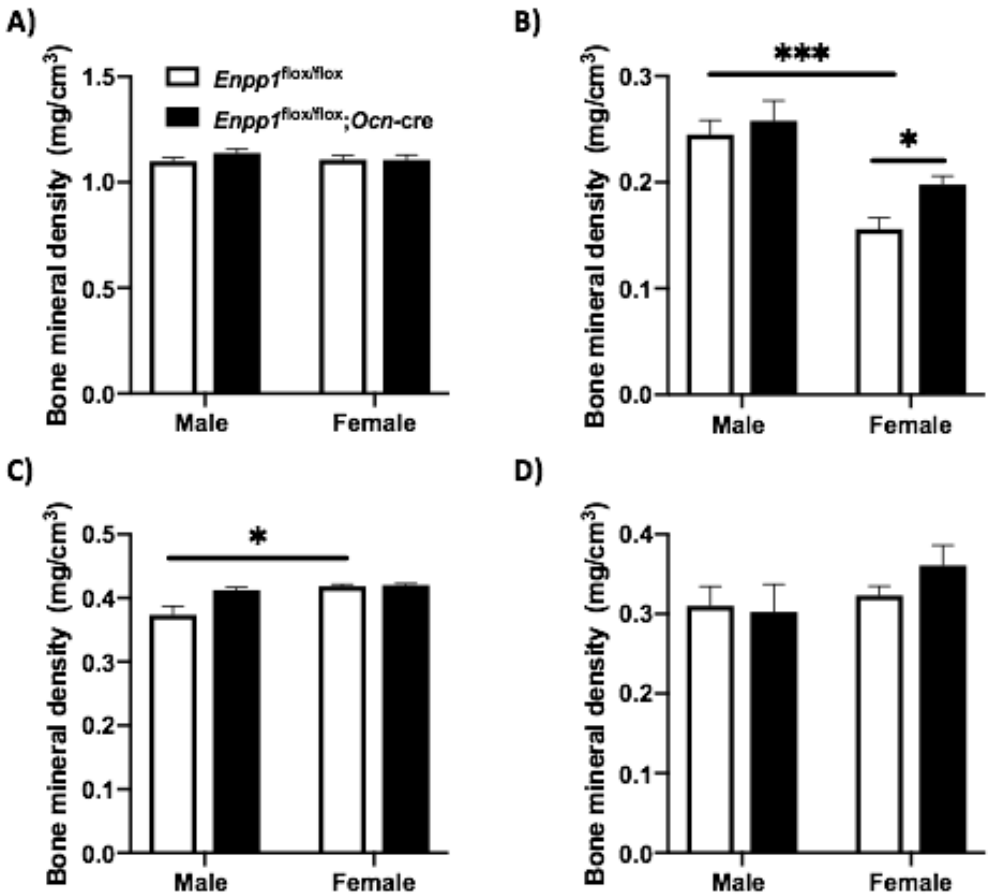

Figure 3.6. µ-CT analysis of tibiae and femora cortical and trabecular bone mineral density from 6-week female mice.

(A) Tibiae cortical and (B) trabecular bone mineral density. (C) femora cortical and (D) trabecular bone mineral density. Data are presented as the mean ± S.E.M (n≥3). Significance denoted by **P*<0.05, ****P*<0.001.

Sex	Genotype	Maximum Load (N)	Deflection at Maximum Load (mm)	Work to Maximum Load (J) 10^{-3}	Stiffness 10^3 (N/m)	Load at Rupture (N)	Deflection at Rupture (mm)	Work to Rupture (J) 10^{-3}
Female	*Enpp1*$^{flox/flox}$	7.75 (1.06)	0.51 (0.07)	1.89 (0.09)	26.39 (6.68)	5.42 (0.74)	0.69 (0.12)	2.97 (0.24)
	Enpp1$^{flox/flox}$;*Ocn*-cre	8.07 (0.85)	0.57 (0.05)	2.33 (0.18)	26.87 (5.03)	5.95 (0.60)	0.82 (0.08)	4.19 (0.24)**
Male	*Enpp1*$^{flox/flox}$	11.79 (1.75)	0.63 (0.06)	3.59 (0.47)	36.53 (6.39)	8.25 (1.23)	1.05 (0.23)	6.92 (0.78)
	Enpp1$^{flox/flox}$;*Ocn*-cre	12.88 (0.27)	0.56 (0.04)	3.91 (0.35)	40.36 (2.23)	9.02 (0.19)	0.91 (0.07)	7.70 (0.62)

Table 3.6. 3-point bending analysis of femora from 6-week old mice reveals an absence of functional consequence from osteoblast-specific NPP1 ablation.

Values are shown for femora dissected from 6-weeks and 22-weeks of age from female and male *Enpp1*$^{flox/flox}$ and *Enpp1*$^{flox/flox}$*;Ocn-cre* mice. Bones were tested to fracture, whereby fracture points were identified from the load-extension curve whereby the maximum load decreased rapidly to 70% of the maximum value. The maximum stiffness was defined as the maximum gradient of the rising portion of the load-extension curve. Data are presented as mean ± S.E.M (n≥4). Significance between genotype is denoted by ***P*<0.01.

Sex	Genotype	Maximum Load (N)	Deflection at Maximum Load (mm)	Work to Maximum Load (J) 10^{-3}	Stiffness 10^3 (N/m)	Load at Rupture (N)	Deflection at Rupture (mm)	Work to Rupture (J) 10^{-3}
Female	*Enpp1*$^{flox/flox}$	4.72 (0.24)	0.52 (0.03)	1.34 (0.04)	13.97 (1.35)	3.30 (0.17)	0.86 (0.11)	5.69 (1.11)
	Enpp1$^{flox/flox}$;*Ocn*-cre	5.19 (0.78)	0.66 (0.09)	1.91 (0.44)	22.56 (4.92)	3.63 (0.54)	0.82 (0.16)	3.87 (0.89)
Male	*Enpp1*$^{flox/flox}$	8.17 (0.41)	0.65 (0.04)	3.17 (0.44)	21.26 (1.24)	5.72 (0.28)	0.90 (0.09)	5.76 (1.20)
	Enpp1$^{flox/flox}$;*Ocn*-cre	7.15 (0.41)	0.71 (0.04)	3.01 (0.33)	17.82 (0.97)	5.03 (0.35)	1.20 (0.10)*	6.53 (0.79)

Table 3.7. 3-point bending analysis of tibiae from 6-week old mice an absence of functional consequence from osteoblast-specific NPP1 ablation.

Bones from *Enpp1*$^{flox/flox}$ and *Enpp1*$^{flox/flox}$*;Ocn-cre* were tested to fracture, whereby fracture points were identified from the load-extension curve whereby the maximum load decreased rapidly to 70% of the maximum value. The maximum stiffness was defined as the maximum gradient of the rising portion of the load-extension curve. Data are presented as mean ± S.E.M (n≥4). Significance between genotype is denoted by *P<0.05.

3.4.7. Histomorphometry analysis of juvenile mice using Bioquant OSTEO software

To further investigate the micro-architecture of the bone, and to investigate the mineralisation of the bone tissue, a histomorphometry assessment was conducted using Bioquant software on sectioned sections of the femora, as this is the bone where I observed the majority of architectural differences by μ-CT analysis by assessing specific regions (See section 3.3.7). This region is determined as the region of interest and is below the growth plate. For all stains, the same region was assessed. This analysis was performed to support and confirm the findings observed by μ-CT analysis, and in particular to assess osteoid and adiposity, which is a limitation of basic μ-CT analysis. Overall, one sex-specific difference was observed in the histomorphometry analysis: female *Enpp1*$^{flox/flox}$ mice have significantly decreased trabecular diameter compared to male *Enpp1*$^{flox/flox}$ mice at 6-weeks of age (0.05 mm vs. 0.07 mm; $P<0.05$) (Fig. 3.7B). Several genotype-specific differences were also observed. Male *Enpp1*$^{flox/flox}$;*Ocn*-cre mice demonstrated significantly reduced spacing between their trabeculae compared to *Enpp1*$^{flox/flox}$ control mice (0.05 mm vs. 0.08 mm; $P<0.05$) (Fig. 3.7A). Male *Enpp1*$^{flox/flox}$;*Ocn*-cre exhibit increased bone volume compared to *Enpp1*$^{flox/flox}$ controls (0.28 μm^2 vs. 0.17 μm^2; $P<0.05$) as did female mice (0.24 μm^2 vs. 0.15 μm^2; $P<0.05$) (Fig. 3.7E). Additionally, male *Enpp1*$^{flox/flox}$;*Ocn*-cre mice demonstrate increased bone volume/tissue volume compared to *Enpp1*$^{flox/flox}$ controls (0.28 vs. 0.17; $P<0.05$) (Fig. 37F). Females *Enpp1*$^{flox/flox}$;*Ocn*-cre mice show significantly decreased osteoid surface (8.42 mm vs. 15.68 mm; $P<0.05$) (Fig. 3.7G) and decreased osteoid surface/bone surface (0.073 mm vs. 0.51 mm; $P<0.05$) (Fig. 3.7H) compared to *Enpp1*$^{flox/flox}$ female controls. This suggests less osteoid tissue, which can be explained by increased bone tissue volume observed in the *Enpp1*$^{flox/flox}$;*Ocn*-cre mice. The osteoid width of the female *Enpp1*$^{flox/flox}$;*Ocn*-cre mice was also significantly increased compared to *Enpp1*$^{flox/flox}$ controls (7.46 mm vs. 6.28 mm; $P<0.05$) (Fig. 3.7K), in keeping with findings from μ-CT of a significantly increased width of bone (periosteal and endosteal diameter analysis). The female *Enpp1*$^{flox/flox}$;*Ocn*-cre mice also demonstrate significantly increased bone marrow adiposity volume compared to *Enpp1*$^{flox/flox}$ controls (0.002 μm^3 vs 0.001 μm^3; $P<0.05$) (Fig. 3.7N).

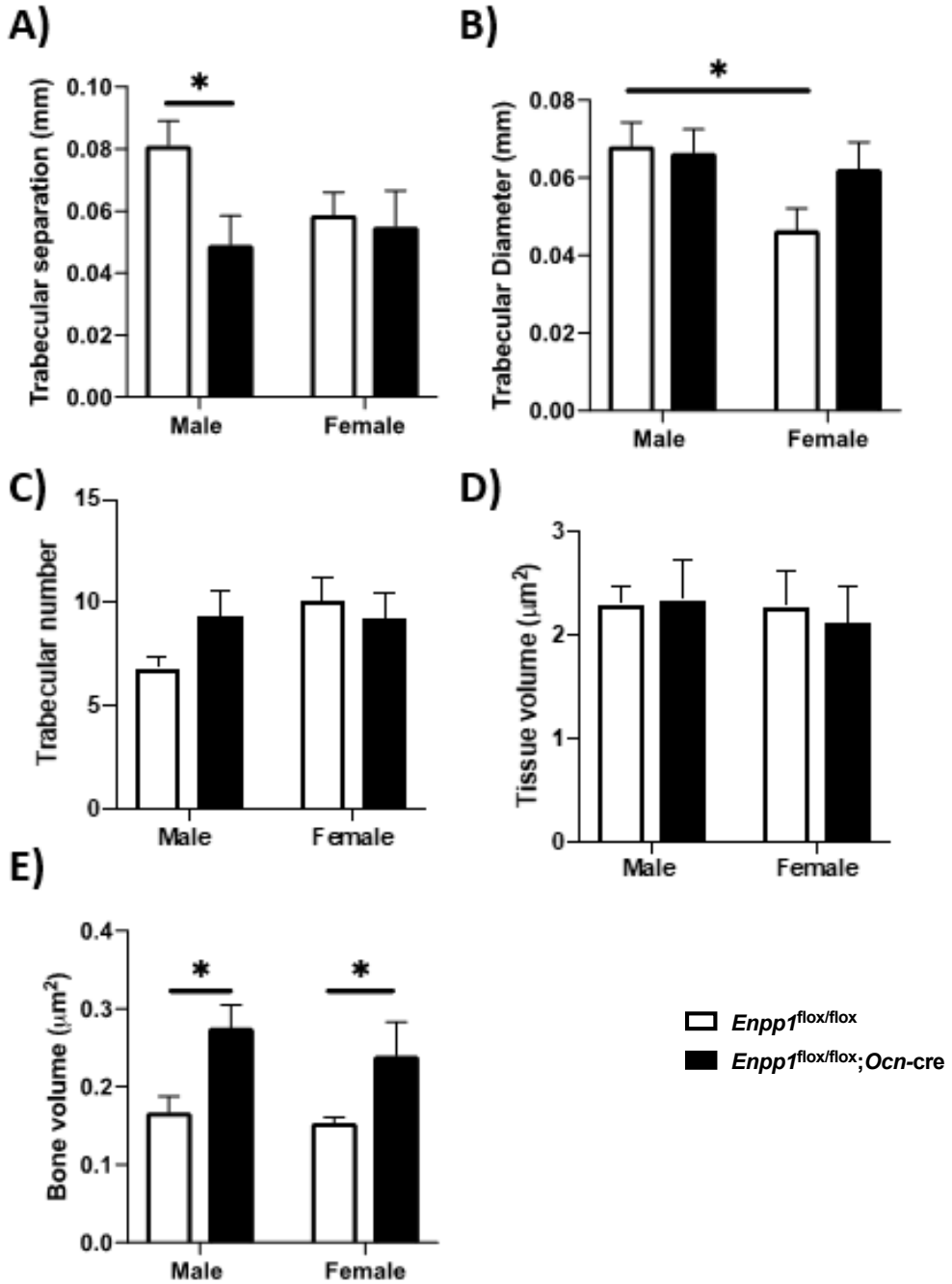

Figure 3.7 Part 1. Histomorphometry analysis of 6-week old male and female femora demonstrates increased bone volume in osteoblast-specific NPP1 ablated mice.

Parameters investigated include (A) trabecular separation, (B) trabecular diameter, (c) trabecular number, (D) trabecular tissue volume and (E) Bone volume. Data are presented as mean ± S.E.M ($n \geq 5$). Significance is denoted by $*P<0.05$.

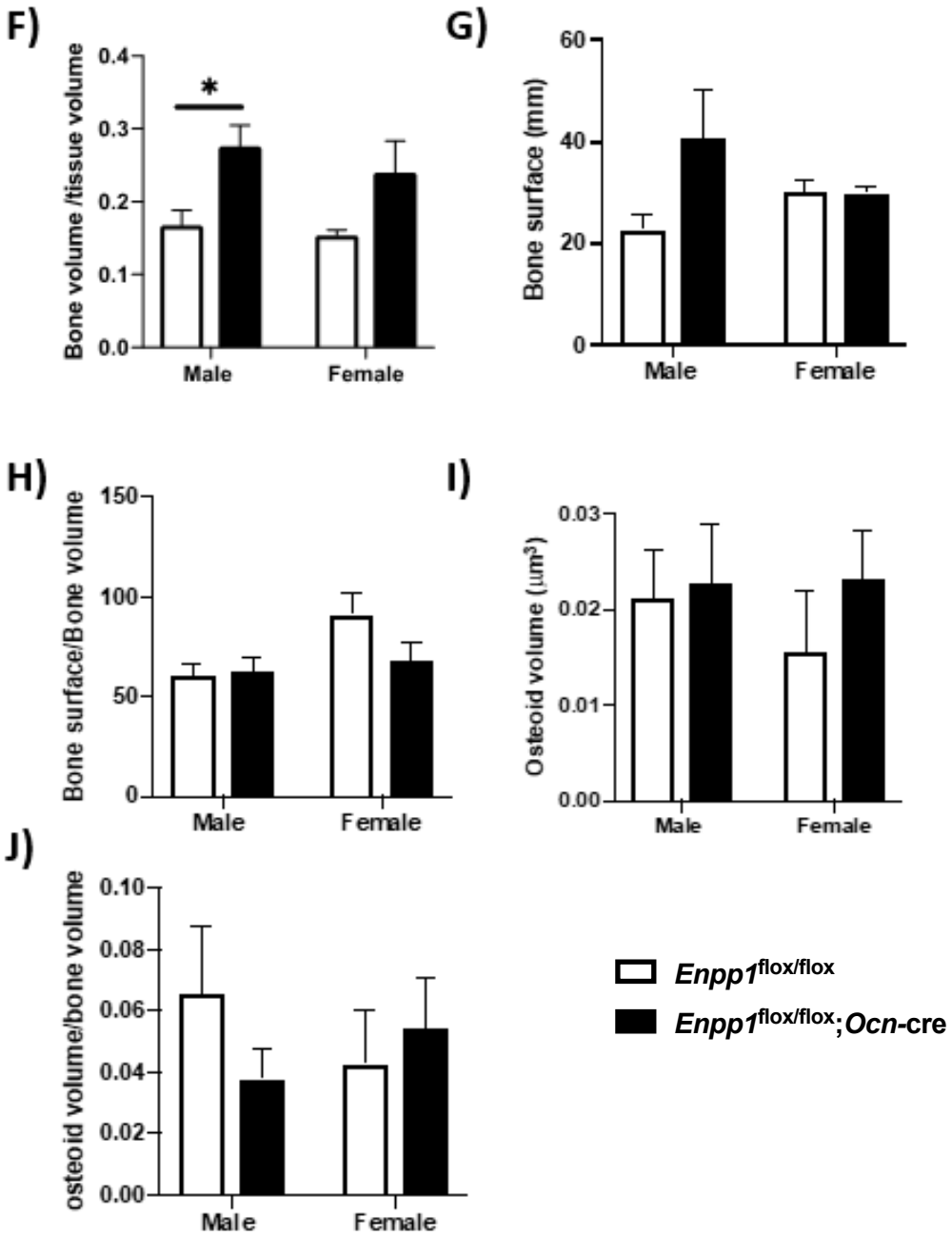

Figure 3.7: Part 2. Histomorphometry analysis of 6-week old male and female femora reveals largely significant differences between genotype.

Parameters investigated include (G) Bone surface, (H) Bone surface/bone volume, (I) osteoid volume, (J) osteoid volume/bone volume. Data are presented as mean ± S.E.M (n≥5). Significance is denoted by *P<0.05.

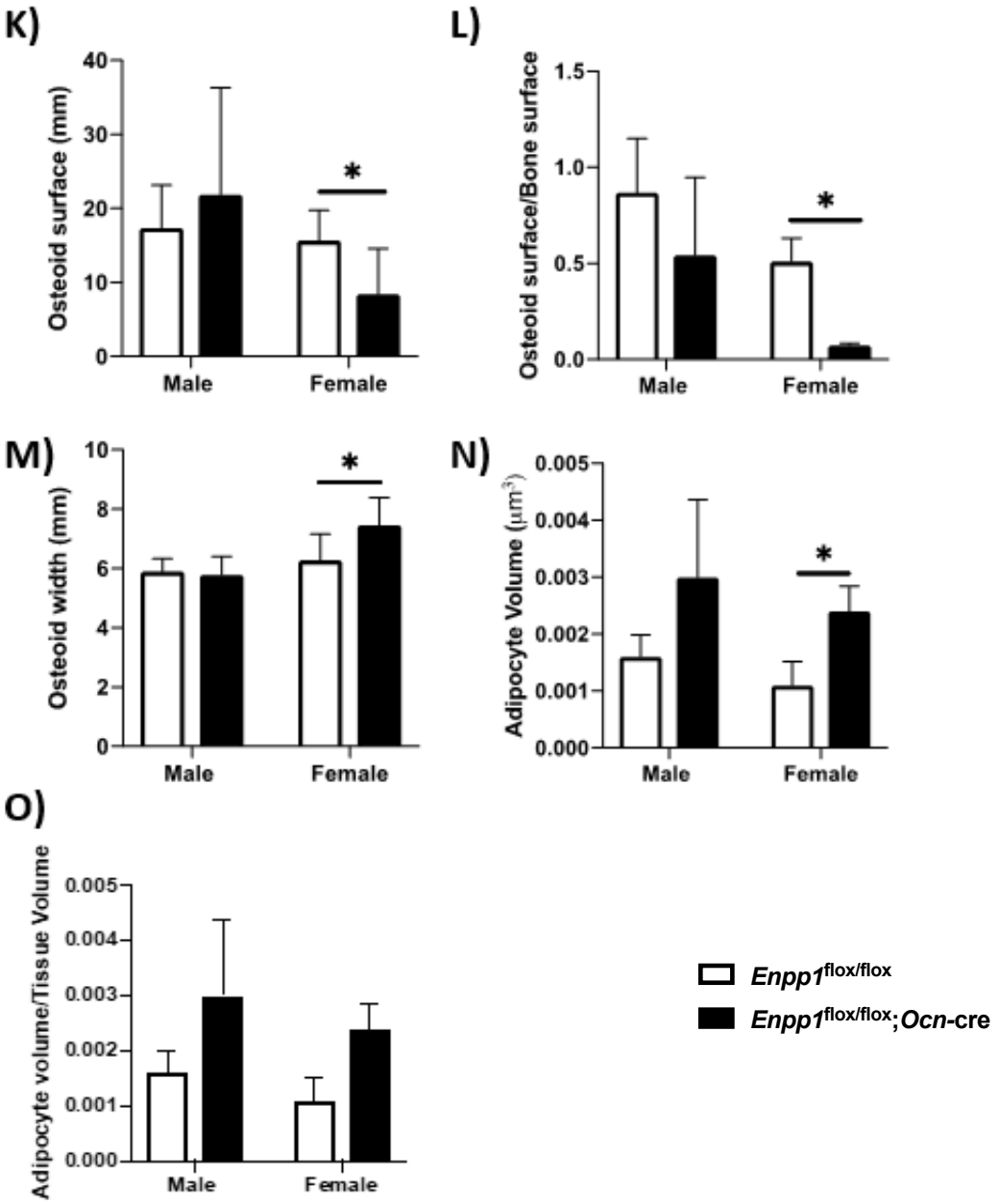

Figure 3.7: Part 3. Histomorphometry analysis of 6-week old male and female femora demonstrates increased mineralized bone and bone material in female osteoblast-specific NPP1 ablated mice.

Parameters investigated include (K) Osteoid surface, (L) Osteoid surface/bone surface, (M) Osteoid width, (N) Adipocyte volume and (O) adipocyte volume/tissue volume. Data are presented as mean ± S.E.M (n≥5). Significance is denoted by *P<0.05.

3.4.8. μ-CT analysis of bone marrow adiposity of 16-week old male mice

Given that the histomorphometry data indicated a genotype effect on adipocyte volume, μ-CT was next utilised to analyse bone marrow adiposity using osmium staining. At the time of analysis, 6-week old samples bone samples were no longer available. The 16-week old male *Enpp1*$^{flox/flox}$;*Ocn*-cre and *Enpp1*$^{flox/flox}$ mouse long bones were utilised to determine whether a genotype effect on marrow adiposity could be detected by μ-CT. Whilst this cannot be considered reflective of the 6-week old mice, it does provide information on the marrow adipose tissue of skeleton which has not reached full maturity. The use of this technique is of notable importance, given that marrow adipose tissue is not evenly distributed throughout the bone marrow of long bones, and histomorphometric analysis of one bone section area may not be representative of the total bone marrow adiposity. Indeed, the conventional quantitative analysis of marrow adipose tissue is dependent upon sectioning to overcome issues associated with uneven distribution, yet this comes with limitations including being labour and resource-intensive, and is inconsistent between individuals and laboratories. The utilisation of osmium tetroxide staining and μ-CT analysis represents a rapid, systemic and reproducible method to quantitate marrow adipose tissue. The analysis conducted focused on four different regions:

1. The tibia-fibular junction to the distal end of the bone
2. The growth plate to the tibia-fibular junction
3. The proximal epiphyseal region
4. The total bone

Analysis of male 16-week old mice tibiae did not reveal any significant differences between genotypes for the regions analysed (Fig. 3.8). Unfortunately, the male femora and female age-matched mice were not available for analysis, representing a limitation of the data obtained by osmium staining.

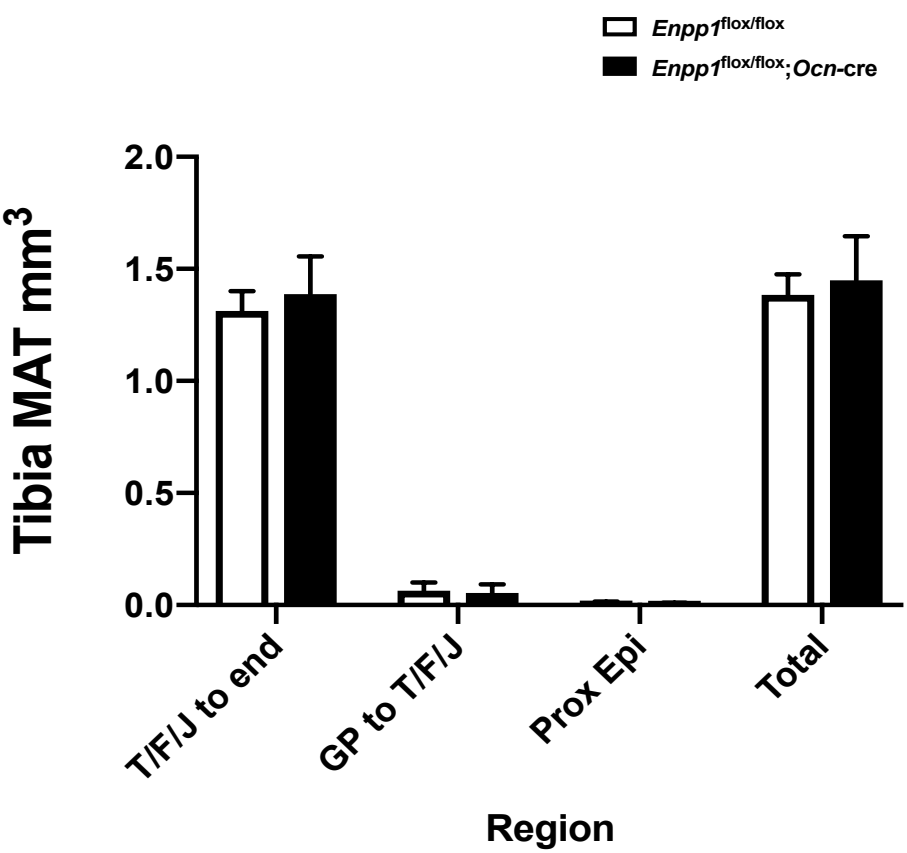

Figure 3.8. μ-CT analysis of osmium stained tibiae for marrow adiposity reveals no difference between genotype.

Four regions of interest were analysed including (1) the tibia-fibular junction (T/F/J) to distal end of bone, (2) the growth plate (GP) to T/F/J, (3) the proximal epiphysis (Prox. Epi) and (4) the total bone. Data are presented as the mean ± S.E.M (n≥4).

3.4.9. Gross anatomy - body mass and long bone length of adult mice

Given that the analysis of 6-week old *Enpp1*$^{flox/flox}$;*Ocn*-cre and *Enpp1*$^{flox/flox}$ mice revealed a bone phenotype, the adult (22-weeks of age) mice were next investigated. The aim was to determine whether the genotype-specific differences observed in the *Enpp1*$^{flox/flox}$;*Ocn*-cre and *Enpp1*$^{flox/flox}$ juvenile mice were recapitulated in the developed skeleton of the 22-week old adult mice. As observed at 6-weeks of age, sex-specific differences were observed concerning the weight of mice at 22-weeks of age. Here, I observed that the male *Enpp1*$^{flox/flox}$;*Ocn*-cre mice were significantly heavier than the female *Enpp1*$^{flox/flox}$;*Ocn*-cre mice (30.99 g vs. 22.12 g; $P<0.001$) (Fig. 3.9A), and the same was true for *Enpp1*$^{flox/flox}$ male mice compared to *Enpp1*$^{flox/flox}$ female mice (31.90 g vs. 24.77 g; $P<0.001$). No difference in body weight was observed between genotype, suggesting that the osteoblast-specific NPP1 ablation is not significant to abrogate growth as observed in the global *Enpp1*$^{-/-}$ mice (Huesa et al., 2014). Regarding long bone length, no difference in length was observed between genotype for female mice regarding the tibiae (Fig. 3.9B) or femora (Fig. 3.9C). Male *Enpp1*$^{flox/flox}$;*Ocn*-cre mice exhibit increased tibiae length (17.80 mm vs. 17.32 mm; $P<0.05$), and decreased femora length (15.30 mm vs. 17.32 mm; $P<0.001$) compared to age-matched *Enpp1*$^{flox/flox}$ male mice (Fig. 3.9B, 3.9C). Furthermore, female 22-week old *Enpp1*$^{flox/flox}$ mice exhibited significantly shorter femora length compared to male *Enpp1*$^{flox/flox}$ (15.23 mm vs. 17.32 mm; $P<0.001$) (Fig. 3.9C) – an expected result given the significantly smaller size of female mice compared to male mice at this age.

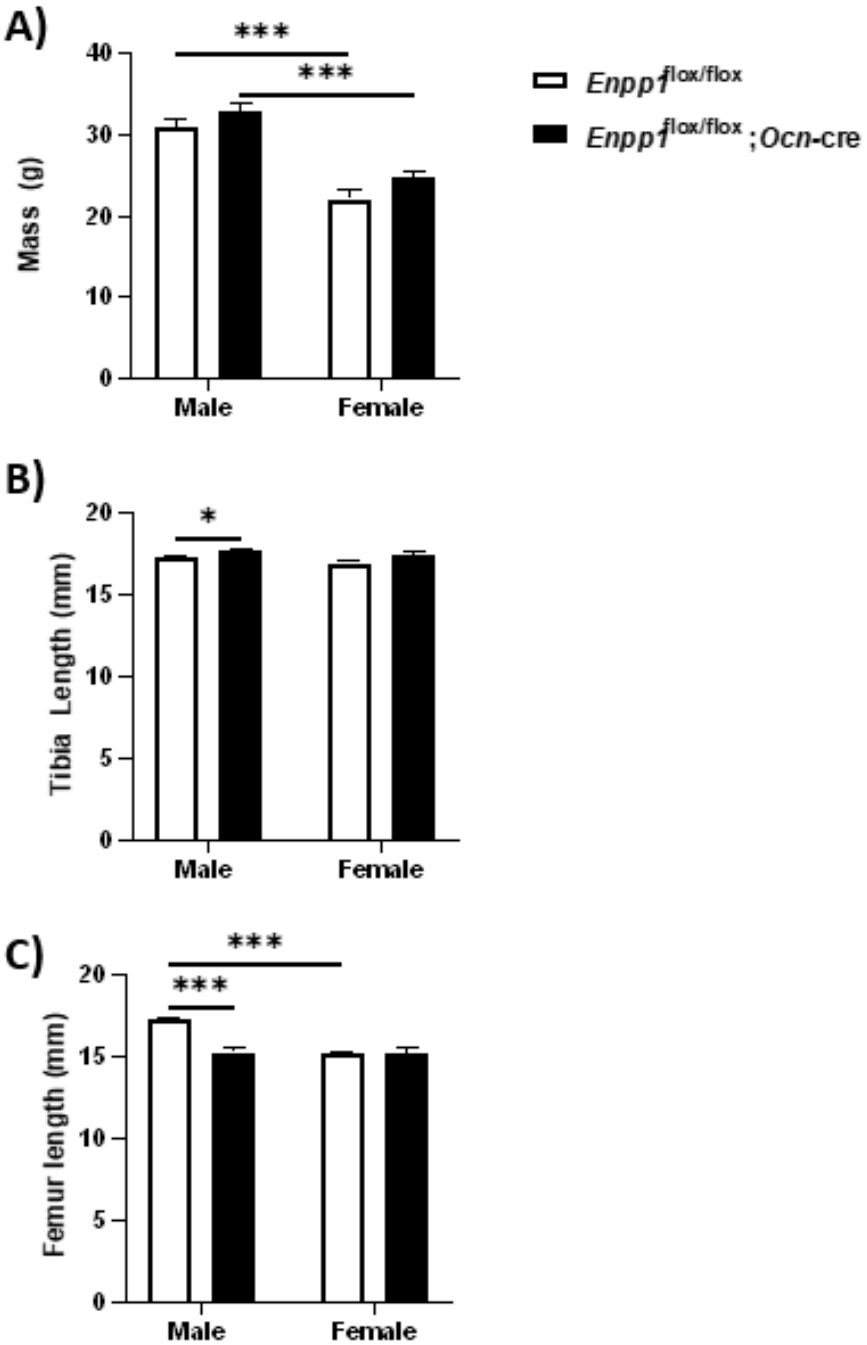

Figure 3.9. The mass and long bone length of male and female 22-week old mice demonstates genotype and sex-specific differences.

(A) The mass at 6-weeks of age for *Enpp1*$^{flox/flox}$;*Ocn*-cre and *Enpp1*$^{flox/flox}$ male and female mice and the (B) tibiae and (C) femora length. Dare represented as the mean ± S.E.M (n=6). Significance is denoted by **P*<0.05, ****P*<0.001.

3.4.10. Serum markers of bone resorption and formation in adult mice

Quantification of serum markers of bone resorption and formation showed no sex-specific differences for either *Enpp1*$^{flox/flox}$;*Ocn*-cre or *Enpp1*$^{flox/flox}$ mice at 22-weeks of age (Fig. 3.10A, 4.10B). Female mice showed no difference in bone resorption (CtX) (Fig. 3.13A) or bone formation (P1NP) markers between genotypes (Fig. 3.10B). Male *Enpp1*$^{flox/flox}$;*Ocn*-cre mice had similar Ctx levels (Fig. 3.10A) but significantly reduced P1NP levels (355.81 pg/ml vs. 535.32 pg/ml; $P<0.001$) compared to *Enpp1*$^{flox/flox}$ controls (Fig. 3.10B). This suggests that male *Enpp1*$^{flox/flox}$;*Ocn*-cre mice have a reduced osteoblast activity and the female *Enpp1*$^{flox/flox}$;*Ocn*-cre mice were unaffected.

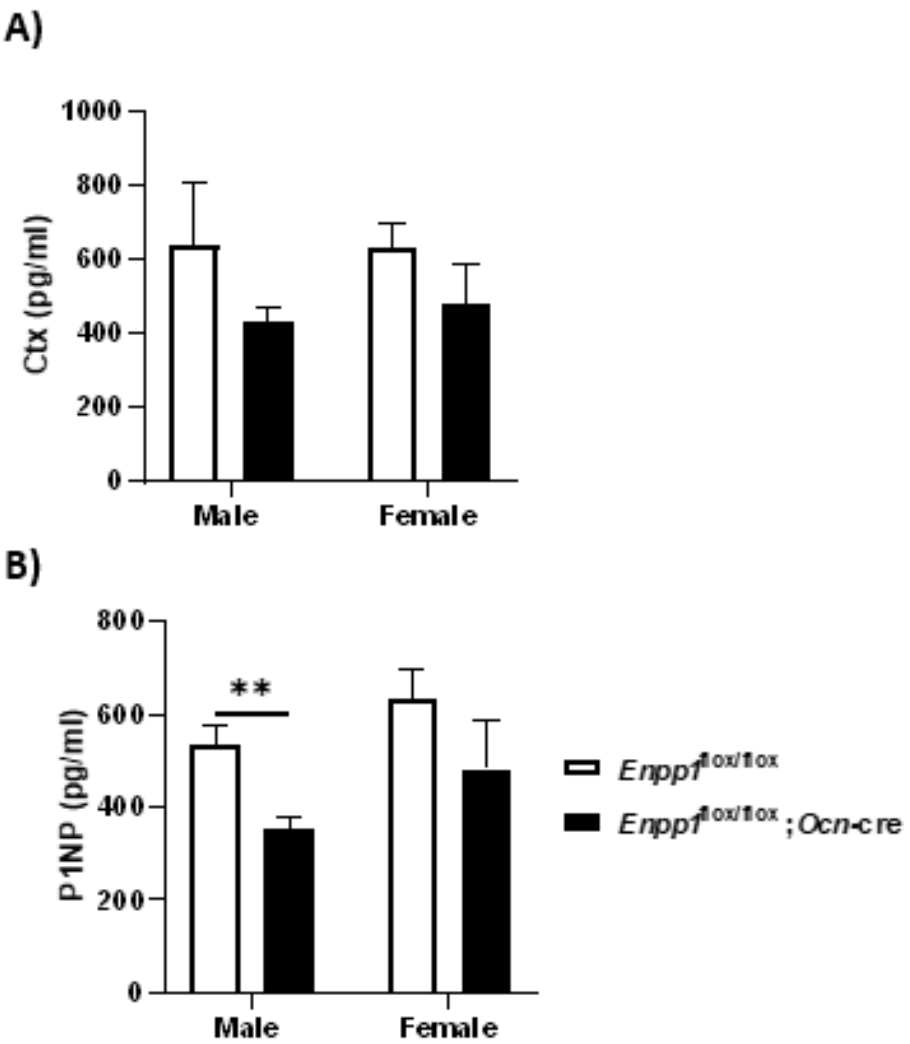

Figure 3.10. Serum concentration of Ctx and P1NP from male and female adult mice are largely unaltered between genotypes.

(A) marker of bone resorption (Ctx) and of (B) bone formation (P1NP). Data are presented as the mean ± S.E.M (n=6). Significance is denoted by, ***P*<0.01

3.4.11. μ-CT analysis of the long bones of adult mice

The investigation of the micro-architecture of 6-week old mice using μ-CT revealed notable significant difference between genotypes, evident mostly in the female cohorts. Upon analysis of the male 22-week old mice, no difference was observed between genotype regarding femora or tibiae trabecular (Table 3.8) or cortical (Table. 3.9) bone. As with the 6-week old mice, the changes were evident amongst the female cohorts. Female *Enpp1*$^{flox/flox}$;*Ocn*-cre mice exhibited significantly increased femora trabecular bone volume/tissue volume (13.34% vs. 7.79%; *P*<0.05), indicative of overall increased bone tissue compared to *Enpp1*$^{flox/flox}$ mice (Table 3.9). The female *Enpp1*$^{flox/flox}$;*Ocn*-cre mice showed significantly decreased femora structural model index (SMI) (1.72 vs. 2.12; *P*<0.05) which suggests a more plate-like, as opposed to rod-like, geometric organization of bone compared to the *Enpp1*$^{flox/flox}$ controls (Table. 3.10). Furthermore, the *Enpp1*$^{flox/flox}$;*Ocn*-cre female mice demonstrated increased trabecular number (2.43 vs. 1.57; *P*<0.05) compared to *Enpp1*$^{flox/flox}$ controls (Table 3.10).

When considering the cortical parameters, female 22-week old *Enpp1*$^{flox/flox}$;*Ocn*-cre mice also demonstrated increased bone mass. The femora endosteal diameter (Endo. Di) is significantly greater in the *Enpp1*$^{flox/flox}$;*Ocn*-cre mice compared to *Enpp1*$^{flox/flox}$ mice (1.66 mm vs. 0.84mm; *P*<0.05) (Table 3.9) indicating a wider bone. Additionally, the femora cortical bone volume was significantly increased in the *Enpp1*$^{flox/flox}$;*Ocn*-cre mice compared to *Enpp1*$^{flox/flox}$ mice (1.05 mm^3 vs. 0.59 mm^3; *P*<0.001) (Table 3.11). Largely, the tibiae cortical bone showed no changes between genotype in the parameters investigated, although trabecular thickness was significantly increased in the *Enpp1*$^{flox/flox}$;*Ocn*-cre mice compared to *Enpp1*$^{flox/flox}$ mice (0.17 mm vs. 0.13; *P*<0.05) (Table 3.11).

Bone	Genotype	BV/TV (%)	Tr. Pf.	SMI	Tr. Th. (mm)	Tr. No.	Tr. Sp. (mm)
Femur	*Enpp1*$^{flox/flox}$	16.03 (2.69)	17.12 (5.15)	1.63 (0.30)	54.38 (3.50)	2.92 (0.32)	0.201 (0.001)
	Enpp1$^{flox/flox}$;*Ocn*-cre	16.57 (2.23)	13.79 (3.20)	1.42 (0.18)	50.73 (2.14)	3.23 (0.35)	0.199 (0.007)
Tibia	*Enpp1*$^{flox/flox}$	14.44 (1.45)	20.81 (4.08)	1.93 (0.24)	53.33 (1.29)	2.71 (0.21)	0.199 (0.009)
	Ocn-Cre;Enpp1$^{flox/flox}$	16.32 (1.34)	16.87 (1.38)	1.65 (0.13)	50.15 (1.42)	3.21 (0.05)	0.187 (0.004)

Table 3.8. µ-CT analysis of tibiae and femora trabecular bone from 22-week male mice reveals no difference between genotypes.

The following parameters were measured; per cent bone volume (BV/TV), trabecular patterning factor (Tr. Pf.), structural model index (SMI), trabecular thickness (Tr. Th.), trabecular number (Tr. No.), trabecular spacing (Tr. Sp.). Data are presented as the mean ± S.E.M ($n \geq 6$).

Bone	Genotype	Peri. Di (mm)	Endo. Di (mm)	BV (mm^3)	Ct. Th (mm)	Po(op) (%)
Femur	*Enpp1*$^{flox/flox}$	2.56 (0.16)	2.15 (0.17)	0.92 (0.06)	173.29 (3.33)	2.43 (0.23)
	Enpp1$^{flox/flox}$;*Ocn*-cre	2.57 (0.09)	2.24 (0.10)	0.96 (0.03)	168.79 (4.84)	2.75 (0.20)
Tibia	*Enpp1*$^{flox/flox}$	1.97 (0.06)	1.37 (0.06)	0.91 (0.05)	156.61 (4.24)	4.87 (0.36)
	Ocn-Cre;Enpp1$^{flox/flox}$	2.05 (0.04)	1.55 (0.04)	0.98 (0.03)	162.53 (4.42)	4.88 (0.98)

Table 3.9. µ-CT analysis of tibiae and femora cortical bone from 22-week male mice reveals no difference between genotype.

The following parameters were measured; periosteal diameter (Peri. Di.), endosteal diameter (Endo. Di), bone volume (BV), cortical thickness (Ct. Th.), open porosity (per cent) (Po(op)). Data are presented as the mean ± S.E.M ($n \geq 6$).

Bone	Genotype	BV/TV (%)	Tr. Pf.	SMI	Tr. Th. (mm)	Tr. No.	Tr. Sp. (mm)
Femur	*Enpp1*$^{flox/flox}$	7.79 (4.50)	28.70 (16.57)	2.12 (1.23)	0.05 (0.03)	1.57 (0.91)	0.266 (0.15)
	Enpp1$^{flox/flox}$;*Ocn*-cre	13.34(1.52)*	16.60 (2.59)	1.72 (0.12)*	0.05 (0.001)	2.43 (0.23)*	0.24 (0.09)
Tibia	*Enpp1*$^{flox/flox}$	7.89 (3.47)	17.64 (7.79)	1.68 (0.55)	0.21 (0.18)	1.34 (0.50)	0.34 (0.08)
	Ocn-Cre;Enpp1$^{flox/flox}$	12.75 (1.29)	17.90 (3.02)	1.97 (0.12)	0.06 (0.002)	2.32 (0.38)	0.26 (0.03)

Table 3.10. **µ-CT analysis of tibiae and femora trabecular bone from 22-week female mice demonstrates significant differences in the femora.**

The following parameters were measured; per cent bone volume (BV/TV), trabecular patterning factor (Tr. Pf.), structural model index (SMI), trabecular thickness (Tr. Th.), trabecular number (Tr. No.), trabecular spacing (Tr. Sp.). Data are presented as the mean ± S.E.M ($n \geq 3$). Significance is denoted by *$P<0.05$.

Bone	Genotype	Peri. Di (mm)	Endo. Di (mm)	BV (mm^3)	Ct. Th (mm)	Po(op) (%)
Femur	*Enpp1*$^{flox/flox}$	1.14 (0.02)	0.84 (0.003)	0.59 (0.28)	0.11 (0.90)	1.72 (0.5)
	Enpp1$^{flox/flox}$;*Ocn*-cre	2.19 (0.07)	1.66 (0.05)*	1.04 (0.03)**	0.19 (0.004)	3.13 (0.18)
Tibia	*Enpp1*$^{flox/flox}$	1.16 (0.38)	0.74 (0.23)	0.73 (0.20)	0.13 (0.03)	3.34 (0.91)
	Ocn-Cre;Enpp1$^{flox/flox}$	1.63 (0.06)	1.05 (0.04)	1.00 (0.03)	0.17 (0.007)*	4.12 (0.03)

Table 3.11. µ-CT analysis of tibiae and femora cortical bone from 22-week female mice reveals significant differences between genotypes.

The following parameters were measured; periosteal diameter (Peri. Di.), endosteal diameter (Endo. Di), bone volume (BV), cortical thickness (Tb. Th.), open porosity (per cent) (Po(op)). Data are presented as the mean ± S.E.M (n≥3). Significance is denoted by *P<0.05, **P<0.01.

Analysis of the epiphyseal bone of 22-week old male mice revealed no micro-architectural differences between genotypes (Fig. 3.11A-3.11F). The female *Enpp1*$^{flox/flox}$;*Ocn*-cre exhibited increased epiphyseal trabecular number (5.60 vs. 5.03; *P*<0.01) (Fig. 3.11B) and a decreased trabecular pattern factor compared to *Enpp1*$^{flox/flox}$ mice (7.06 vs 13.83; *P*<0.05) indicating a greater quantity and connectedness of trabeculae (Fig. 3.11E). All other parameters were unchanged between genotypes for female mice.

Whilst 6-week old mice revealed largely no micro-architectural differences to the subchondral bone, changes regarding the subchondral bone were more evident at 22-weeks of age. For male mice, only the medial trabecular thickness showed genotype changes, whereby the male *Enpp1*$^{flox/flox}$;*Ocn*-cre mice exhibited increased thickness (0.10 mm vs. 0.08 mm; *P*<0.05) compared to *Enpp1*$^{flox/flox}$ control mice (Fig. 3.12E). As with the majority of μ-CT findings, significant differences between genotypes were most prolific amongst the female cohorts of mice. Indeed, female *Enpp1*$^{flox/flox}$;*Ocn*-cre mice demonstrated increased lateral subchondral bone volume (0.28 mm^3 vs. 0.21 mm^3; *P*<0.05) (Fig. 3.12A), increased lateral subchondral bone trabecular thickness (0.10 mm vs. 0.08 mm; *P*<0.001) (Fig. 3.12B), increased medial subchondral bone volume (0.26 mm^3 vs 0.20 mm^3; *P*<0.05) (Fig. 3.12D) and increased medial subchondral bone trabecular thickness (0.10 mm vs. 0.08mm; *P*<0.01) (Fig. 3.12E) compared to female *Enpp1*$^{flox/flox}$ mice. Neither male nor female mice showed a genotype-specific difference in subchondral bone porosity (Fig. 3.12C).

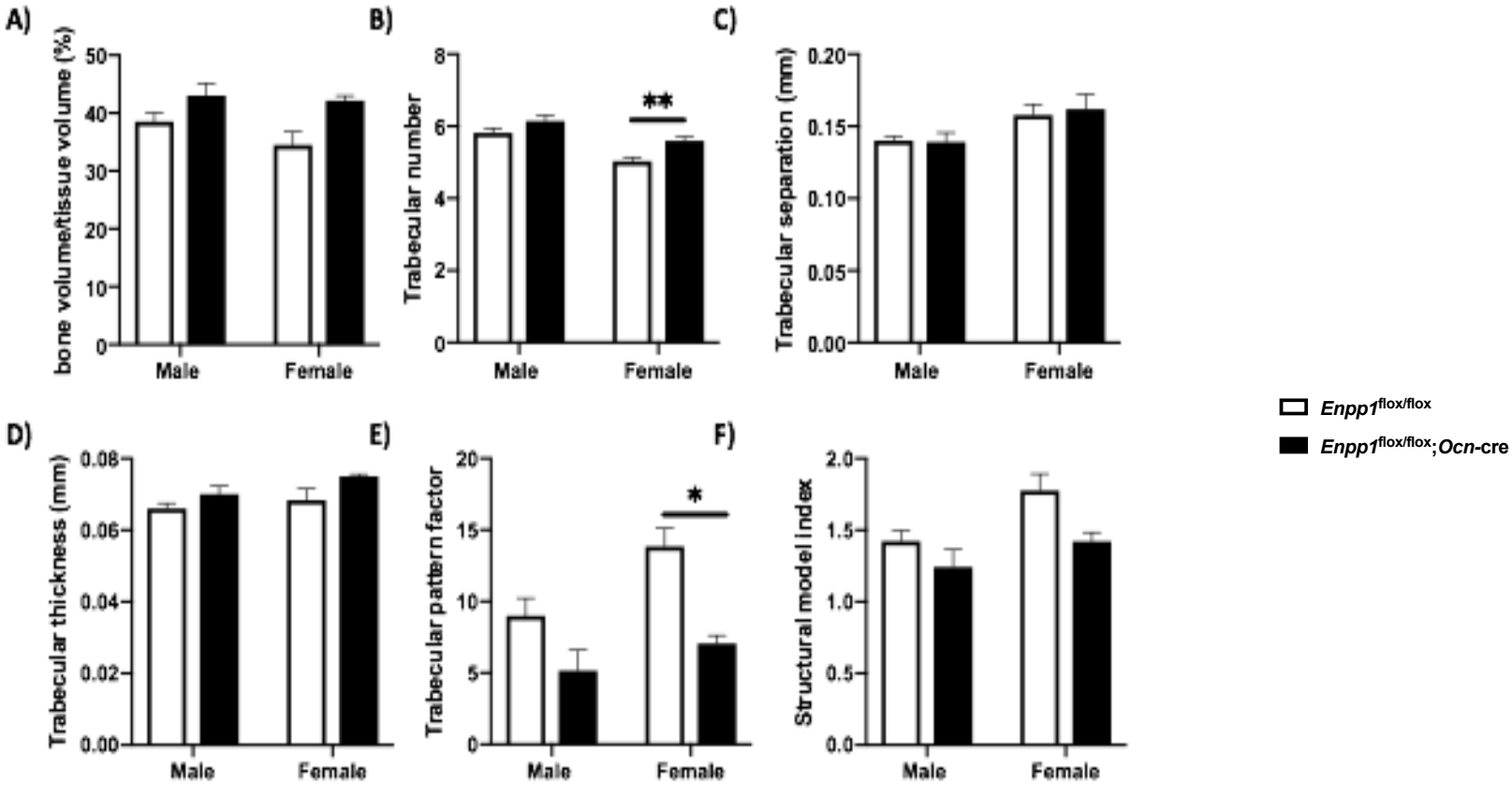

Figure 3.11. µ-CT analysis of the epiphyseal bone from male and female mice reveals significant differences between genotype for female mice.

The parameters analysed include the trabecular (A) bone volume/tissue volume, (B) trabecular number, (C) trabecular separation, (D) trabecular thickness, (E) trabecular pattern factor and (F) structural model index. Data are presented as the mean ± S.E.M (n≥3). Significance is denoted by **P*<0.05.

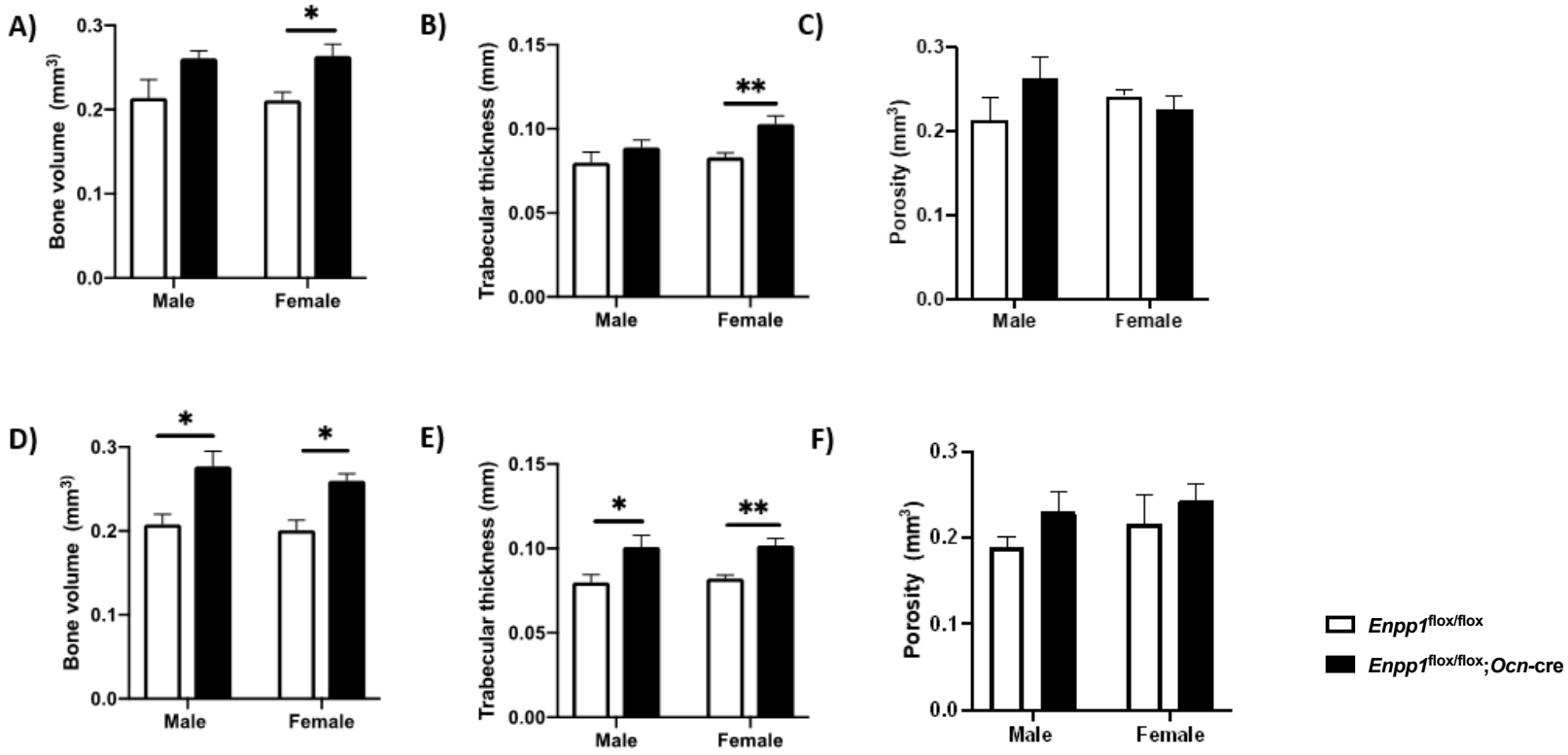

Figure 3.12. µ-CT analysis of the lateral and medial subchondral bone from 22-week old male and female mice reveals genotype specific differences.

The subchondral bone parameters measured include (A) lateral bone volume, (B) lateral trabecular thickness, (C) lateral porosity, (D) medial bone volume, (E) medial trabecular thickness and (F) medial bone porosity. Data are presented as the mean ± S.E.M (n≥3). Significance is denoted by **P*<0.05, ***P*<0.01.

3.4.12. Analysing the mechanical properties of long bones in adult mice

To determine whether the alterations in the 22-week old long bones translates to altered mechanical properties, three-point bending analysis was performed. For both female and male mice, no differences in mechanical properties of the tibia and femora were observed between genotypes (Table. 3.12, 3.13). There was one exception however, female *Enpp1*$^{flox/flox}$;*Ocn*-cre tibiae exhibit increased deflection at rupture compared to female *Enpp1*$^{flox/flox}$ mice (0.95643 mm vs. 0.58949 mm; $P<0.05$).

3.4.13. Analysing bone mineral density of long bones of adult mice

To determine whether osteoblast-specific NPP1 ablation resulted in long-term alterations to bone mineral density, bone mineral density of 22-week old mice long bones were determined using μ-CT analysis. Analysis revealed largely similar bone mineral density in male and female mice of both genotypes which included the tibiae cortical (Fig. 3.13A) trabecular (Fig. 3.13B) and the femora trabecular (Fig. 3.13D) bone. Whilst, the femora cortical bone mineral density was similar in male mice of different genotypes it was significantly decreased in female *Enpp1*$^{flox/flox}$;*Ocn*-cre mice compared to female *Enpp1*$^{flox/flox}$ mice (0.21 mg/cm^3 vs. 0.30 mg/cm^3; $P<0.05$) (Fig. 3.13C).

Sex	Genotype	Maximum Load (N)	Deflection at Maximum Load (mm)	Work to Maximum Load (J)	Stiffness (N/m)	Load at Rupture (N)	Deflection at Rupture (mm)	Work to Rupture (J)
Female	*Enpp1*$^{flox/flox}$	12.69966 (1.6)	0.42100 (0.0)	0.00269 (0.0)	54310.34796 (6873.2)	8.88976 (1.1)	0.44410 (0.1)	0.00296 (0.0)
	Enpp1$^{flox/flox}$;*Ocn*-cre	13.46749 (1.4)	0.42038 (0.0)	0.00281 (0.0)	62177.38960 (6991.7)	9.42725 (1.0)	0.57964 (0.1)	0.00484 (0.0)
Male	*Enpp1*$^{flox/flox}$	13.88379 (0.9)	0.45496 (0.0)	0.00337 (0.0)	51344.89394 (8073.9)	9.71865 (0.6)	0.65151 (0.0)	0.00567 (0.0)
	Ocn-Cre;Enpp1$^{flox/flox}$	15.70142 (1.6)	0.43553 (0.0)	0.00360 (0.0)	56149.58460 (13693.2)	10.99100 (0.1)	0.55927 (0.1)	0.00528 (0.0)

Table 3.12. 3-point bending of 22-week old femora demonstrates unaltered function as a result of osteoblast-specific NPP1 ablation.

Values are shown for femora dissected from 6-weeks and 22-weeks of age from female and male *Enpp1*$^{flox/flox}$;*Ocn*-cre and *Enpp1*$^{flox/flox}$ mice. Bones were tested to fracture, whereby fracture points were identified from the load-extension curve whereby the maximum load decreased rapidly to 70% of the maximum value. The maximum stiffness was defined as the maximum gradient of the rising portion of the load-extension curve. Data are presented as mean ± S.E.M (n≥6). No significant findings.

Sex	Genotype	Maximum Load (N)	Deflection at Maximum Load (mm)	Work to Maximum Load (J)	Stiffness (N/m)	Load at Rupture (N)	Deflection at Rupture (mm)	Work to Rupture (J)
Female	*Enpp1*$^{flox/flox}$	9.06721 (1.0)	0.47210 (0.0)	0.00220 (0.0)	43413.66196 (17904.9)	5.78719 (0.6)	0.58949 (0.0)	0.00568 (0.0)
	Enpp1$^{flox/flox}$;*Ocn*-cre	8.41447 (0.2)	0.62041 (0.1)	0.00318 (0.0	23008.40164 (537.8)	5.87139 (0.2)	0.95643 (0.1)*	0.00576 (0.0)
Male	*Enpp1*$^{flox/flox}$	8.79618 (0.4)	0.51960 (0.0)	0.00244 (0.0)	25682.26337 (3135.1)	6.31046 (0.5)	0.65009 (0.1)	0.00463 (0.0)
	Ocn-Cre;Enpp1$^{flox/flox}$	8.97221 (0.3)	0.55040 (0.0)	0.00248 (0.0)	24944.95816 (2891.6)	6.28055 (0.6)	0.82220 (0.1)	0.00438 (0.0)

Table 3.13. 3-point bending showing largely unaltered mechanical strength of 22-week old tibiae.

Values are shown for femora dissected from 6-weeks and 22-weeks of age from female and male *Enpp1*$^{flox/flox}$;*Ocn*-cre and *Enpp1*$^{flox/flox}$ mice. Bones were tested to fracture, whereby fracture points were identified from the load-extension curve whereby the maximum load decreased rapidly to 70% of the maximum value. The maximum stiffness was defined as the maximum gradient of the rising portion of the load-extension curve. Data are presented as mean ± S.E.M (n≥6). Significance is denoted by *P<0.05.

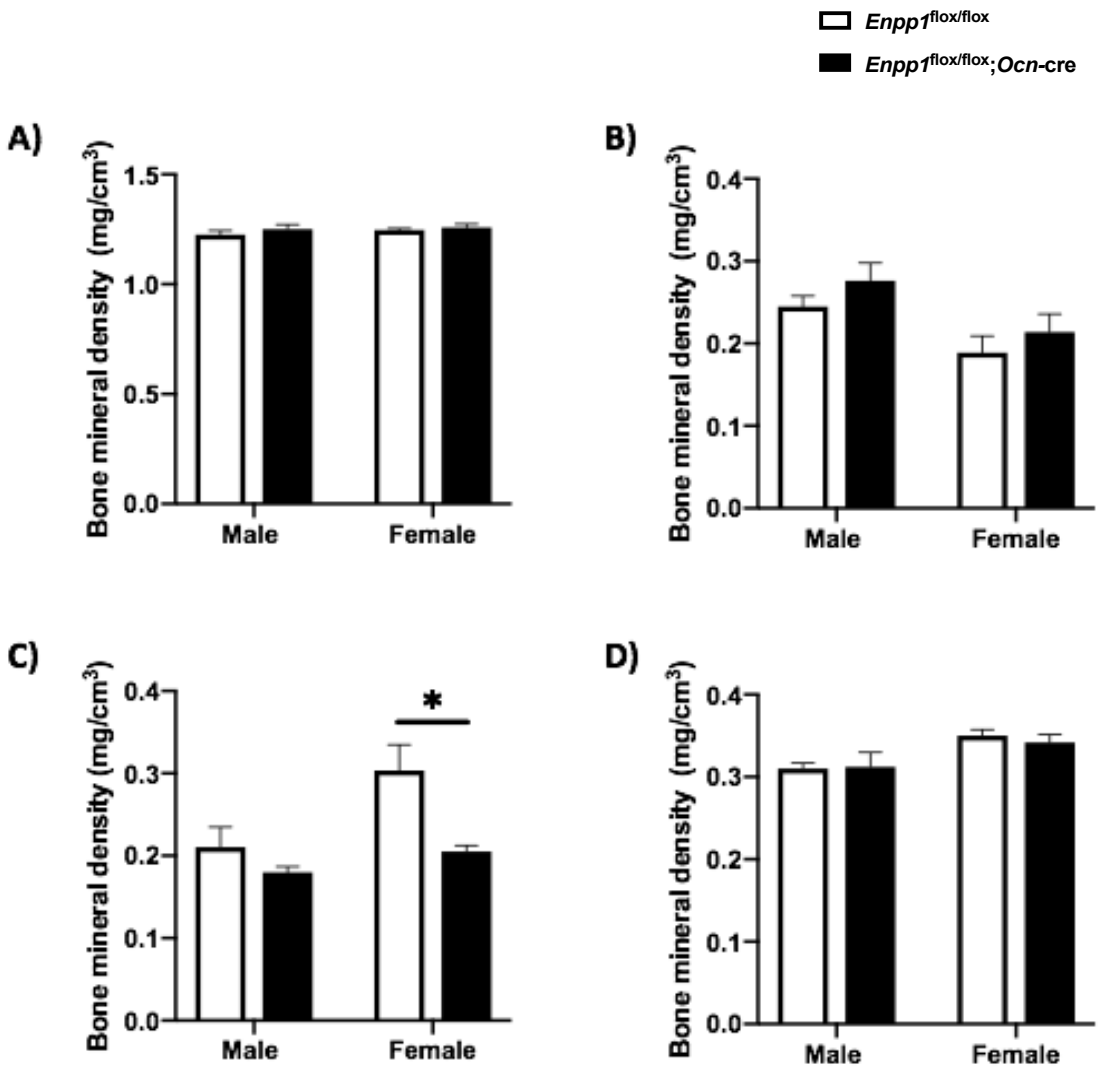

Figure 3.13. Tibiae and femora cortical and trabecular bone mineral density of 6-week female mice demonstrates largely no differences between genotype.

(A) Tibiae cortical and (B) trabecular bone mineral density. (C) femora cortical and (D) trabecular bone mineral density. Data are presented as the mean ± S.E.M (n≥3). Significance denoted by **P*<0.05.

3.5. Discussion

As detailed in section 4.1, previous studies have demonstrated that NPP1 is critical in the regulation of skeletal mineralisation (Okawa et al., 1998b, Hessle et al., 2002, Johnson et al., 2003, Johnson et al., 2005, Li et al., 2013, Li et al., 2014b, Albright et al., 2015). These studies involved the use of global knockouts or naturally occurring mutants of *Enpp1*. As such, the cell-specific contributions of NPP1 to the observed skeletal phenotype remain unknown.

The current study demonstrates that juvenile osteoblast-specific NPP1 knockout mice have largely unaltered body-weight, contradicting the findings of global *Enpp1*$^{-/-}$ mice which present with significantly reduced body weight at 6-weeks of age (Huesa et al., 2014). The long bone length of osteoblast-specific NPPP1 were unaffected, reflecting findings observed for global *Enpp1*$^{-/-}$ mice (Huesa et al., 2014). Furthermore, the markers of resorption and formation of bone were unchanged, again reflecting findings observed for 6-week old global *Enpp1*$^{-/-}$ mice, suggesting unaltered osteoblast and osteoclast activity (Huesa et al., 2014).

This study revealed that the systemic (serum) concentration of PP_i was similar in both osteoblast-specific NPP1 knockout mice and their controls. This contradicts findings in *Enpp1* global knockout and mutated mice, whereby serum PP_i is routinely reported as decreased (Sakamoto et al., 1994, Okawa et al., 1998b, Okawa et al., 1999, Rutsch et al., 2001, Hessle et al., 2002). These findings indicate that the ablation of NPP1 in osteoblasts cannot recapitulate the alterations to systemic PP_i observed when NPP1 is deleted within every tissue. It is likely that the liver, which is reported as a major contributor of systemic PP_i, generating up to 60% of overall PP_i, generates significant quantities of PP_i in the osteoblast-specific knockout mouse such that systemic PP_i is unaltered between genotypes (Terkeltaub, 2001, Terkeltaub, 2006). This likely explains the absence of pathological (ectopic) joint and soft tissue mineralisation observed in the osteoblast-specific NPP1 knockout mice, whereas the global *Enpp1*$^{-/-}$ mice present with aberrant and pathological aortic and kidney mineralisation likely due to systemically decreased PP_i (Mackenzie et al., 2012). An alternate hypothesis exists that tissues undergo mineralisation due to the local (i.e. tissue-specific) levels of PP_i. To further investigate this, alternate cell-specific NPP1 ablated mouse models should be developed and characterised regarding the mineralisation capacity of tissue

whereby the enzyme is no longer present. One such example would be the liver-specific NPP1 conditional knockout.

Previous investigations of global *Enpp1*$^{-/-}$ mice have demonstrated reduced long bone mineral content, with reduced bone volume fraction and trabecular thickness (Mackenzie et al., 2012). This finding is intriguing, given that the majority of studies looking at *Enpp1* knockout mice have reported an accompanying decrease of systemic PP_i concentration. One would expect this decreased PP_i to be associated with increased bone formation. The paradoxical hypermineralisation of soft tissue and joints alongside decreased long bone mineralisation and bone volume observed in the global *Enpp1* knockout mouse indicates that the mechanism through which NPP1 exerts its control of mineralisation are complex and multiple (Mackenzie et al., 2012, Huesa et al., 2014). This led to the hypothesis that there are cell-specific contributions towards the multiple possible mechanisms of NPP1 function. Indeed, it is evident that there are liver cell-specific contributions of NPP1 in regarding metabolic phenotype. A virus-mediated liver-specific *Enpp1* deficient mouse model demonstrated a 25% lower plasma glucose (Zhou et al., 2009). However, until this point the osteoblast-specific actions of NPP1 regarding both metabolic and skeletal phenotype was unknown. Interestingly, the osteoblast-specific *Enpp1* mouse model analysis reported in this chapter did not reveal significantly increased systemic PP_i – contradictory to the global *Enpp1* knockout. This indicates an extra-osteoblastic role of NPP1 in regulation of systemic serum PP_i.

To determine whether micro-architectural changes occurred in the long bones as a result of osteoblast-specific NPP1 ablation a comprehensive high-resolution μ-CT analysis was conducted. This included the regions of mid-diaphyseal cortical and trabecular bone, the epiphyseal trabecular bone, the lateral subchondral bone of the femorotibial joint, and the medial subchondral bone of the femorotibial joint. Most notably, this work for the first time demonstrated that the ablation of NPP1 (at the site of the osteoblast) resulted in an increased bone mineral density. As such, the suggested mechanism of local reduction of PP_i due to decreased local NPP1 activity (in the osteoblast) drives an increase in mineral deposition within the ECM.

The 6-week old mice with an osteoblast-specific NPP1 ablation present with a notable skeletal phenotype, whereby there is an increase in bone mass and bone volume. This is in keeping with my hypothesis for this mouse model. This was confirmed at multiple levels, including comprehensive μ-CT analysis. The 6-week old *Enpp1*$^{flox/flox}$;*Ocn*-cre demonstrate notable differences in the trabecular and cortical mid-diaphyseal femora and cortical parameters indicative of overall increased bone tissue. It is important to note here that the genotype-specific differences observed in μ-CT were more prolific amongst female mice compared with male mice. Furthermore, the data presented in this chapter indicates that the architectural alterations observed in the 6-week old *Enpp1*$^{flox/flox}$;*Ocn*-cre bones does not translate to altered biomechanics in the juvenile age. As the skeleton is still developing at this age time point, it is pertinent to look at later time points (*e.g.* once skeletal maturity has been reached) to see if the results noted here are recapitulated in a mature skeleton.

The μ-CT analysis revealed notable differences in bone architecture between genotypes. Alterations to bone architecture are known to be associated with changes to mechanical function. To determine whether the osteoblast-specific NPP1 ablation resulted in ability to resist load as a product of altered architecture, 3-point bending assessment was conducted. No notable difference in mechanical function were observed, suggesting that the changes observed in μ-CT are not able to alter the mechanical function of the bone.

The use of histological analysis of the bone (distal femora) of 6-week old mice supported the findings of μ-CT, indicating increased *Enpp1*$^{flox/flox}$;*Ocn*-cre bone mass. This observation was more evident in female juvenile cohorts and less evident in male cohorts. Histological analysis revealed increased bone marrow adiposity in *Enpp1*$^{flox/flox}$;*Ocn*-cre mice, however, this was not reflected in the more detailed μ-CT analysis of osmium stained bones; this is suggestive of non-uniform dispersal of marrow adipose tissue throughout the bone. A deleterious imbalance of adipocytes and osteoblasts are commonly reported in pathological situations including ageing and diabetes – whereby an increase in bone marrow adipose tissue occurs at the expense of osteoblast renewal (Justesen et al., 2001, Botolin and McCabe, 2007, Muruganandan et al., 2009)

This occurs due to the common progenitor lineage of mesenchymal stem cells for adipocytes and osteoblasts (Caplan, 1991, Teitelbaum, 2000). Furthermore, the adipocytes are reported to secrete a large number of signalling molecules that can affect bone homeostasis and bone remodelling (*e.g.* adiponectin) (Pajvani et al., 2003). The absence of adipocyte changes observed in the *Enpp1*$^{flox/flox}$;*Ocn*-cre mice at this stage indicates protection against, or at least absence, of the pathological osteoblast/bone marrow relationship. To further investigate this, it is necessary to conduct a metabolic challenge for the osteoblast-specific NPP1 knockout mice to induce a diabetic phenotype and investigate potential pathological effects of marrow adipose tissue expansion during caloric excess and glucose dysregulation in the mouse model (as discussed in chapter 6). Taken together, this histomorphometry analysis indicates an increase in the mineralised tissue alongside a reduction in osteoid tissue and potential increased bone marrow adiposity, most evident in female cohorts of *Enpp1*$^{flox/flox}$;*Ocn*-cre compared to *Enpp1*$^{flox/flox}$ controls.

The investigation of skeletal phenotype continued, whereby the adult 22-week old mice were next assessed. Here, the expected sex-different results were observed, including longer length bones in male mice compared to female mice. The female *Enpp1*$^{flox/flox}$;*Ocn*-cre mice demonstrate no differences in bone length, however, the male *Enpp1*$^{flox/flox}$;*Ocn*-cre mice exhibited increased tibiae and decreased femora length which is suggestive of altered loading on the long bones. The relationship between loading and altered bone growth plate dynamics is published, indicating increased growth plate chondrocytes resultant of sustained mechanical loading (Stokes et al., 2002). Alterations to bone length in association with load in mouse models is also well published. For example, Killion *et al.,* demonstrate that paralysis of a mouse hind limb by disruption of the sciatic nerve at post-natal day 8 results in altered gait and altered load. These mice present with significantly reduced bone limb length at 8-weeks of age as a result of decreased loading, with the contralateral limb of the same mouse used as control (Killion et al., 2017).

Largely no differences were observed in the markers of bone formation or resorption at 22-weeks, reflecting the 6-week old mice, and as such, the altered femora length is not attributed to altered osteoblast or osteoclast activity in the 22-week old mice. The difference

in bone length may also be attributable to the difference in sex hormones between male and female mice. It is well established that testosterone treatment results in an increase in bone accrual, and that androgens cause an upregulation of the androgen receptor on osteoblasts (Kasperk et al., 1997, Wiren et al., 1997, Wiren et al., 1999, Khosla et al., 2001, Seeman, 2001). Therefore, the greater long bone length observed in the male *Enpp1*$^{flox/flox}$;*Ocn*-cre mice compared to female counterparts is likely endocrine-related (Ornoy et al., 1994).

The data presented in this chapter demonstrates significant changes for both male and female *Enpp1*$^{flox/flox}$;*Ocn*-cre mice cortical porosity. One limitation of this dataset is related to the voxel scanning resolution. A standard scanning resolution of 4-5 μm was used in this thesis for the assessment of long bones via μ-CT analysis (Basillais et al., 2007, Cardoso et al., 2013). However, a resolution of less than 4 μm (ideally 1 μm) should be used to separate the vascular porosity from osteonal canals (Palacio-Mancheno et al., 2014). Indeed, it is reported that at a 4 μm resolution, vascular porosity and vascular canal diameters were underestimated, osteocyte lacunae was poorly detected and vascular canal separation was over-estimated (compared to 1 μM scans) in Sprague Dawley rat long bones. Regarding the data in this thesis, no difference in osteoclast activity was observed in the osteoblast-specific NPP1 ablated mice. As such, we can posit that the altered porosity observed was not due to increased osteoclast activity/altered osteoblast and osteoclast balance (and associated osteoporotic phenotype) (Teitelbaum, 2000). To support the μ-CT data, a detailed histomorphometric analysis of the cortical bone porosity may have been conducted using established protocols such as that described by Qiu *et al.* (Qiu et al., 2003), although this too has limitations including variability or practice between individuals.

In addition, the cortical porosity of the tibiae and femora was assessed at one particular anatomical region, specifically a 1 mm region which is 0.4 mm from the growth plate. The micro-porosity of bone plays an important role in bone biology and in the mechanical quality of the bone. Assessing porosity has often been conducted in order to investigate mechanical property of bone. However, recent findings by Nunez *et al* demonstrate that the posterior region of the tibiofibular junction of 15 week old mice have higher porosity (in the form of vascular canals) compared to the anterior, lateral and medial regions. Furthermore, the

anterior and posterior regions of intracortical vascular networks were assessed and demonstrated notable differences in porosity (Nunez et al., 2018). This translated into thinner cortices within the posterior cortex after 10 months of life, with no changes to the rest of the cortex (Nunez et al., 2018). By not assessing porosity in this more detailed way, potential regional changes in the *Enpp1*$^{flox/flox}$;*Ocn*-cre may have been overlooked.

It is recognised in several animal species that subchondral bone plays an important role in supporting the functional loading (exercise) of a joint following locomotion, along with articular cartilage (Camp et al., 2014, Smith et al., 2016, Adebayo et al., 2017, Li et al., 2017b, Fang et al., 2018). When derangements of the subchondral bone occur, progression to osteoarthritis may follow (Lajeunesse et al., 2003). The subchondral bone is a dynamic tissue, which can respond to various stresses, including acute and prolonged (chronic) joint stress (Radin and Rose, 1986, Young et al., 1991, Ding, 2010). The thickening of the trabecular bone, as observed in the *Enpp1*$^{flox/flox}$;*Ocn*-cre mice, is associated with increased subchondral bone modelling, which in turn can lead to stiffer bones, with decreased elasticity and shock absorption (Radin et al., 1970, Goldring, 2009, Ding, 2010). These findings suggest that the subchondral bone is thickening, resulting in a stronger bone. This may be due to the increased or altered activity of osteoblasts at the subchondral site, or decreased osteoclastic activity in the *Enpp1*$^{flox/flox}$;*Ocn*-cre mice.

The global *Enpp1*$^{-/-}$ mice present with changes consistent with an osteoarthritic phenotype (Jin et al., 2018). Indeed, an alternate explanation could exist for the thickening of the *Enpp1*$^{flox/flox}$;*Ocn*-cre mice subchondral bone. This may be observed when the subchondral bone is no longer able to compensate for physiological stresses and the subchondral bone thickens, which affects the ability of the articular cartilage to withstand mechanical load due to increased stress at the base of the articular cartilage (Sophia Fox et al., 2009). This typically manifests as deep, horizontal clefts within the articular cartilage, and perpetuates osteoarthritic changes within the joint (Stewart and Kawcak, 2018). The resultant maladaptive bone modelling can manifest as a mechanical failure (whereby the bone fractures) or as subtler changes whereby the ability of bone to sustain activity demands occurs.

To conclude, a greater number of significant differences in the bone phenotype are evident in the female juvenile osteoblast-specific NPP1 ablated mice, notably increased bone mass. The *Enpp1*$^{flox/flox}$;*Ocn*-cre mice potentially have decreased local PP_i, which leads to this altered bone phenotype with concomitant unchanged systemic PP_i levels. This may explain the bone-specific mineralisation changes and the absence of ectopic calcification in the *Enpp1*$^{flox/flox}$;*Ocn*-cre mice. The absence of altered biomechanical properties of *Enpp1*$^{flox/flox}$;*Ocn*-cre mice suggests that the increase in bone formation does not alter the bone functionality. As such, the osteoblast-specific NPP1 is important in the regulation of skeletal formation and mineralisation. Additionally, the absence of osteoblast-specific NPP1 is not enough to recapitulate the severe mineralisation defects observed in the global NPP1 knockout mice (Huesa et al., 2014).

Therefore, NPP1 from other organs, such as the liver, is likely to play a role in the regulation of mineralisation. The potential role of other organs and more complex mechanisms through which NPP1 may exert its action will be discussed in chapter 7. To further understand the osteoblast-specific NPP1 ablated mouse model mineralisation phenotype, particularly at a mechanistic level, it was important to establish an *in vitro* model of the NPP1 ablated osteoblasts. This further analysis aimed to assess the calcification propensity and possible mechanisms underlying the minerlisation phenotype, to determine whether this reflects the basic and functional bone phenotype at the gross level. The use of cell lines and primary cell culture to asses these themes is described in Chapter 4.

(*This page has been left intentionally blank)*

Chapter 4. Investigating the profile of *Enpp1* expression during osteoblast matrix mineralisation *in vitro*.

4.1 Introduction

As is discussed in chapter 1, the formation of bone is a tightly coordinated process which involves osteoblasts. The newly laid down osteoid becomes mineralised, whereby osteoblasts mineralise their ECM by promoting the formation of HA crystals (Caetano-Lopes et al., 2007). This involves a highly regulated series of physiochemical and biochemical processes. The process of mineralisation relies upon levels of Ca^{2+} and P_i which, when at saturation levels, permit the initiation of HA crystal formation. This, in turn, is governed by the actions of a large network consisting of mineralisation promoters and mineralisation inhibitors (Fig. 4.1).

Although found in virtually all cell types (*e.g.* liver, kidney, brain) (Harahap and Goding, 1988), there is a relatively higher expression of ENPP1 (and thus ENPP1-specific activity) in osteoblasts and chondrocytes, where it plays a major role in the regulation of HA mineral nucleation (Terkeltaub, 2006). This is regulated through the catabolism of ATP through hydrolysis to generate PP_i which potently inhibits the accumulation of HA crystals and thus mineralisation (Meyer, 1984). It is the balance of PP_i generation relative to the PP_i degradation (yielding P_i) which holds the extracellular PP_i levels in check and thus regulates the pro/anti mineralisation environment. It is important to note that there are other sources of P_i generation as demonstrated in Fig 4.1. This ensures that pathological calcification is avoided and physiological mineralisation permitted. The absence of the ENPP1-catalysed generation of PP_i *in vivo* results in a striking spontaneous calcification which has been demonstrated in a variety of different mouse models (Hosoda et al., 1981, Okawa et al., 1998a, Banakh et al., 2002, Anderson et al., 2004, Anderson et al., 2005b, Terkeltaub, 2006, Babij et al., 2009). The generation of PP_i by ENPP1 also provides a substrate reservoir for the action of ALP-catalysed P_i generation, a pro-mineralising phenomenon. The coordinated actions of these two proteins regulate the ratio of PP_i/P_i. Disruptions to this ratio results in abnormal calcification: this is evident in several naturally occurring diseases (GACI, PXE, and hypophosphatasia) (Choi et al., 2011, Bishop, 2015, Nitschke and Rutsch, 2017).

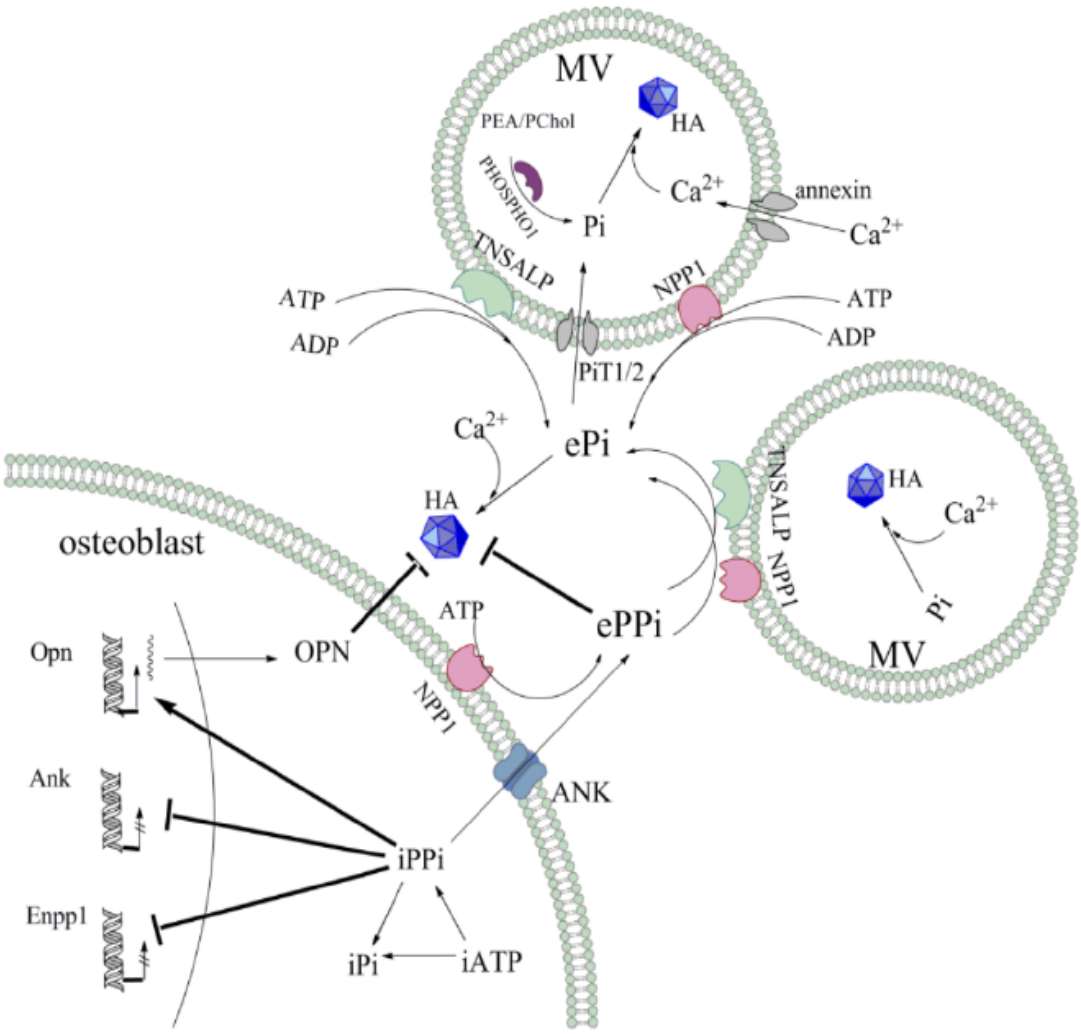

Figure 4.1. A schematic representation of regulators involved in mineralisation.

The HA crystals are composed of P_i and Ca^{2+}. In the MVs, P_i is generated by the function of PiT1/2, as well as by the hydrolysis of the phosphomonoesters including PEA and PChol by PHOSPHO1. The Ca^{2+} transport is mediated by annexin channels that allow influx into the MVs. The extracellular pyrophosphate (ePP_i) pool is derived both by NPP1 which generates PPi via ATP hydrolysis. Additionally, ePP_i is transported to the extracellular by ANK transporter at the level of the chondrocyte and osteoblast membranes. For both tissue non-specific alkaline phosphatase (TNSALP) and NPP1, the hydrolysis of ATP, ADP and PP_i contributes to the extracellular P_i (eP_i) pool, though TNSALP is more efficient than NPP1 at the level of the MVs. Moreover, a negative feedback loop exists in intracellular. PPi, which is produced by NPP1 and transported by ANK, inhibits the expression of *Enpp1* and *Ank*. Together with ePP_i, *Opn* expression inhibits HA crystal propagation and growth (Zhou et al., 2012)

The osteoblast is key to the formation of bone, both in early development and throughout the lifespan, whereby osteoblasts facilitate the repair of damaged bone and the formation of bone in response to mechanical demand (Frost, 1994). To study bone development, notably concerning humans, non-invasive research techniques needed to be created and used. The development of *in vitro* cell culture models, including cells lines and use of primary cells has catalysed our gain-of-knowledge for bone formation and the mechanisms/interactions involved.

To study osteoblast matrix mineralisation, a variety of clonal cell model systems have been previously employed. The most commonly used cell line to investigate osteoblast matrix mineralisation is the MC3T3-E1 – an osteoblast-like clonal and non-transformed cell line. This cell line was first isolated and reported in 1981 (Kodama et al., 1981, Sudo et al., 1983). There are over 50 sub-clones of MC3T3 cells (Wang et al., 1999b). Of these sub-clones, MC3T3-E1 sub-clone c14 represents a fast mineralising sub-clone (Houston et al., 2016). In the presence of ascorbic acid (AA) and β-glycerophosphate (β-GP), these cells are reported to develop nodules of mineralisation (Franceschi and Iyer, 1992, Chentoufi et al., 1993, Beck et al., 2000). It is important to note that cell lines themselves may not fully represent the primary cells from which they were developed. Due to this, the scientific community has increasingly used primary cells (in this case, primary osteoblasts) isolated commonly from the calvaria and less commonly from long bones (such as the femur) (Taylor et al., 2014). This line of investigation is of increasing importance when considering the specific contributions of a gene, tissue, or cell type to a phenomenon. As such, the use of primary osteoblast cell culture to investigate matrix mineralisation and temporal changes throughout the time course of mineralisation was fully utilised in this study and described within.

The previous chapter has demonstrated an increase in mineralisation and bone formation at the site of the long bone, including the tibia and the femora, for the osteoblast-specific ablated mouse model. These changes are evident at the microarchitectural level. However, it is not evident from the bone phenotyping of chapter 3 whether there are altered cellular capabilities for mineralization regarding the osteoblast-specific NPP1 ablated mouse model.

This chapter aimed to assess the osteoblasts function by using the well established isolation of osteoblasts form the calvaria of experimental mice.

4.2. Hypothesis

I hypothesised that primary osteoblasts isolated from the *Enpp1*$^{flox/flox}$;*Ocn*-cre mouse will have a more rapid onset of matrix mineralisation (cultured in mineralising conditions) than primary osteoblasts isolated from the *Enpp1*$^{flox/flox}$ mouse which will resemble MC3T3-E1 sub-clone c14 matrix minerlisation. I further hypothesised that this will be due to lower levels of PP_i. This abnormal hypermineralisation phenotype will be rescued via TNAP inhibition such that PP_i levels are returned to physiological levels.

4.3 Aims

To investigate the expressions of genes associated with mineralisation *in vitro,* both established osteoblast-like (fast mineralising) MC3T3-E1 sub-clone c14 cells and primary calvarial osteoblasts isolated from the osteoblast-specific NPP1 knockout mouse model (*Enpp1*$^{flox/flox}$;*Ocn*-cre) and age-matched controls (*Enpp1*$^{fl0x/flox}$) were utilised. For both cell lines and primary osteoblasts, cells were cultured in mineralising media to investigate the following aims;

I. Changes in gene expression of both MC3T3-E1 sub-clone c14 cell line and primary osteoblasts isolated from *Enpp1*$^{flox/flox}$;*Ocn*-cre mice in comparison to *Enpp1*$^{flox/flox}$ control mice throughout time course in mineralisation medium.

II. Whether the inhibition of TNAP via the addition of a small molecule TNAP inhibitor to the mineralisation media will rescue any potential mineralisation abnormalities of the isolated primary osteoblasts.

III. Any potential difference in the metabolic capacity of primary osteoblasts isolated from the from *Enpp1*$^{flox/flox}$;*Ocn*-cre mouse model compared to age-matched *Enpp1*$^{flox/flox}$ controls.

4.4 Materials and methods

4.4.1. MC3T3-E1 sub-clone c14 and primary cell culture

MC3T3-E1 sub-clone c14 cells were seeded in 6-well plates at a density of 100,000 cells per well. When confluent, the media for cells was supplemented with 5 mM β-GP and 50 μg/ml AA (Section 2.2.6). Primary osteoblasts were isolated from 2-5 day old pups and cultured as (Section 2.2.5)(Appendix III for schematic representation of primary osteoblast isolation from calvaria). Confluent primary cultures were maintained for up to 28 days in primary osteoblast media supplemented with 5 mM β-GP and 50 μg/ml AA.

4.4.2. qPCR analysis of MC3T3-E1 sub-clone c14 and primary osteoblast gene expression throughout mineralisation time course

At defined time points, RNA was extracted from both MC3T3-E14 sub-clone c14 and primary osteoblasts using Qiagen RNeasy kit, as per the manufacturer's protocol. Subsequently, cDNA was prepared (Section 2.3.2.) and was used at a concentration of between 5 and 15 ng/μl for qPCR analysis (Section 2.3.3). qPCR was performed using the SYBR green detection method on a Stratagene Mc3000P real-time qPCR system. Primers were purchased from PrimerDesign Ltd, or designed in house and synthesised by Sigma and Eurofins (Appendix I). Reactions were run in duplicate, and results were normalised to *β-actin* and *GAPDH* housekeeping genes and relative gene expression was determined using the ΔΔCt method (Livak and Schmittgen, 2001).

4.4.3. Calcium deposition

Media from the cellular monolayers was discarded and the cell monolayers were washed with PBS. Next, 500 μl of 0.6 M HCl was added to the monolayer and incubated at 4°C. A commercially available calcium assay Kit (Randox, County Antrim, UK) was used to quantify the calcium deposition in the cells, with samples and standard run in duplicate. The mechanism underpinning this assay is based on the binding between O-cresolphthalein complexone and calcium ions in an alkaline media. For each experiment, a negative control was included using the leaching solution (0.6 M of HCl) in place of the sample. Calcium standards, provided by the kit, were used as instructed to determine the calculation for

calcium concentration. As such, 5.25 µl of calcium standard/negative control with 0.6 M HCl or sample was added to a 96-well plate in duplicate. Next, 250 µl of 1:1 ratio of 2-amino-2-methyl-propan-1-ol (R1) and O-Cresolphthalein complexone 8-Hydroxyquinoline, HCl (R2) were added to each well. The Optical Density was read using Synergy HT Multi Mode Microplate reader (BioTek) at a wavelength of 570 nm. Calcium content was determined using the following equation:

$$\text{Concentration} = \left(\frac{\text{mmol}}{\text{L}}\right) = \left(\frac{\text{Sample OD}}{\text{Standard OD}}\right) = \text{standard concentration } \left(\frac{\text{mmol}}{\text{L}}\right)$$

4.4.5. Alizarin Red S staining and quantification

The media from cellular monolayers was discarded and cellular monolayers were washed with PBS. Cells were then incubated with 4% paraformaldehyde (PFA; pH 7.0) for 15 minutes at room temperature (RT). The PFA was discarded, and cellular monolayers washed three times with PBS. Subsequently, 2% (w/v) Alizarin Red S Stain (pH 4.2; Sigma, Dorset, UK) was added and incubated at room temperature for 10 minutes. Cellular monolayers were washed with water until excess staining had been removed. The cellular monolayer was allowed to dry and was photographed, after which the cells were stored dry at -20°C. When required, bound Alizarin red S stain was solubilised using 10% cetylpyridinium chloride (Sigma-Aldrich). Samples were collected and run in duplicate, using cetylpyridinium chloride as a blank, in a 96-well plate to measure the optical density at 570 nm. Optical density was determined using the synergy HT multimode Microplate reader (BioTek, Bedfordshire, UK).

4.4.4. ALP activity

MC3T3-E1 sub-clone c14 cells and primary osteoblasts were harvested in 500 µl of 1% Triton-x-100 with 1 mM $MgCl_2$. TNAP activity was analysed using Thermo-line TNAP reagent (Thermo-line, Melbourne, Australia) (Farquharson et al., 1995). Enzymatic activity of TNAP was measured using *p*-nitrophenyl phosphate (pNPP) as substrate. The optical density of the reaction product p-nitrophenol was read at 405 nm by the Synergy HT multimode Microplate reader (BioTek, Bedfordshire, UK). Protein concentration was determined using the Bio-Rad

DC assay (Section 3.4.5) and total TNAP activity was expressed as nmoles pNPP hydrolysed/min/mg protein.

4.4.5 Bio-Rad DC assay

The medium of the cellular monolayer was discarded and cell monolayers were washed with PBS to remove excess media. An appropriate volume of 0.1 M NaOH 0.1% SDS lysis buffer was added to the cell monolayer and incubated at RT on a shaker for 1 hour. The cells were scraped and collected into Eppendorf tubes. Tubes were subsequently vortexed and centrifuged at 10,000 *g* for 10 seconds to remove condensation. To quantify protein concentrations, Bio-Rad DC Protein Assay (Bio-Rad Hertfordshire, UK) was used according to manufacturer's instruction, with a protein standard of γ globulin used to obtain a standard curve. For both protein standard and protein, 5 µl of the samples were run in duplicate on a 96-well plate, with 25 µl alkaline copper tartrate (Reagent A) and 200 µl Folin's reagent (Reagent B) subsequently added. The 96-well plate was incubated at RT for 15-60 minutes before absorbance measurement (at a wavelength of 590 nm) using the synergy HT multimode Microplate reader (BioTek, Bedfordshire, UK).

4.4.6. Seahorse metabolic analysis of primary osteoblasts

Calvarial osteoblasts from age-matched *Enpp1*^{floxflox} and *Enpp1*$^{flox/flox}$;*Ocn*-cre mice were extracted (Section 2.2.5) and plated on a Seahorse XF24 microplate at a density of 10,000 cells per well in 150 µL of primary osteoblast medium. The plate was transferred to a 37°C CO_2 incubator until 100% confluency was reached (approximately 1 day). Osteoblasts were washed in 500 µl XF assay media supplemented with 25 mM glucose and 10 mM pyruvate and placed in a non-CO_2 incubator at 37°C for 1 hour before the start of the assay. Calvarial osteoblasts were then exposed to oligomycin (1 µM - a complex V inhibitor, that inhibits respiration by inhibiting ATP synthase), the uncoupling agent carbonyl cyanide p-trifluoromethoxyphenylhydrazone (FCCP - (3 µM)), antimycin A (that inhibits respiration by inhibiting oxidation of ubiquinol in the electron transport chain) and rotenone (1 µM - complex I inhibitor involved in the inhibition of the mitochondrial respiratory chain). All reagents were prepared for the assay from 2.5 mM Seahorse stock solutions (Seahorse Bioscience, Massachusetts, US). Following equilibration, the Seahorse plate was placed in the Seahorse XF24 Analyser. Oxygen consumption rate (OCR; an indicator of aerobic

respiration) and extracellular acidification rate (ECAR; an indicator of glycolysis) values are shown as pMoles/min compared at three different time points per condition. For the Seahorse metabolic analysis optimisation of drug concentrations was conducted, and subsequently, Seahorse experiments were run twice at optimal drug concentrations. All data were normalised to total protein concentration by sulforhodamine B staining. The data shown in the assays are an average of at least three different wells per group for one Seahorse Run. This work was performed with the assistance of Dr Rod Carter.

4.4.7. Serum PP_i Assay

Serum samples were collected (Section 2.9.3) and stored at -80°C until required. Caution was taken to avoid aspiration of air during sample collection. Plasma was subsequently transferred to separation tubes (Sartorius Centristart, 1,300,000 MW 123 79E) and filter-centrifuged at 2000 *g* for 25 minutes at 4°C. Supernatant was collected and stored at -80°C until required. Subsequently, 35 μL PP_i master mix (Section 2.9.3) and 5 μl of sample were added to opaque 96-well plates, with samples run in duplicate. The plate was briefly centrifuged, followed by incubation at 37°C for 30 minutes followed by heat inactivation at 95°C for 10 minutes. The 96-well plate was shortly spun down, and 30 μL of sample was transferred to a new 96-well plate. 15 μL of BacTiter Glo (Promega G8230) pre-warmed to room temperature was added, and plate briefly centrifuged and incubated at room temperature for 10 minutes. Luminescence was subsequently measured using the synergy HT multimode Microplate reader (BioTek, Bedfordshire, UK) at 24°C. Master-mix without enzyme was used for blank, and a standard curve determined using known concentrations of PP_i. This technique was developed in collaboration with Janna Zoll and Professor Olivier Le Saux of University of Hawaii. I optimised this technique for implementation in this experiment to measure serum PP_i of the *Enpp1*$^{flox/flox}$;*Ocn*-cre and *Enpp1*$^{flox/flox}$ mice.

4.4.8. Treatment with TNAP inhibitor.

Primary osteoblasts from *Enpp1*$^{flox/flox}$;*Ocn*-cre and *Enpp1*$^{flox/flox}$ control mice were plated at a density of 100,000 cells per well in a 6-well plate. When confluent, the culture media was supplemented with 5 mM β-GP and 50 μg/ml AA (Section 2.2.1) and addition of 30 μM TNAP

inhibitor 2,5-Dimethoxy-N-(quinolin-3-yl)benzenesulfonamide-referred to as MLS-0038949 (Sigma) (Huesa et al., 2015a). Confluent primary cultures were maintained for up to 28 days in primary osteoblast media supplemented with 5 mM β-GP and 50 μg/ml AA and TNAP inhibitor MLS-0038949 (Sigma). The cellular layers were analysed for calcium content by a Randox assay and stained for Alizarin red S (Sections 3.4.3. and 3.4.5) at days 0, 21 and 28.

4.5. Results

4.5.1. Investigating the mineralisation profile of the mouse cell Line MC3T3-E1 sub-clone c14

4.5.1.1. Analysing calcium content of MC3T3-E1 sub-clone c14 cells

an *in vitro* pilot study regarding the mineralising profile of a well-established, mineralisation-competent murine pre-osteoblastic cell line (MC3T3-E1 sub-clone c14) was conducted prior to investigating primary osteoblast cell mineralization. These results were used to draw comparisons of the mineralisation profile of the primary calvarial osteoblasts isolated from the *Enpp1*$^{flox/flox}$;*Ocn*-cre and *Enpp1*$^{flox/flox}$ control mice. These MC3T3-E1 sub-clone c14 cells were cultured with the addition of β-GP, which is a commonly used organic phosphate source and AA which is required for collagen secretion into the ECM (Chung et al., 1992, Altaf et al., 2006). At day 0, the Alizarin red S staining (representing calcium deposition in ECM) was minimal (0.07 AU) (Fig. 4.2A) indicating a low level of mineral deposition. Culture of cells under mineralisation conditions resulted in a significant increase of Alizarin red S staining at day 14 (0.24 AU vs. 0.07 AU; $P<0.01$) and day 21 (0.53 AU vs. 0.07 AU; $P<0.001$) (Fig, 4.2A). The total calcium deposition was significantly increased following 21 days of culture in mineralising conditions (0.64 AU vs. 0.22 AU; $P<0.001$) (Fig. 4.2B). These data indicate the formation of a mineralised matrix by MC3T3-E1 sub-clone c14 cells over a 21-day culture period in mineralisation conditions.

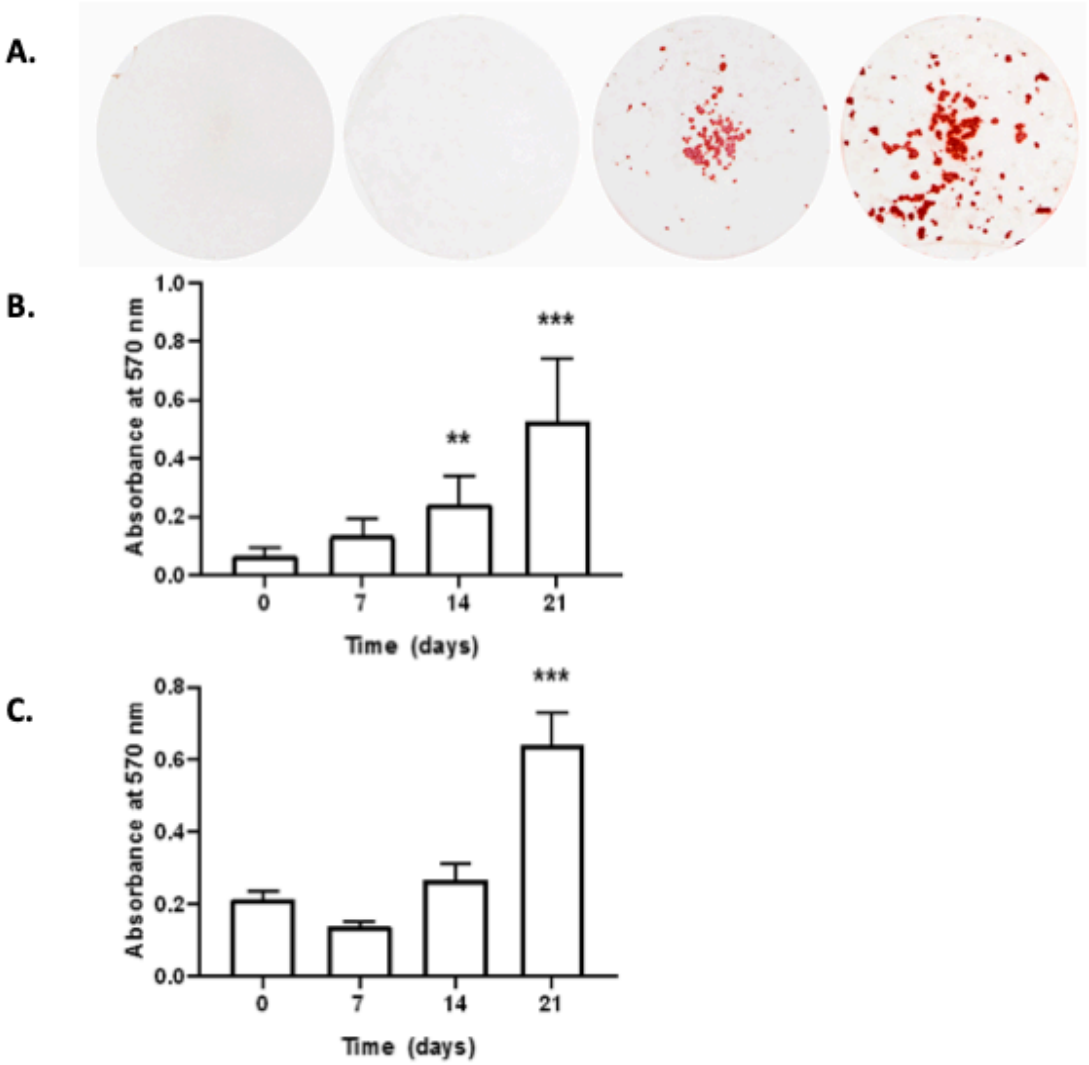

Figure 4.2. Analysis of increased temporal calcium deposition in MC3T3-E1 sub-clone c14 cells.

A) MC3T3-E1 sub-clone c14 cellular monolayers stained with Alizarin red S, (B) quantification of Alizarin red S and (C) quantification of deposited calcium content by absorbance. Data are presented as the mean ± S.E.M (n=6) in comparison to day 0. Significance is denoted by $^{**}P<0.01$, $^{***}P<0.001$.

4.5.1.2. Analysing the relative changes of mRNA in MC3T3-E1 sub-clone c14 cells

The mRNA expression of genes associated with mineralisation was determined at all mineralisation condition time points (day 0, 7, 14 and 21). A significant decrease in *Ank* fold change, compared to day 0, was observed by day 7 (0.70 vs. 1.00; *P<0.05)* and day 14 (0.41 vs. 1.00, *P*<0.001) (Fig. 4.3A). The *Ank* mRNA expression was increased at day 21 comparable to day 0 (Fig. 4.3A). A significant decrease in the fold change of *Pit1* was observed by day 7 (0.36 vs. 1.00, *P*<0.001), as was *Enpp1* (0.33 vs. 1.00; *P*<0.001) and was maintained until day 21 (Fig. 4.3B, Fig. 4.3C). A significant increase in *Alpl* mRNA expression was observed by day 7 (119.33 vs. 1.00; *P*<0.001) and was maintained until day 21 (Fig. 4.3D). No significant differences in *Runx2* (Fig. 4.3D) *or Phospho1* (Fig 4.3E) mRNA expression were observed throughout the mineralisation time course for MC3T3-E1 sub-clone c14 cells (Fig. 4.3E-G).

4.5.1.3 Investigating ALP activity in MC3T3-E1 sub-clone c14 cells

To investigate the activity of TNAP throughout the time course mineralisation study, a commercially available ALP kinetic assay was used. To normalise results, the Bradford assay was used to quantify protein at each time point. The ALP activity, normalised to total protein, was significantly decreased, compared to day 0, following 21 days in mineralisation media (107.14 nmols pNPP hydrolysed/min/mg protein vs. 454.00 nmols pNPP hydrolysed/min/mg protein, *P* <0.01) (Fig. 4.4).

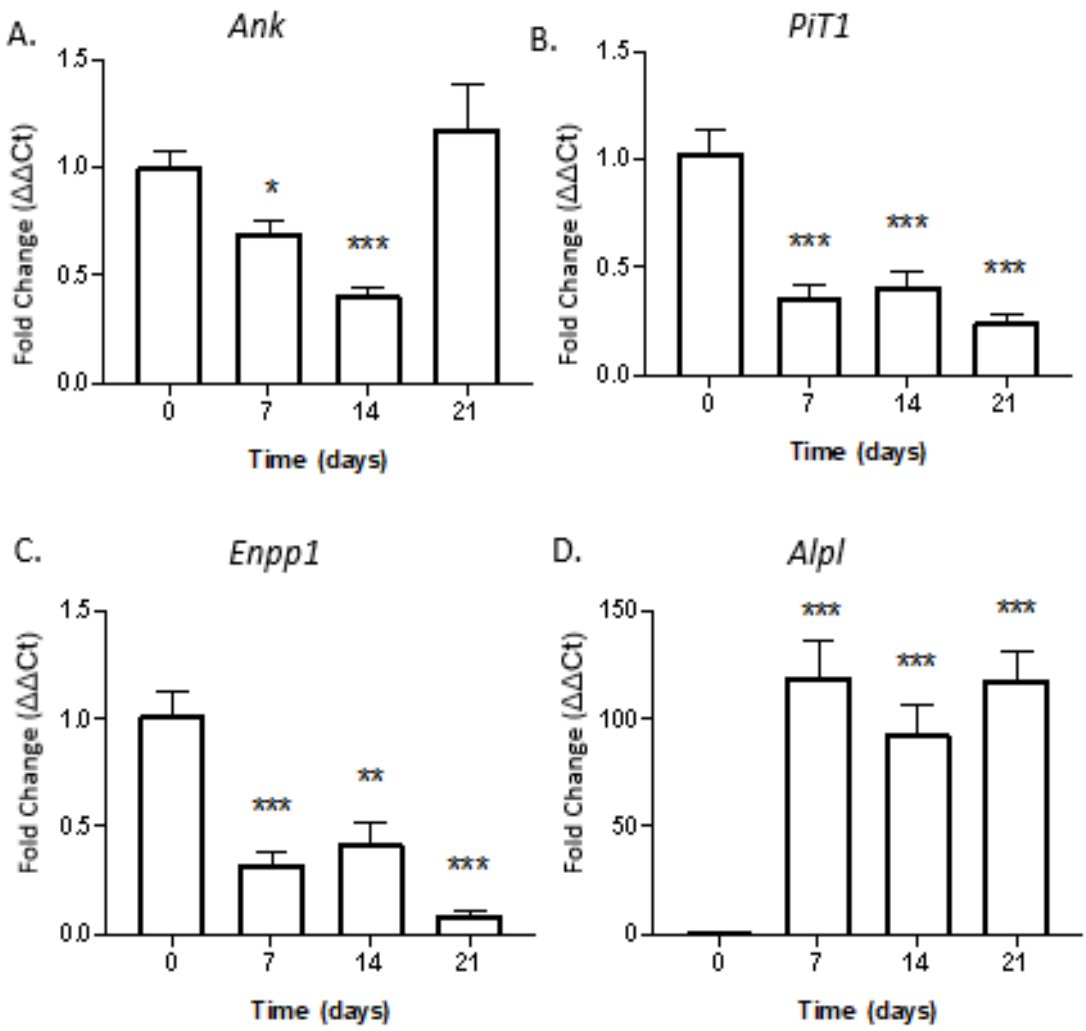

Figure 4.3. Part 1. Assessing the relative change of bone-associated mRNA expression in MC3T3-E1 sub-clone c14 cells demonstrates changes to *Ank, PiT1, Enpp1* and *Alpl.*

To assess the relative change of mRNA in MC3T3-E1 sub-clone c14 cells, qPCR was conducted. Cells were grown for 0, 7, 14 and 21 days post-confluence in mineralisation media and subsequently analysed for (A) *Ank,* (B) *Pit1*, (C) *Enpp1* and (D) *TNAP.* The mRNA values generated were normalised to *β-actin* and *Gapdh* housekeeping genes. Data are presented as the mean ± S.E.M (number of wells assessed per time point: n=6) in comparison to day 0. Significance is denoted by **P*<0.05, ***P*<0.01, ****P*<0.001.

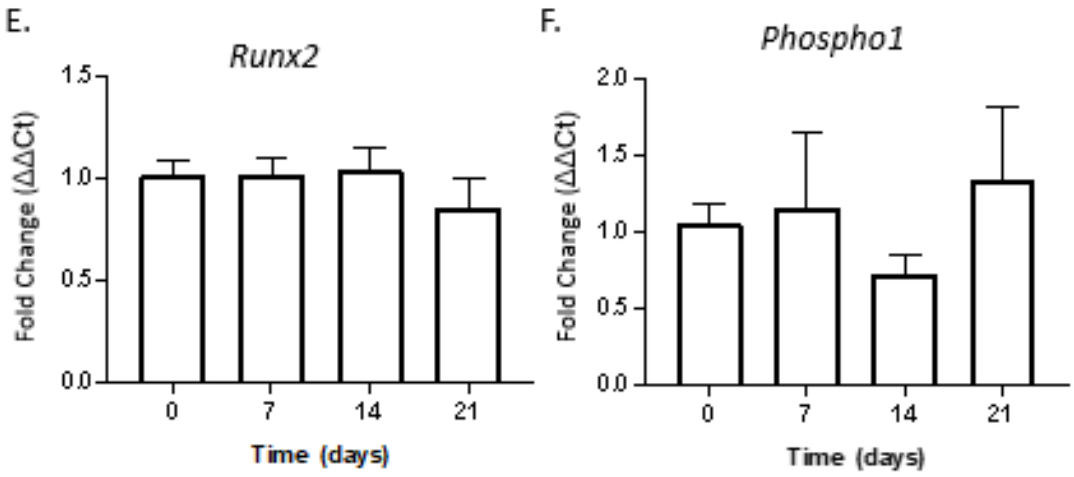

Figure 4.3: Part 2. Assessing the relative change of bone-related mRNA expression in MC3T3-E1 sub-clone c14 cells.

To assess the relative change of mRNA in MC3T3-E1 sub-clone c14 cells, qPCR was conducted. Cells were grown for 0, 7, 14 and 21 days post-confluence in minerlisation media and subsequently analysed for mRNA expression of (E) *Runx2* and (F) *Phospho1*. The mRNA values generated were normalised to *β-actin* and *Gapdh* housekeeping genes. Data are presented as the mean ± S.E.M (number of wells assessed per time point: n=6) in comparison to day 0.

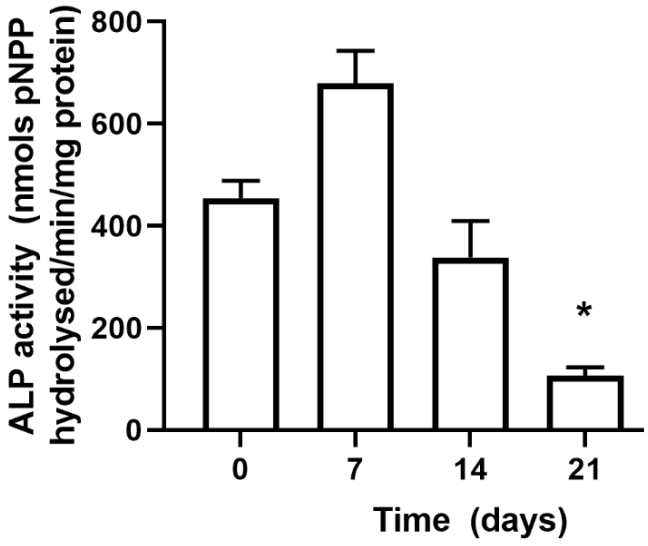

Figure 4.4. ALP activity in MC3T3-E1 sub-clone c14 cells decreases after 21 days *in vitro*.

ALP activity was determined and normalised to total protein. Data are presented as the mean ± S.E.M (n=6) in comparison to day 0. Significance is denoted by *P<0.05.

4.5.2. Investigating the matrix mineralisation profile of primary osteoblasts isolated from *Enpp1*$^{flox/flox}$;*Ocn*-cre and *Enpp1*$^{flox/flox}$

4.5.2.1. Analysing calcium deposition of primary osteoblasts

Representative images of Alizarin red S stained cellular monolayers show progressively increasing stain intensity over the time course for both *Enpp1*$^{flox/flox}$;*Ocn*-cre and *Enpp1*$^{flox/flox}$ isolated primary osteoblasts (Fig. 4.5A). Assessment of temporal changes of staining intensity revealed a significant increase in Alizarin red S staining by day 28 for *Enpp1*$^{flox/flox}$ isolated primary osteoblasts (1.57 O.D at 570 nm vs. 0.06 units O.D at 570 nm; $P<0.001$) (Fig. 4.5B). The Alizarin red S staining was significantly increased by day 21 for *Enpp1*$^{flox/flox}$;*Ocn*-cre isolated primary osteoblasts (1.06 O.D at 570 nm vs. 0.06 O.D at 570 nm; $P<0.01$) and was maintained until day 28 (Fig. 4.5C). When observing genotype-specific difference in matrix mineralisation throughout the time course, a significant increase in Alizarin red S staining was evident at day 28, in cultures of osteoblasts from *Enpp1*$^{flox/flox}$;*Ocn*-cre compared to cultures of *Enpp1*$^{flox/flox}$ osteoblasts (2.50 O.D at 570 nm vs. 1.58 O.D at 570 nm; $P<0.05$) (Fig. 4.5D).

Total calcium deposition of primary osteoblast cells was also analysed to investigate temporal and genotype-specific differences. The *Enpp1*$^{flox/flox}$ isolated primary osteoblast demonstrate significantly increased calcium deposition by day 14 in mineralisation conditions compared to day 0 (18.01 µg/ml vs. 5.76 µg/ml; $P<0.05$) (Fig. 4.6A). A significant increase in calcium deposition for the *Enpp1*$^{flox/flox}$ isolated primary osteoblasts was also observed at day 21 and day 28 compared to day 0 (Fig. 4.6A). Reflecting the Alizarin red S staining, a significant increase in total calcium deposition was observed at the early time point of day 7 for the *Enpp1*$^{flox/flox}$;*Ocn*-cre isolated primary osteoblasts compared to day 0 (5.97 µg/ml vs 0.94 µg/ml; $P<0.001$) (Fig. 4.6B). A significant increase in calcium deposition was also observed at day 21 and day 28 compared to day 0 (Fig. 4.5B). Genotype-specific differences were also investigated over the mineralisation time course. By day 14, the *Enpp1*$^{flox/flox}$;*Ocn*-cre isolated primary osteoblasts demonstrate a significantly increased calcium deposition compared to *Enpp1*$^{flox/flox}$ isolated primary osteoblasts (27.72 µg/ml vs. 18.02 µg/ml, $P<0.05$) (Fig. 4.6C). This was also observed for day 21 ($P<0.01$) and day 28 ($P<0.001$) (Fig. 4.6C). These data demonstrate an enhanced ability of the *Enpp1*$^{flox/flox}$;*Ocn*-cre isolated primary osteoblasts to mineralise their matrix.

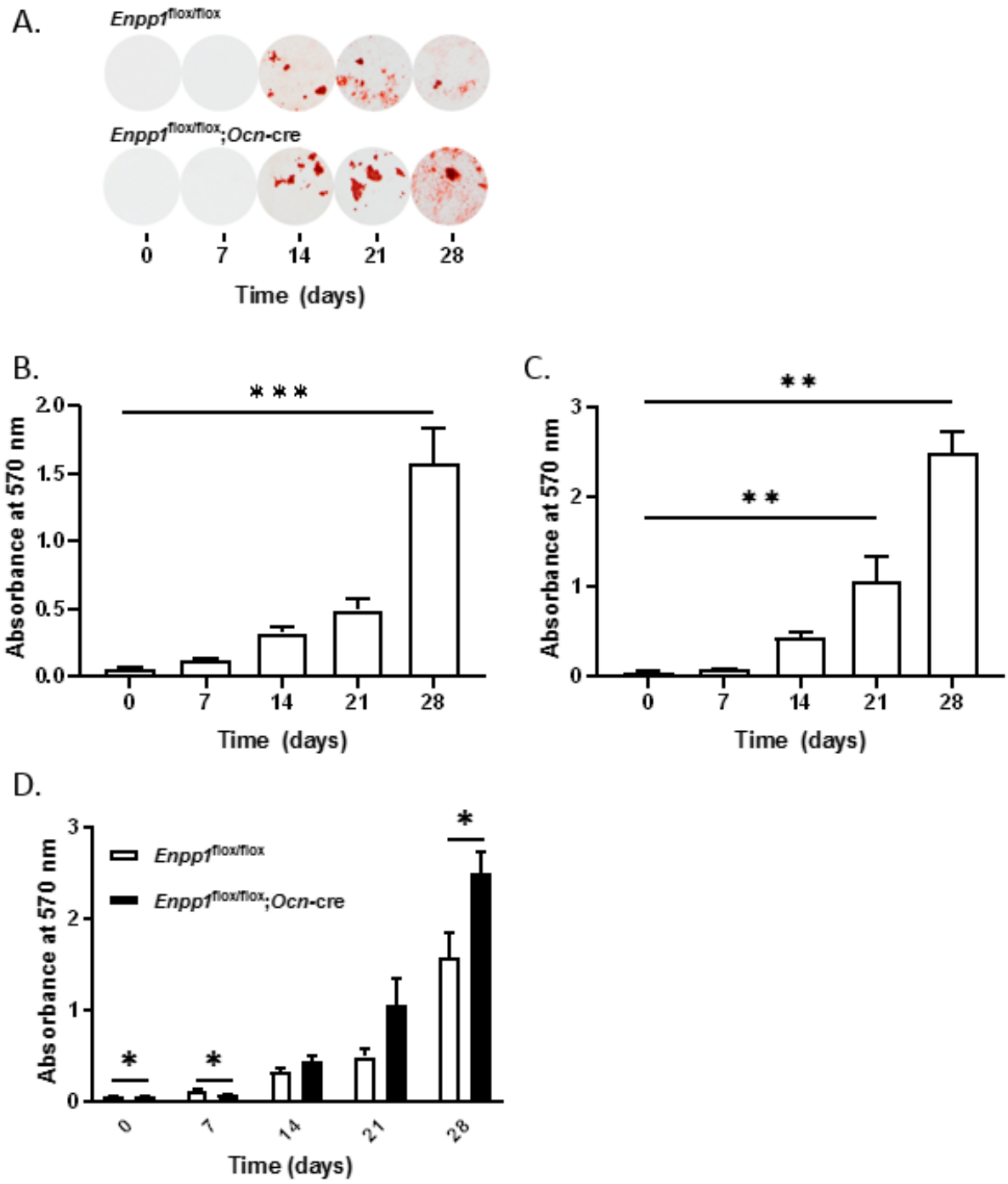

Figure 4.5. Increased calcium content in the primary osteoblasts of osteoblast-specific NPP1 ablated mice by Alizarin red S staining.

(A) Primary osteoblast cellular monolayers stained with Alizarin red S, absorbance determined quantification of Alizarin red S stain from (B) *Enpp1*$^{flox/flox}$ and (C) *Enpp1*$^{flox/flox}$;*Ocn*-cre isolated primary osteoblasts showing significance over time course and (D) showing significance between genotype over time (days) in mineralisation media post confluence. Data are presented as the mean ± S.E.M (n=6). Significance is denoted by **P*<0.05, ***P*<0.01, ****P*<0.001.

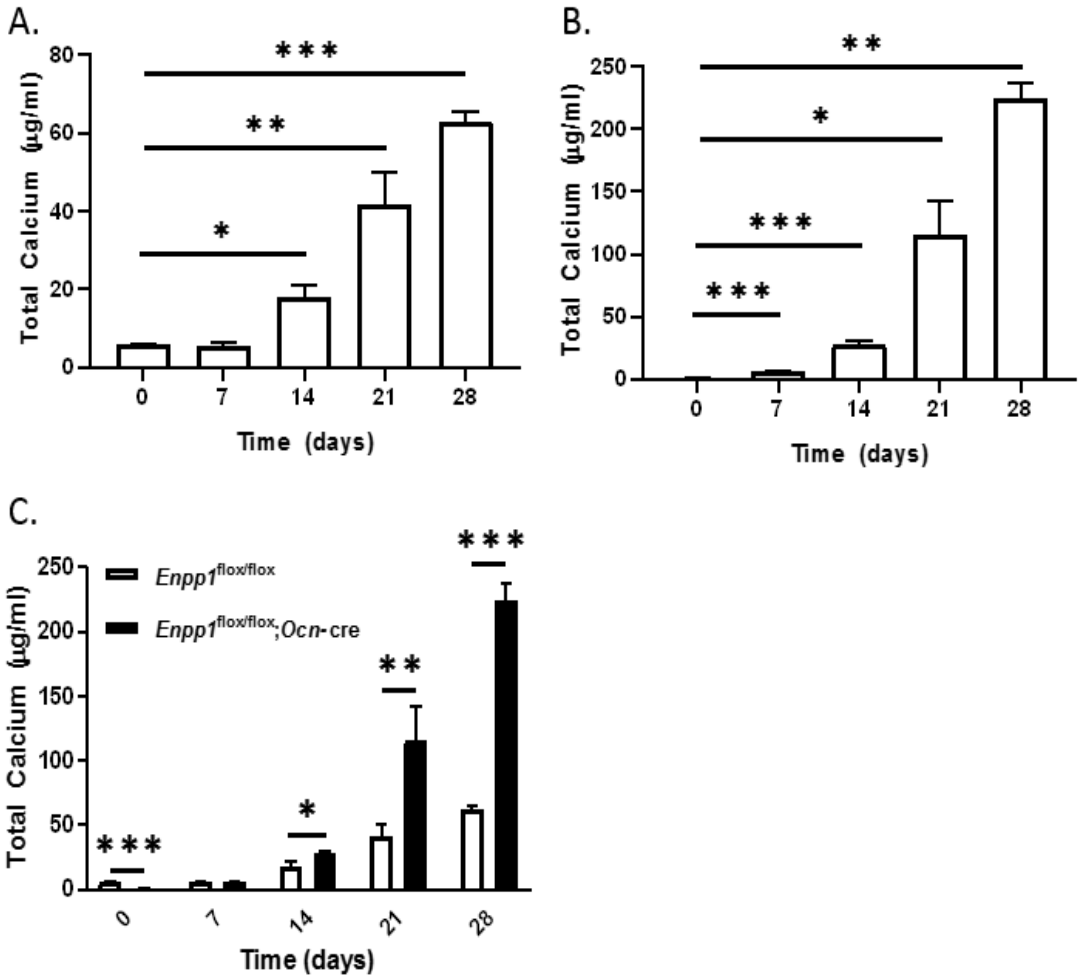

Figure 4.6. Primary osteoblast total calcium content is increased in the primary osteoblasts of osteoblast-specific NPP1 ablated mice.

Total protein concentration of (A) *Enpp1*$^{flox/flox}$ and (B) *Enpp1*$^{flox/flox}$;*Ocn*-cre isolated primary osteoblasts showing significance increase over the time course and (D) showing significance between genotype over time (days) in mineralisation media post confluence. Data are presented as the mean ± S.E.M (n=6). Significance is denoted by **P*<0.05, ***P*<0.01, ****P*<0.001.

4.5.2.2. Analysing the mRNA expression of key osteogenic and mineralisation genes in primary osteoblast cells.

Genotype-specific changes of mRNA expression in cultured primary osteoblast cells isolated from *Enpp1*$^{flox/flox}$;*Ocn*-cre and *Enpp1*$^{flox/flox}$ mouse calvaria were analysed by qPCR. At day 0, *Bglap* mRNA expression was significantly increased in *Enpp1*$^{flox/flox}$;*Ocn*-cre primary osteoblasts compared to *Enpp1*$^{flox/flox}$ (fold change 1.31 vs. 1.00; $P<0.05$) (Fig. 4.7A). At day 21 only, a significant decrease in *Bglap* and *Opn* (0.38 vs. 22.91; $P<0.05$) (Fig. 4.7A, Fig. 4.7B) mRNA expression was observed in *Enpp1*$^{flox/flox}$;*Ocn*-cre primary osteoblasts compared to *Enpp1*$^{flox/flox}$ isolated primary osteoblasts. At day 21, a significant increase in *Phospho1* (38.12 vs. 1.00; $P<0.05$) (Fig. 4.7C) and *Runx2* (18.30 vs. 3.00; $P<0.01$) (Fig. 4.7D) mRNA expression was observed for *Enpp1*$^{flox/flox}$;*Ocn*-cre primary osteoblasts compared to *Enpp1*$^{flox/flox}$ isolated primary osteoblasts. No significant differences in mRNA expression of *Mgp* (Fig 4.7F) or *Fgf23* (Fig 4.7G) were noted between genotype. It is important to note that many of the changes at specific time points for differences in mRNA expression of genes were not significant between genotypes or temporal time points. The general trend observed was that a significant difference in mRNA expression of genes was evident at day 21 but was not observed at other time points.

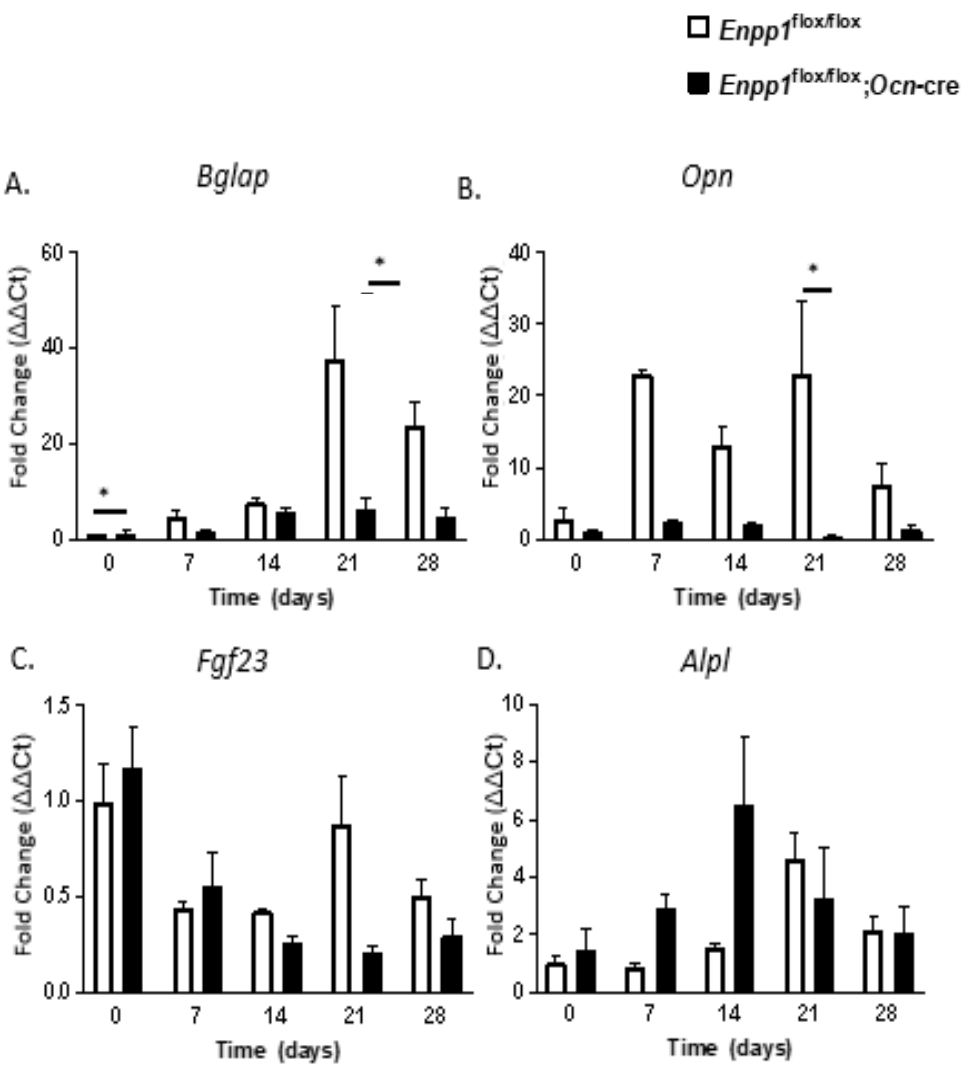

Figure 4.7. Part 1. Bone-Related mRNA expression in primary osteoblasts shows significant differences between genotype for *Bgalp, Opn, Runx2 and Phospho1.*

To assess the relative changes in mRNA levels of primary osteoblasts, qPCR was conducted. Cells were grown for 0, 7, 14, 21 and 28 days post-confluence in mineralisation media and subsequently analysed for (A) *Bglap,* (B) *Opn*, (C) *Fgf23* and (D) *Alpl.* The mRNA values generated were normalised to *β-actin* and *Gapdh* housekeeping genes. Data are presented as the mean ± S.E.M (n=6). Significance is denoted by **P*<0.05.

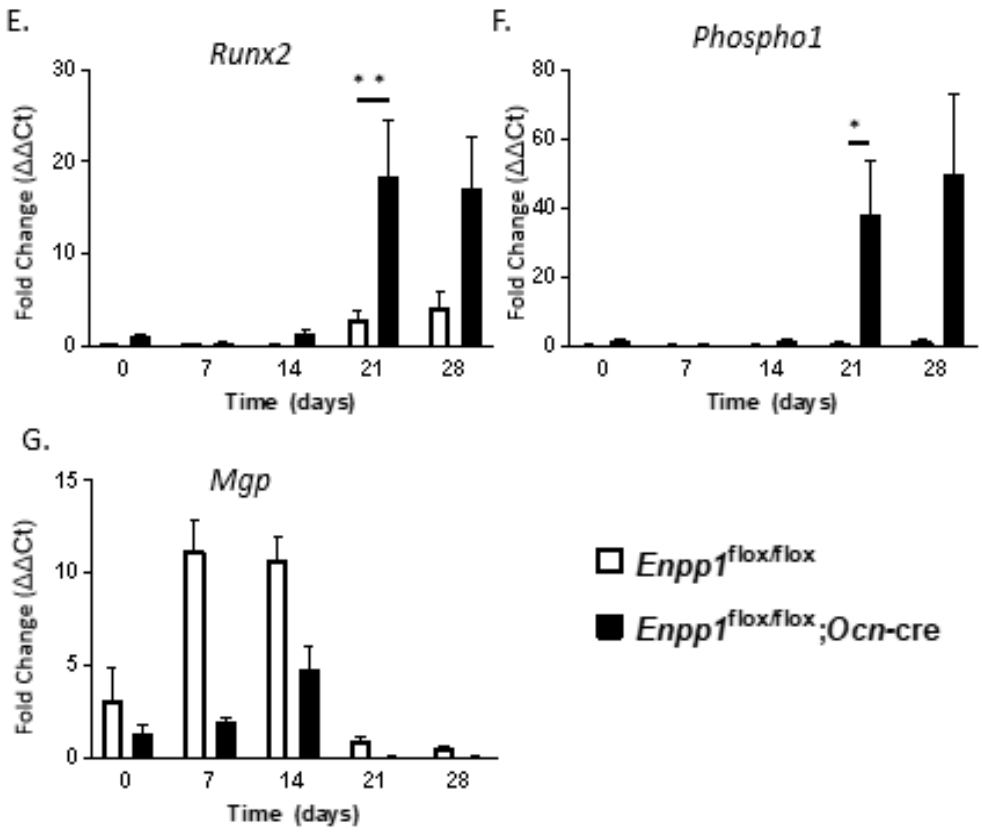

Figure 4.7: Part 2. Bone-Related mRNA expression in primary osteoblasts shows significant differences between genotype for *Bgalp, Opn, Runx2 and Phospho1*.

To assess the relative change of mRNA in primary osteoblasts, qPCR was conducted. Cells were grown for 0, 7, 14, 21, and 28 days post-confluence in mineralisation media and subsequently analysed for (E) *Runx2*, (F) *Phospho1* and (G) *Mgp.* The mRNA values generated were normalised to *β-actin* and *Gapdh* housekeeping genes. Data are presented as the mean ± S.E.M (n=6). Significance is denoted by **P*<0.05, ***P*<0.01.

4.5.2.3. Analysing the relative change of extracellular PP_i in primary osteoblast cells

Given that the *Enpp1*$^{flox/flox}$;*Ocn*-cre isolated primary osteoblasts were able to mineralise their matrix more in comparison to *Enpp1*$^{flox/flox}$ isolated primary osteoblasts, the next aim was to determine if this was due to differences in extracellular PP_i levels between genotypes. Once cells had reached confluence, (day 0) a PP_i assay was conducted and samples normalised to protein concentration. Initial studies aimed to optimise conditions to generate a standard curve (concentrations as follows; 0, 0.16, 0.31, 0.63, 1.25, 2.5 and 5 µM PPi) in α-MEM media which was subsequently used throughout the primary osteoblast cell culture experiments. Analysis of PP_i concentrations revealed a significant decrease in the extracellular media concentration in the *Enpp1*$^{flox/flox}$;*Ocn*-cre isolated primary osteoblasts compared to the *Enpp1*$^{flox/flox}$ controls when normalised to total protein (1.51 vs 1.02 µM/mg/ml; *P*<0.01) (Fig. 4.8).

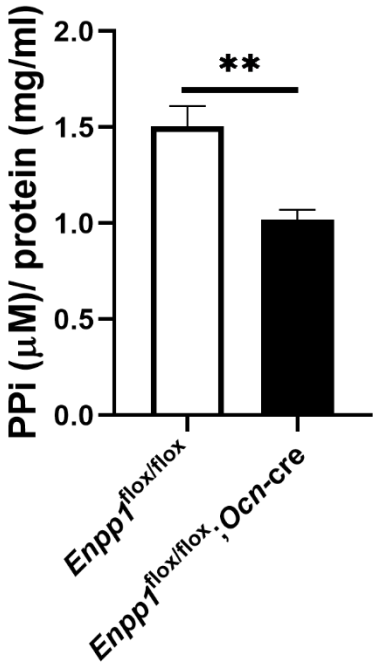

Figure 4.8. Extracellular pyrophosphate concentration in primary osteoblast cells from osteoblast-specific NPP1 mice is significantly reduced.

To assess the difference in extracellular PP_i between osteoblast cells isolated from *Enpp1*$^{flox/flox}$;*Ocn*-cre and *Enpp1*$^{flox/flox}$ mice a PP_i assay was conducted. Cells were grown to confluence and the media was collected. Total extracellular PP_i normalised to total protein was calculated. Data are presented as the mean ± S.E.M (n=6). Significance is denoted by **P<0.01.

4.5.3. Analysing the effect of TNAP inhibition on primary osteoblast matrix mineralisation

Given that TNAP reduces PP_i by hydrolysis to P_i, the inhibition of TNAP in Enpp1$^{flox/flox}$;Ocn-*cre* primary osteoblasts cultured in minerlisation media was hypothesised to restore the P_i/PP_i ratio, and result in the restoration of normal matrix mineralisation. To investigate this, primary osteoblasts isolated from both genotypes of mice were cultured under mineralisation conditions with the addition of 30 µM TNAP-specific inhibitor MLS-0038949. Samples were collected at day 0 and day 21 (where Enpp1$^{flox/flox}$;Ocn-*cre* demonstrated significantly increased mineralisation compared to Enpp1$^{flox/flox}$ controls), whereby cells from both genotypes demonstrated matrix mineralisation with the addition of the TNAP inhibitor MLS-0038949. Staining with Alizarin red S (Fig. 4.9A) and quantitative analysis (Fig 3.9B) demonstrated that both Enpp1$^{flox/flox}$;Ocn-*cre and* Enpp1$^{flox/flox}$ primary osteoblasts have a minimal level of calcium deposition at day 0, which was increased by day 21 with addition of MLS-0038949, with no evident differences between genotype (Fig. 4.9A).

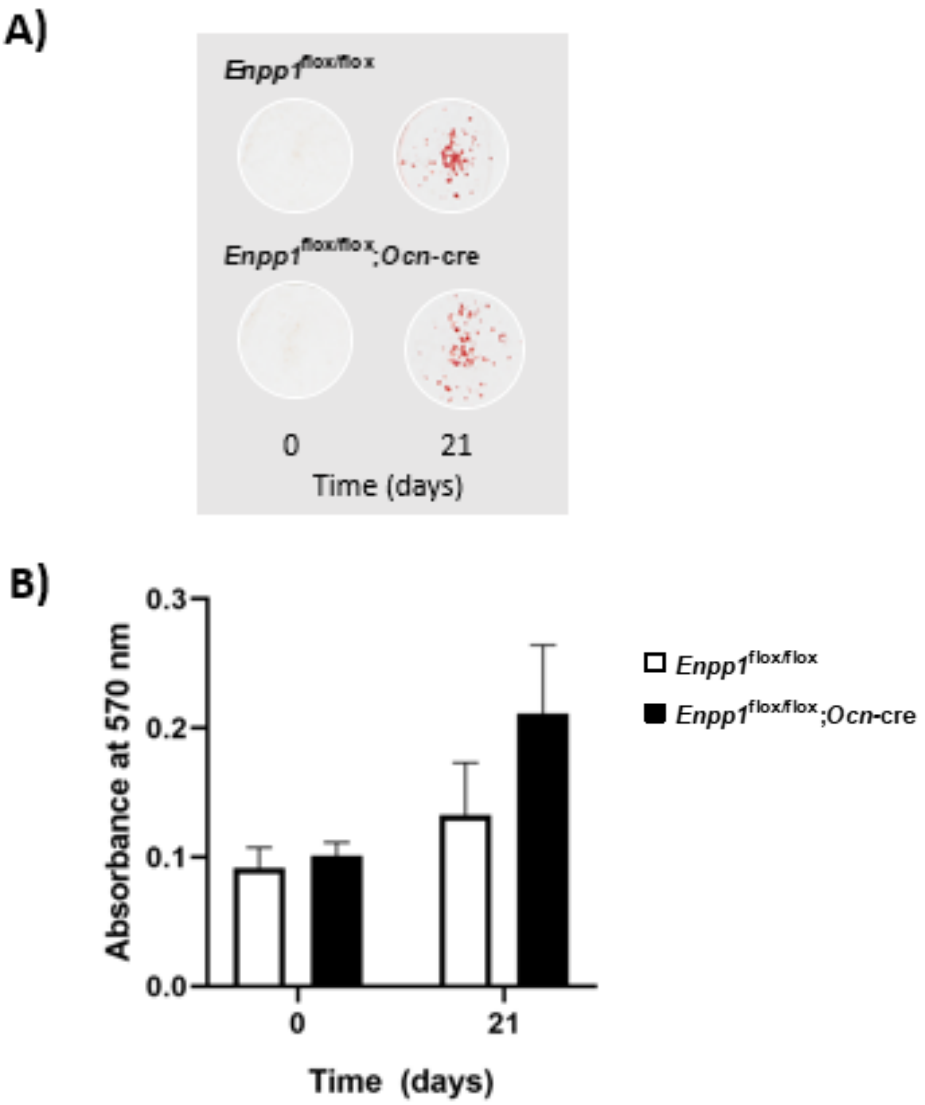

Figure 4.9. Analysis of calcium deposition following TNAP inhibition of primary osteoblasts.

Primary osteoblasts were treated with 30 µM TNAP inhibitor MLS-0038949 during mineralisation time-course. (A) Primary osteoblast cellular monolayers stained with Alizarin red S, (B) quantification of Alizarin red S. Data are presented as the mean ± S.E.M (n=6) and compared to day 0.

4.5.4. Analysing metabolic differences in primary osteoblast cells

Given the evidence that bone may contribute to global energy homeostasis (Ducy et al., 2000), I next aimed to investigate whether the *Enpp1*$^{flox/flox}$;*Ocn*-cre primary osteoblasts increased propensity to mineralise their matrix was associated with altered cellular metabolic function. The SeahorseXF-24 extracellular flux analyser was used to measure OCR (indicative of aerobic respiration) and ECAR (and indicator of glycolytic function) via metabolic stress testing. It was observed that the *Enpp1*$^{flox/flox}$;*Ocn*-cre isolated osteoblasts exhibit altered respiration compared to *Enpp1*$^{flox/flox}$ isolated primary osteoblasts. Basal respiration was significantly decreased in *Enpp1*$^{flox/flox}$;*Ocn*-cre cells compared to *Enpp1*$^{flox/flox}$ cells (56.60 pMol/min vs 64.06 pMol/min; $P < 0.01$) as was ATP linked respiration (45.73 pMol/min vs. 50.97 pMol/min; $P<0.05$) (Fig. 4.10A, Fig 3.10B). No significant difference in maximal respiration or leak respiration were observed between genotypes (Fig. 4.10C, Fig. 4.10D). By analyzing ECAR as an indicator of glycolytic function, the *Enpp1*$^{flox/flox}$;*Ocn*-cre osteoblasts demonstrated impaired approximate glycolytic capacity (under conditions of ATP mitochondrial inhibition) (4.91 pMol/min vs. 5.73 pMol/min; $P<0.05$), and decreased approximate glycolytic capacity (under conditions of ATP mitochondrial inhibition) (9.35 pMol/min vs. 12.73 pMol/min; $P<0.01$) (Fig. 4.10E, Fig. 4.10F) compared to *Enpp1*$^{flox/flox}$ isolated osteoblasts.

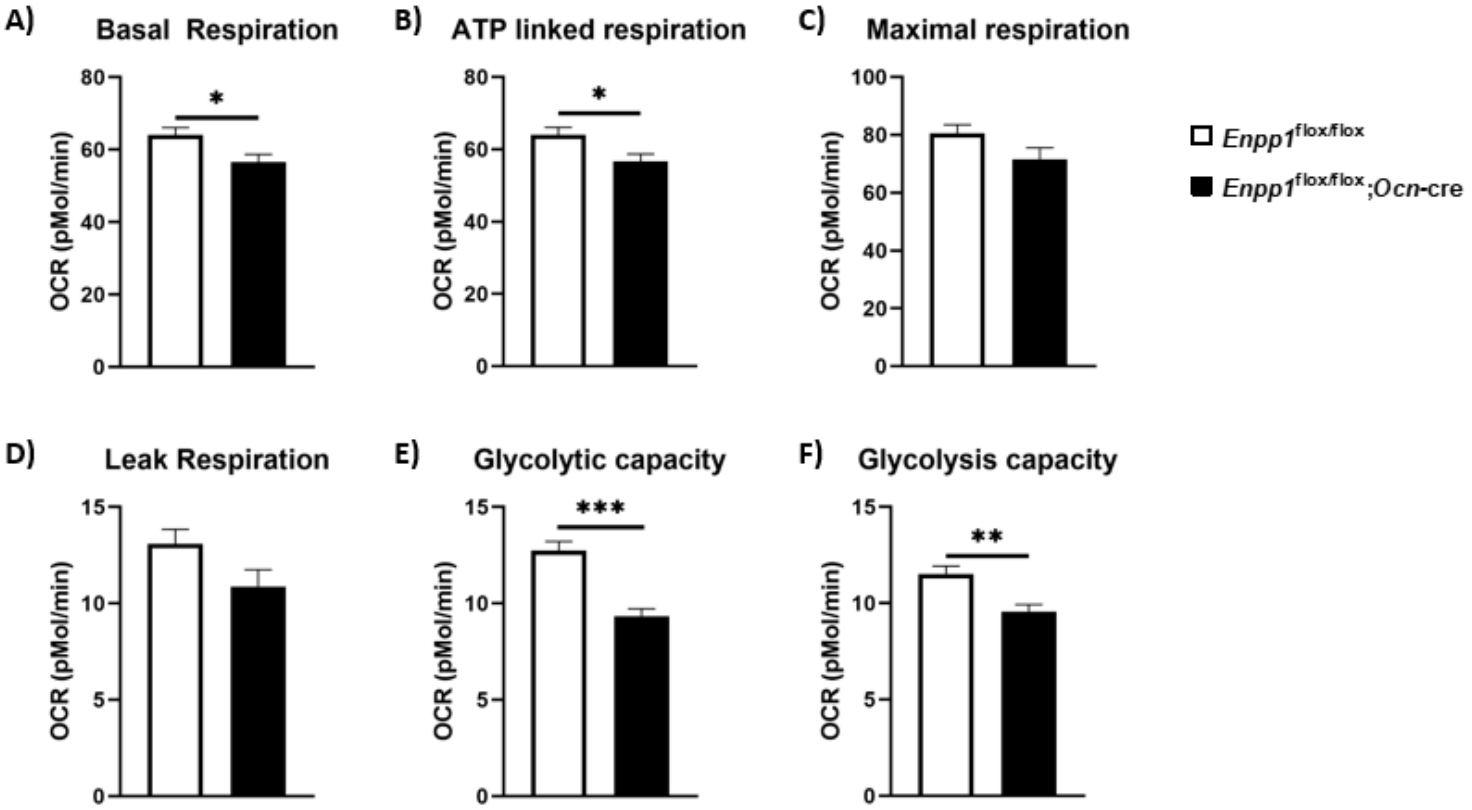

Figure 4.10. *Enpp1$^{flox/flox}$;Ocn*-cre primary osteoblasts demonstrate decreased aerobic respiration and glycolytic function.

Seahorse Metabolic Analysis of primary osteoblasts isolated from the calvariae of *Enpp1$^{flox/flox}$;Ocn*-cre and *Enpp1$^{flox/flox}$* mice. (A) Basal respiration, (B) ATP-linked respiration, (C) Maximal Respiration, (D) Leak Respiration, (E) Approximate glycolytic function (mitochondrial inhibition conditions) and (F) Approximate glycolysis function (respiratory inhibition conditions). Data presented as the mean ± S.E.M (n=3). Significance was denoted by **P*<0.05, ***P*<0.01, ****P*<0.001.

4.6. Discussion.

The development of *in vitro* techniques have allowed for a more in-depth probing and analysis of the osteoblast phenotype and greater elucidation of the mechanisms involved regarding the mineralisation of their matrix. The requirement for available osteoblast cells for *in vitro* research was met by the development of cell lines, many of which have now been well characterised, both in their direct behaviour and in their comparison to human osteoblasts as a suitable model of mineralisation. Here, I have characterised the mineralisation of the MC3T3-E1 sub-clone C14 cell line - a non-transformed cell line derived from mouse calvariae bone (Wang et al., 1999a). This MC3T3-E1 sub-clone 14 cell type was originally isolated by Sudo *et al* and represents one of the most commonly used cell lines for *in vitro* studies relating to physiological and pathological aspect of bone biology (Sudo et al., 1983). The use of these cell lines has led to the understanding of the temporal expression of key regulators and the development of ECM mineralisation.

The investigation of MC3T3-E1 sub-clone c14 cells presented in this thesis demonstrates the capability of this cell line to mineralise their matrix over a 21-day culture period when cultured in mineralisation media. This was evidenced by the increasing intensity of Alizarin red S staining, which reached quantitative significance after 14 days of culture. These results are indicative of an increase of the calcium deposition within the matrix and reflect previous findings of MC3T3-E1 sub-clone c14 mineralisation studies utilizing AA and β-GP supplemented mineralisation media (Kawazoe et al., 2004).

Furthermore, the relative mRNA expression of MC3T3-E1 sub-clone c14 *Enpp1* was significantly decreased by day 7, compared to day 0, and this diminished expression was maintained throughout time-course. Given that ENPP1 generates extracellular PP_i, this observed decrease is likely also contributing towards mediating the P_i/PP_i ratio to favour mineralisation. Runx2 is a recognised driver of osteoblast differentiation. Throughout the time-course, no significant difference in *Runx2* mRNA expression was observed. This may indicate that the MC3T3-E1 sub-clone c14 cells achieved mature osteoblasts status before the onset of mineralisation evidenced through Alizarin red S staining and calcium assay analysis (Komori, 2010). To fully determine the maturity of osteoblasts, further analysis of mature osteoblast markers must be conducted. Such markers include collagen type I, alkaline

phosphatase and bone matrix proteins including osteopontin, bone sialoprotein and osteocalcin. These markers are well recognised as determinants of mature osteoblast status may be assessed for protein expression *in situ* by immunohistochemistry (Liu et al., 1997, Staines et al., 2012b, Neve et al., 2013).

The decrease of *Ank* expression, a transmembrane protein that transports intracellular PP_i to the extracellular milieu (Hakim et al., 1984b, Kim et al., 2010) likely contributes to ensuring a P_i/PP_i ratio to facilitate mineral formation in the ECM. Previous studies have demonstrated that ank/ank mutant mice present with ectopic calcification due to a C-terminal intracellular domain truncation (Ho et al., 2000), demonstrating the importance of ANK in regulating matrix mineralisation. The return of the relative levels of *Ank* expression at day 21 to levels comparable of day 0 is indicative of the increasing the extracellular PP_i levels once significant mineralisation of the matrix was achieved. Interestingly the levels of *Pit1* expression showed a significant decrease at all of the time points investigated; given that *Pit*1 expression is often considered a ubiquitous supplier of P_i with important roles in the mineralisation process this is intriguing.

The analysis of PiT1 null mice has revealed that this transporter protein is critical in embryonic development. Complete deletion of *PiT1* leads to embryonic lethality, reportedly by E12.5, and hypomorphic and null alleles resulted in late embryonic lethality between E14.5 and E16.5 (Beck et al., 2010). Although the work by Beck *et al.,* did not evidence any early skeletal formation defects, *in vitro* studies have demonstrated the involvement of PiT1 in bone mineralisation, reflecting findings *in vivo* that *PiT1* is preferentially expressed in chondrocytes (Palmer et al., 2001, Bourgine et al., 2011). A recent paper by *Chande* et al., reports a heterozygous mouse model with an over-expression of PiT1 which is not associated with embryonic lethality. This mouse model is designed as a transgenic mouse expressing a C-terminal influenza hemagglutinin epitope-tagged human PiT1 (hPiT1) transporter which is regulated by a cytomegalovirus/chicken beta-actin/rabbit beta-globin gene promoter and a loxP-stop-LoxP cassette. This design allows for conditional activation of transgene expression, whereby expression of the resultant HA-hPiT1 (determined by qPCR) was found to be expressed at 10-fold higher levels than that of endogenous mouse Pit1 in multiple

tissues including cultured primary calvaria osteoblasts (Chande et al., 2019). Analysis of bone phenotype by μ-CT revealed no alteration in long bone (femora) mineral density and unaltered mineral metabolism. Conversely, investigations in the role of Pit1 in vascular smooth muscle cells (immortalised) showed that when intracellular Pi is increased via PiT1 over-expression, the cells develop a mineralising phenotype as opposed to their usual contractile phenotype (Li et al., 2006). Additionally, knockdown of *PiT1* expression via gene silencing results in the inhibition of P_i uptake by vascular smooth muscle cells (Li et al., 2006). Further investigations have revealed that mineralisation is either downregulated or upregulated, respectively, with under- and over-expression of *PiT1* in osteoblast cultures (Yoshiko et al., 2007). Taken together, the *in vitro* data suggests that PiT1 is important in the regulation of bone formation by its roles in P_i regulation. Additionally, *in vivo* data seems to suggest that over-expression of PiT1 does not result in alteration of bone mineralisation.

The data in this chapter demonstrates that TNAP expression was increased by day 7. The observed increase in *Alpl*, is consistent with previous findings (Hessle et al., 2002, Narisawa et al., 2007). In addition, the data presented in this chapter reveals that no significant differences in *Phospho1* mRNA expression were observed with time in culture. PHOSPHO1 has been identified as an initiator of MV-mediated mineralisation, whereby it generates P_i within the MV to facilitate HA deposition (Roberts et al., 2007a). As such, it is possible that an increase in *Phospho1* mRNA expression would be expected to accompany the increased mineralisation observed in the MC3T3-E1 sub-clone c14 cells over time. Indeed, studies of MC3T3-E1 sub-clone c14 cells grown in minerlisation conditions (presence of AA and calcium chloride) demonstrated a mineralisation of their ECM after 10 days in culture. In addition, the *Phospho1* mRNA expression was significantly increased throughout the time course, reportedly with approximately 150-fold higher expression compared to day 0 (Houston et al., 2016).

However, it has been demonstrated that the absence of PHOSPHO1 does not prevent the intra-vesicular deposition of mineral (Yadav et al., 2011b). Therefore, PHOSPHO1 activity at the basal levels observed at day 0 in this chapter is likely sufficient to allow the initiation of mineralisation in this experiment. Observations of *Phospho1* knockout mice (*Phospho1*$^{-/-}$)

have hypomineralised bone, with abnormal growth plates, spontaneous fracture, osteomalacia, scoliosis and bowed bones in early life (Yadav et al., 2011a). TNAP knockout mice also manifest a hypomineralisation phenotype, which is reflective of infantile hypophosphatasia, concluding that *Alpl*$^{-/-}$ mice are unable to initiate mineralisation *in vivo* (Wennberg et al., 2000). Furthermore, the double ablation of *Phospho1* and *Alpl* in mice results in the complete lack of skeletal mineralisation and perinatal lethality (Yadav et al., 2011a). Together, this data indicates that TNAP and PHOSPHO1 have distinct roles, and this is reflected in the cell culture results reported in this thesis. At this point, it is essential to take into account that the study assessed genes, but not proteins. Indeed, this represents a limitation to the findings given that the changes in mRNA may not directly related to protein activity.

Although the MC3T3-E1 sub-clone c14 cell lines provide a convenient and accessible model their use should be limited to appropriate and specific scientific questions whereby the analysis and extrapolation of their results should be completed with care. In future experiments, it would be worthwhile examining the protein expression to determine if this reflected the observed changes in mRNA expression. For this chapter, the MC3T3-E1 sub-clone c14 cells were studied to develop a mineralisation profile of osteoblast-like cells over three weeks. This was important to give a baseline comparison sample to use when considering results from the osteoblast-specific ablated NPP1 primary osteoblasts, which are to be cultured under the same conditions. This involves the use of β-GP (to promote mineralisation) and AA (required for collagen secretion). These experiments demonstrated that the optimum culture conditions to induce matrix mineralisation of osteoblasts and other cell types (*e.g.* vascular smooth muscle cells) (Quarles et al., 1992, Franceschi et al., 1994, Steitz et al., 2001, Collet et al., 2007, Hong et al., 2010).

The data presented in this chapter demonstrate that the *Enpp1*$^{flox/flox}$;*Ocn*-cre primary osteoblasts can mineralise their matrix to a greater extent, and faster, than the *Enpp1*$^{flox/flox}$ control primary osteoblasts. The matrix mineralisation of the *Enpp1*$^{flox/flox}$ control isolated primary osteoblasts is consistent with previous studies showing calvarial osteoblasts forming mineralised multicellular nodules under minerlisation conditions *in vitro* (Hessle et al., 2002,

Patel et al., 2019). As such, the ablation of NPP1 in osteoblasts results in increased mineralisation, reflected by qualitative and quantitative Alizarin red S staining and calcium deposition analysis.

Typically, a positive correlation between the expression of *Runx2, Alpl and Bglap* is observed during mineralisation. Although no late time points investigated revealed significant differences in *Bglap* expression*,* only *Runx2* expression demonstrated significantly increased mRNA expression in the *Enpp1*$^{flox/flox}$;*Ocn*-cre isolated primary osteoblasts compared to *Enpp1*$^{flox/flox}$ controls. Intriguingly, *Alpl* was significantly decreased in the *Enpp1*$^{flox/flox}$;*Ocn*-cre isolated primary osteoblasts, although at all other time points a trend of increased *Alp* activity in the *Enpp1*$^{flox/flox}$;*Ocn*-cre isolated primary osteoblasts was observed. This suggests an alternative origin for high P_i levels: this is possibly achieved through significantly increased PHOSPHO1 expression, whereby relative mRNA levels were notably increased in the *Enpp1*$^{flox/flox}$;*Ocn*-cre isolated primary osteoblasts, however, this was only observed at day 21. This is supportive of a matrix-vesical derived origin of HA mineral within the *Enpp1*$^{flox/flox}$;*Ocn*-cre primary osteoblasts (Stewart et al., 2006).

No significant differences between *Enpp1*$^{flox/flox}$;*Ocn*-cre and *Enpp1*$^{flox/flox}$ isolated primary osteoblasts for *Mgp* expression – a recognised inhibitor of bone mineralisation, were observed, indicating that the osteoblast-specific ablation of *Enpp1* is enough of a driving force to lead to increased mineralisation even when *Mgp* levels remain low and unchanged (Murshed et al., 2004). These findings are consistent with the literature which reports that *Mgp* expression is generally low in skeletal tissue so as not to inhibit mineralisation (and comparatively higher in soft tissue so at to not permit mineralisation) (Price et al., 1983, Hale et al., 1988, Cancela et al., 1990, Theuwissen et al., 2012).

Given that one of the critical functions of NPP1 is to generate PP_i from ATP, it was of interest to analyse the extracellular PP_i concentration in the media from cultured cells. As expected, this was shown to be significantly decreased in the *Enpp1*$^{flox/flox}$;*Ocn*-cre primary osteoblasts

possibly indicating the primary mechanism through which the hypermineralisation phenotype of these cultures is facilitated. As demonstrated in chapter 3, the *Enpp1*$^{flox/flox}$;*Ocn*-cre mice display a significant increase in bone formation (and bone mineral density) compared to *Enpp1*$^{flox/flox}$ controls. As such, it is possible to consider that the *Enpp1*$^{flox/flox}$;*Ocn*-cre isolated primary osteoblasts have a higher metabolic demand than those from their control. Indeed, with increased bone formation and matrix mineralisation, a greater proportion of proteins (*e.g.* collagen and extracellular matrix proteins) and HA mineral must be synthesised and released which is associated with energetic cost. The skeleton is recognised as an endocrine organ, with roles in systemic metabolism and abilities to regulate energy. This concept of bone-regulated metabolism was first suggested and understood when *Fgf23* was recognised as critical in regulating phosphate metabolism and thus bone mineralisation (Murshed et al., 2005). Secondly, the understanding of systemic functions of OCN (as detailed in chapter 1) which regulates glucose via insulin signalling recognised the skeleton as a mediator of energy metabolism (Karsenty et al., 2012). It is important to consider that bone formation (modelling and remodelling) is also associated with high-energetic demand, and thus may influence energy metabolism. As such, I investigated both the aerobic respiration and glycolytic functions of the isolated primary osteoblasts. The literature reports that isolated primary osteoblasts are capable of utilizing both aerobic glycolysis and oxidative phosphorylation during their differentiation *in vitro* and that once a cellular maturity is reached a heavier reliance on aerobic glycolysis was observed (Guntur et al., 2014). Furthermore, it has been demonstrated that the stimulation of aerobic glycolysis (via stabilisation of the Hif1α complex) in pre-osteoblasts leads to the increased osteoblast formation from pre-osteoblasts and bone formation in mice (Regan et al., 2014). It is therefore suggested that glycolysis is a notable metabolic feature of osteoblasts, and is critical to their phenotype.

The predominance of glycolysis when cells exhibit a high energy demand is seemingly counter-intuitive, given that glycolysis yields less ATP than aerobic respiration. However, it has been reported in several studies from the 1950's and 1980's that aerobic glycolysis is the main mechanism of glucose production in osteoblasts (Borle et al., 1960, Cohn and Forscher, 1962). This preliminary work was conducted using slices of bone and was later confirmed in primary osteoblasts isolated from calvariae (Peck et al., 1964). The mature osteoblasts

increased reliance on glycolysis is likely related to the large-scale production of ECM proteins required for bone formation. More recent *in vivo* analysis of primary osteoblasts has demonstrated that mature osteoblasts preferentially utilise aerobic glycolysis over oxidative phosphorylation (Guntur et al., 2014)

The results presented in this chapter demonstrate a significant reduction in the glycolytic function indicators investigated (that is, the approximation of glycolytic function under both mitochondrial inhibition and full respiratory inhibition conditions, determined through the Seahorse Mitochondrial Stress Test). This suggests that the deletion of *Enpp1* within bone is detrimental to the metabolic functionality of the osteoblasts, leading to impaired energy production compared to the controls.

Further research in recent years has identified the osteoblasts as being implicated in the regulation of systemic glucose metabolism, evident in mouse model studies (Esen and Long, 2014). Insulin and bone are intimately linked, whereby insulin is necessary for healthy post-natal bone acquisition (Manolagas and Weinstein, 1999). Mice which lack the IR specifically in osteoblasts exhibit decreased trabecular bone volume and decreased bone formation, with reduced osteoblast numbers and structural strength (Fulzele et al., 2010, Clemens and Karsenty, 2011, Thrailkill et al., 2014). In wild-type mice, insulin serves an anabolic function, stimulating osteoblasts to proliferate and subsequently differentiate (Yang et al., 2010). Given that the osteoblast-specific IR null mice exhibit significant insulin resistance following chronic high-fat diet feeding, the insulin-bone relationship may be affected by the osteoblast-specific *Enpp1* ablation.

It is indeed well reported that decreased glycolysis is associated with diabetes and glucose metabolism dysregulation in mouse models (Guo et al., 2012). As such, the suppressed glycolytic function in the *Enpp1*$^{flox/flox}$;*Ocn*-cre primary osteoblasts compared to *Enpp1*$^{flox/flox}$ controls may contribute to the worsening metabolic phenotype observed. It is important to note that the knowledge of metabolic profile for bone cells remains largely undetermined. Furthermore, the artificial environment in which *in vitro* experiments are conducted may alter substrate utilisation and the overall metabolic function of the cells thereby making it

hard to extrapolate data. These two factors demonstrate a notable limitation of this study. A better understanding of the bioenergetics of cells is critical to understand a holistic view of the metabolic regulation of bone, and the ever-increasingly complex role of bone in regulating energy metabolism. This knowledge may aid in the treatment of metabolic and bone diseases.

The analysis of TNAP inhibition revealed no significant differences in mineralisation between genotypes at day 0 and day 21, evidenced through qualitative and quantitative Alizarin red S staining. This preliminary data to show that the absence of TNAP activity, coupled with the absence of osteoblast-specific NPP1 activity results in the absence of hypermineralisation phenotype likely due to a restored P_i/PP_i ratio. This *in vitro* finding reflects the *in vivo* finding of normalised skeletal mineralisation in knockout mice null for both *Alpl* and *Enpp1* (Hessle et al., 2002). The TNAP inhibitor cell culture data in this chapter would benefit from more detailed additional analysis to add credence to argument including mRNA, protein and total calcium analysis.

It is important to note that alternate methods of osteoblast isolation of mice exist. One such example is that of primary osteoblast isolation from the long bones. This may represent a suitable alternative isolation of osteoblasts, overcoming several limitations experienced I calvaria osteoblast isolation. For example, calvaria osteoblast isolation may result in a number of cell types in the final isolation including osteoclast precursor cells and fibroblasts (Peck et al., 1964, Burger et al., 1986). In addition, isolation from long bones would likely have yielded greater numbers of cells compared to the isolation of cells from individual calvaria of mice. This chapter would have benefitted from adopting more than one method of primary osteoblast isolation. Furthermore, chapter 3 demonstrates interesting sexual dimorphism with regard to the bone phenotype of the osteoblast-specific NPP1 ablated mouse. Due to the requirement to isolate primary osteoblasts from individual calvaria, it was not possible to separate the calvaria by sex to investigate whether sexual dimorphism was also observed in the mineralisation capacity of the primary osteoblast. It would have been of great interest, and likely easier practical implementation, to assess sexual dimorphism and

minerlisation capacity of osteoblast by assessing the temporal mineralszation of adenoviral *Enpp1* knockdown osteoblasts isolated from long-bones of wild-type mice.

Overall, the data presented in this chapter demonstrates that cultures of *Enpp1*$^{flox/flox}$;*Ocn*-cre primary osteoblasts demonstrate a hypermineralisation phenotype with concomitant decreased extracellular PP_i concentration and alterations to metabolic function.

(*This page has been left intentionally blank)*

Chapter 5. Investigating the role of osteoblast-specific NPP1 ablation on metabolism.

5.1. Introduction

The global NPP1 knockout mouse (*Enpp1*$^{-/-}$) mouse presents with a notable metabolic phenotype when reared on a control diet (Huesa et al., 2014). Chronic deficiency of NPP1 resulted in changes in whole-body glucose metabolism, whereby adult global *Enpp1*$^{-/-}$ mice present with decreased glucose-stimulated insulin secretion (GSIS) peak across the duration of a GTT, indicating insulin sensitisation (Huesa et al., 2014). The *Enpp1*$^{-/-}$ mice also presented with unaltered serum total OCN levels (Huesa et al., 2014). However, further investigation revealed that the *Enpp1*$^{-/-}$ mice exhibit increased serum concentrations of the bioactive form of OCN (under-carboxylated (GLU13), and un-carboxylated GLU)), along with increased bone resorption (Huesa et al., 2014). NPP1 is recognised as a negative regulator of insulin signalling: these data suggest that the ablation of NPP1 results in metabolic protection via increased osteoclastic bone resorption (Maddux et al., 2006a, Goldfine et al., 2008, Prudente et al., 2009, Huesa et al., 2014). The resulting acidic environment facilitates undercarboxylated-OCN or uncarboxylated-OCN formation and increased insulin sensitivity (Nesbitt and Horton, 1997, Salo et al., 1997, Ivaska et al., 2004, Ivaska et al., 2005, Booth et al., 2013, Huesa et al., 2014, Wei and Karsenty, 2015b).

The insulin-sensitive phenotype observed in the *Enpp1*$^{-/-}$ mice may be due to the ablation of NPP1 in insulin-sensitive tissues such as the liver, adipose, and the skeletal muscle, and/or due to increased bone turn over involving both the osteoblasts and osteoclasts. Recent advancements in the refinement of mouse genetics and techniques employed to investigate metabolism and cellular bioenergetics have greatly improved our understanding of the cellular mechanisms that regulate energy metabolism. The last two decades have led to unexpected observations in genetically modified mice, revealing novel endocrine pathways whereby bone cells communicate with other centres of metabolic control (*e.g.* OCN signalling to the pancreas to regulate insulin secretion and thus glucose concentration) (Ducy et al., 1996, Lee et al., 2007, Oury et al., 2011, Guntur and Rosen, 2012, Oldknow et al., 2014, Wei et al., 2014, Wei and Karsenty, 2015a, Karsenty and Olson, 2016). This has resulted in recognition of the role that the skeleton, or more specifically of the different skeletal cell types, plays in overall bioenergetics (Lee et al., 2007, DiGirolamo et al., 2012, Guntur and Rosen, 2012, Guntur et al., 2014, Faienza et al., 2015, Lee et al., 2017, Suchacki et al., 2017).

Given that the skeleton completely replaces itself every 10 years (Manolagas, 2000), and that bone contributes a significant proportion of total body mass, the action of osteoblasts to generate bone can understandably be associated with a notable energetic demand (Borisov and Marei, 1974, Manolagas, 2000, Vaananen et al., 2000, Karsenty et al., 2012, Zhang et al., 2015, Suchacki et al., 2017). Bone cells require a significant proportion of the body's overall fuel supply, and as such, they compete with other highly metabolic (and energy-consuming) tissues (Riddle and Clemens, 2017). This basic notion can explain why it is critical that bone cells communicate with other tissues through hormones to influence global energy metabolism. Secondly, osteoblasts are programmed at various stages in their development to optimise their energy production in accordance with increased functional demand in their lifestyle such as when they need to synthesis a large amount of ECM collagen (Riddle and Clemens, 2017).

The research of the last 20 years points towards increasingly complex interplays between bone, fat and other metabolically important organs, through shared regulatory mechanisms of energy metabolism (Ducy et al., 1996, Lee et al., 2007, Zhou et al., 2009, Ferron et al., 2010a, Oury et al., 2011, DiGirolamo et al., 2012, Guntur and Rosen, 2012, Mackenzie et al., 2012, Oldknow et al., 2014, Wang et al., 2014b, Faienza et al., 2015, Wei and Karsenty, 2015a, Karsenty and Olson, 2016, Zoch et al., 2016, Du et al., 2016, Suchacki et al., 2017, Roberts et al., 2019a, Shan et al., 2019). Basic and translational research must be conducted to investigate the integrated skeletal-metabolic mechanisms to better understand the role of specific cell types in bone health, energy metabolism, and human health and disease. Given the recognised role of NPP1 in insulin signalling, the notable metabolic phenotype of *Enpp1*$^{-/-}$ mice, and the understanding of the energetic demands of osteoblasts, this chapter aimed to investigate the metabolic phenotype of mice lacking NPP1 specifically in the osteoblast utilising the novel *Enpp1*$^{flox/flox}$;*Ocn*-cre mouse (Esen and Long, 2014, Guntur et al., 2014, Huesa et al., 2014). Therefore, the overarching aim of this chapter was to compare the metabolic phenotype of *Enpp1*$^{flox/flox}$;*Ocn*-cre mouse and *Enpp1*$^{flox/flox}$ control mice.

5.2. Hypothesis

The osteoblast-specific ablation of *Enpp1* will result in increased insulin sensitivity of control-diet fed mice reflecting the metabolically protected phenotype of the global *Enpp1*$^{-/-}$ mice. A bone phenotype reflecting that of the juvenile *Enpp1*$^{flox/flox}$;*Ocn*-cre mice (chapter 3) will be observed for 16-weeks of age control-fed *Enpp1*$^{flox/flox}$;*Ocn*-cre mice.

5.3. Aims

I. To analyse the metabolic phenotype of 16-week old *Enpp1*$^{flox/flox}$;*Ocn*-cre and *Enpp1*$^{flox/flox}$ mice.

II. To analyse the bone phenotype of 16-week old *Enpp1*$^{flox/flox}$;*Ocn*-cre and *Enpp1*$^{flox/flox}$ mice.

5.4. Materials and methods

5.4.1. Animal generation, food, weighing, and consumption

The *Enpp1*$^{flox/flox}$;*Ocn*-cre and age-matched *Enpp1*$^{flox/flox}$ control mice were generated (Section 2.7.1) and male mice were fed a control-diet from 4-weeks of age until culling at 16-weeks of age (Section 2.7.2). The weight of consumed food was calculated each week. The weights of the mice were measured each week (Section 2.7.2).

5.4.2. Gross analysis

At 16-weeks of age, mice were culled and weight at cull was recorded. Tibiae and femora from male *Enpp1*$^{flox/flox}$;*Ocn*-cre and *Enpp1*$^{flox/flox}$ mice were collected at dissection and used for histological analysis (Section 5.4.5). The length of these long bones were measured using DigiMax digital Vernier callipers (R. S. Components Ltd, Corby, Northants, UK). Mice were dissected and soft tissues were collected (Section 2.6.3).

5.4.3. Glucose tolerance and insulin tolerance testing

Male mice aged 16-weeks were weighed and fasted for 4-hours before administration of 2 mg D-glucose per g of body weight by oral gavage (for GTT) or 0.5 mU of insulin per g of body weight by intraperitoneal injection (for ITT). Blood glucose and circulating insulin was calculated (Section 2.7.4).

5.4.4. Serum OCN analysis and biochemistry

Total OCN and uncarboxylated-OCN was measured as previously described (Ferron *et al.,* 2010) (Section 2.9.2). Julian Berger of Columbia University (USA) kindly completed this work. Glucose stimulated insulin secretion (GSIS) was detected by ELISA (ChrystalChem, Chicago, IL, USA) (Section 2.9.2).

5.4.5. Histological analysis

Soft tissues were collected from *Enpp1*$^{flox/flox}$;*Ocn*-cre *and Enpp1*$^{flox/flox}$ mice culled at 16-weeks of age (Section 2.6.3). Tissues were prepared for microscopic analysis by fixing in 10% NBF (Section 2.9.1). Sections were paraffin-embedded after fixing (Section 2.9.2). Fat pads, liver, and pancreas sections were stained with H&E (Section 2.9.3). The pancreatic islet number and islet size in H&E stained sections was determined (Section 2.9.9). The number and area of H&E stained adipocytes in fat pad sections was assessed (Section 2.9.10). Liver sections were stained with Weigert's haematoxylin and fast-green to assess architecture, and with picosirius red to assess fibrotic damage. Dr Timothy Kendal of the University of Edinburgh kindly performed the liver analysis (Section 2.9.11).

5.4.6. Immunohistochemistry of pancreas

Pancreatic tissue was collected (Section 2.6.3) and prepared for microscopic analysis by fixing in 10% NBF (Section 2.9.1). Pancreas sections were cut at 5 µM in thickness and insulin production was identified by immunohistochemistry (Section 2.9.12) to identify insulin-secreting pancreatic β-cells.

5.4.7. Analysis of liver triglyceride content

Following euthanasia of male mice at 16-weeks of age, livers were collected, frozen, and stored at -80° C. Tissue was prepared and total triglyceride was measured using a Triglyceride (TG) Assay (Sentinel Diagnostics, Milan, Italy) (Section 2.9.4).

5.4.8. mRNA analysis of metabolic tissues

mRNA was extracted from metabolic tissues (including liver, fat pads, and *quadriceps femoris*) using a Qiagen RNeasy kit according to the manufacturer's instructions. cDNA was prepared (Section 2.3.2) and was used at 5 ng/μl for RT-qPCR analysis (Section 2.3.3). Results were normalised to β-*actin* and *Gapdh* housekeeping gene and the relative gene expression level was calculated using the ΔΔCT method (Livak and Schmittgen, 2001).

5.4.9. Three-point bending of long bones

The tibiae and femora from male *Enpp1*$^{flox/flox}$;*Ocn*-cre and *Enpp1*$^{flox/flox}$ mice were collected. Three-point bending was conducted using an LXR materials testing machine (Lloyds Instruments, West Sussex, U.K.) (Section 2.6.1).

5.4.10. μ-CT of long bones

The tibiae and femora from 16-week old male *Enpp1*$^{flox/flox}$;*Ocn*-cre and *Enpp1*$^{flox/flox}$ mice were collected, fixed in 10% NBF for 24 hours and subsequently stored in 70% ethanol. The bones were scanned using a μ-CT (Skycan 1172, Bruker, Aartselaar, Belgium) to assess trabecular architecture and cortical geometry (Section 2.6.2).

5.4.11. Catwalk analysis

Gait analysis was recorded using a CatWalk XT gait analysis system. Mice were familiarised with the equipment before the recording of data. Data were collected from male *Enpp1*$^{flox/flox}$;*Ocn*-cre *and Enpp1*$^{flox/flox}$ mice at 14-weeks of age (Section 2.7.5).

5.5. Results

5.5.1. *Enpp1*$^{flox/flox}$*;Ocn*-cre mice demonstrate unaltered body mass and food consumption.

Given that findings of the global *Enpp1*$^{-/-}$ mice revealed a notable metabolic phenotype following control diet feeding, I reasoned that the osteoblast-specific NPP1 knockout mouse may recapitulate this protected metabolic phenotype. This is grounded in two phenomena: firstly, that the *Enpp1*$^{-/-}$ mice demonstrate an overall alteration of development including reduced body mass and secondly that NPP1 is a recognised negative regulator of insulin signalling (Maddux et al., 1995, Maddux and Goldfine, 2000, Mackenzie et al., 2012, Huesa et al., 2014). The *Enpp1*$^{flox/flox}$;*Ocn*-cre demonstrates no significant changes in body weight gain from 4-weeks of age to 16-weeks of age (Fig 5.1A) compared to *Enpp1*$^{flox/flox}$ mice. The food consumption per mouse was similar in both genotypes over this duration of study (Fig. 5.1B).

5.5.2. *Enpp1*$^{flox/flox}$*;Ocn*-cre mice demonstrate unaltered insulin sensitivity, reduced liver mass and increased muscle mass

The *Enpp1*$^{flox/flox}$;*Ocn*-cre mice exhibited unaltered glucose tolerance (Fig. 5.2A), insulin tolerance (Fig. 5.2B), and GSIS (Fig. 5.2C). Given that there can be a degree of variation between individual mice for responses to glucose and insulin, the area under the curve for each test was calculated. This technique is widely used to diagnose impaired glucose tolerance (Ayala et al., 2010). The area under the curve analysis for GTT (Fig. 5.2D), ITT (Fig 5.2E), and GSIS (Fig 5.2F) revealed no significant differences between genotype. To ensure that the absence of any changes in glucose metabolism and insulin sensitivity were not a product of altered organ mass and function, gross analysis of organ mass was conducted at necroscopy. These analyses revealed no significant changes for the *Enpp1*$^{flox/flox}$;*Ocn*-cre mouse in the mass (mg/g total body mass) of brown fat, subcutaneous fat, gonadal fat, mesenteric fat, spleen, pancreas or kidney compared to *Enpp1*$^{flox/flox}$ counterparts (Fig. 5.3). Interestingly, however, *Enpp1*$^{flox/flox}$;*Ocn*-cre mice demonstrated significantly reduced liver mass (49.10 mg/g total body mass vs. 58.57 mg/g total body mass; $P<0.05$) (Fig. 5.3). Given the critical importance of the liver in metabolic function, this warranted further investigation and histological analysis (Section 5.5.4). In addition, the left and right *quadriceps femoris*

muscles were significantly increased in mass in the *Enpp1*$^{flox/flox}$;*Ocn*-cre mice compared to *Enpp1*$^{flox/flox}$ controls (Left: 8.45 mg/g total body mass vs. 7.46 mg/g total body mass; $P<0.05$: Right: 8.48 mg/g total body mass vs. 7.38 mg/g total body mass; $P<0.01$) (Fig. 5.3). The gain of muscle *quadriceps femoris* muscle mass is indicative of increased loading via exercise, and as such it was pertinent to further investigate the altered muscle mass by analysing the gait of these mice (Section 5.5.3) (Soffe et al., 2016, White et al., 2016).

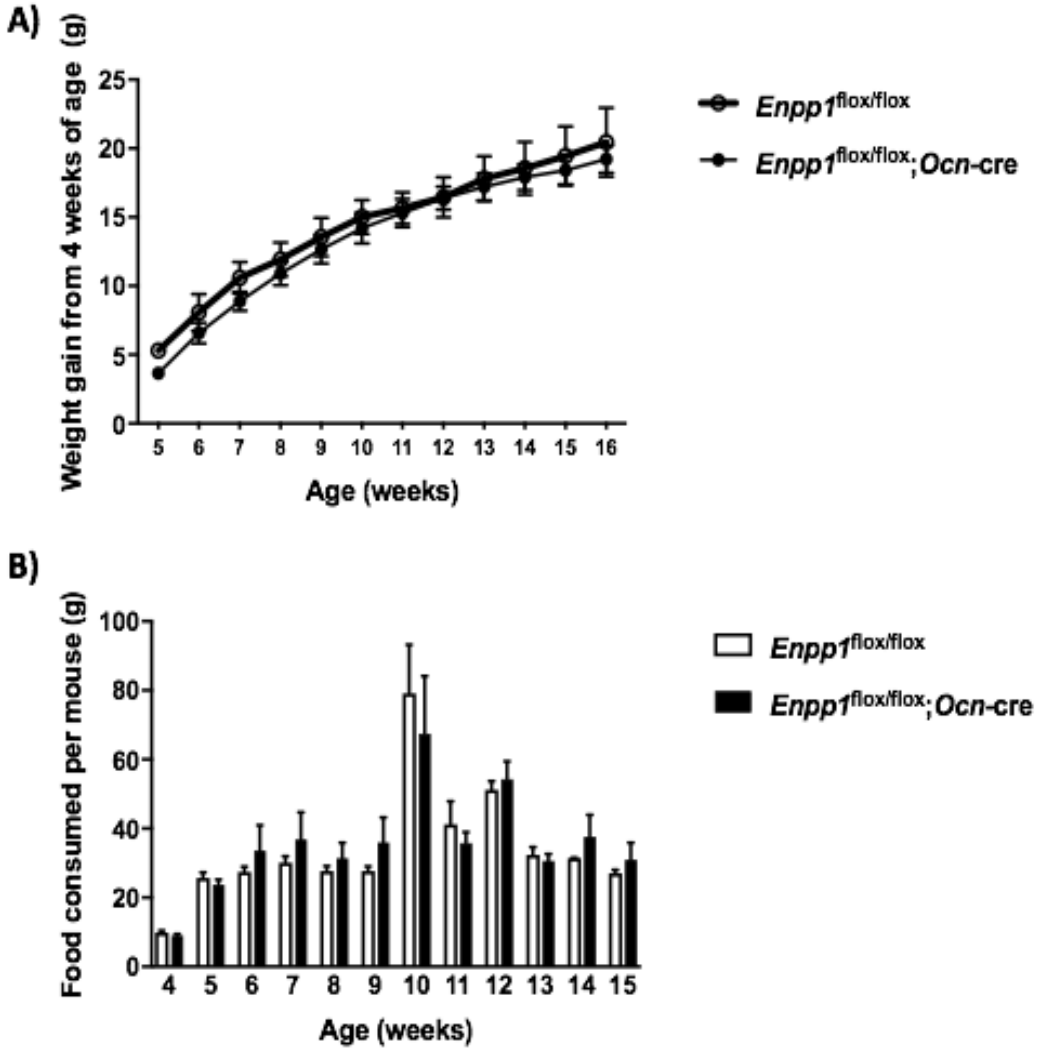

Figure 5.1. Weight gain and food consumption of mice is not altered between genotype.

(A) Analysis of *Enpp1*$^{flox/flox}$;*Ocn*-cre and *Enpp1*$^{flox/flox}$ mice. There was no significant difference in weight gain between genotype. To ensure this was not a result of disparity in feeding, (B) weekly food consumption was calculated revealing no difference between genotype throughout the time-course. Data are presented as the mean ± S.E.M (n≥4). No significant findings observed.

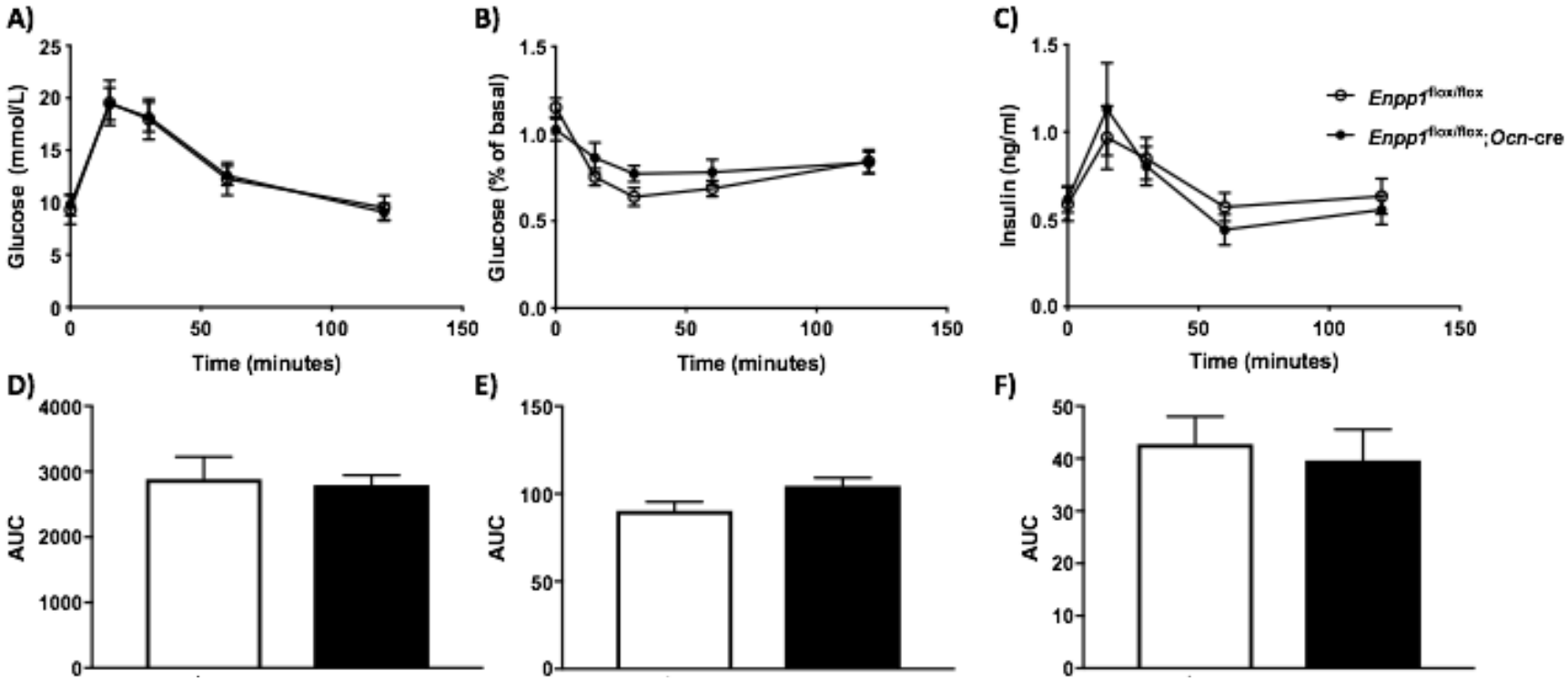

Figure 5.2. Assessment of glucose tolerance and insulin sensitivity is not altered between genotype.

Metabolic analysis of 16-week old male *Enpp1*$^{flox/flox}$;*Ocn*-cre and *Enpp1*$^{flox/flox}$ mice. (A) GTT and (D) area under the curve, (B) ITT and (E) area under the curve and (C) GSIS and (F) area under the curve showed similar blood glucose levels of *Enpp1*$^{flox/flox}$;*Ocn*-cre compared to *Enpp1*$^{flox/flox}$ mice. Data are presented as the mean ± S.E.M (n≥6). No significant findings observed.

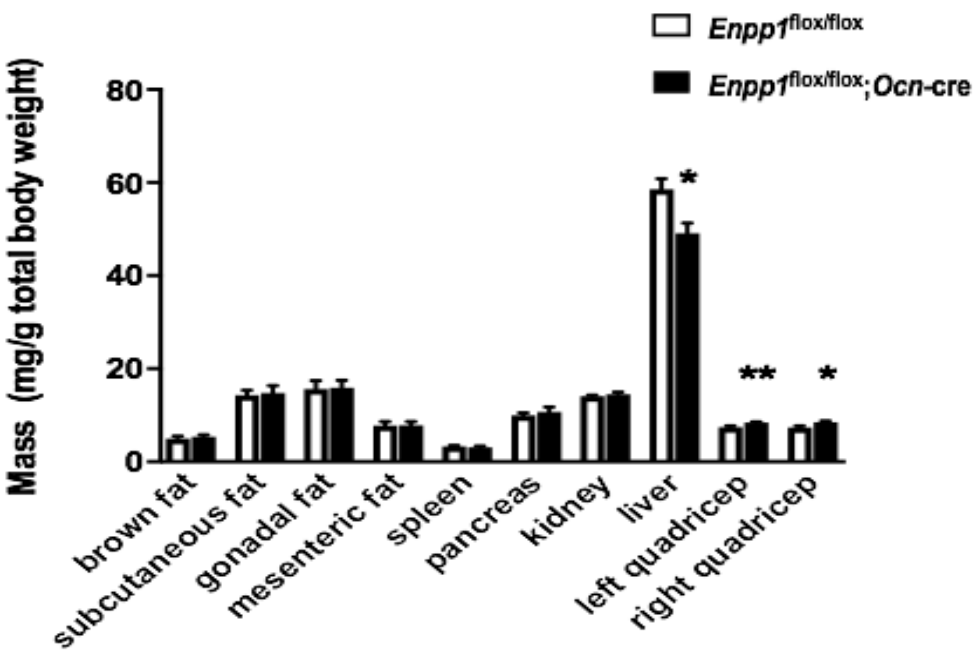

Figure 5.3. Organ mass at 16-weeks of age reveals differences in mass between genotype for liver, left and right *quadriceps femoris* muscle.

The *Enpp1*$^{flox/flox}$;*Ocn*-cre and *Enpp1*$^{flox/flox}$ mice were culled at 16-weeks of age and then dissected. The tissues were removed and weighed: brown fat, subcutaneous fat, gonadal fat, mesenteric fat, spleen, pancreas, kidney, liver, left quadriceps, and right quadriceps. Dissection analysis revealed that the liver mass (mg/g body total body weight) of *Enpp1*$^{flox/flox}$;*Ocn*-cre mice was significantly reduced, whereas left and right *quadriceps femoris* were significantly greater in mass compared to the *Enpp1*$^{flox/flox}$ control mice. Data are presented as the mean ± S.E.M (n≥4). Significance denoted by *P<0.05, **P<0.01.

5.5.3 *Enpp1*$^{flox/flox}$*;Ocn-cre* mice exhibit altered gait

Results from CatWalk gait analysis did not show any changes in stride length of the *Enpp1*$^{flox/flox}$;*Ocn*-cre mice compared to *Enpp1*$^{flox/flox}$ controls (Fig. 5.4). However, *Enpp1*$^{flox/flox}$;*Ocn*-cre mice did present with a number of altered gait parameters. *Enpp1*$^{flox/flox}$;*Ocn*-cre mice exhibit significantly increased initial dual stance (0.06 s vs. 0.027 s; *P*<0.05) (Fig. 5.5A), increased front paw base of support (1.53cm vs. 1.32 cm; *P*<0.05) (Fig. 5.5B), increased support girdle (1.85% vs. 1.12%; *P*<0.05) (Fig. 5.5C), decreased right front left front coupling (47.35% vs 50.89%; *P*<0.05) (Fig. 5.5D), increased right hind left front coupling (79.08% vs. 50.89%; *P*<0.05) (Fig. 5.5E) and left hind foot maximum intensity (48.54 % vs. 42.38 %; *P*<0.05) (Fig. 5.5F) compared to *Enpp1*$^{flox/flox}$ control mice.

5.5.4. Analysis of *Enpp1*$^{flox/flox}$*;Ocn*-cre mice liver histology and triglyceride content.

Given the alterations to the mass of the liver for the *Enpp1*$^{flox/flox}$;*Ocn*-cre (Fig. 5.3), it was important to assess the general histology of the liver to investigate if any tissue damage had occurred. A detailed histological appraisal by Dr Timothy Kendall indicated no pathological alterations were observed in the *Enpp1*$^{flox/flox}$;*Ocn*-cre *mice* or *Enpp1*$^{flox/flox}$ controls. The *Enpp1*$^{flox/flox}$;*Ocn*-cre mice and *Enpp1*$^{flox/flox}$ controls revealed no fibrosis and tissue damage through inflammation. Given the metabolic protection of the global *Enpp1*$^{-/-}$ mouse, I next wanted to investigate whether the decreased liver size of the *Enpp1*$^{flox/flox}$;*Ocn*-cre mouse was due to a decrease in liver triglyceride deposition. However, analysis of this revealed no significant difference between the genotypes (Fig. 5.6). Therefore, the liver mass difference between genotypes is likely not attributable to any triglyceride storage changes nor tissue pathological tissue damages.

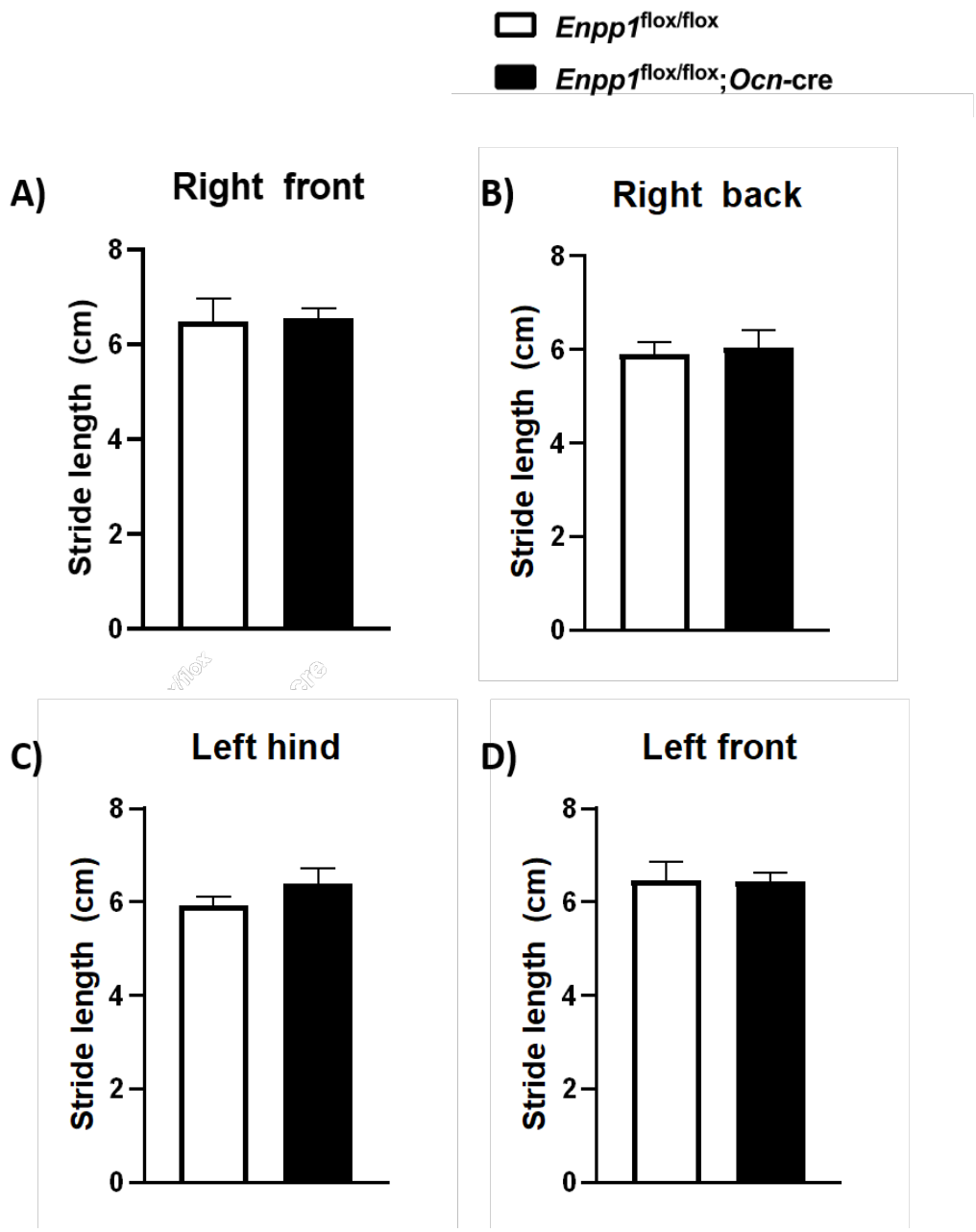

Figure 5.4. The stride length of mice is not altered between genotype.

The gait of male *Enpp1*$^{flox/flox}$;*Ocn*-cre and *Enpp1*$^{flox/flox}$ mice were assessed at 14-weeks of age. Stride length of the (A) right front, (B) right back, (C) left hind and (D) left front legs. Data are presented as the mean ± S.E.M (n≥6). No significant findings observed.

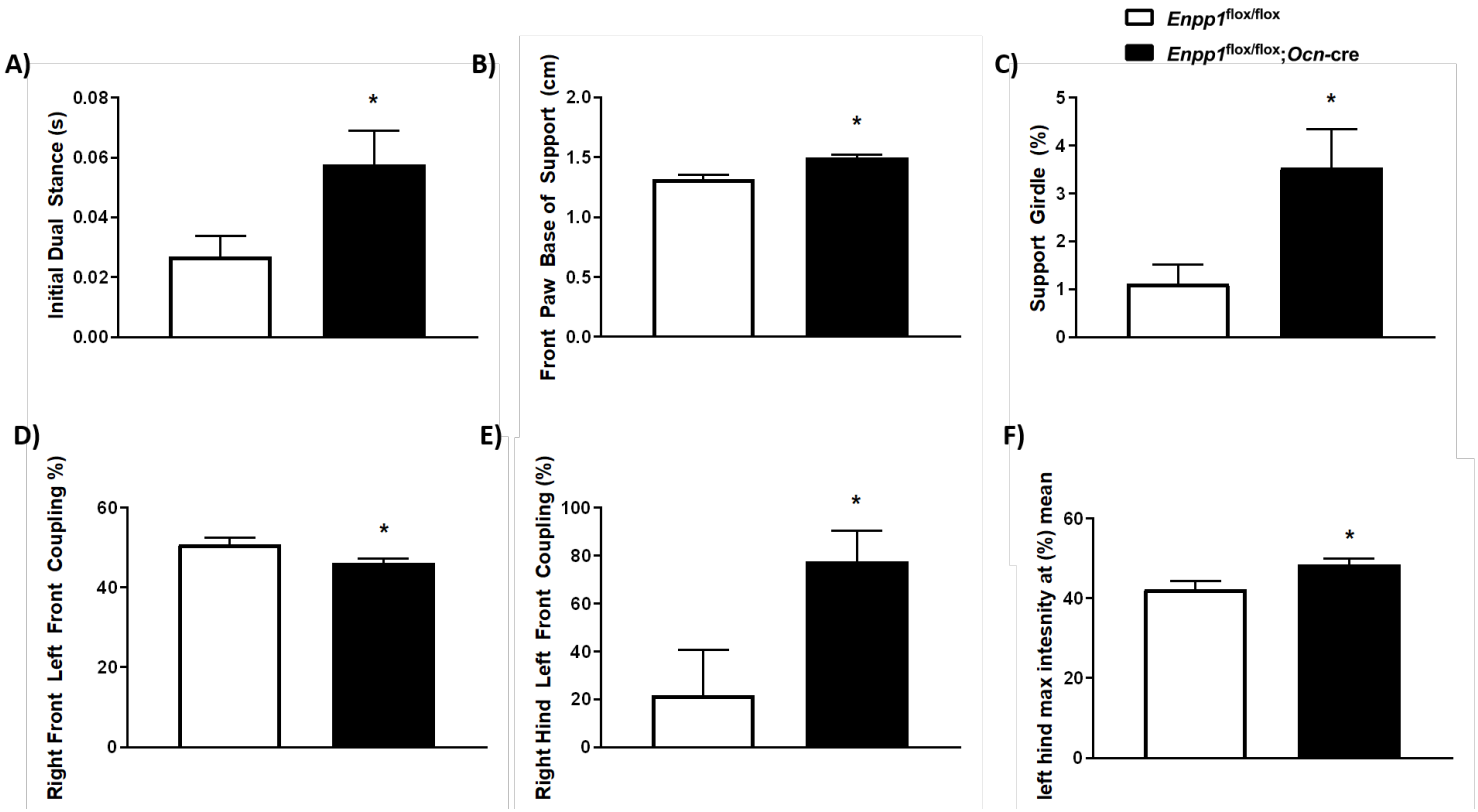

Figure 5.5. Gait analysis reveals an unstable gait in the osteoblast-specific NPP1 ablated mouse model.

The gait of male *Enpp1*$^{flox/flox}$;*Ocn*-cre and *Enpp1*$^{flox/flox}$ mice were assessed at 14-weeks of age. Parameters showing significant differences included (A) initial dual stance, (B) front paw base of support, (C) support girdle, (D) right front let front coupling, (E) right hind left front coupling and (F) Left hind max intensity at (%) mean. Data are presented as the mean ± S.E.M (n≥6). Significance denoted by *P<0.05.

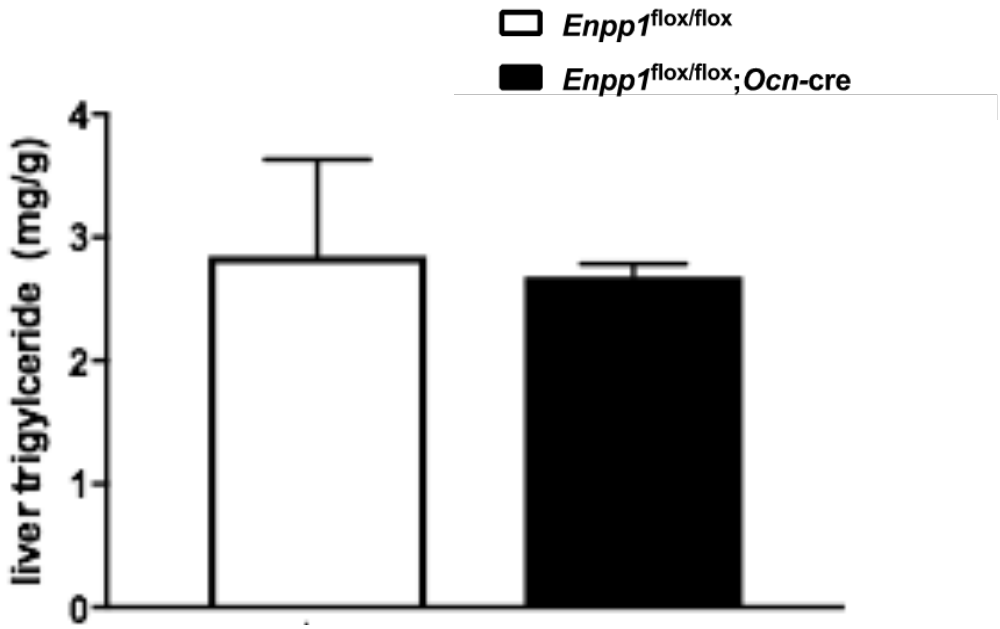

Figure 5.6. Liver triglyceride quantification reveals no differences between genotype.

Quantitative analysis of liver triglyceride demonstrates no difference between genotype in triglyceride content. Images are representative. Data are presented as the mean ± S.E.M (n≥4). No significant findings observed.

5.5.5. *Enpp1*$^{flox/flox}$*;Ocn*-cre mice exhibit increased uncarboxylated-OCN and unaltered pancreata.

Analysis demonstrated an unaltered serum concentration of total OCN (Fig. 5.7A). When considering only uncarboxylated-OCN, the *Enpp1*$^{flox/flox}$*;Ocn*-cre mice present with a significantly increased serum concentration compared to *Enpp1*$^{flox/flox}$ controls (Fig. 5.7B) (22.87 ng/ml vs. 11.74 ng/ml; $P<0.05$). Given that undercarboxylated-OCN or uncarboxylated-OCN exerts a systemic effect on the pancreas, whereby it promotes insulin secretion, the insulin-secreting islets of the pancreas were next analysed. The *Enpp1*$^{flox/flox}$;*Ocn*-cre mice demonstrate no significant difference in the size (Fig. 5.7C) or number (Fig 5.7D) of insulin-secreting pancreatic islets. This indicates that osteoblast-specific NPP1 ablation does not result in the alteration of pancreatic beta-cell function, despite the significant changes to the uncarboxylated-OCN secretion.

5.5.6. Analysis of adipocytes from the white and brown fat depots

The analysis of organ mass following culling at 16-weeks of age revealed no significant difference in the mass of the white fat depots (mg/g total body weight) (Fig. 5.8). To determine whether the deletion of osteoblast-specific NPP1 resulted in an alteration of the adipocyte's ability to store lipid, the average number and average area of adipocytes for each of the white adipocyte depots were analysed. This revealed no significant difference between genotype for adipocyte number (Fig. 5.8A) or adipocyte area (Fig. 5.8B) in any of the three white fat depots. To determine whether there was variation in the adipocyte size, a size-frequency distribution of adipocytes for the subcutaneous fat pad (Fig 5.8C), the gonadal fat pad (Fig. 5.8D) and the mesenteric fat pad (Fig 5.8E) was conducted. This revealed a minor increase in the number of larger adipocytes in the subcutaneous and the gonadal fat pad of the *Enpp1*$^{flox/flox}$;*Ocn*-cre mice compared to the *Enpp1*$^{flox/flox}$ controls. Overall, the size distribution of adipocytes did not largely vary in the depots investigated. This suggests that there is no alteration in the hyperplasia or hypertrophy of the white adipocytes in the *Enpp1*$^{flox/flox}$;*Ocn*-cre mice. The number of adipocyte nuclei per field for brown fat showed no differences between genotype (Fig. 5.9). This indicates no change in brown fat adipogenesis, hyperplasia or hypertrophy as a result of osteoblast-specific NPP1 ablation in mice.

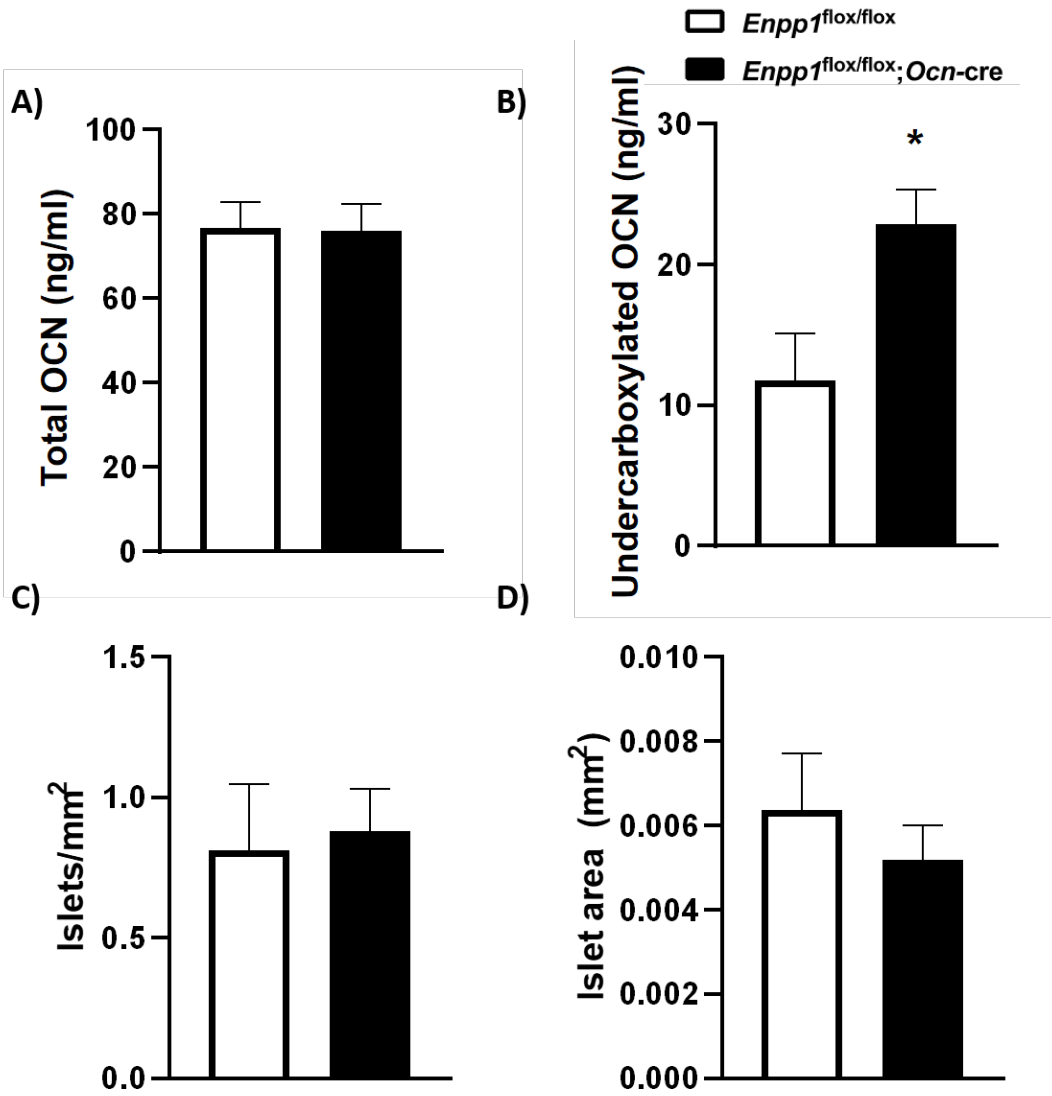

Figure 5.7. Osteoblast-specific NPP1 ablated mice have increased undercarboxylated OCN and unaltered pancreatic islet morphology.

Analysis of (A) total serum OCN and (B) undercarboyxlated-OCN, and the (C) area and (D) number of insulin-secreting pancreatic islets determined through immunohistochemistry and ImageJ quantitation. Data are presented as the mean ± S.E.M (n≥6). Significance denoted by *P<0.05.

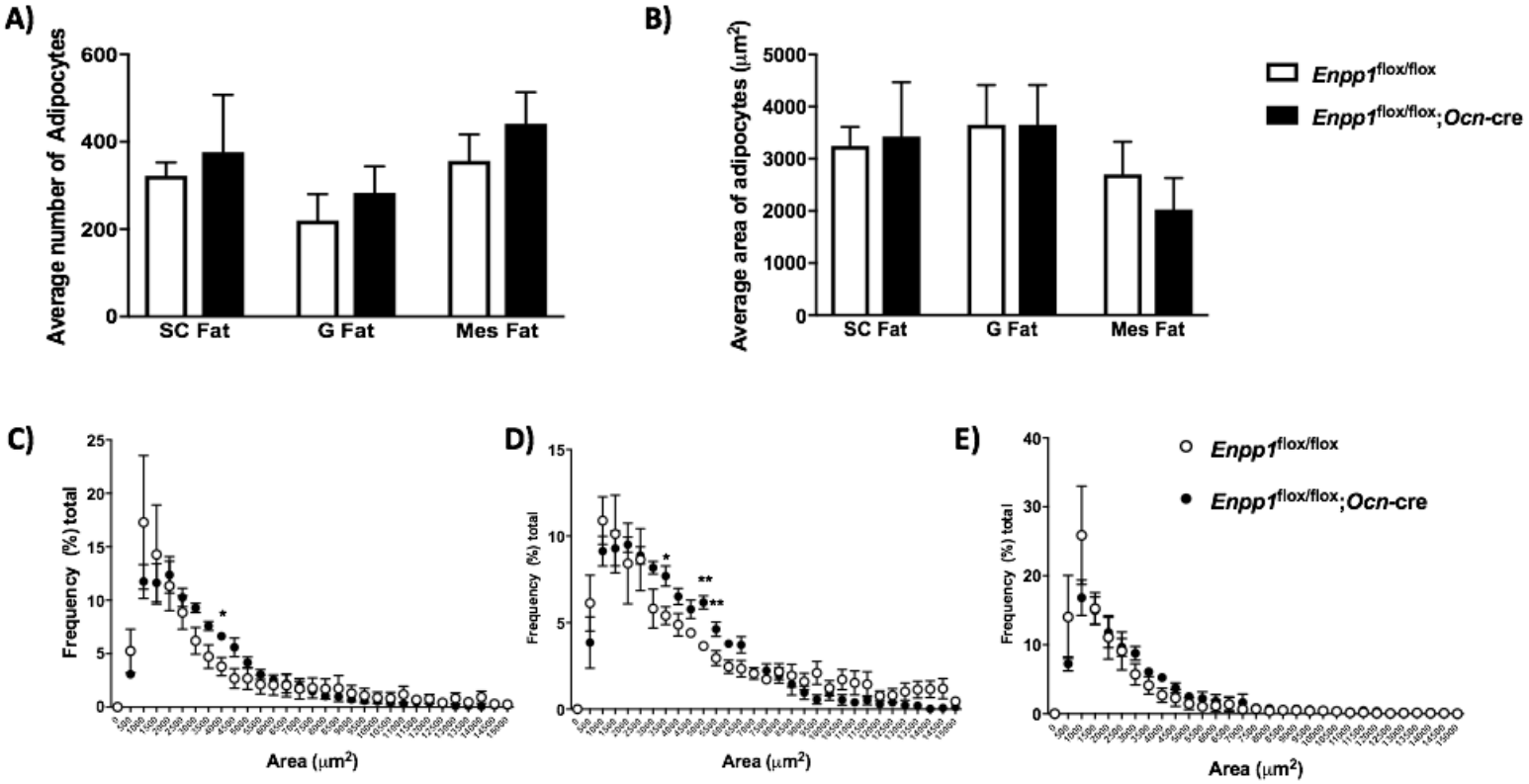

Figure 5.8. Analysis of the white fat depots adipocyte number, area, and size-frequency distribution is largely unchanged between genotypes.

The average (A) number and (B) area of adipocytes for the subcutaneous (SC), gonadal (G) and mesenteric (Mes) fat pad were analysed. The size-frequency distribution of adipocytes was analysed for the (C) SC, (D) G and (E) Mes fat pads. Data are presented as the mean ± S.E.M (n≥6). Significance denoted by **P*<0.05, ***P*<0.01.

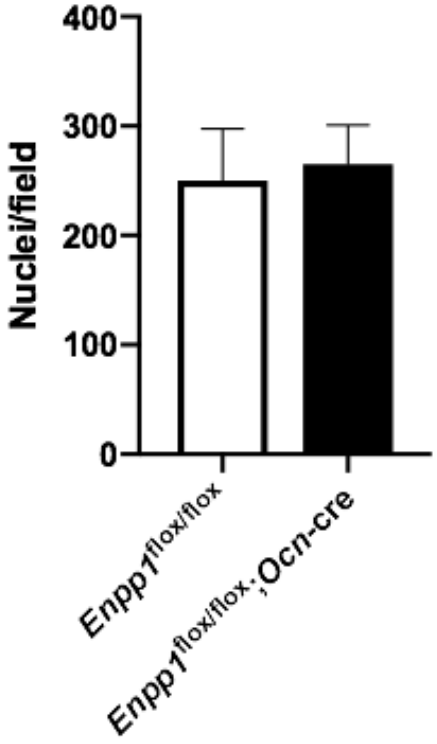

Figure 5.9. Quantitative assessment of brown adipose tissue nuclei reveals no difference between genotypes.

Analysis of H&E stained nuclei from *Enpp1*$^{flox/flox}$;*Ocn*-cre and *Enpp1*$^{flox/flox}$ mice revealed no difference in nuclei/field. Data are presented as the mean ± S.E.M (n=4). No significant findings observed.

5.5.7. Analysis of metabolic genes in metabolic tissues

The expression of genes associated with metabolism was evaluated in key metabolic tissues including *quadriceps femoris* muscle, brown fat, liver and white adipocytes (gonadal adipocytes). For the *quadriceps femoris* muscle, the glucose transporter (GLUT) receptors were analysed. This included Solute Carrier Family 2 Member 1 (*Slc2a1),* Solute Carrier Family 2 Member 2 (*Scl2a2),* Solute Carrier Family 2 Member 4 (*Scl2a4),* Solute Carrier Family 2 Member 10 *(Slc2a10)* and Solute Carrier Family 2 Member 12 (*Scl2a12).* These genes are reported in the literature to play key roles in metabolism (Mueckler and Thorens, 2013, Deng and Yan, 2016, Navale and Paranjape, 2016). No significant difference in the expression of any of the GLUT receptors of the investigated was noted (*Slc2a1, Slc2a2, Slc2a4, Slc2a10, Slc2a12*) for *Enpp1*$^{flox/flox}$;*Ocn*-cre mice compared to *Enpp1*$^{flox/flox}$ controls (Fig. 5.10A-E). Similarly, no difference in the mRNA expression of GLUT receptors (*Slc2a1, Sl2a2, Slc2a1,* and *Slc2a12*; Fig 5.11A-D) between genotypes was observed within the gonadal fat depot.

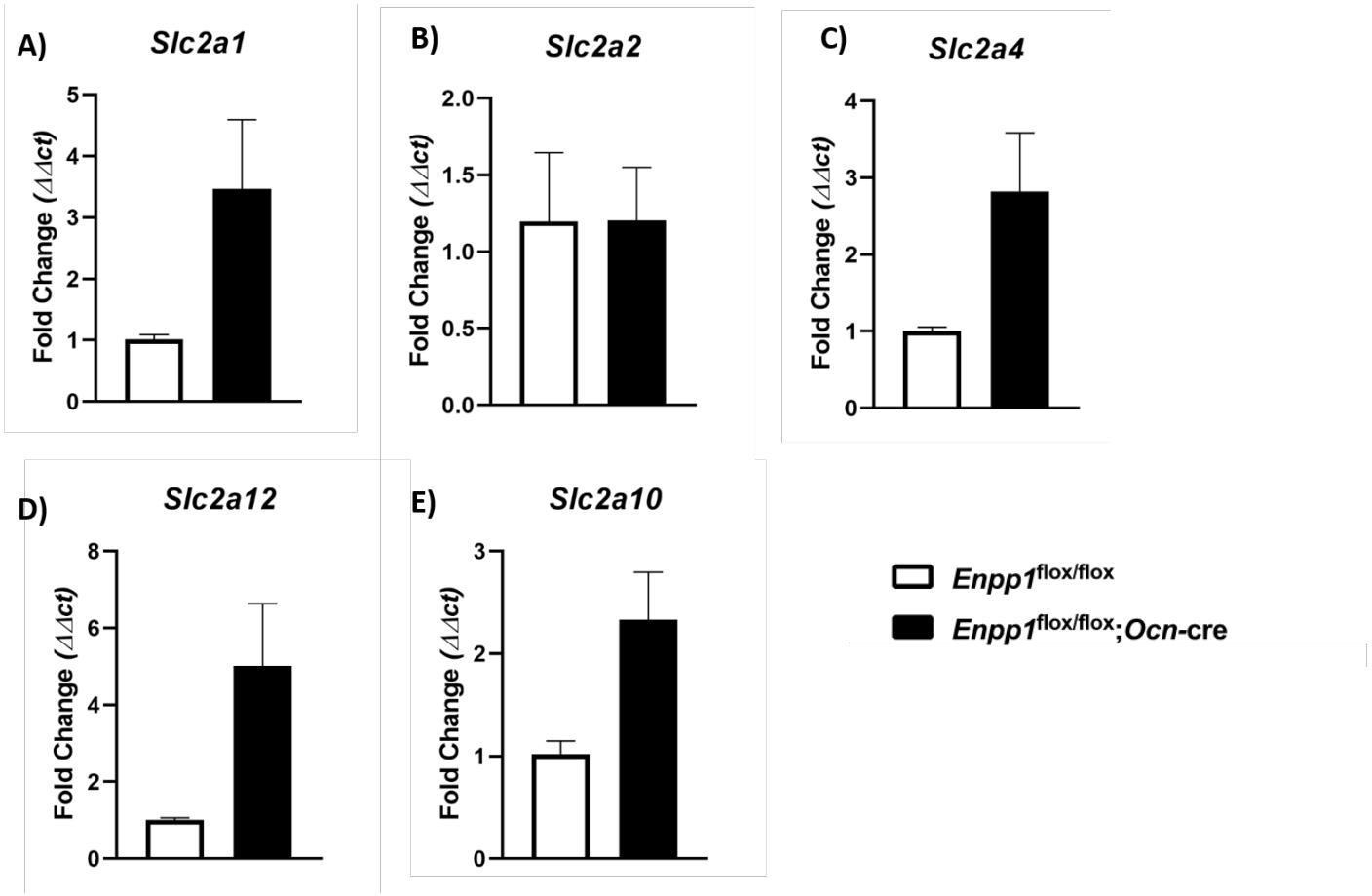

Figure 5.10. Analysis of the GLUT receptors of *quadriceps femoris* muscle reveals no differences between genotypes.
The *quadriceps femoris* mRNA expression of selected GLUT receptors including (A) *Slc2a1*, (B) *Slc2a2*, (C) *Slc2a4,* (D) *Slc2a10* and (E) *Slc2a12* was analysed. mRNA values generated were normalised to the geometric mean of *Gapdh* and *β-actin* house-keeping genes. Data are presented as the mean ± S.E.M (n=4). No significant findings observed.

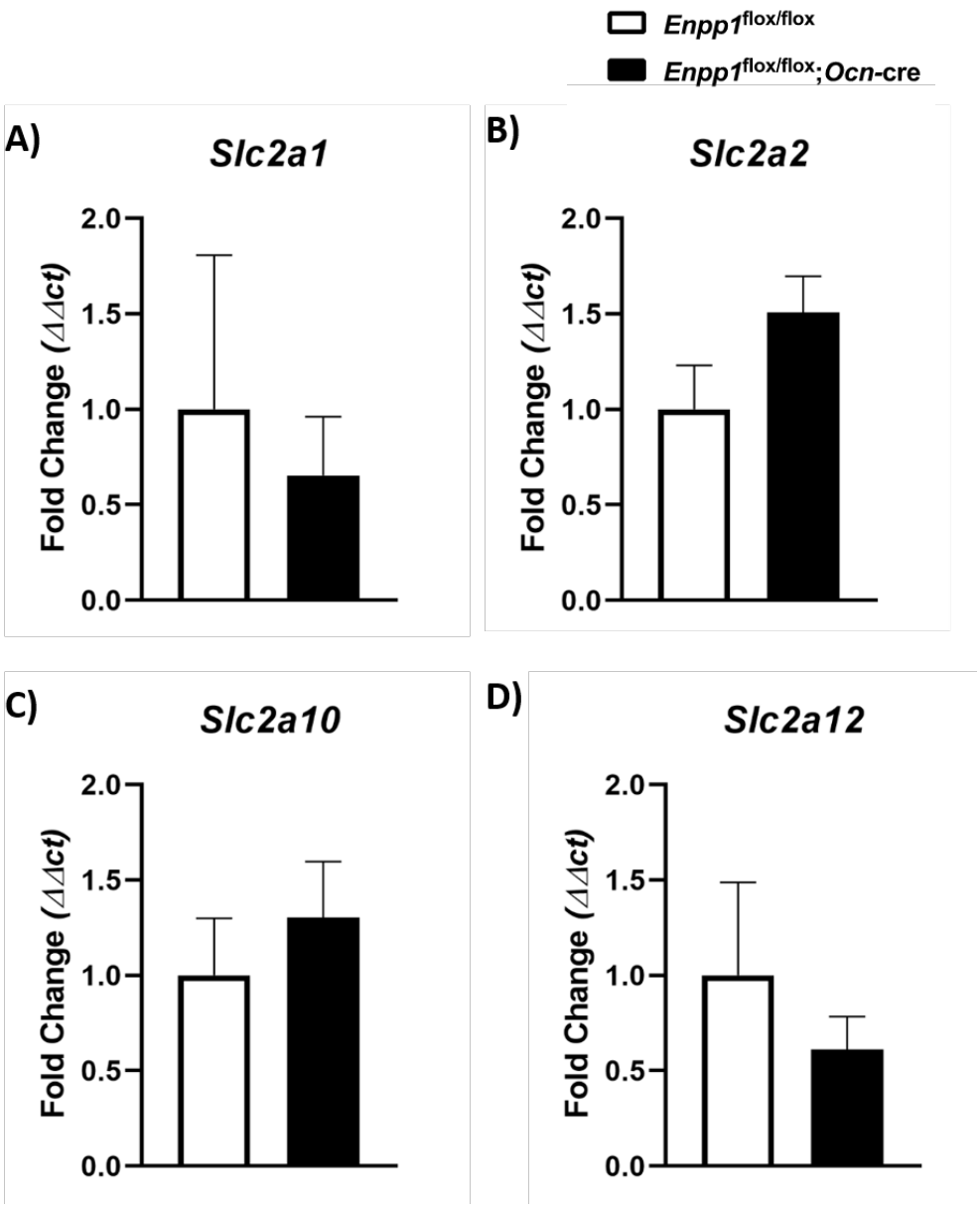

Figure 5.11. Analysis of the GLUT receptors of gonadal fat pad reveals no difference between genotypes.

The gonadal fat pad mRNA expression of selected GLUT receptors including (A) *Slc2a1*, (B) *Slc2a2*, (C) *Slc2a10,* (D) *Slc2a12* was analysed. mRNA values generated were normalised to the geometric mean of *Gapdh* and β-*actin* house-keeping genes. Data are presented as the mean ± S.E.M (n=4). No significant findings observed.

The liver was next analysed. Again, reflecting other metabolic tissues, no difference between genotype for the mRNA expression of the liver-expressed GLUT receptor (*Slc2a2*) was observed (Fig. 5.12A). No difference in the mRNA expression of liver peroxisome proliferator-activated receptor alpha (PPARα) was observed (Fig 5.12B). The liver phosphoenolpyruvate carboxykinase *(Pck1)* mRNA expression was significantly increased in *Enpp1*$^{flox/flox}$;*Ocn*-cre mice compared to *Enpp1*$^{flox/flox}$ control mice (Fold change of 1.81 vs. 1.00; $P<0.05$) (Fig. 5.12C).

The analysis of brown adipose tissue mRNA expression revealed largely unaltered expression of metabolic genes including; *Slc2a1, Slc2a4,* uncoupling protein-1 (*Ucp1),* uncoupling protein 2 (*UCP2),* diacylglycerol O-acyltransferase 2 *(Dgat2),* and lipoprotein lipase *(Lpl)* (Fig. 5.13. The mRNA expression of diacylglycerol O-acyltransferase 1 (*Dgat1)* was significantly reduced in the *Enpp1*$^{flox/flox}$;*Ocn*-cre mice compared to *Enpp1*$^{flox/flox}$ controls (Fold change of 0.45 vs. 1.00; $P<0.05$) (Fig 5.13E). This enzyme is involved in the synthesis of triglycerides (Yen et al., 2008, Liu et al., 2012). However, *Dgat2* mRNA expression remained unchanged between genotypes (Fig. 5.13F), and this enzyme is involved in the synthesis of triglycerides (Yen et al., 2008, Liu et al., 2012).

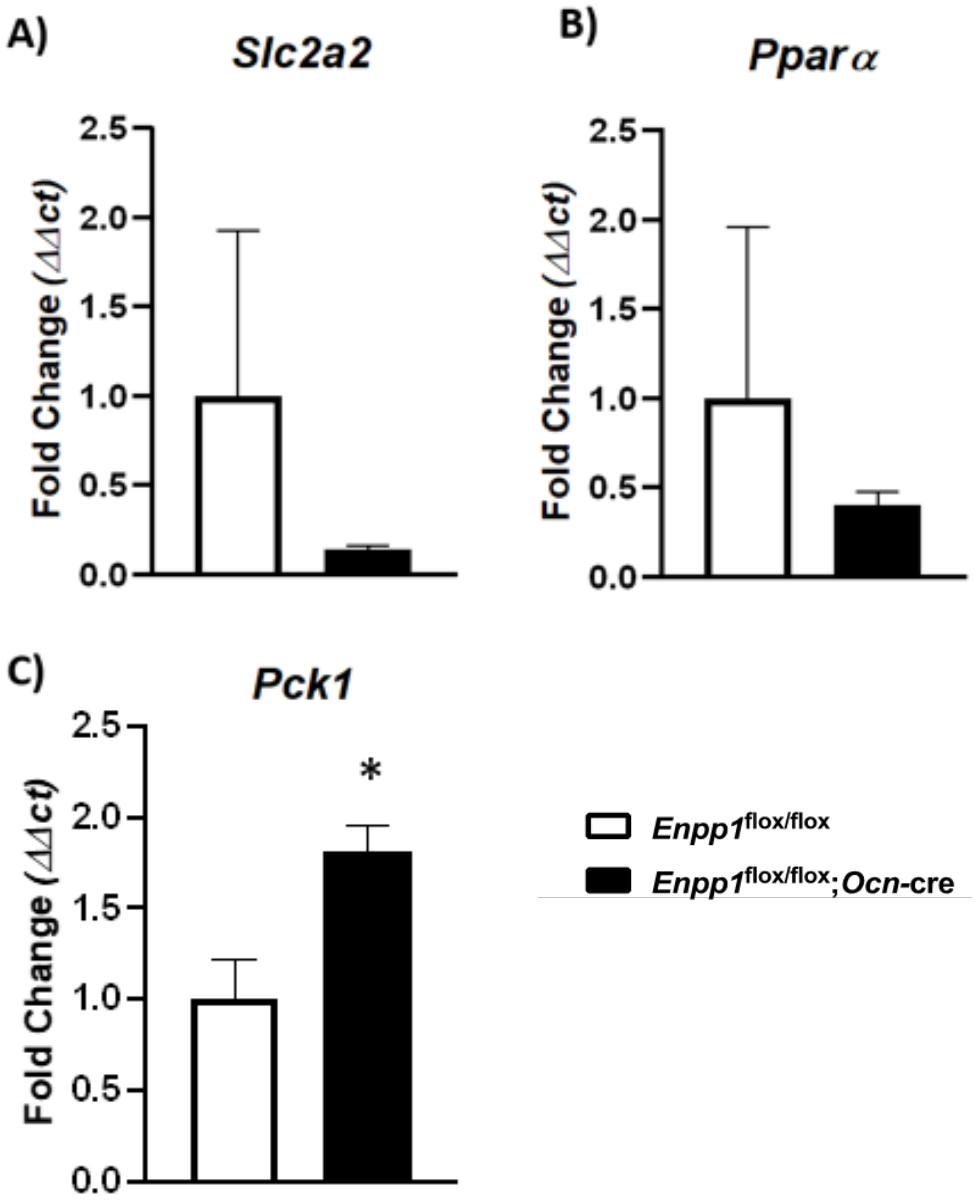

Figure 5.12. Analysis of liver metabolic genes demonstrates increased *Pck1* in osteoblast-specific NPP1 ablated mice.

The liver mRNA expression of selected metabolic genes including (A) *Slc2a2*, (B) *Pparα*, (C) *Pck1,* (D) *Slc2a12* was analysed. mRNA values generated were normalised to the geometric mean of *Gapdh* and β-*actin* house-keeping genes. Data are presented as the mean ± S.E.M (n=4), Significance denoted by **P*<0.05.

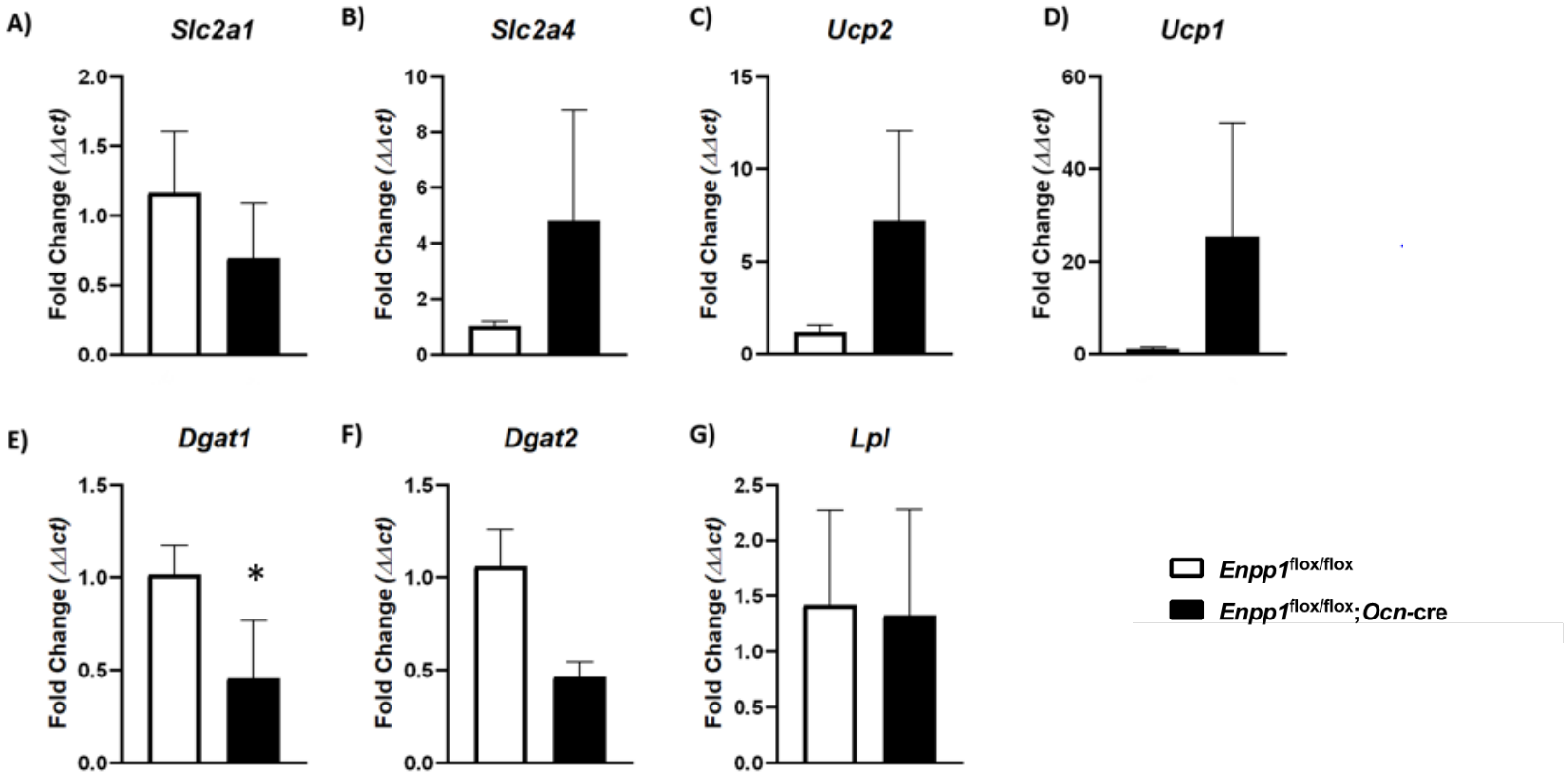

Figure 5.13. Analysis of selected brown adipose tissue metabolic genes reveals largely no difference in expression between genotypes.

The brown fat mRNA expression of selected metabolic genes including (A) *Slc2a1*, (B) *Slc2a4*, (C) *Ucp1,* (D) *Ucp2,* (E) *Dgat1* (F) *Dgat2 and* (G) L*pl* was analysed. mRNA values generated were normalised to the geometric mean of *Gapdh* and β-*actin* house-keeping genes. Data are presented as the mean ± S.E.M (n=4). Significance denoted by **P*<0.05.

5.5.8. Analysis of long bone micro-architecture, length and mechanical strength.

To investigate whether osteoblast-specific ablation of *Enpp1* caused alterations to bone architecture at 16-weeks of age, a μ-CT analysis of the diaphyseal bone of tibiae and femora from male *Enpp1*$^{flox/flox}$;*Ocn*-cre and *Enpp1*$^{flox/flox}$ mice was conducted. For the tibia, no genotype differences were observed for the analysed trabecular parameters (Fig. 5.14) or cortical parameters (Fig. 5.15). For the femora, no significant differences between genotype were observed for trabecular (Fig. 5.16) or cortical (Fig. 5.17) diaphyseal bone. These results reflect the absence of difference in skeletal phenotype of 22-week old male *Enpp1*$^{flox/flox}$;*Ocn*-cre mice (chapter 4). The length of long bones was also assessed to determine whether a disparity in growth was evident at 16-weeks of age for the *Enpp1*$^{flox/flox}$;*Ocn*-cre mice. No significant difference between genotype was observed regarding tibia or femora length nor mechanical properties (Table 5.1). This too reflects observations of the skeletal phenotype of male mice at 22-weeks of age (chapter 3).

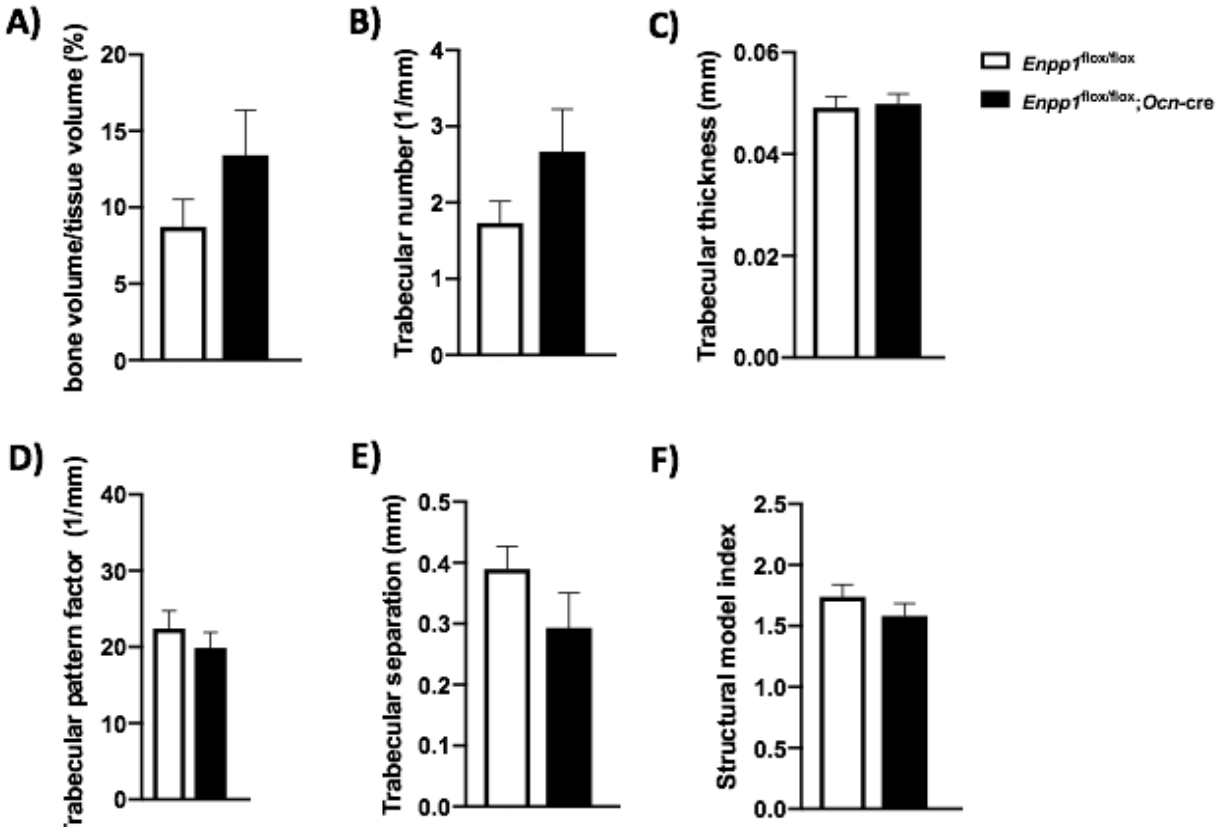

Figure 5.14. µ-CT analysis of tibiae trabecular bone from 16-week male mice demonstrates no difference between genotypes.

The following parameters were measured; (A) percent bone volume (BV/TV), (B) trabecular number, (C) trabecular thickness, (D) trabecular pattern factor, (E) trabecular separation and (F) Structural model index. Data are presented as the mean ± S.E.M ($n \geq 3$). No significant findings observed.

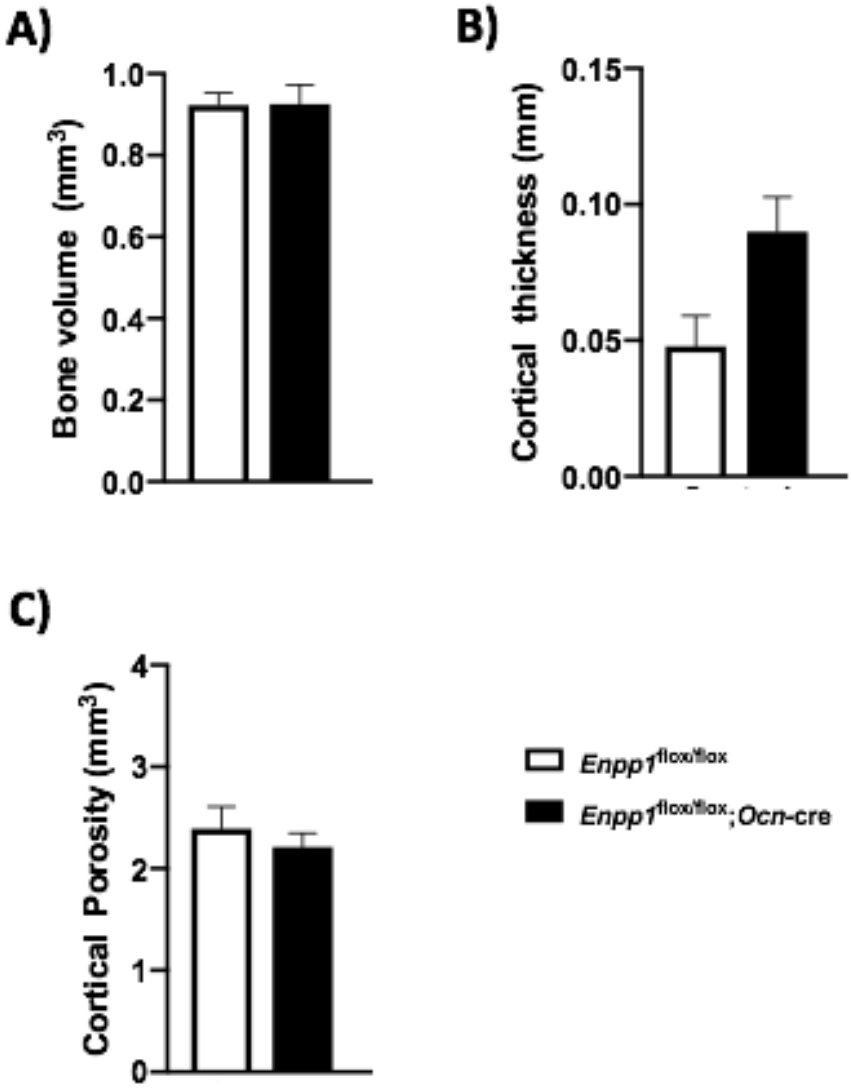

Figure 5.15. µ-CT analysis of tibiae trabecular bone from 16-week male mice demonstrates no difference between genotypes.

The following parameters were measured; (A) bone volume, (B) cortical thickness and (C) cortical porosity. Data are presented as the mean ± S.E.M (n≥3). No significant findings observed.

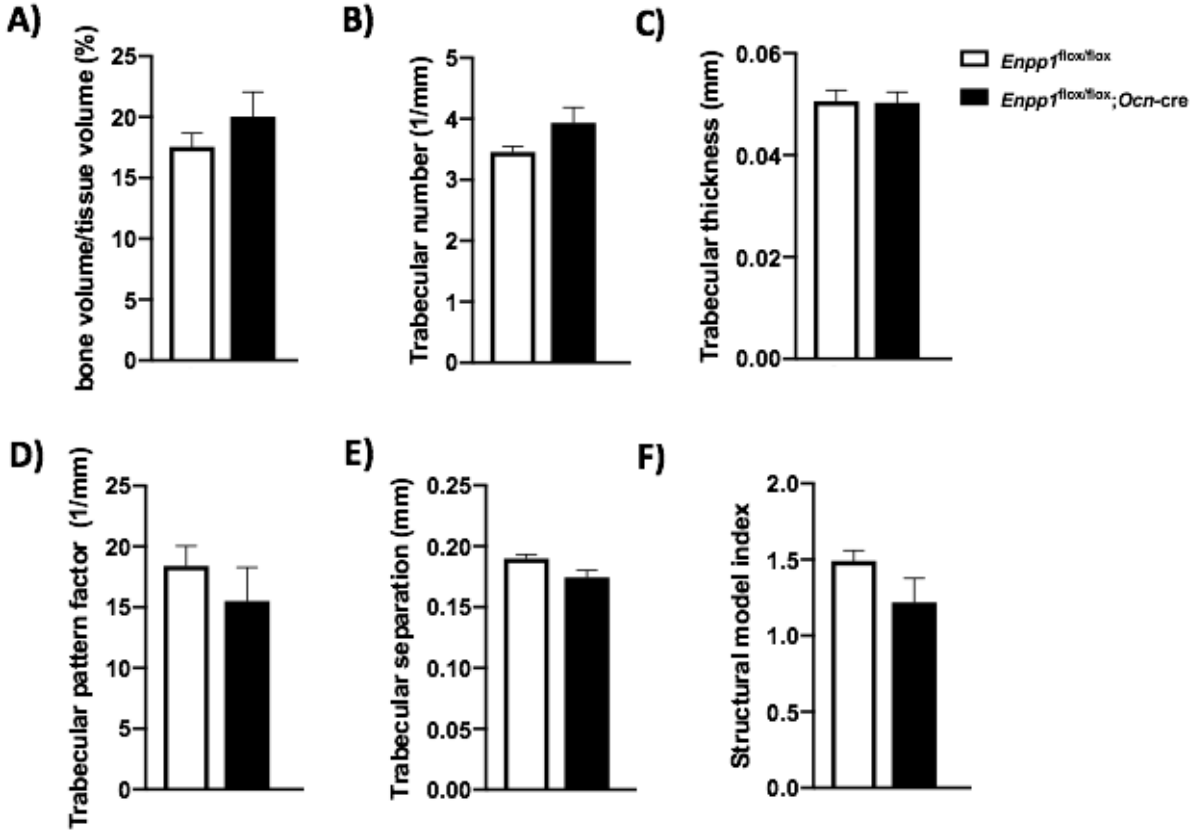

Figure 5.16. µ-CT analysis of femora trabecular bone from 16-week male mice reveals no differences between genotypes.

The following parameters were measured; (A) percent bone volume (BV/TV), (B) trabecular number, (C) trabecular thickness, (D) trabecular pattern factor, (E) trabecular separation and (F) Structural model index. Data are presented as the mean ± S.E.M (n≥3). No significant findings observed.

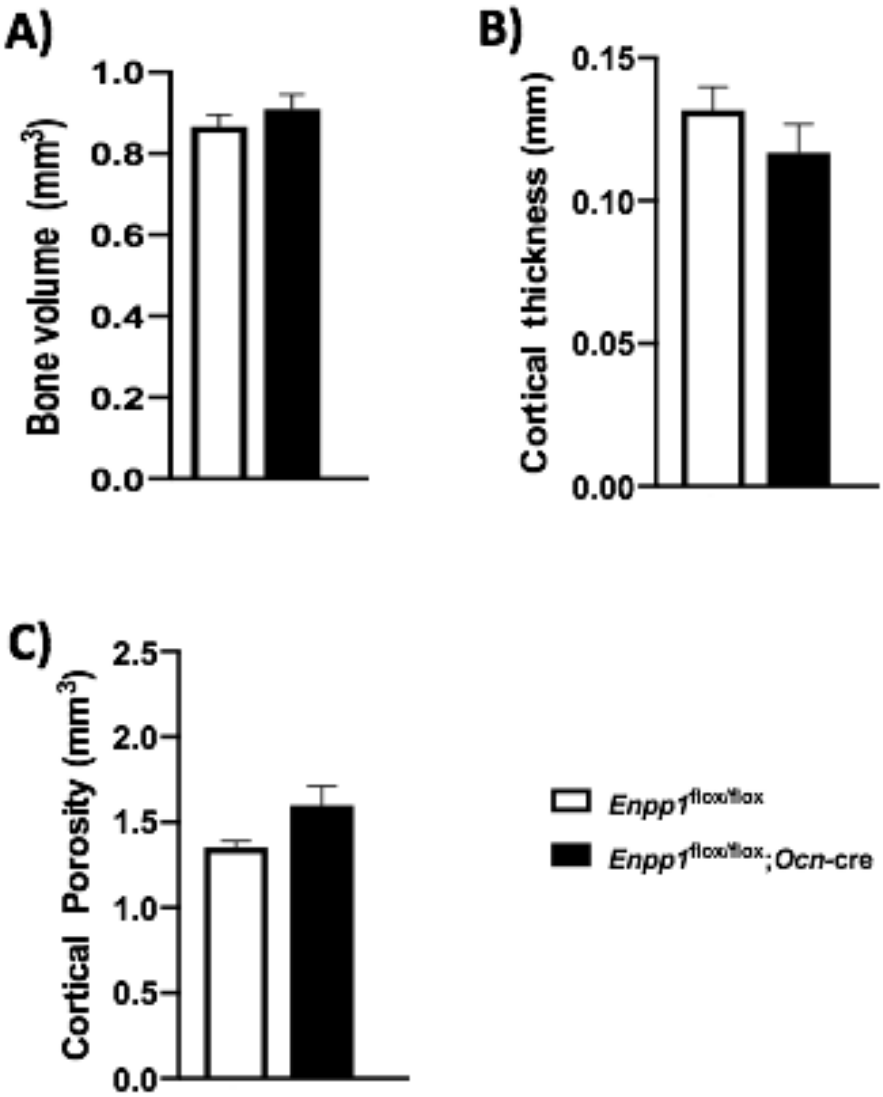

Figure 5.17. : µ-CT analysis of femora trabecular bone from 16-week male mice reveals no difference between genotypes.

The following parameters were measured; (A) bone volume, (B) cortical thickness and (C) cortical porosity. Data are presented as the mean ± S.E.M (n≥3). No significant findings observed.

Bone	Genotype	Length	Maximum Load (N)	Deflection at maximum load (mm)	Work to maximum Load x10^3 (J)	Stiffness x10^3 (N/m)	Load at Rupture (N)	Deflection at Rupture (mm)	Work to rupture x10^3 (J)
Tibia	*Enpp1$^{flox/flox}$*	17.4 (0.03)	8.87 (0.55)	0.67 (0.10)	3.39 (0.57)	25.09 (1.22)	6.49 (0.36)	0.84 (0.13)	4.81 (1.49)
	Enpp1$^{flox/flox}$;Ocn-cre	17.3 (0.03)	9.47 (0.90)	0.60 (0.05)	2.10 (0.21)	25.12 (2.89)	6.66 (0.61)	0.92 (0.09)	5.01 (0.92)
Femur	*Enpp1$^{flox/flox}$*	15.4 (0.02)	8.8 (3.32)	0.34 (0.10)	1.79 (4.76)	61.67 (6.93)	6.21 (2.32)	0.47 (0.16)	6.20 (0.38)
	Enpp1$^{flox/flox}$;Ocn-cre	15.6 (0.02)	16.78 (1.13)	0.57 (0.03)	4.67 (0.28)	51.34 (8.07)	11.75 (0.79)	0.68 (0.04)	5.67 (0.62)

Table 5.1. Length and mechanical properties of long bones from 16-week old male mice reveals no functional differences between genotypes.

Gross analysis of long bones revealed no difference in length (n=6). Assessment of mechanical strength via 3-point bending analysis revealed no significant differences between genotype in measured parameters. Data are presented as the mean ± S.E.M (n≥4). No significant findings observed.

5.6. Discussion

NPP1 has previously been demonstrated as a critical regulator of bone mineralisation via generation of PP_i (Rutsch et al., 2003, Li et al., 2014b, Huesa et al., 2015b). Moreover, I have demonstrated for the first time that the osteoblast-specific ablation of NPP1 results in increased bone mass and mineral density (chapter 3). Additionally, increased matrix mineralisation was evident in the cultured of osteoblasts isolated from *Enpp1*$^{flox/flox}$;*Ocn*-cre mice (chapter 4). In the current chapter, the metabolic phenotype of 16-week old male *Enpp1*$^{flox/flox}$;*Ocn*-cre and *Enpp1*$^{flox/flox}$ control mice was assessed.

The use of genetically modified animals, integrated physiology and clinical observations has greatly improved our understanding of bone and energy metabolism. Previous studies revealed a notable metabolic phenotype, including increased insulin sensitivity, of the global *Enpp1*$^{-/-}$ mouse (Huesa et al., 2014). The literature has not previously assessed the osteoblast-specific contributions of NPP1 to the metabolic phenotype observed in the global *Enpp1*$^{-/-}$ mouse despite many reports acknowledging the role that osteoblasts (and bone in general) play within whole organism metabolism (DiGirolamo et al., 2012, Lee et al., 2017, Motyl et al., 2017).

Chapter 3 of this thesis revealed that the *Enpp1*$^{flox/flox}$;*Ocn*-cre mice demonstrate increased long bone mass and mineralisation. The formation of bone has indeed been associated with metabolic cost (Motyl et al., 2017), and as such, I aimed to investigate whether the osteoblast-specific ablation of NPP1 would result in a concomitant skeletal and metabolic phenotype.

The data presented in this chapter reveals that there is not a notable metabolic phenotype in the control-diet fed 16-week old male *Enpp1*$^{flox/flox}$;*Ocn*-cre mice. The data in this chapter does not confirm my original hypothesis that *Enpp1*$^{flox/flox}$;*Ocn*-cre mice would recapitulate the metabolic phenotype observed in the *Enpp1*$^{-/-}$ mice. The *Enpp1*$^{flox/flox}$;*Ocn*-cre mice present with no alterations to their body weight, food consumption, glucose tolerance, insulin tolerance or GSIS. Furthermore, necroscopy results largely do not reflect changes in metabolic tissue mass observed in the *Enpp1*$^{-/-}$ mice. Despite the altered weight of the liver

in the *Enpp1*$^{flox/flox}$;*Ocn*-cre, this did not translate to altered function evident through histological analysis and quantitative investigation of liver triglyceride content. The increased muscle mass of the *quadriceps femoris* is a likely product of the altered gait observed in the *Enpp1*$^{flox/flox}$;*Ocn*-cre mice indicative of increased instability in movement. Given that the 6-week old *Enpp1*$^{flox/flox}$;*Ocn*-cre present with notable alterations to their long bones length and microarchitecture, the gait alterations may be a consequence of the altered juvenile bone development and resultant skeletal phenotype.

Interestingly, when the 16-week old control-diet fed male *Enpp1*$^{flox/flox}$;*Ocn*-cre mouse long bones were assessed, no bone phenotype was revealed. Given that the 22-week old male *Enpp1*$^{flox/flox}$;*Ocn*-cre mice also do not present with notable bone phenotype (chapter 3), this new evidence adds credence to the conclusion that osteoblast-specific NPP1 ablation results in altered juvenile mouse bone formation but not adult bones. Given that this bone phenotype is not maintained throughout the lifespan of the mouse, it is possible that an alternate source of PP_i is compensating for the locally reduced PP_i product of the osteoblast-specific ablation. This could come from the liver, which produces the majority of plasma PP_i (Jansen et al., 2014, Kauffenstein et al., 2018). The analysis of a liver-specific NPP1 ablated mouse model would be important for determining whether liver-derived PP_i is critical in the regulation of mineralisation and bone development.

The *Enpp1*$^{flox/flox}$;*Ocn*-cre mice did present with increased uncarboxylated-OCN yet this was not capable of providing metabolic protection for the *Enpp1*$^{flox/flox}$;*Ocn*-cre mice, which did not demonstrate insulin sensitivity. This is perplexing, given that OCN is recognised to increase insulin sensitivity and secretion (Lee et al., 2007, Karsenty et al., 2012). Adipose tissue, including white adipose tissue and thermogenic active brown adipose tissue, are complex and play important roles in energy homeostasis regulation (Fonseca-Alaniz et al., 2007). They act as reservoirs for storing lipids as a source of energy and are capable of secreting paracrine factors to act on metabolic tissues (Ahima and Flier, 2000, Kershaw and Flier, 2004). If the fat stores are not able to store energy, fat deposition in other tissues that regulate glucose may occur; this is a risk factor for insulin resistance and T2DM (Rutkowski et al., 2015, Reilly and Saltiel, 2017). I aimed to ensure that there was physiological storage

of fat within the adipocytes. By determining this, it is possible to eliminate lipotoxicity as a contributor to why the increased uncarboxylated-OCN did not result in increased insulin sensitivity in the *Enpp1*$^{flox/flox}$;*Ocn*-cre mice

The analysis of organ mass at cull revealed no significant difference in the mass of the white fat depots (mg/g total body weight). However, this does not reflect the morphology or health of the individual adipocyte. Adipocytes are highly dynamic and can be structurally modified (Drolet et al., 2008, Spalding et al., 2008, Jo et al., 2009). For example, when in a caloric excess, adipocytes can undergo tissue remodelling and increase in number (hyperplasia) and size (hypertrophy) (Cawthorn et al., 2014, Hardouin et al., 2016). Healthy adipocytes should be relatively uniform and should be able to adapt in-keeping with the energy storage requirements which come hand in hand with energy excess (Faust et al., 1978). Energy excess can occur through two basic mechanisms: increased caloric intake (food excess) or decreased caloric output (*e.g*. decreased locomotion) (Hill and Commerford, 1996, Sandoval et al., 2008, Hill et al., 2012). Adipocytes may be deranged in a variety of metabolic-related disorders including T2DM, dietary-induced obesity, or conditions whereby the adipocyte is directly affected such that lipid storage ability is limited (*e.g.* lipodystrophy) (Goralski et al., 2007, Garg, 2011). Histological analysis revealed adipocyte morphology and size distribution, comparable between genotypes, suggesting no alteration to the adipocyte capability to store fat.

The brown adipose tissue thermogenic function may differ between genotypes: this may offer one explanation for why the global *Enpp1*$^{-/-}$ mice demonstrate metabolic protection. Brown adipose tissue is capable of thermogenesis, and this releases a large amount of energy as heat (Smith and Hock, 1963, Cypess et al., 2009, Lee et al., 2010). This process is a contributor to the regulation of whole-body energy metabolism, although the extent of this is debated within the literature (Muzik et al., 2013, Carpentier et al., 2018, Fernández-Verdejo et al., 2019). For example, brown adipose tissue may account for up to 60% of 'non-shivering' thermogenesis in small mammals (Heldmaier and Buchberger, 1985, Foster et al., 2007). To combat obesity, a caloric deficit must be obtained by either restricting food intake or promoting energy expenditure. Classically, this has been achieved by increased exercise,

although the medical community has progressed to include surgical intervention (*e.g.* gastric bypass surgery) which alters satiety and/or fat malabsorption (Plourde et al., 2014, Grenier-Larouche et al., 2017, Narayanaswami and Dwoskin, 2017, Lean et al., 2018). These interventions result in profound anti-diabetic and anti-obesity effects (Khera et al., 2016).

It may also be possible to alter energy homeostasis to promote exercise and non-exercise related thermogenesis, thus combating obesity and T2DM. The scientific and medical community has a renewed interest in determining the roles of BAT as a potential target in the treatment of metabolic conditions including obesity and T2DM by promoting energy expenditure in this metabolic tissue (Cypess and Kahn, 2010, Nedergaard and Cannon, 2010, Tseng et al., 2010, Bonet et al., 2013, Trayhurn, 2018). This involves delineating the role of different genes and factors in brown tissue behaviour. This is of particular interest given that studies demonstrate that cold exposure (5-8 hours), which activates brown adipose tissue, lead to increased basal and insulin-stimulated whole-body glucose disposal (Chondronikola et al., 2014). As such, the activation of brown adipose tissue may be a pertinent therapeutic target for T2DM management. The data presented in this chapter revealed no difference in brown adipose tissue morphology or nuclei number was observed between genotypes. Therefore, NPP1 appears not to be a critical regulator of brown adipose tissue activity regarding control-fed dietary conditions. Additionally, no alterations to the pancreas were evident between genotypes. To assess the function of metabolic tissues, mRNA expression was analysed. This did not reveal any notable upregulation of metabolic genes, supporting a largely unaltered metabolic phenotype amongst the *Enpp1*$^{flox/flox}$;*Ocn*-cre mice.

Interestingly, the mRNA expression of the brown fat Diacylglycerol O-Acyltransferase 1 (*Dgat1)* was significantly reduced in the *Enpp1*$^{flox/flox}$;*Ocn*-cre mice. This enzyme is involved in the synthesis of triglycerides (Chitraju et al., 2017). However, *Dgat2* mRNA expression remained unchanged between genotypes, and this enzyme is involved in the synthesis of triglycerides (Cases et al., 1998). A recent study has revealed that following regular chow feeding, *Dgat1* and *Dgat2* can compensate for each other and that either enzyme is fully capable of catalysing triglyceride synthesis for storage under basal conditions (Chitraju et al.,

2017). As such, the alterations of *Dgat1* mRNA expression with the absence of *Dgat2* changes are largely insignificant concerning metabolic health and function.

No difference in the mRNA expression of liver peroxisome proliferator-activated receptor alpha (PPARα) were observed. This transcription factor is a major regulator of lipid metabolism in the liver and is responsible for the regulation of mitochondria and fatty acid oxidation (Kersten et al., 1999). However, the liver phosphoenolpyruvate carboxykinase *(Pck1)* mRNA expression was significantly increased in *Enpp1*$^{flox/flox}$;*Ocn*-cre mice compared to *Enpp1*$^{flox/flox}$ controls. This gene is one of the main control points for the regulation of gluconeogenesis (Millward et al., 2010). It has been shown that the deletion of *Pck1* in mice results in increased plasma free fatty acid levels and is a contributing factor to insulin resistance (Millward et al., 2010) (Hanson and Garber, 1972). As such, the deletion of *Enpp1* within the osteoblast serves to increase liver *Pck1* expression and promote fatty acid oxidation and metabolic protection. This may indicate a bone-liver metabolic axis involving NPP1.

A possible limitation of this study was that observations were only made in male mice. However, by studying only male mice, I have eliminated the influence of oestrogen signalling regarding metabolic phenotype. Indeed, an increasing body of evidence, including human and murine based studies, has linked altered oestrogen signalling with metabolic dysregulation, including the metabolic syndrome (Heine et al., 2000, Munoz et al., 2002, Bryzgalova et al., 2006, Eshtiaghi et al., 2010, Matic et al., 2013).

In conclusion, the results presented in this chapter highlight that the osteoblast-specific ablation of NPP1 in mice does not recapitulate the phenotype of the global *Enpp1*$^{-/-}$ mice. Importantly, I have demonstrated that the osteoblast-specific ablation of NPP1 results in increased uncarboxylated-OCN, but that this is not able to facilitate improved insulin sensitivity. Given that NPP1 is recognised as a pathogenic factor for insulin resistance, it is important to assess the *Enpp1*$^{flox/flox}$;*Ocn*-cre following metabolic stress in the form of chronic high-fat diet feeding. The metabolic protection may only emerge following such a challenge,

and as such phenotyping of high-fat diet fed *Enpp1*$^{flox/flox}$;*Ocn*-cre male mice was next conducted in chapter 6.

(*This page has been left intentionally blank)*

Chapter 6. Investigating the role of osteoblast-specific ablation of NPP1 on the metabolic phenotype of chronically high-fat diet fed mice.

6.1 Introduction

Obesity is recognised as the single most important risk factor for the development of T2DM (Tuomilehto et al., 2001a, Belkina and Denis, 2010). T2DM itself is characterised by a resistance to insulin-stimulated glucose uptake, resulting in decompensation of systemic glucose metabolism (Cefalu, 2001, Reaven, 2004, Dongiovanni et al., 2010, Sinaiko and Caprio, 2012). The scientific community has made notable progress in understanding glucose metabolism: however, the mechanisms and regulation of glucose metabolism in health and disease remain incompletely understood. In a chronic overfeeding situation the peripheral IR-associated signalling will be altered, and reduced sensitivity to insulin-mediated glucose regulation will occur (Nagy and Einwallner, 2018). High-fat diet fed mice are frequently used as a model for diet-induced insulin resistance (Winzell and Ahrén, 2004). The subsequent utilisation of an oral GTT can shed light on the peripheral disposal of orally adminstered glucose and insulin secretion (Nagy and Einwallner, 2018). Additionally, the ITT will glean insights into the regulation of whole-body insulin action. When these GTT and ITT data are considered together, they can characterise the metabolic phenotype (Ayala et al., 2010, Alquier and Poitout, 2018, Nagy and Einwallner, 2018). By assessing specific knockout mouse models, this can identify genes important in glucose homeostasis. This work aids in the understanding of metabolic pathogenesis and identifying possible therapeutic interventions.

Insight has already been gained regarding the role of NPP1 in diabetes (Dong et al., 2005, Maddux et al., 2006a, Bacci et al., 2007, Bhatti et al., 2010, Di Paola et al., 2011, Pan et al., 2011, Huesa et al., 2014). It is recognised that NPP1 binds to the α-subunit of the IR, impairing the insulin stimulation of the IR and thus abrogating its downstream signalling (Goldfine et al., 2008). There are multiple clinical and basic research observations that link ENPP1 in humans (and mice) to insulin resistance and T2DM (Grupe et al., 1995, Maddux et al., 1995, Frittitta et al., 1998, Maddux and Goldfine, 2000, Abate et al., 2003, Dong et al., 2005, Bacci et al., 2007, Di Paola et al., 2011, Frittitta et al., 2001, Huesa et al., 2014, Pan et al., 2011). For example, *ENPP1* expression was assessed and was increased in the muscle cells from insulin-resistant human patients (Maddux et al., 2006b, Goldfine et al., 2008). The insulin from these cells was also found to be incapable of promoting the IR autophosphorylation which occurs as a result of insulin binding to the α-subunit of the IR (Maddux et al., 1995). This has also been demonstrated *in vitro* (Grupe et al., 1995). Human mammary epithelial

cells (MCF7 cells) were isolated and induced to overexpress *ENPP1*. As a result, decreased insulin responsiveness was observed in these cells (Grupe et al., 1995).

Animal studies have also been enlightening regarding the role of ENPP1 and insulin resistance. Indeed, overexpression of ENPP1 in a variety of primary cell types including muscle, liver and adipose tissue induces insulin resistance and glucose intolerance in rodent models (Maddux et al., 1995, Dong et al., 2005, Maddux et al., 2006a, Pan et al., 2011, Pan et al., 2012). Recent investigations into the metabolic phenotype resulting from the knockdown of NPP1 have demonstrated that the global ablation of NPP1 results in improved insulin sensitivity in mice (Huesa et al., 2014). However, the cell-specific contributions towards the metabolic phenotype observed in the global *Enpp1*$^{-/-}$ mouse have not been delineated.

Given that the worldwide incidence of T2DM is set to reach over 640 million adults in 2040 (Ogurtsova et al., 2017), its burden is undeniable for the health of developed and developing countries. T2DM itself is a common, yet multifactorial syndrome, the incidence of which is rapidly increasing due to the contribution of a variety of factors, namely obesity (Weigensberg and Goran, 2009, Ershow, 2009, Al-Goblan et al., 2014, Wu et al., 2014). As such, it is of great importance to comprehend the genetic components which underlie the predisposition to diabetes and insulin resistance including considering the roles that such genes play in obesogenic settings. The high-fat diet model is crucial to understand this.

For the treatment of T2DM, the scientific community could aim to normalise the basic defects that occur in diabetes, including insulin resistance. T2DM is caused by inadequate β-cell compensation in response to insulin resistance which results in a relative insulin deficiency, culminating in hyperglycemia (Butler et al., 2003, Del Guerra et al., 2005, Florez, 2008, McCarthy, 2010, Ashcroft and Rorsman, 2012, Cerf, 2013). T2DM is closely associated with obesity, as one its main pathological causes of insulin resistance. As such, the majority of animal models are obese, and their primary importance is in understanding obesity-induced insulin resistance and its effects (King and Bowe, 2016b). Animal models have long been used to understand insulin actions, obesity and T2DM (King and Bowe, 2016b). Examples include

monogenic mouse models which aid in understanding insulin resistance development in an obesity phenotype. One frequently used monogenic mouse model of altered leptin signalling is the $Lep^{ob/ob}$ mouse, which has no functional leptin, resulting in hyperphagia. These mice, as an effect of this, develop obesity, hyperinsulinemia and hyperglycemia (Lindstrom, 2007, Wang et al., 2014a). Obesity can also be induced by feeding a rodent a high-fat diet, whereby weight gain, associated insulin resistance, and aberrant glucose metabolism can be observed following chronic feeding (of 8 weeks or more) (Surwit et al., 1998, Winzell and Ahrén, 2004). The method of chronic high-fat diet feeding was utilised for the studies described in this chapter.

Attention must be given to specific genes, including *ENPP1*, to understand the contribution to the pathogenesis of T2DM and to better diagnose, treat and eventually prevent incidence. This underpins the importance of this chapter, which investigates and profiles the metabolic phenotype of the osteoblast-specific NPP1 ablated mouse model under obesogenic conditions (via chronic high-fat diet feeding). This recapitulates the energy imbalance observed in a significant proportion of our human population and is critical to our understanding of cell-specific contributions of certain genes to global energy metabolism.

The previous analysis of global *Enpp1*$^{-/-}$ mice revealed that, following a high-fat diet challenge, the global *Enpp1*$^{-/-}$ mice exhibit a pronounced resistance to obesity (Huesa et al., 2014). My initial studies of the *Enpp1*$^{flox/flox}$*;Ocn*-cre mice revealed no difference in weight gain compared to *Enpp1*$^{flox/flox}$ mice on a control-diet (Chapter 5). A metabolic phenotype may only present when the mouse is experiencing a chronic high caloric intake (i.e. under obesogenic conditions). As such, the *Enpp1*$^{flox/flox}$*;Ocn*-cre mice were fed a 60% fat diet from 4- to 16-weeks of age.

6.2. Hypothesis

Following chronic high-fat diet feeding, a protected metabolic phenotype, with resistance to obesity will be evident in the osteoblast-specific NPP1 ablated mouse. These mice will present with a bone phenotype reflecting the juvenile 6-week old *Enpp1*$^{flox/flox}$*;Ocn*-cre and *Enpp1*$^{flox/flox}$ mice.

6.3. Aims

I. Analyse the metabolic phenotype of the high-fat diet challenged *Enpp1*$^{flox/flox}$*;Ocn*-cre and *Enpp1*$^{flox/flox}$ mice.

II. Analyse the bone phenotype of high-fat diet *Enpp1*$^{flox/flox}$*;Ocn*-cre and *Enpp1*$^{flox/flox}$ mice.

6.4. Materials and methods

6.4.1. Animal generation, food, weighing and consumption.

The *Enpp1*$^{flox/flox}$*;Ocn*-cre and age-matched *Enpp1*$^{flox/flox}$ control mice where generated (Section 2.7.1). Male mice were fed a high-fat diet from 4-weeks of age until cull at 16-weeks of age (Section 2.7.2). Male high-fat diet fed mice were fed a high-fat diet from 4-weeks of age until cull at 16-weeks of age (Section 2.7.2). The weight of consumed food was calculated each week. The weights of the mice were analysed each week (Section 2.7.2).

6.4.2. Gross analysis

At 16-weeks of age, mice were culled and weight at cull was recorded. Tibiae and femora from male *Enpp1*$^{flox/flox}$*;Ocn*-cre and *Enpp1*$^{flox/flox}$ mice aged 16-weeks were taken at dissection and soft tissue removed. The length of these long bones were measured using DigiMax digital Vernier callipers (R. S. Components Ltd, Corby, Northants, UK). Mice were dissected and soft tissues were collected (Section 2.6.3).

6.4.3. Glucose tolerance and insulin tolerance testing

Male mice aged 16-weeks were weighed and fasted for 4-hours prior to administration of 2 mg D-glucose per g of body weight was administered by oral gavage (for GTT) or 0.5 mU of insulin per g of body weight was administered by intraperitoneal injection (for ITT). Blood glucose and circulating insulin was calculated (Section 2.7.4).

6.4.4. Serum OCN analysis and biochemistry

Total OCN and uncarboxylated-OCN was measured as previously described (Ferron *et al.,* 2010) (Section 2.9.2). Julian Berger of Columbia University (USA) kindly completed this work. Glucose stimulated insulin secretion (GSIS) was detected by ELISA (ChrystalChem, Chicago, IL, USA) (Section 2.9.2).

6.4.5. Histological analysis

Soft tissues were collected from *Enpp1*$^{flox/flox}$*;Ocn*-cre *and Enpp1*$^{flox/flox}$ mice culled at 16-weeks of age (Section 2.6.3). Tissues were prepared for microscopy analysis by fixing in 10% NBF (Section 2.9.1). Sections were paraffin-embedded after fixing (Section 2.9.2). Fat pads, liver and pancreas sections were stained with H&E (Section 2.9.3). Islet number and size was determined in H&E stained sections of pancreas (Section 2.9.9). The number and area of adipocytes in fat pads was determined (Section 2.9.10). Liver sections were stained with Weigert's haematoxylin and fast-green to assess architecture, and with picosirius red to assess fibrotic damage (Section 2.9.11).

6.4.6. Immunohistochemistry of pancreas

Pancreas tissue was collected (Section 2.6.3) and prepared for microscopy analysis by fixing in 10% NBF (Section 2.9.1). Pancreas sections were taken at 5 µM and were stained for insulin by immunohistochemistry (Section 2.9.12) to identify pancreatic β-cells.

6.4.7. Analysis of liver triglyceride content

Following euthanasia of livers were collected, frozen, and stored at -80° C. Tissue was prepared and total triglyceride was measured using a Triglyceride (TG) Assay (Sentinel Diagnostics, Milan, Italy).

6.4.8. mRNA analysis of metabolic tissues

mRNa samples were extracted from metabolic tissues (including liver, fat pads and *quadriceps femoris*) using a Qiagen RNeasy kit according to the manufacturer's instructions. cDNA was prepared (Section 2.3.2) and was used at 5 ng/μg for RT-qPCR analysis (Section 2.3.3). Results were normalised to β-*actin* and *Gapdh* housekeeping gene and the relative gene expression level was calculated using the ΔΔCT method (Livak and Schmittgen, 2001).

6.4.9. Three-point bending of long bones

The tibiae and femora from *Enpp1*$^{flox/flox}$*;Ocn*-cre and *Enpp1*$^{flox/flox}$ mice were collected. Three-point bending also conducted on tibiae and femora using a LXR materials testing machine (Lloyds Instruments, West Sussex, U.K.) (Section 2.6.1).

6.4.10. μ-CT of long bones

The tibiae and femora from *Enpp1*$^{flox/flox}$*;Ocn*-cre and *Enpp1*$^{flox/flox}$ mice were collected, fixed in 10% NBF for 24 hours and subsequently stored in 70% ethanol. The bones were scanned using a micro-computed tomography (μ-CT) system (Skycan 1172, Bruker, Aartselaar, Belgium) to assess trabecular architecture and cortical geometry (Section 2.6.2).

6.4.11. Catwalk analysis

Gait analysis was recorded using a CatWalk XT gait analysis system. Mice were familiarised with the equipment prior to the recording of data. Data was collected from male *Enpp1*$^{flox/flox}$*;Ocn*-cre *and Enpp1*$^{flox/flox}$ mice at 14-weeks of age (Section 2.7.5).

6.5. Results

6.5.1. *Enpp1*$^{flox/flox}$*;Ocn*-cre do not demonstrate resistance to obesity following chronic high-fat diet challenge

The *Enpp1*$^{flox/flox}$*;Ocn*-cre mice demonstrate no significant changes in body weight gain from 4-weeks of age to 16-weeks of age (Fig 6.1A) compared to *Enpp1*$^{flox/flox}$ mice. Furthermore, no difference between genotype in food consumption per mouse was observed (Fig. 5.1B).

6.5.2. *Enpp1*$^{flox/flox}$*;Ocn*-cre demonstrate glucose intolerance, insulin resistance and increased brown fat and liver mass

The *Enpp1*$^{flox/flox}$*;Ocn*-cre mice on a high-fat diet exhibited a decreased ability to regulate their glucose following the administration of an oral glucose bolus (GTT) (Fig. 6.2A), which was reflected in the area under the curve analysis (4849.25 arbitrary units (AU) vs. 3913.88 AU; $P<0.05$) (Fig. 6.2D). In addition, the *Enpp1*$^{flox/flox}$*;Ocn*-cre mice demonstrated reduced ability to respond to insulin and decrease their glucose compared to *Enpp1*$^{flox/flox}$ control mice, indicative of insulin resistance, notably at time points of 30 minutes (0.73 % of basal glucose vs. 0.52 % of basal glucose; $P<0.05$) and 120 minutes (0.90 % of basal vs. 0.58 % of basal; $P<0.01$) (Fig. 6.2B). However, this did not translate to statistical significance when area under the curve was analysed (Fig. 6.2E). The GSIS was also comparable in both genotypes (Fig. 6.2C, 6.2F). To ensure that the absence of any changes in glucose metabolism and insulin sensitivity were not the product of altered organ mass and function, gross analysis of organ mass was conducted at necroscopy. These analyses revealed no significant changes for the *Enpp1*$^{flox/flox}$*;Ocn*-cre mouse in the mass (mg/g total body mass) of white fat (subcutaneous, gonadal or mesenteric), spleen, pancreas, kidney or *quadriceps femoris* muscle compared to *Enpp1*$^{flox/flox}$ control mice (Fig. 6.3). The liver was further analysed to determine whether such pathological non-alcoholic fatty liver disease (NAFLD) or non-alcoholic steatohepatitis (NASH) changes had occurred (Section 6.5.3).

The weight of brown fat of *Enpp1*$^{flox/flox}$*;Ocn*-cre was increased following high-fat diet feeding (8.78 mg/g vs. 7.18mg/g; $P<0.05$) compared to *Enpp1*$^{flox/flox}$ control mice (Fig. 6.3). The brown fat of the high-fat diet fed *Enpp1*$^{flox/flox}$*;Ocn*-cre mice was significantly increased compared to *Enpp1*$^{flox/flox}$ control mice (8.78 mg/g total body weight vs. 7.18 mg/g total body weight;

P<0.05). The thermogenic capacity of this fat depot was analysed to investigate whether this could contribute to the metabolic phenotype observed (Section 6.5.4).

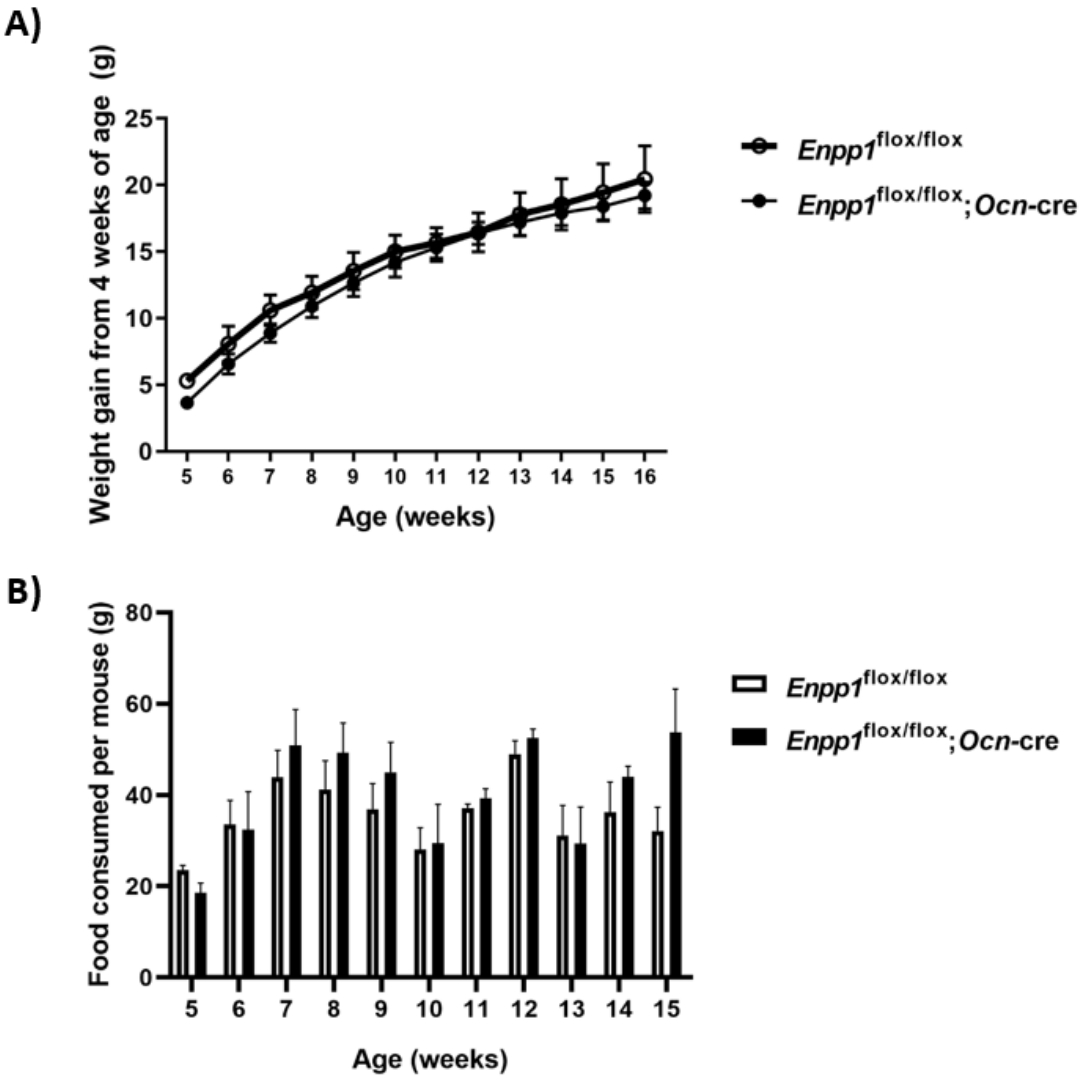

Figure 6.1. Weight gain and food consumption of high-fat diet fed mice reveals no difference between genotypes.

(A) Mass of high-fat diet *Enpp1*$^{flox/flox}$*;Ocn*-cre and *Enpp1*$^{flox/flox}$ mice weighed each week revealed no significant difference between genotype in weight gain. To ensure this was not a result of disparity in feeding, (B) weekly food consumption was calculated revealing no significant difference between genotype throughout the time course. Data are presented as the mean ± S.E.M (n≥4). No significant findings observed.

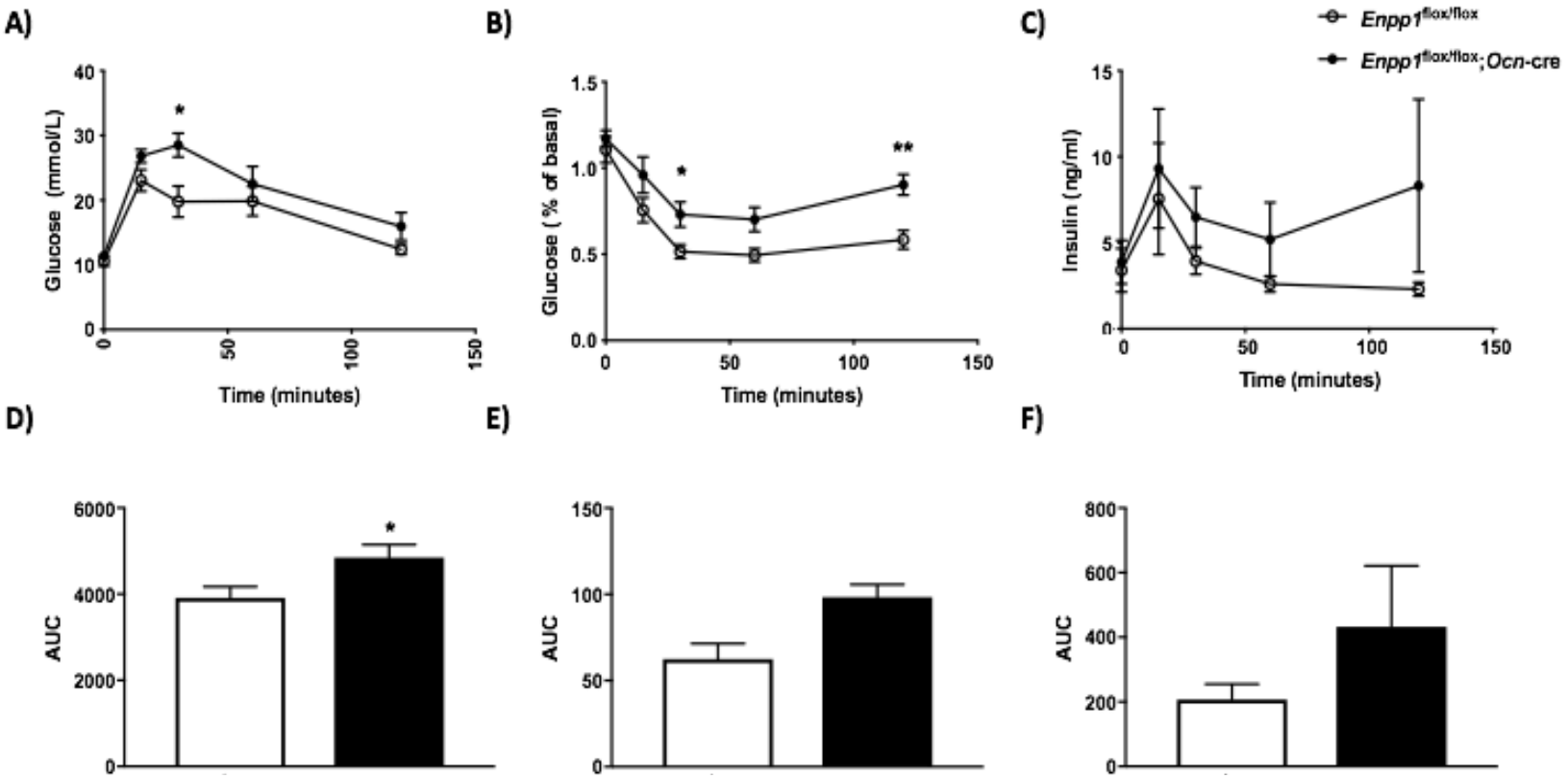

Figure 6.2. Assessment of glucose tolerance and insulin sensitivity of high-fat diet fed mice reveals insulin resistance and glucose intolerance in the osteoblast-specific NPP1 ablated mice.

Metabolic analysis of 16-week old control fed male *Enpp1*$^{flox/flox}$*;Ocn*-cre and *Enpp1*$^{flox/flox}$ mice. (A) GTT and (D) area under curve, (B) ITT and (E) area under the curve and (C) GSIS and (F) area under the curve shows no difference in reduction of blood glucose levels of *Enpp1*$^{flox/flox}$*;Ocn*-cre mice compared to *Enpp1*$^{flox/flox}$ mice. Data are presented as the mean ± S.E.M (n≥6). Significance denoted by **P*<0.05, ***P*<0.01.

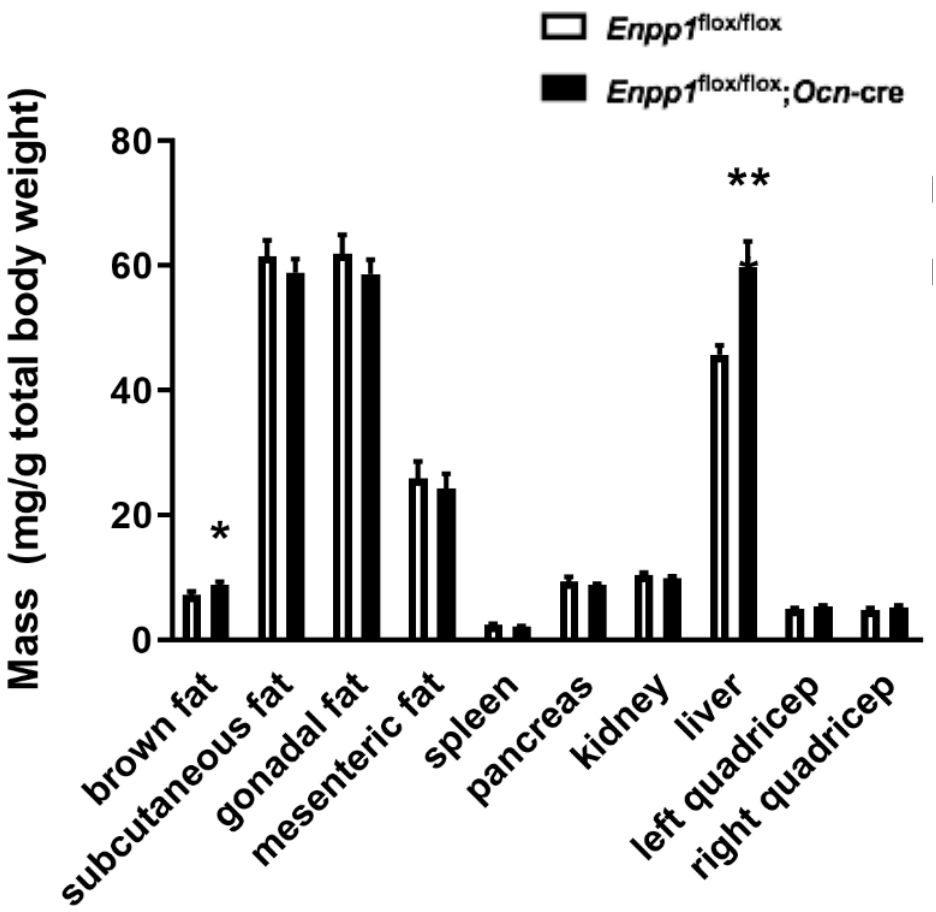

Figure 6.3. High-fat diet fed osteoblast-specific ablated NPP1 mice have greater brown fat pad and liver mass.

The *Enpp1*$^{flox/flox}$*;Ocn*-cre and *Enpp1*$^{flox/flox}$ mice were culled at 16-weeks of age and then dissected. The outlined tissues were removed and weighed: brown fat, subcutaneous fat, gonadal fat, mesenteric fat, spleen, pancreas, kidney, liver, left quadriceps and right quadriceps. Dissection analysis revealed that the liver mass (mg/g body total body weight) of *Enpp1*$^{flox/flox}$*;Ocn*-cre mice was significantly reduced, whereas left and right *quadriceps femoris* were significantly heavier than the *Enpp1*$^{flox/flox}$ counterpart mice. Data are presented as the mean ± S.E.M (n≥4). Significance denoted by **P*<0.05, ***P*<0.01.

6.5.3. Analysis of *Enpp1*$^{flox/flox}$*;Ocn*-cre liver histology and triglyceride content.

The control-diet fed *Enpp1*$^{flox/flox}$*;Ocn*-cre mice exhibit livers of decreased mass, but with no abnormal liver pathology or adiposity alterations between genotypes (chapter 5, Section 5.5.4). Given that the high-fat fed *Enpp1*$^{flox/flox}$*;Ocn*-cre mice have livers of significantly increased mass compared to *Enpp1*$^{flox/flox}$ control mice (59.81 mg/g total body weight vs. 45.70 mg/g total body weight; $P<0.01$) (Fig. 6.3), I next assessed the liver histology and triglyceride content in collaboration with Dr Timothy Kendall. The high-fat fed *Enpp1*$^{flox/flox}$ mice demonstrated extensive small droplet macro-vesicular steatosis (5/6 of mice investigated) with no inflammation or fibrosis.

Of the 6 *Enpp1*$^{flox/flox}$*;Ocn*-cre mice assessed, five presented with no detectable steatosis nor inflammation or steatosis. However, the remaining mouse presented with small droplet steatosis comparable to the *Enpp1*$^{flox/flox}$ mice (Huesa et al., 2014). Assessment of the liver triglyceride content was conducted and demonstrated that the *Enpp1*$^{flox/flox}$;Ocn-*cre* mice have significantly increased triglyceride content (9.65 mg/g vs. 5.21 mg/g; $P<0.05$) (Fig. 6.4) compared to *Enpp1*$^{flox/flox}$ control mice. Therefore, the *Enpp1*$^{flox/flox}$*;Ocn-cre* mice have raised fatty acid content of the liver which may account for the increased mass (compared to *Enpp1*$^{flox/flox}$ controls) yet this does not present as steatosis.

6.5.4. *Enpp1*$^{flox/flox}$*;Ocn*-cre mice exhibit unaltered OCN and pancreata

The osteoblast-specific NPP1 ablation of control-diet fed mice results in altered OCN carboxylation status, as observed in the *Enpp1*$^{-/-}$ mice (Fig. 5.5B). This was not observed following high-fat diet feeding, whereby no difference in total (Fig. 6.5A) or uncarboxylated-OCN (Fig. 6.5B) was observed between the two genotypes. Given that undercarboxylated and/or uncarboxylated-OCN exerts a notable effect on the pancreas, whereby it promotes insulin secretion, the insulin-secreting islets of the pancreas were next analysed. The *Enpp1*$^{flox/flox}$*;Ocn*-cre mice demonstrate no significant difference in the size (Fig. 6.5C) or number (Fig 6.5D) of insulin-secreting pancreatic islets compared to *Enpp1*$^{flox/flox}$ control mice. This indicates that osteoblast-specific NPP1 ablation does not result in the alteration of pancreatic β-cell function or OCN activity following high-fat diet feeding.

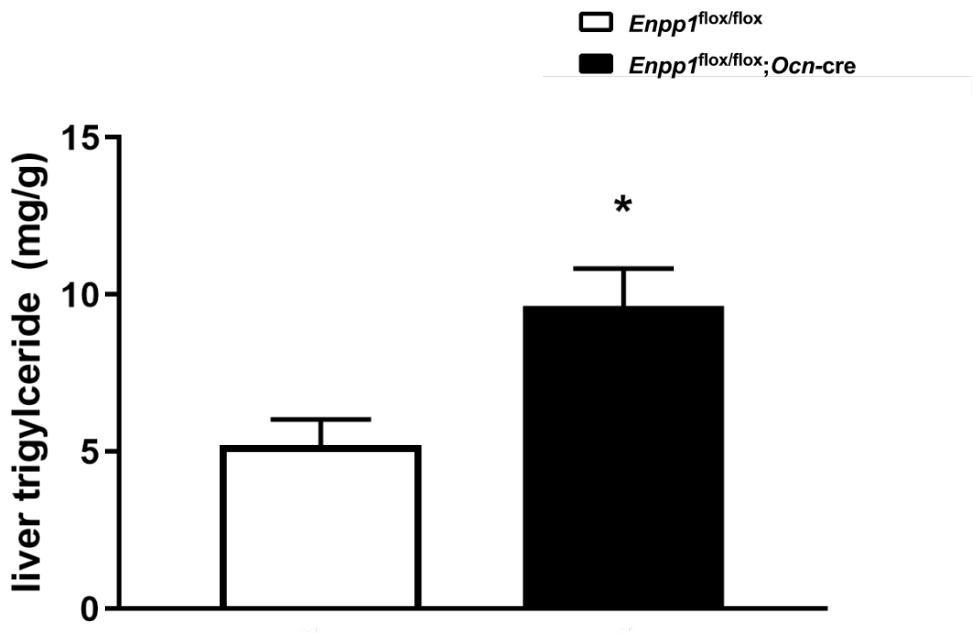

Figure 6.4. High-fat diet fed osteoblast-specific NPP1 ablated mice have grater liver triglyceride content.

Quantitative analysis of liver triglyceride demonstrates no difference between genotype in triglyceride content. Data are presented as the mean ± S.E.M (n≥4). Significance denoted by *P<0.05.

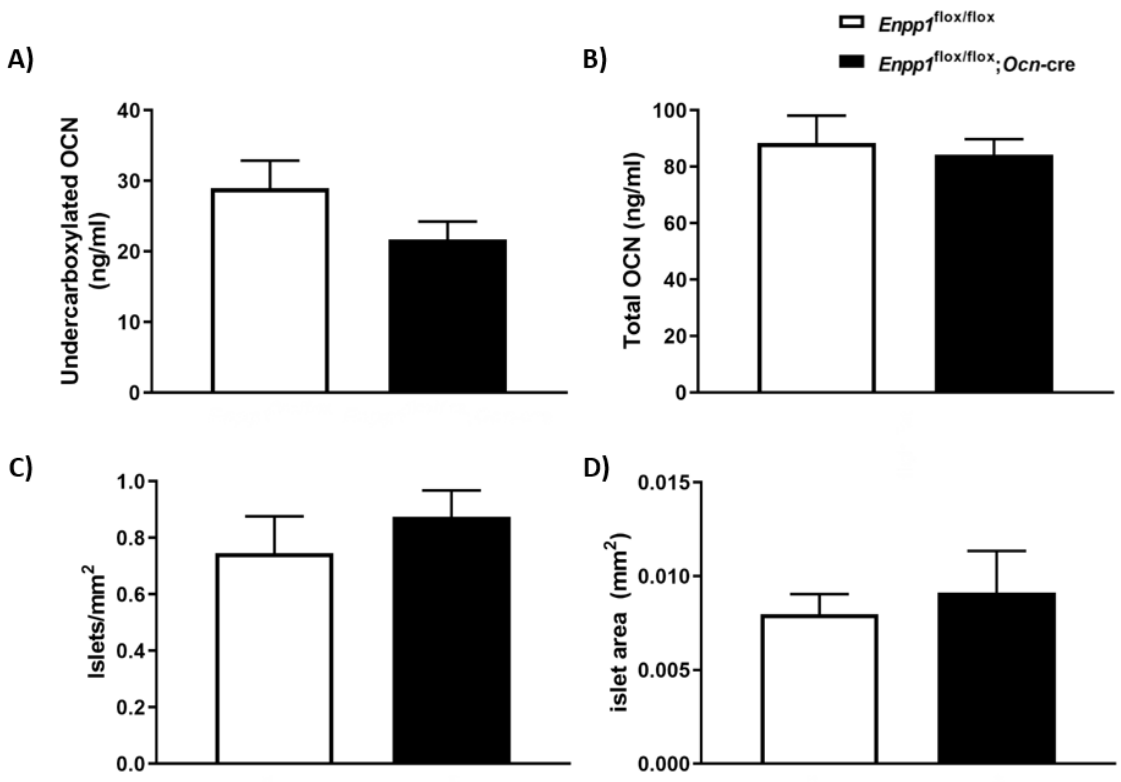

Figure 6.5. Analysis of serum OCN and insulin-secreting pancreatic islets of high-fat diet fed mice demonstrates no difference between genotype.

Analysis of high-fat diet fed *Enpp1*$^{flox/flox}$*;Ocn*-cre and *Enpp1*$^{flox/flox}$ mice (A) total serum OCN and (B) undercarboyxlated-OCN and the (C) area, and (D) number of insulin-secreting pancreatic islets determined through immunohistochemistry and ImageJ quantitation Data are presented as the mean ± S.E.M (n=6). No significant findings observed.

6.5.5. Analysis of adipocytes from the white and brown fat depots

The analysis of organ mass at cull revealed that high-fat diet fed *Enpp1*$^{flox/flox}$*;Ocn*-cre mice have significantly increased brown fat mass (Fig. 6.3), yet unaltered white adipose tissue mass (mg/g total body weight) (Fig. 6.3) compared to *Enpp1*$^{flox/flox}$ control mice. To assess whether these data were associated with altered morphology and health of adipose tissue, further histology to assess adipocyte number and size-frequency distribution and qPCR to analyse mRNA expression was conducted. No significant difference in subcutaneous or mesenteric fat depot adipocyte area (Fig. 6.6A) or adipocyte number (Fig. 6.6B) was observed between genotype. However, *Enpp1*$^{flox/flox}$*;Ocn*-cre mice demonstrate significantly greater average area of gonadal fat pad adipocytes (6215.91 µm^2 vs. 3051.27 µm^2; P<0.01) (Fig. 6.6A), and a significantly reduced number of adipocytes/micrograph (85.18 adipocytes/micrographs vs. 283.19 adipocytes/micrographs; P<0.01) (Fig. 6.6B) compared to *Enpp1*$^{flox/flox}$ controls.

Analysis of the adipocyte size distribution from each of the white adipocyte depots revealed no significant difference in the size distribution for the gonadal (Fig. 6.6D) and mesenteric fat pads (Fig. 6.6E). The *Enpp1*$^{flox/flox}$*;Ocn*-cre mice demonstrated an overall slight increase in larger sized subcutaneous adipocytes (4.18 % of total adipocytes vs. 2.02% of total adipocytes at size of 6500 µm^2; P<0.01) (Fig. 6.6C) compared to *Enpp1*$^{flox/flox}$ control mice. This suggests that overall there is little alteration in the hyperplasia or hypertrophy of the white adipocytes in the *Enpp1*$^{flox/flox}$*;Ocn*-cre mice.

The number of brown fat adipocyte nuclei per field were similar between genotype (Fig. 6.7). This may indicate no change in brown fat adipogenesis, hyperplasia or hypertrophy as a result of osteoblast-specific NPP1 knockout, although the overall mass of brown adipose tissue (mg/g total body weight) was significantly increased compared to controls.

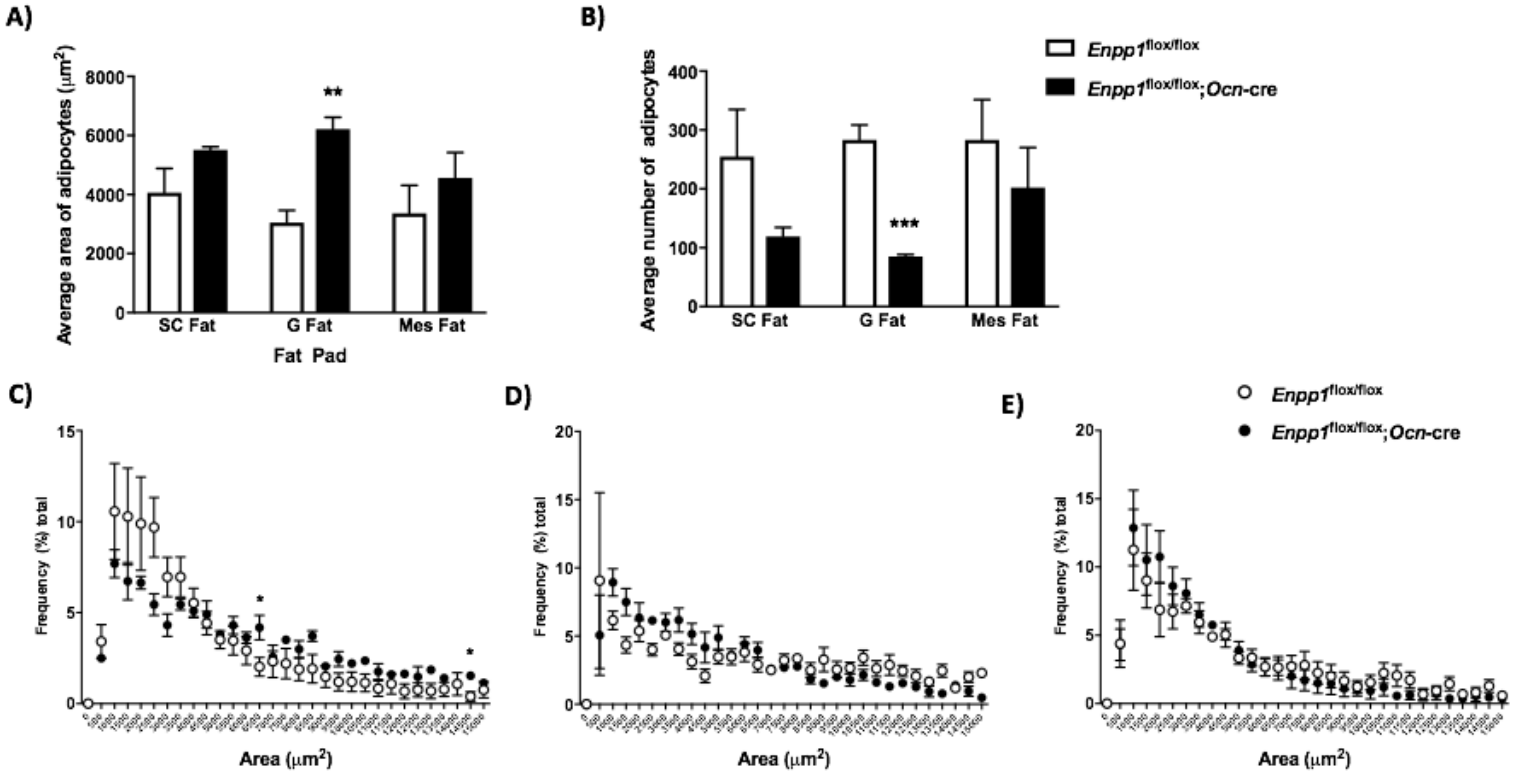

Figure 6.6. Analysis of the white fat depot adipocyte number, area and size-frequency distribution of high-fat diet fed mice demonstrates difference between genotype in the gonadal adipose depot.

The average (A) number and (B) area of adipocytes for the subcutaneous (SC), gonadal (G) and mesenteric (Mes) fat pad were analysed. The size-frequency distribution of adipocytes was analysed for the (C) SC, (D) G and (E) Mes fat pads. Data are presented as the mean ± S.E.M (n≥6). Significance denoted by **P*<0.05, ***P*<0.01, ****P*<0.001.

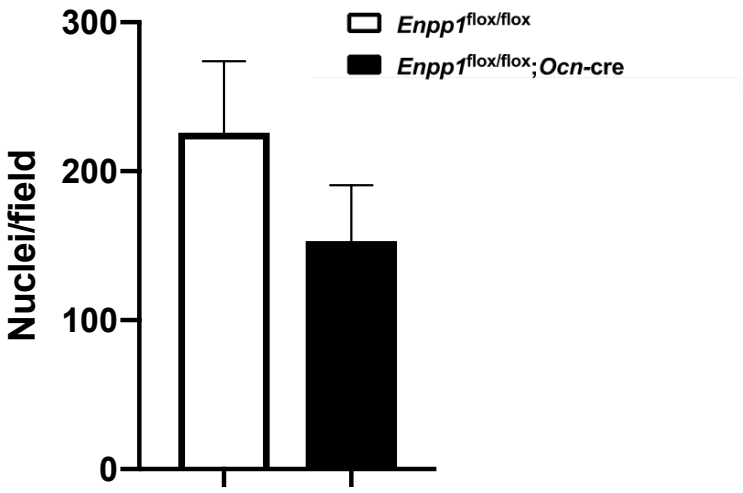

Figure 6.7. Quantitative assessment of brown adipose tissue nuclei of high-fat diet fed mic reveals no difference between genotype.

Analysis of H&E stained nuclei from high-fat diet fed *Enpp1*$^{flox/flox}$*;Ocn*-cre and *Enpp1*$^{flox/flox}$ mice reveals no difference in nuclei/field. Data are presented as the mean ± S.E.M (n=4). No significant findings observed.

6.5.6. Analysis of metabolic genes in metabolic tissues from high-fat diet fed mice.

The *Enpp1*$^{flox/flox}$*;Ocn*-cre mice had a significantly lower level of *Slc2a2* mRNA expression compared to the *Enpp1*$^{flox/flox}$ control mice (0.44 fold change vs. 1; $P<0.05$) (Fig 6.8B). No significant difference in any of the other GLUT receptors investigated were observed for *Enpp1*$^{flox/flox}$*;Ocn*-cre mice compared to *Enpp1*$^{flox/flox}$ controls (Fig. 6.8A, Fig. 6.8C-E). Similarly, no significant difference between genotype for the GLUT receptors investigated in gonadal adipose tissue was observed (Fig. 6.9A-D).

Furthermore, the mRNA expression of metabolic genes for liver and brown adipose tissue were analysed. Given that there were mass changes between genotypes for both these organs following high-fat diet changes, it was important to assess whether gene function was also altered. No significant difference in mRNA expression for the genes assessed were observed for the liver (Fig. 6.10A-C) or brown adipose tissue (Fig. 6.11A-G).

6.5.6. Analysis of long bone micro-architecture, length and mechanical strength.

To investigate whether osteoblast-specific ablation of *Enpp1* caused alterations to bone architecture in high-fat diet fed mice at 16-weeks of age, μ-CT analysis of the diaphyseal bone of tibiae and femora from male *Enpp1*$^{flox/flox}$*;Ocn*-cre and *Enpp1*$^{flox/flox}$ mice was conducted. For the tibiae, no genotype differences were observed for the analysed trabecular parameters (Fig. 6.12). The cortical tibial assessed parameters revealed a significant increase in the cortical porosity of *Enpp1*$^{flox/flox}$*;Ocn*-cre mice compared to *Enpp1*$^{flox/flox}$ controls (2.78 mm^3 vs. 2.03 mm^3; $P<0.05$) (Fig. 6.13C). For the femora, no significant differences between genotype were observed for trabecular (Fig. 6.14) or cortical (Fig. 6.15) diaphyseal bone.

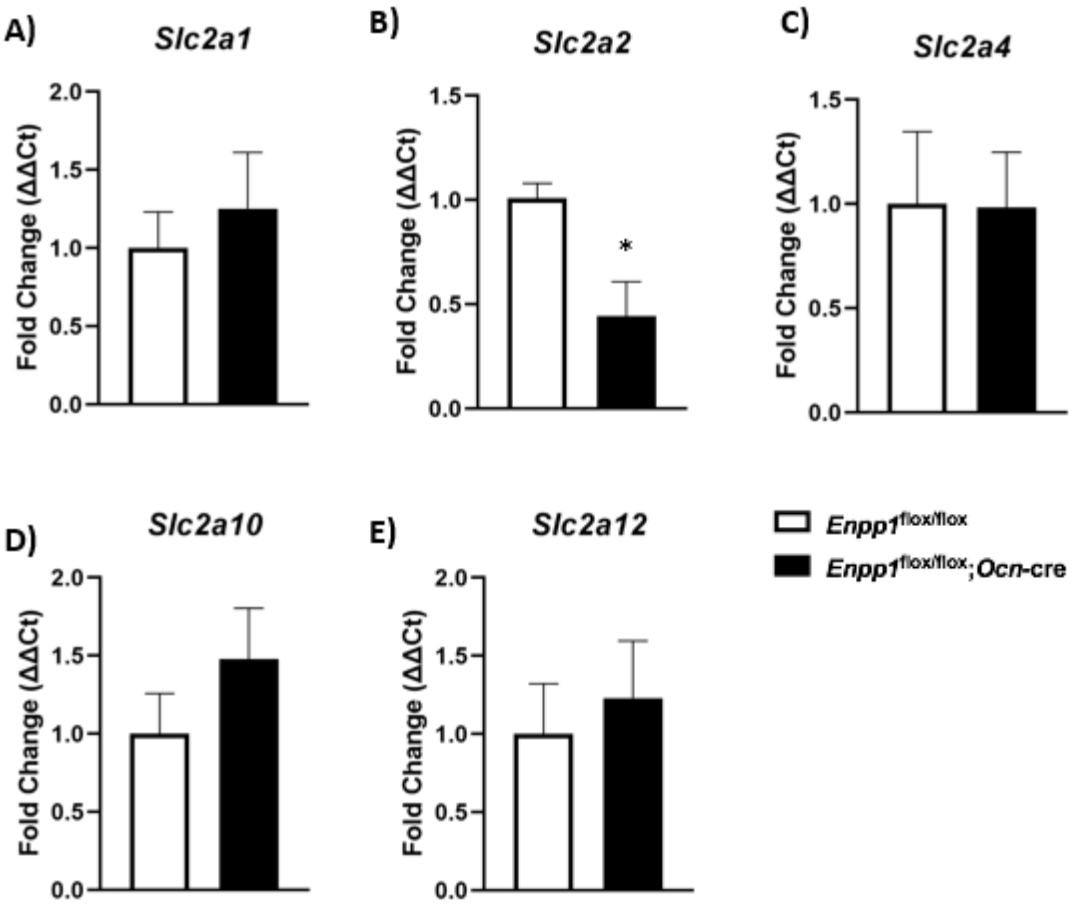

Figure 6.8. The mRNA expression of GLUT receptors of *quadriceps femoris* muscle of high-fat diet fed mice is largely unchanged between genotypes.

The *quadriceps femoris* mRNA expression of selected GLUT receptors including (A) *Slc2a1*, (B) *Slc2a2*, (C) *Slc2a4,* (D) *Slc2a10,* and (E) *Slc2a12* was analysed. mRNA values generated were normalised to the geometric mean of *Gapdh* and *β-actin* house-keeping genes. Data are presented as the mean ± S.E.M (n=4). Significance denoted by **P*<0.05.

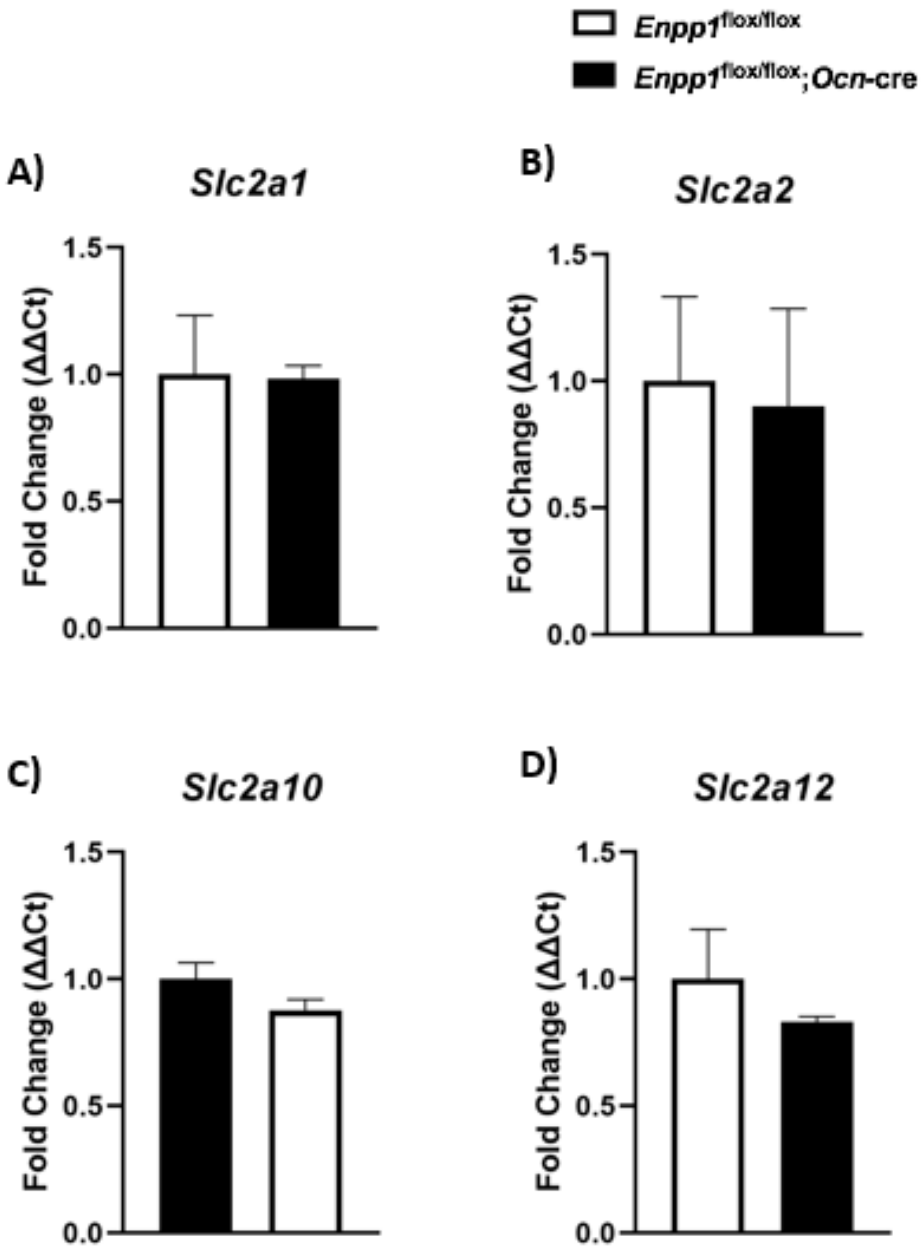

Figure 6.9. The mRNA expression of GLUT receptors of gonadal fat pad of high-fat diet fed mice in unaltered between genotypes.

The gonadal fat pad mRNA expression of selected GLUT receptors including (A) *Slc2a1*, (B) *Slc2a2*, (C) *Slc2a10,* and (D) *Slc2a12* was analysed. mRNA values generated were normalised to the geometric mean of *Gapdh* and β-*actin* house-keeping genes. Data are presented as the mean ± S.E.M (n=4). No significant findings observed.

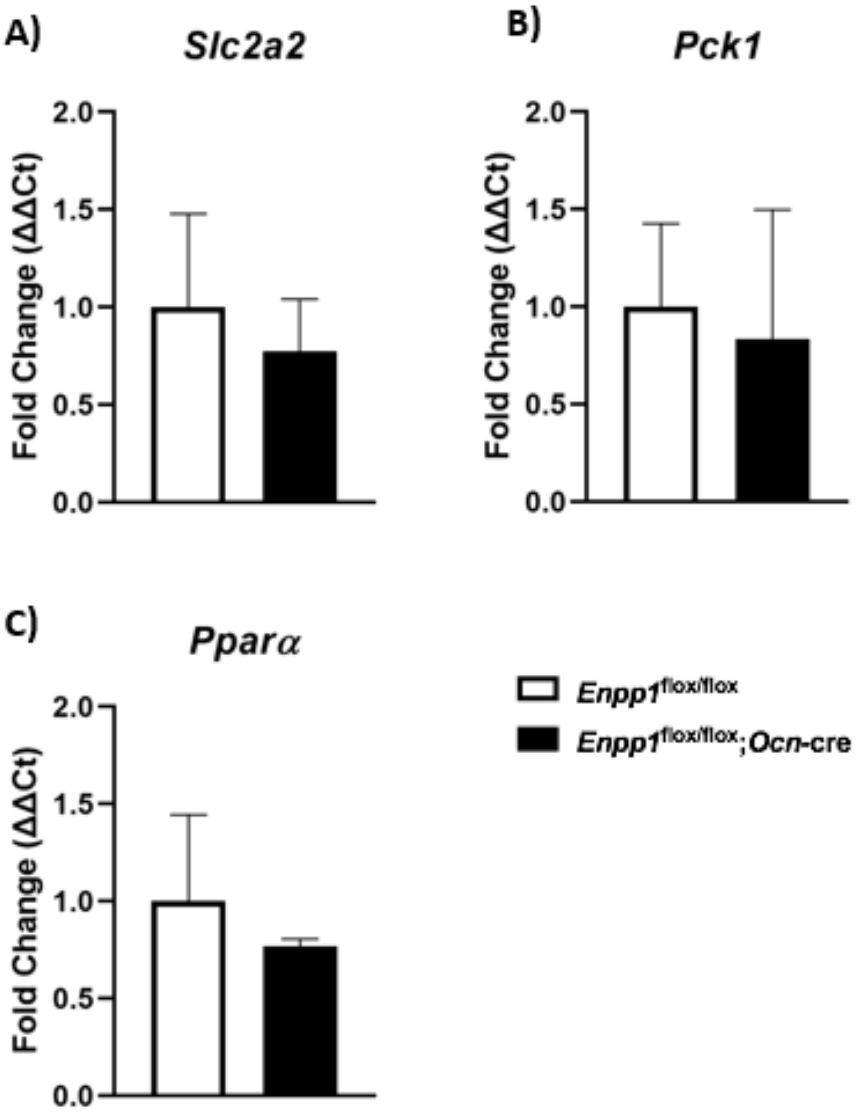

Figure 6.10. The mRNA expression of liver tissue-associated metabolic genes of high-fat diet fed mice is unchanged between genotypes.

The brown fat mRNA expression of selected metabolic genes including (A) *Slc2a1*, (B) *Slc2a4*, (C) *Ucp1,* (D) *Ucp2,* (E) *Dgat1* (F) *Dgat2*, and (G) L*pl* was analysed. mRNA values generated were normalised to the geometric mean of *Gapdh* and β-*actin* house-keeping genes. Data are presented as the mean ± S.E.M (n=4). No significant findings observed.

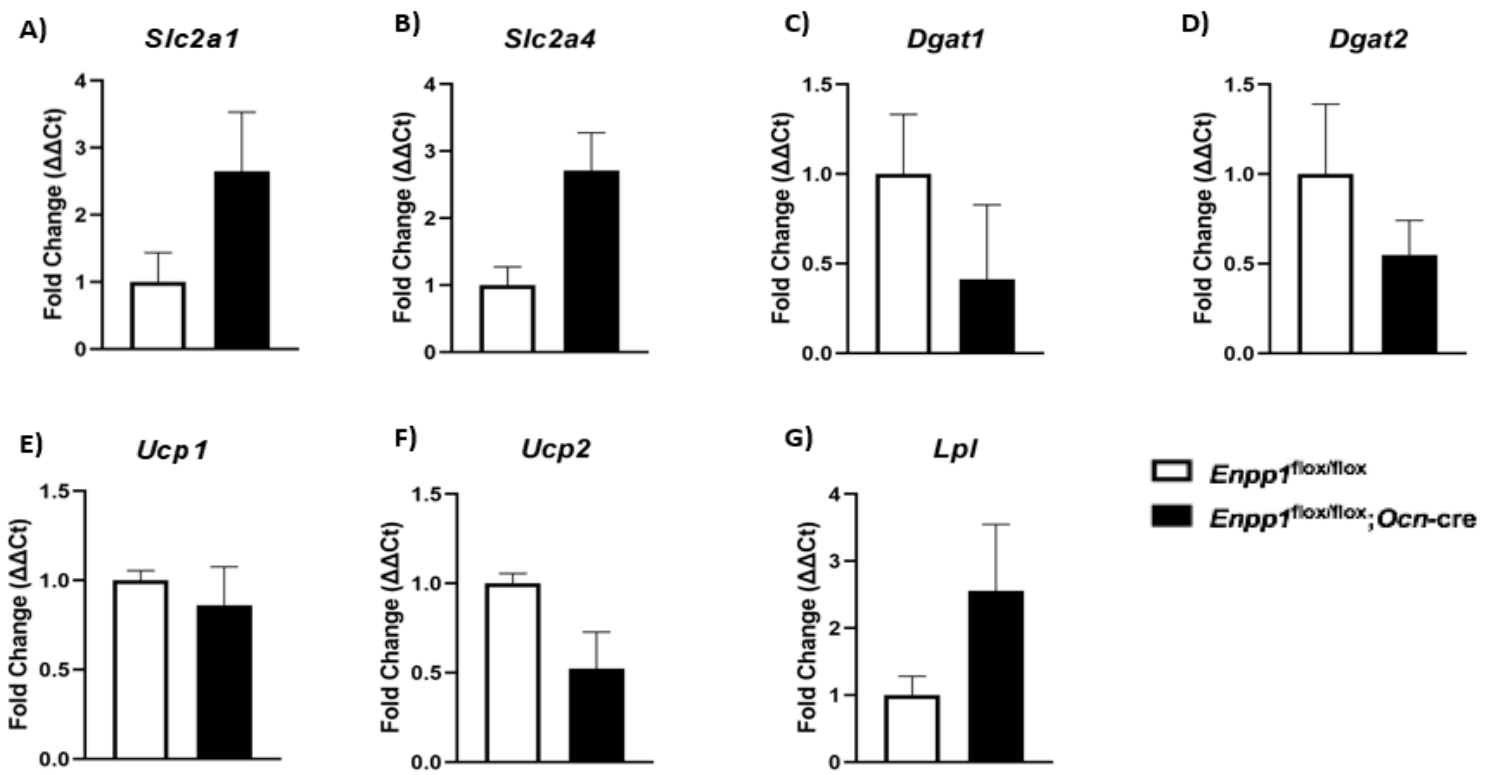

Figure 6.11. The mRNA expression of brown adipose tissue-associated metabolic genes of high-fat diet fed mice is unchanged between genotypes.

The brown fat mRNA expression of selected metabolic genes including (A) *Slc2a1*, (B) *Slc2a4*, (C) *Ucp1,* (D) *Ucp2,* (E) *Dgat1* (F) *Dgat2*, and (G) L*pl* was analysed. mRNA values generated were normalised to the geometric mean of *Gapdh* and β-*actin* house-keeping genes. Data are presented as the mean ± S.E.M (n=4). No significant findings observed.

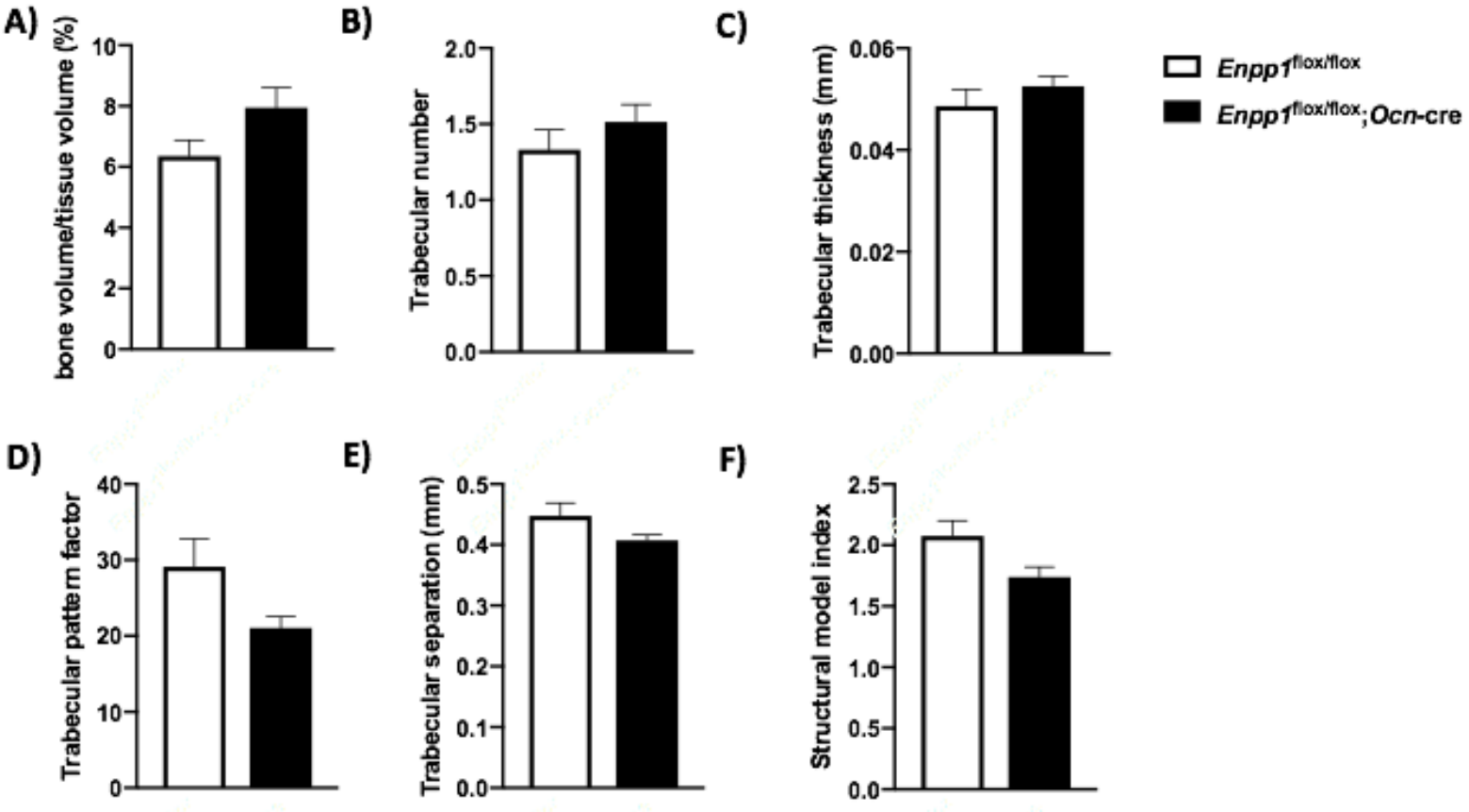

Figure 6.12. µ-CT analysis of tibiae trabecular bone of high-fat diet fed mice reveals no difference between genotypes.

The following parameters were measured; (A) bone volume (BV/TV), (B) trabecular number, (C) trabecular thickness, (D) trabecular pattern factor, (E) trabecular separation, and (F) structural model index. Data are presented as the mean ± S.E.M (n≥3). No significant findings observed.

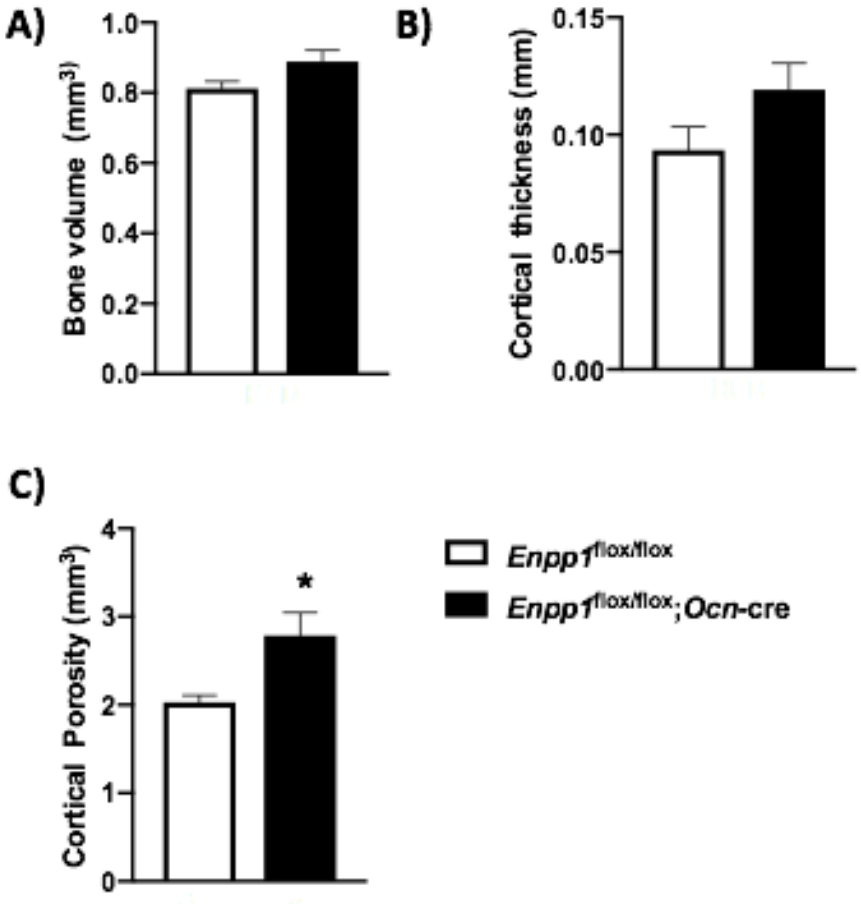

Figure 6.13. µ-CT analysis of tibiae cortical bone of high-fat diet fed mice shows increased cortical porosity of osteoblast-specific NPP1 ablated mice.

The following parameters were measured; (A) bone volume, (B) cortical thickness and (C) cortical porosity. Data are presented as the mean ± S.E.M (n≥3). Significance is denoted by *P<0.05.

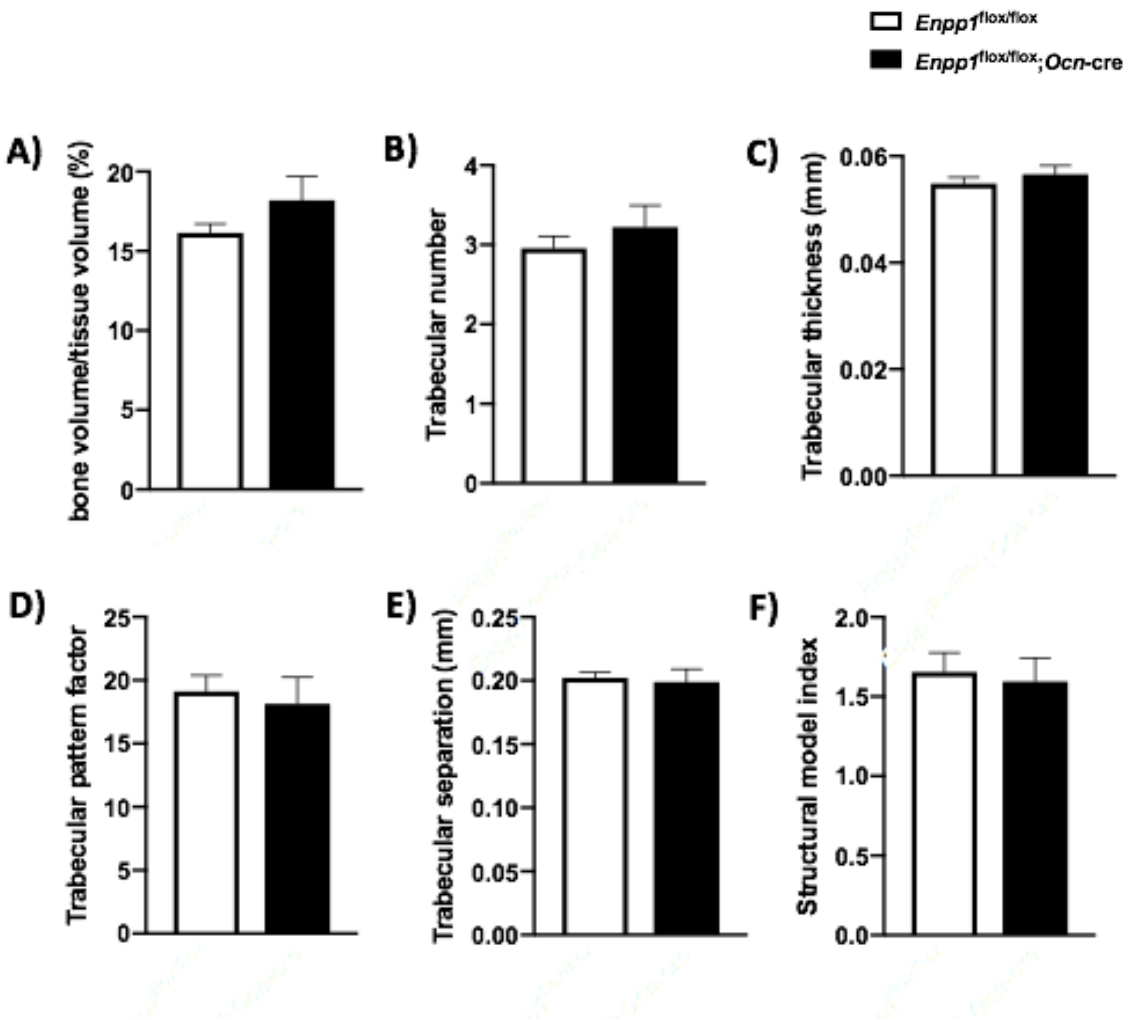

Figure 6.14. µ-CT analysis of femora trabecular bone of high-fat diet fed mice demonstrates no differences between genotypes.

The following parameters were measured; (A) percent bone volume (BV/TV), (B) trabecular number, (C) trabecular thickness, (D) trabecular pattern factor, (E) trabecular separation and (F) Structural model index. Data are presented as the mean ± S.E.M ($n \geq 3$). No significant findings observed.

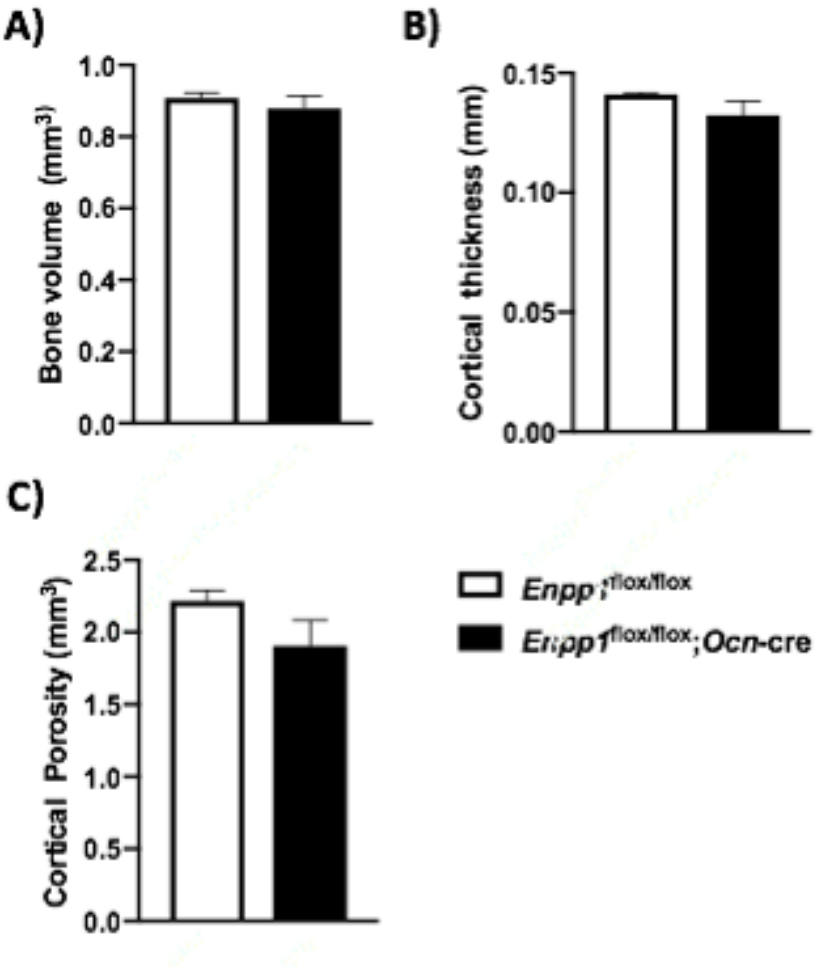

Figure 6.15. µ-CT analysis of femora cortical bone of high-fat diet fed mice reveals no differences between genotypes.

The following parameters were measured; (A) bone volume, (B) cortical thickness, (C) cortical porosity. Data are presented as the mean ± S.E.M (n≥3). No significant findings observed.

6.5.6. Analysis of long bone marrow adipose tissue by osmium staining

The analysis of differing bone marrow adipose depots in the tibiae revealed no significant difference in adipocyte quantification between genotype (Fig 6. 16), nor did it reveal a diet-effect, whereby there was not a notable expansion of adipocyte tissue following chronic high-fat diet feeding. The total femoral marrow adipose tissue reflected these findings, with no difference observed between genotype, nor between diet-type. (Fig. 6.17).

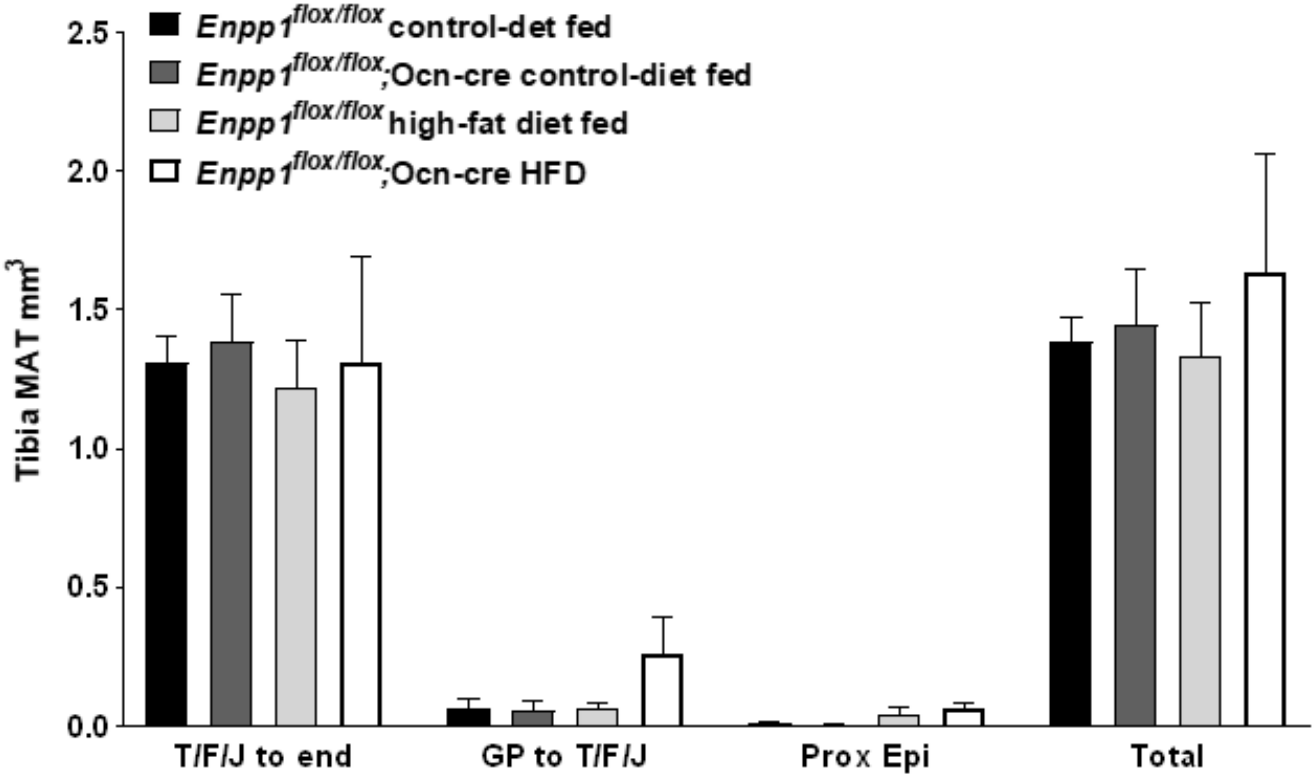

Figure 6.16. Osmium staining of tibiae marrow adipose tissue of high-fat diet fed mice shows no difference between genotypes.

The marrow adipose tissue of control diet fed (CD) and high-fat diet fed (HFD) *Enpp1$^{flox/flox}$;Ocn-cre* and *Enpp1$^{flox/flox}$* mice quantified by osmium tetroxide staining and μ-CT analysis. This included the different anatomical regions, including tibia-fibula junction (T/F/J) to proximal end, proximal growth plate (GP) to T/F/J, proximal epiphysis (Prox Epi) and the bone marrow from the total length of the tibiae. Data are presented as the mean ± S.E.M (n≥3). No significant findings observed.

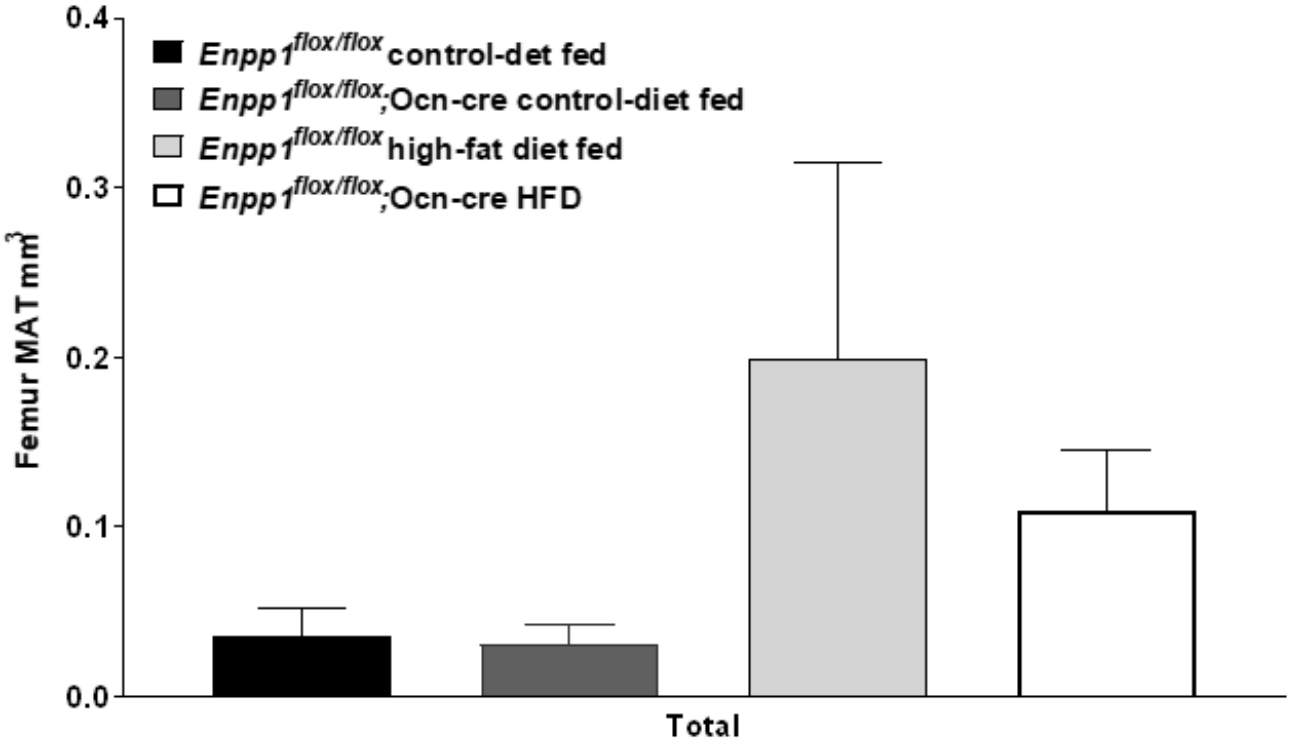

Figure 6.17. Osmium staining of total femoral marrow adipose tissue of high-fat diet fed mice shows no difference between genotypes..

The marrow adipose tissue of control diet fed (CD) and high-fat diet fed (HFD) *Enpp1$^{flox/flox}$;Ocn-cre* and *Enpp1$^{flox/flox}$* mice quantified by osmium tetroxide staining and μ-CT analysis. Data are presented as the mean ± S.E.M (n≥3). No significant findings observed.

6.6. Discussion

Previous work to this thesis has well established the metabolic phenotype changes that occur following high-fat diet feeding in mice (Winzell and Ahrén, 2004, King and Bowe, 2016a, Nagy and Einwallner, 2018). This has been instrumental in aiding the understanding of metabolic syndrome pathophysiology, including the disease states of obesity and T2DM (Lindstrom, 2007, Wang et al., 2014a, King and Bowe, 2016b). The use of a high-fat diet feeding model can allow for the probing of a genes function within the obesogenic landscape. I have utilised this model to understand the role of osteoblast-specific NPP1, to determine whether this confers metabolic protection as evidenced in the global *Enpp1*$^{-/-}$ knockout mice.

Chapter 3 of this thesis revealed that the *Enpp1*$^{flox/flox}$*;Ocn*-cre mice demonstrate increased long bone mass and mineralisation. The formation of bone has been associated with metabolic cost, and as such, I aimed to investigate whether the osteoblast-specific ablation of NPP1 would result in a concomitant skeletal and metabolic phenotype, perhaps only being evident under situations of chronic caloric excess. For this chapter, male mice were used to assess the effect of high-fat diet between genotypes in order to avoid the confounding effects estrogen may have on dietary induced phenotypes (Acharya et al., 2019a, Yepuru et al., 2010, Litwak et al., 2014, Acharya et al., 2019b, Ting et al., 2017, Omotola et al., 2019).

The data presented in this chapter reveals that the osteoblast-specific ablation of NPP1 in mice confers a lack of metabolic protection. These findings are not consistent with my original hypothesis that the ablation of NPP1 in osteoblasts would result in increased insulin sensitivity and provide overall protection against the detrimental effects of chronic obesogenic feeding. The observed increase of the *Enpp1*$^{flox/flox}$*;Ocn*-cre mice liver mass at necroscopy can be explained by the increased liver triglyceride content, a typical change following high-fat diet feeding (Eisinger et al., 2014).

Lipidomic analysis has revealed that approximately 60% of the lipids altered in mice fed a high-fat diet were also altered in the serum (Eisinger et al., 2014). Further studies would be informative to delineate the altered lipid species expansion in the liver and the serum of the

Enpp1$^{flox/flox}$*;Ocn*-cre mice to determine if this reflected literature reported alterations of lipids in high-fat diet fed rodent models of obesity. For example, Seferovic *et al.,* report notable changes in liver lipids involved in the sphingolipid pathway, which has been implicated by others in high-fat diet models, after only 1-week of high-fat diet challenge of mice (Clements and Reynertson, 1977, Yang et al., 2009, Seferovic et al., 2018). Furthermore, ultra-performance liquid chromatography–quadrupole time-of-flight mass-spectrometry analysis of high-fat diet fed C57BL/6J mice revealed a significantly altered triglyceride level compared to controls (Nam et al., 2015). Notably, this included a difference in the acyl chain length and degree of unsaturation (Nam et al., 2015). Continued investigation of the *Enpp1*$^{flox/flox}$*;Ocn*-cre lipid profile and triglyceride content may identify novel pathways of bone-specific NPP1 and liver lipid synthesis and storage.

The absence of fibrosis and steatosis in the *Enpp1*$^{flox/flox}$*;Ocn*-cre mice reported by Dr Timothy Kendall of the University of Edinburgh perhaps hints that safer storage of triglyceride in the liver is occurring. Typically, following high-fat diet feeding, mice will develop a fatty liver NAFLD which may progress to NASH (Kohli and Feldstein, 2011, Takahashi et al., 2012, Clapper et al., 2013, Savari et al., 2019, Velázquez et al., 2019). The caloric excess of mice in chronic high-fat feeding conditions leads to excess energy. This excess energy leads to an increase of non-esterified fatty acids and pro-inflammatory cytokine release (White and Marette, 2014, Després and Lemieux, 2006). This increases fat deposition in the liver (Despres, 2006, Tilg and Hotamisligil, 2006, Clapper et al., 2013) and is reflective of the major risk factors for the development of metabolic syndrome in humans (Hariri and Thibault, 2010, James et al., 2012).

An alternative explanation for increased liver mass and triglyceride content with no inflammation and fibrosis could be that the hepatocytes exhibit a higher than usual turnover of fatty acids, with increased transient storage in the form of triglycerides in lipid droplets. A study by Salmon and Hems revealed that genetically obese *ob/ob* mice exhibit significantly increased hepatic triglyceride and phospholipid synthesis compared with lean mice (Salmon and Hems, 1973). The use of a methionine-choline deficient (MCD) diet will rapidly and reliably induce measurable (mainly macro-vesicular) hepatic steatosis in rodents following 2-

4 weeks of feeding (Weltman et al., 1996, Sahai et al., 2004, Machado et al., 2015). After this point, progressive inflammatory damage and fibrosis will occur (Sahai et al., 2004, Weltman et al., 1996, Rinella et al., 2008, Stephenson et al., 2018). This highlights an important variation in dietary regimes and outcomes, demonstrating various alterations to the liver phenotype dependent on the composition of the diet. To investigate whether osteoblast-specific NPP1 ablation is truly protective against NAFLD and NASH in the liver, feeding with an MCD diet followed by comprehensive liver phenotyping including lipidomic profiling, proteomic profiling and histological assessment would be informative.

Alternatively, excess lipids may be stored in a different location. For example, the *Enpp1*$^{flox/flox}$*;Ocn*-cre mice demonstrate significantly increased gonadal fat pad mass compared to *Enpp1*$^{flox/flox}$ controls: this may represent an adipose tissue depot site that is more able to expand. Brown fat is an organ which is specialised for energy expenditure. This adipose depot is characterised by several small lipid droplets (multilocular), the presence of many mitochondria, and the unique expression of uncoupling protein 1 (UCP1) (Ravussin and Kozak, 2009, Cannon and Nedergaard, 2010, Nedergaard and Cannon, 2010, Nedergaard et al., 2010, Richard et al., 2010, Richard and Picard, 2011). This protein acts to uncouple oxidative phosphorylation from ATP production, thereby released energy as heat (thermogenesis) (Nicholls and Locke, 1984, Cannon and Nedergaard, 1985, Matthias et al., 2000). Despite the increased brown fat mass, the thermogenic function as evidenced through qPCR analysis was unaltered. The fat pad mass of the *Enpp1*$^{flox/flox}$*;Ocn*-cre mice reflected those of the *Enpp1*$^{flox/flox}$ mice, demonstrating a comparable ability to expand and store excess triglyceride in lipid droplets, whereby adipocytes undergo hypertrophy. This indicates that osteoblast-derived NPP1 does not lead to changes in the metabolic action of brown fat in thermoneutral conditions. However, a more in-depth thermogenic analysis beyond mRNA level (*e.g*. western blot analysis) is needed to confirm brown fat metabolic activity.

Reflecting the results observed in the control-diet fed mice, the high-fat diet fed mice do not present with a notable bone phenotype. The high-fat diet and its effect on bone has been studied and published. These publications demonstrate notable changes evident at the bone

level following 12-weeks of chronic high-fat diet feeding (Wohl et al., 1998, Doucette et al., 2015). Predominantly, an expansion of the bone marrow adipose tissue (BMAT) (184% following 12-weeks of high-fat diet feeding), with a deleterious effect on the skeleton is observed (Doucette et al., 2015). Such deleterious effects include reduced trabecular bone mass (29%) and reduced cortical thickness (5%) (Tencerova et al., 2018) Indeed, this study also demonstrates that it is the expansion of BMAT in response to high-fat diet feeding that exerts the deleterious skeletal changes.

The accumulation of BMAT is reportedly associated with obesity, insulin resistance and T2DM in mice and humans (Lecka-Czernik, 2010, Bredella et al., 2011, Bredella et al., 2013, Doucette et al., 2015, Gawronska-Kozak et al., 2014). To assess the expansion of BMAT following chronic high-fat diet feeding, osmium staining followed by µ-CT analysis was performed as described previously (Scheller et al., 2014, Styner et al., 2014, Styner et al., 2015). This was conducted for the tibiae at various anatomical regions since BMAT expansion occurs heterogeneously throughout the long bones, whereby different regions respond in variable ways to stimuli (Meunier et al., 1971, Minaire et al., 1974, Wronski et al., 1981, Cup et al., 2000, Nuttall and Gimble, 2000, Devlin et al., 2010, Akune et al., 2004, Cawthorn et al., 2014). The sites investigated included the tibia-fibula Junction (T/F/J) to the proximal end of the bone, proximal growth plate (GP) to T/F/J, and proximal epiphysis (Prox Epi), and the bone marrow adipose tissue throughout the total length of the bone. The more proximal regions contain a fat known as regulated marrow adipose tissue (rMAT) which contains adipocytes interspersed with haematopoiesis and which forms shortly after post-natal development (Pichardo et al., 2007, Scheller and Rosen, 2014). Secondly, there is constitutive marrow adipose tissue (cMAT) which is more distal and contains larger white-adipose tissue-like adipocytes (Scheller et al., 2015). The expansion of BMAT following chronic high-fat diet feeding of the *Enpp1*$^{flox/flox}$*;Ocn*-cre mice was assessed by osmium staining, revealing little difference between the control-diet and high-fat diet fed mice. The absence of BMAT expansion may explain the absence of deleterious skeletal effects in the *Enpp1*$^{flox/flox}$*;Ocn*-cre mice.

Previous work has revealed that BMAT increases in high-fat diet fed C57BL/6J mice. These studies routinely report that there is a significant increase in BMAT, yet the trabecular and cortical bone mass remains unchanged (Doucette et al., 2015), or decreased (Cao et al., 2010, Patsch et al., 2011). Experimental and clinical evidence both point towards the reduction of osteoblastogenesis at the expense of adipogenesis, for example, humans with osteoporosis (and decreased bone mass) present with increased marrow adipose tissue (Prockop, 1997, Rosen and Bouxsein, 2006, Rodriguez et al., 2008, Nishio et al., 2012, Ambrosi et al., 2017). This is due to the shared lineage origin of bone marrow mesenchymal stem cells (MSC) for both osteoblast and adipocytes (Kim et al., 2004, Muruganandan et al., 2009, Krings et al., 2012, Ortuño et al., 2013, Muruganandan and Sinal, 2014, Ambrosi et al., 2017). These MSCs are self-renewing and pluripotent. When MSCs differentiate into adipocytes, this can affect bone remodelling by the suppression of intracellular osteogenic signals (such as Runx2, osterix, and β-catenin), while simultaneously promoting the secretion of adipogenic signalling molecules such as leptin, adiponectin, chemerin, omentin-1, resistin, and visfatin (Ambrosi et al., 2017, Krings et al., 2012, Muruganandan et al., 2009, Muruganandan and Sinal, 2014, Ortuño et al., 2013, Kim et al., 2004). The increased bone mass of the juvenile *Enpp1*$^{flox/flox}$*;Ocn*-cre mice compared to *Enpp1*$^{flox/flox}$ control mice was likely facilitated at the expense of the bone BMAT development and expansion (Muruganandan et al., 2009, Muruganandan and Sinal, 2014). To confirm this, assessment of BMAT adipogenesis signalling molecules could be performed by mass-spectrometry and microarray analysis of gene expression (Lee et al., 2004, Welsh et al., 2004, Liu et al., 2011). Further investigation of the osteogenic signalling by assessing osteogenic-associated pathways and protein expression could indicate whether there is increased osteoblastogenesis at the expense of adipogenesis as hypothesised.

Despite the control-diet fed *Enpp1*$^{flox/flox}$*;Ocn*-cre mice presenting with increased uncarboxylated-OCN, this was not observed in the chronic high-fat diet fed mice. This suggests a loss of OCN-associated metabolic protection of the *Enpp1*$^{flox/flox}$*;Ocn*-cre mice following chronic high-fat diet challenge. The normalisation of undercarboxylated and/or un-carboxylated-OCN following high-fat diet feeding has been reported in several mouse studies, including those with targeted gene deletion in osteoblasts (Kashiwagi et al., 2011). An analysis of rats with T2DM revealed significantly decreased undercarboxylated levels,

alongside significantly increased serum triglyceride (Gu et al., 2017). It has been reported that two osteoblast transcription factors (Fork-head box O and activating transcription factor 3) both suppress OCN activity by favouring the expression of embryonic stem cell phosphatase (ESP) (Kode et al., 2012). Insulin binds to its receptor in osteoblasts and is responsible for disengaging it from its role as a substrate for ESP (Lee et al., 2007). As such, the IR is subsequently activated, which activates a molecular pathway inducing bone resorption, which provides the acidic bone ECM that favours OCN decarboxylation (Kode et al., 2012). By upregulating ESP through osteoblast-specific transcription factors, a decrease of undercarboxylated and uncarboxylated-OCN occurs (Lee et al., 2007, Ferron et al., 2010a, Kode et al., 2012). It would be of great interest to investigate whether this mechanism was occurring, and thus explain the loss of difference between genotype of uncarboxylated OCN, in the osteoblast-specific NPP1 ablated high-fat diet fed mice.

In conclusion, the results presented in this chapter highlight that the chronic high-fat diet feeding of osteoblast-specific NPP1 ablated male 16-week old mice is unexpectedly metabolically detrimental. These data also indicated that the *Enpp1*$^{flox/flox}$*;Ocn*-cre mice are incapable of expanding their BMAT and that this may aid in conferring protection of the bone. Further work would be required to assess this. Further work is also required to determine the mechanistic explanations of why ablation of NPP1 at one of its principal sites of action does not result in the metabolic protection observed in the *Enpp1*$^{-/-}$ mice.

Given that *Enpp1*$^{flox/flox}$*;Ocn*-cre mice only have NPP1 ablated from the osteoblast, NPP1 from alternate tissue or cell-type may be responsible for driving the insulin-resistant phenotype in this mouse. The literature reports that NPP1 is expressed ubiquitously, with relatively higher expression levels in certain tissue types including in bone, liver, testis and kidney (Harahap and Goding, 1988, Yano et al., 1985, Funakoshi et al., 1992, Huang et al., 1994). As such, I suggest that the careful assessment of cell-specific ablation of NPP1 from these tissue types be investigated to determine which tissue-knockout can recapitulate the metabolic phenotype observed in the *Enpp1*$^{-/-}$ mouse.

(*This page has been left intentionally blank)*

Chapter 7. Discussion.

7.1. General discussion

The establishment of bone as an endocrine organ, utilisation of mouse models, clinical observations and integrative physiological approaches has led to unanticipated advances within the bone biology field. The contemporary understanding of the roles of the skeleton extends well beyond the traditional views of bone as a structural scaffold, mineral homeostasis regulator and haematopoietic niche. Indeed, the skeleton is now recognised to contribute to systemic glucose metabolism, insulin secretion and response by insulin-target tissues, brain development, male fertility and others (Clemens and Karsenty, 2011, Oury et al., 2011, Wei et al., 2014, Delezie and Handschin, 2018, Shan et al., 2019). These data emerging over the last 20 years have firmly established a bone-endocrine function, and have borne witness to an increase in the number of laboratories working within this field.

The continued study of bone has identified the critical importance of matrix mineralisation regulators (Gurley et al., 2006a, Sweet and Green, 1981, Hakim et al., 1984a, Hessle et al., 2002, Johnson et al., 2003, Harmey et al., 2004, Roberts et al., 2007a, Festing et al., 2009, Collins and Boehm, 2011, Mackenzie et al., 2012, Huesa et al., 2015a, Houston et al., 2016, Tong et al., 2018, Bonnet et al., 2019, Dillon et al., 2019, Roberts et al., 2019b). In recent years, several studies have advocated a non-skeletal role for these regulators in a range of human diseases, including metabolic, cardiovascular and neurodegenerative disease (Maddux et al., 2006a, Malkin et al., 2006, Goldfine et al., 2008, Kiechl et al., 2013, Diaz-Hernandez et al., 2015, Dayeh et al., 2016, Sayols-Baixeras et al., 2016). This is an emerging area of interest and the functional roles and mechanisms of action of these various endocrine factors, phosphatases and phosphodiesterase enzymes in different pathologies are of great interest. Mechanistic insight into the pathways where mineralisation promotors and inhibitors act may identify druggable targets for commonly experienced morbidities, notably those related to metabolism and metabolic syndrome.

The formation of bone and its resorption are events which occur throughout life and are associated with high energetic cost. This has led to the hypothesis that energy metabolism and bone formation regulate one another in a feedback loop. Following work by Professor Gerard Karsenty (Colombia University, New York) and Professor Thomas Clemens (Johns

Hopkins University, Baltimore) which led to the discovery of undercarboxylated (metabolically active) OCN, a hormone secreted specifically by the osteoblast to promote insulin sensitivity (amongst other systemic functions), further evidence has emerged for the metabolic role of bone (Clemens and Karsenty, 2011). Many laboratories are engaged in determining the precise mechanisms, aetiology, genetics and molecular components that are involved in the physiology and pathophysiology of bone-endocrine function.

T2DM represents a notable global health crisis, with a projected incidence of 643 million by 2040 (https://diabetesatlas.org/), 90% of which will be T2DM (Bruno et al., 2005, Holman et al., 2015). The literature reports that the main drivers of T2DM are the rise in obesity, sedentary lifestyle, consumption of energy-dense foods and an ageing population (Chan et al., 2009, Hu, 2011, Polonsky, 2012, Roglic, 2016). However, an individual's genetic architecture also may determine their response to these environmental challenges. This can be characterised as modifiable (*e.g*. environmental) and non-modifiable risk factors (*e.g*. genetics); the combination of these factors may lead an individual to suffer from the metabolic syndrome, including hypertension, dyslipidaemia, insulin resistance, obesity and more (Fig. 7.1). A more comprehensive understanding of the role of mineralisation regulators and their contribution to energy metabolism may be helpful for the identification and development of new preventative, therapeutic and genetic strategies to combat components of the metabolic syndrome, notably, T2DM. This is timely, given that T2DM represents an ever-increasing burden of disease in both developed and low-income countries. For example, the reported increase in health loss from T2DM since 1990 in India is the highest amongst all major non-communicable diseases (Tandon et al., 2018) whilst alarmingly almost 10% of the American population (30.2 million individuals) have diabetes, 23 million of which suffer from T2DM (https://www.cdc.gov/diabetes/data/statistics/statistics-report.html).

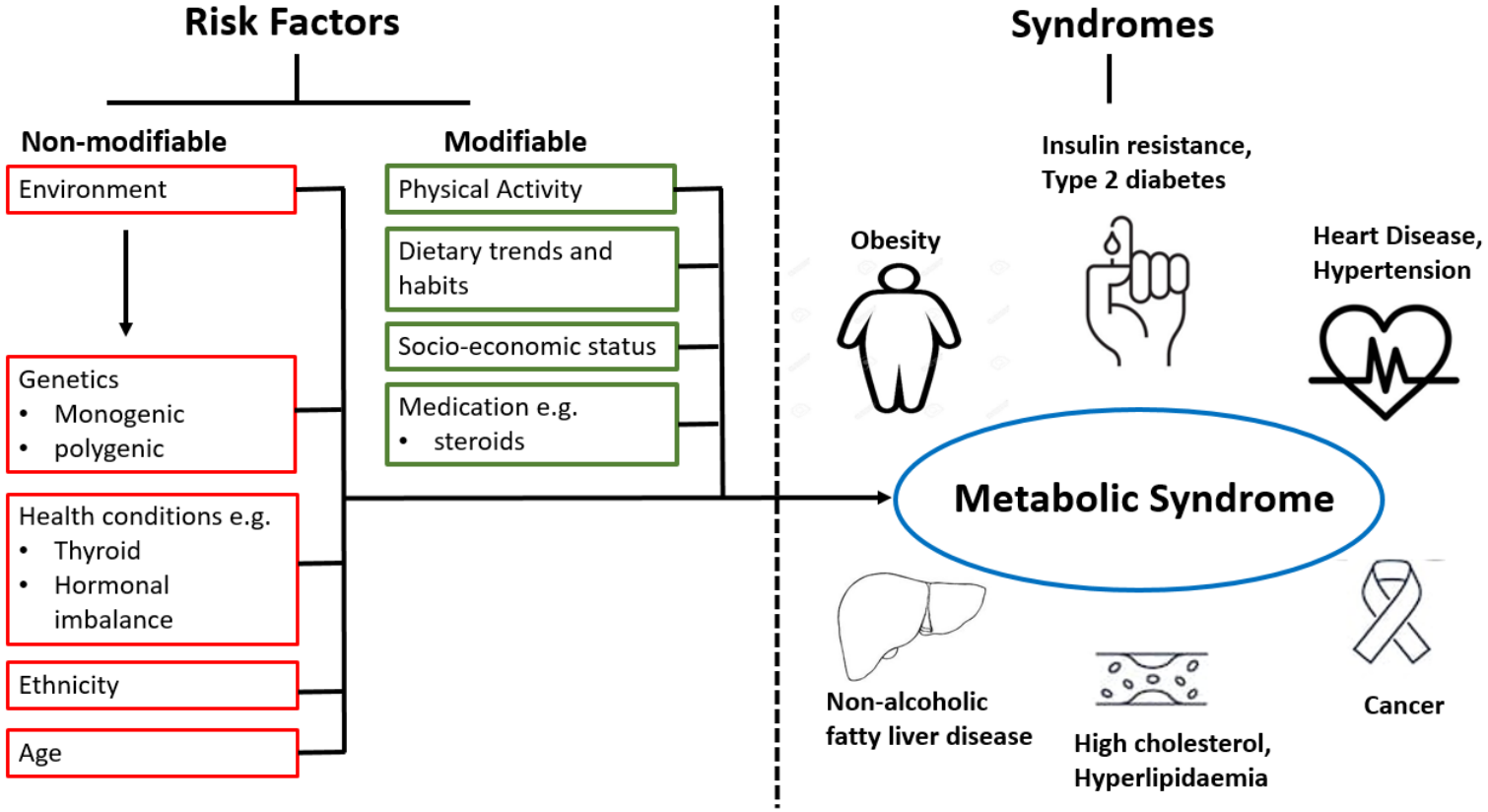

Figure 7.1. Risk factors and disease experienced in the metabolic syndrome.

Schematic figure demonstrating non-modifiable and modifiable risk factors that may contribute to an individuals incidence of metabolic syndrome. The multiple conditions that make up metabolic syndrome are represented on the right hand side of this figure.

Obesity and insulin resistance are preventable and reversible diseases and simple interventions (*e.g.* daily exercise) and alterations to lifestyle (*e.g.* dietary choices) can decrease mass and improve insulin sensitivity (Ross et al., 2000, Assali et al., 2001, Janssen et al., 2002, Toledo et al., 2008). The use of lifestyle intervention strategies has been demonstrated as effective in controlled and randomised trials across the globe, including the Chinese Da Qing study, the Finish Diabetes Prevention Programme, the Indian Diabetes Prevention program and the U.S Diabetes Prevention Programme (Pan et al., 1997, Tuomilehto et al., 2001b, Knowler et al., 2002, Ramachandran et al., 2006). However, the deployment of lifestyle-based intervention strategies throughout entire populations (*e.g.* 52 million people North America) is a massive, and arguably an unachievable task (Florez, 2016).

Alternative strategies have been implored including the use of metformin (dimethylbiguanide). The oral administration of this first-line pharmacological treatment for T2DM results in lowered blood glucose concentrations (Bailey and Turner, 1996, Kirpichnikov et al., 2002). The Diabetes Control and Complications Trial (1993) has demonstrated that there is a casual relation between T2DM and microvascular disease. Patients with T2DM often have several risk factors for the development of atheroma, hypertension, dyslipidaemia and vascular disease (Stout, 1990, DeFronzo and Ferrannini, 1991, Reaven, 1988). A study of insulin-treated patients with T2DM in Japan revealed that improved glycaemic control was associated with decreased progression of microvascular disease (Ohkubo et al., 1995). Such observations have been reflected in further human-based studies, reflecting the vasculoprotective effects of metformin including the UK Prospective Diabetes Study (1998) and others (Bailey, 2008). Various animal models have highlighted that metformin acts to prevent vascular endothelial dysfunction by increasing nitric oxide bioavailability (Mather et al., 2001, Vitale et al., 2005, Sena et al., 2011, Forouzandeh et al., 2014).

The mechanisms of action for metformin and metabolism remain largely unknown, with reports suggesting that a range of organs are targeted including the liver and the gut (Wang et al., 2002, Tiikkainen et al., 2004, Natali and Ferrannini, 2006, Shu et al., 2007, Zema, 2012, Karlsson et al., 2013). Furthermore, metformin use has limitations with reports of

metformin-induced hepatotoxicity and side-effects including dizziness, muscle pain, tiredness, respiratory difficulties, irregular heartbeat, diarrhoea, nausea and vomiting (Baradaran, 2012, Miralles-Linares et al., 2012, Gheshlaghi, 2012, Scheen and Paquot, 2013, Nasri et al., 2014). A population-based study showed that approximately 25% of patients taking prescribed metformin had contraindications to its use (Emslie-Smith et al., 2001). Alternate strategies to tackle T2DM are required and this necessitates continued investigative efforts into the genetic components of the disease.

This thesis has specifically focused on determining the effect of osteoblast-specific ablation of NPP1 on both skeletal and metabolic phenotypes. NPP1 is an indispensable mineralisation regulator through its action whereby extracellular PP_i is generated by ATP hydrolysis. Previous work has demonstrated that the global ablation of NPP1 in mice results in a hypermineralisation of the joints, spinal ankylosis, and ectopic mineralisation (*e.g.* the tunica media of the aorta) (Mackenzie et al., 2012). Previous work also demonstrated that the global ablation of NPP1 is metabolically protective, whereby *Enpp1*$^{-/-}$ mice challenged with high-fat diet were protected against obesity and insulin resistance (Huesa et al., 2014). The cell-specific contributions of NPP1 to these phenotypes remain undetermined. Here, I show that the osteoblast-specific ablation of *Enpp1* engenders an increase in bone mass and bone mineralisation (chapter 3). I demonstrated that this bone phenotype is reflected at the *in vitro* level, whereby primary osteoblasts isolated from the osteoblast-specific *Enpp1*-ablated mouse mineralise their matrix more quickly and to a greater extent compared to their controls (chapter 4). Furthermore, the work presented in this thesis demonstrates that osteoblast-specific *Enpp1* ablation does not result in the alteration of systemic PP_i and is not able to recapitulate the pathological ectopic mineralisation observed in the global *Enpp1*$^{-/-}$.

This thesis has also investigated the effect of osteoblast-specific *Enpp1* ablation on metabolic phenotype. Here, I show that osteoblast-specific *Enpp1* ablation of control-diet fed mice facilitates an increase in uncarboxylated-OCN reflecting observations of the global *Enpp1*$^{-/-}$ mouse. However, following chronic high-fat diet feeding, osteoblast-specific *Enpp1* ablation does not result in metabolic protection as observed in the global *Enpp1*$^{-/-}$ mouse. Indeed, the osteoblast-specific *Enpp1* ablated HFD-fed mice present with an unanticipated worsening of

metabolic phenotype including insulin resistance and obesity. These data demonstrate that the ablation of NPP1 at one of its key sites of action is metabolically detrimental. The metabolic phenotyping conducted would have benefitted from an additional analysis using a euglycemic clamp to further assess insulin sensitivity. This technique is considered the gold-standard method to assess insulin action on glucose utilisation in animals and humans alike (Shen et al., 1970, DeFronzo and Beckles, 1979).

The bone phenotype of the osteoblast-specific *Enpp1* ablated mouse model represents a novel finding. As discussed in chapter 3, there are several mouse models which have been used to investigate *Enpp1* ablation, including transgenic, naturally occurring mutants and knock-out models. However, these models do not report any increase in bone mineral density, as determined by μ-CT or otherwise (*e.g.* ashing, back-scattered scanning electron microscopy or detailed histological assessment). The novel finding demonstrated in this thesis highlights that osteoblast-derived NPP1 is critical in the maintenance of physiological bone mineralisation. However, it appears that osteoblast-derived NPP1 is not critical for the regulation of systemic (*e.g.* ectopic) mineralisation. As hypothesised in this thesis, I propose that osteoblast-specific NPP1 ablation results in the local reduction of PP_i concentration which affects the bone mineralisation but leaves systemic PP_i and the viscera unaffected by pathological mineralisation. This could indicate that circulatory PP_i generated from liver-derived NPP1 may be exerting crucial systemic protective effects against ectopic mineralisation.

The metabolic phenotype of the global *Enpp1*$^{-/-}$ may be governed by liver-specific NPP1. This is supported by reports in the literature from both clinical observations and basic research that highlights the liver as a key NPP1 target (Fig. 7.2). A full serum biochemical analysis of the control-fed female *Enpp1*$^{flox/flox}$*;Ocn*-cre mouse revealed depressed serum albumin, total protein, globulin and cholesterol concentrations compared to controls (Fig. 7.3). A study by Desmarchelier *et al.* revealed that mice on a high-fat diet (termed 'western diet') for 12 weeks demonstrated significantly increased plasma cholesterol levels (Desmarchelier et al., 2012). Furthermore, it is well recognised that the accumulation of hepatic free cholesterol contributes to non-alcoholic fatty liver pathogenesis (Bashiri et al., 2013, Musso et al., 2013).

The reduction of serum cholesterol in female *Enpp1*$^{flox/flox}$*;Ocn*-cre mice may indicate the existence of a protective mechanism against non-alcoholic fatty liver disease. To further, investigate this, gas- and liquid chromatography/mass spectrometry-based profiling of lipidomic and metabolic changes in the liver and plasma of our *Enpp1*$^{flox/flox}$*;Ocn*-cre mice could be conducted as described in previous studies (Tu et al., 2017). Such studies take advantage of non-targeted metabolomics and lipidomic profiling to comprehensively assess mechanisms involved in disease development (Xu et al., 2019). This would facilitate an unbiased probing of potential liver-specific lipid and metabolic pathway changes in the *Enpp1*$^{flox/flox}$*;Ocn*-cre mice related to published libraries for non-alcoholic fatty liver disease in mice (Dumas et al., 2006, Puri et al., 2007, Thomas et al., 2012, Lai et al., 2015). Furthermore, given that the male counterparts revealed no significant differences in serum biochemistry between genotype, it would be pertinent to investigate sex differences in liver function and metabolic phenotype of cell-specific NPP1 knockout mice in future studies (Fig. 7.3). A suggested future study, therefore, could take advantage of analysing an *Enpp1*$^{flox/flox}$;Albumin-cre mouse model, including basic metabolic profiling and bone phenotyping in an aim to further elucidate the cell-specific mechanisms of NPP1.

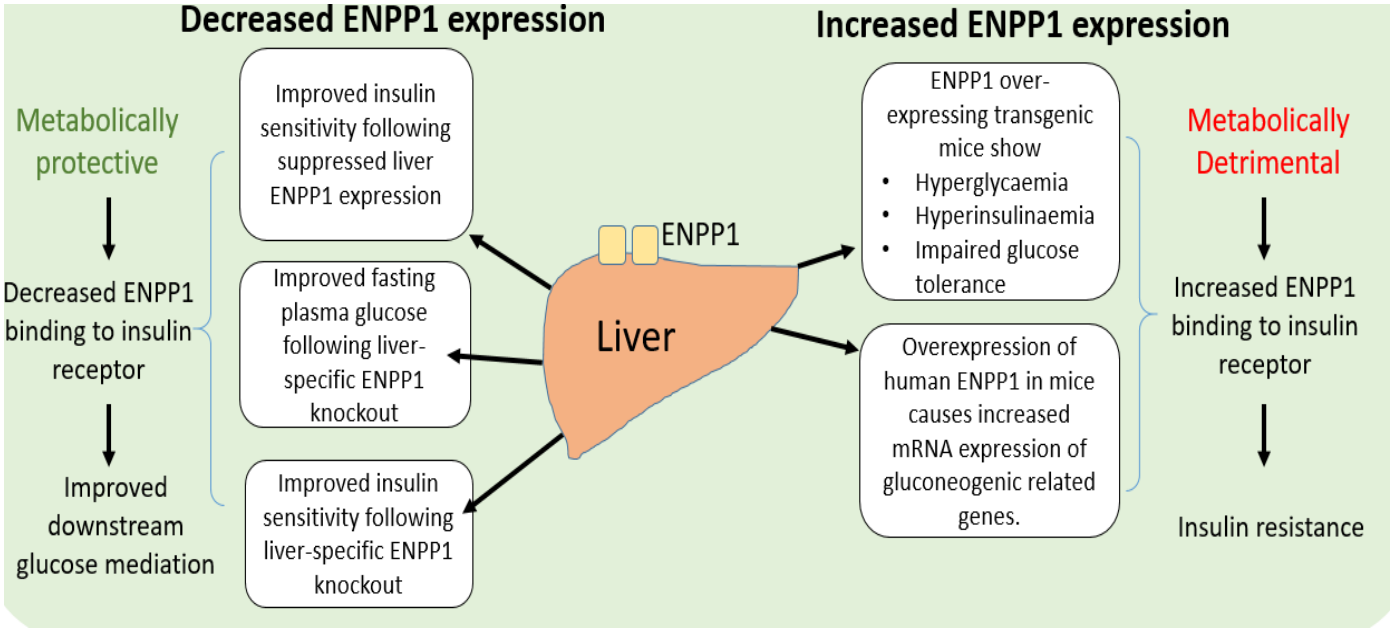

Figure 7.2. Schematic representing the proposed role and downstream effects of ENPP1 expression in the liver.

Decreased ENPP1 expression is associated with improved metabolic phenotype, whereby increased ENPP1 expression is associated with worsening metabolic phenotype. Results summarised include both clinical and basic observations from human and mouse models.

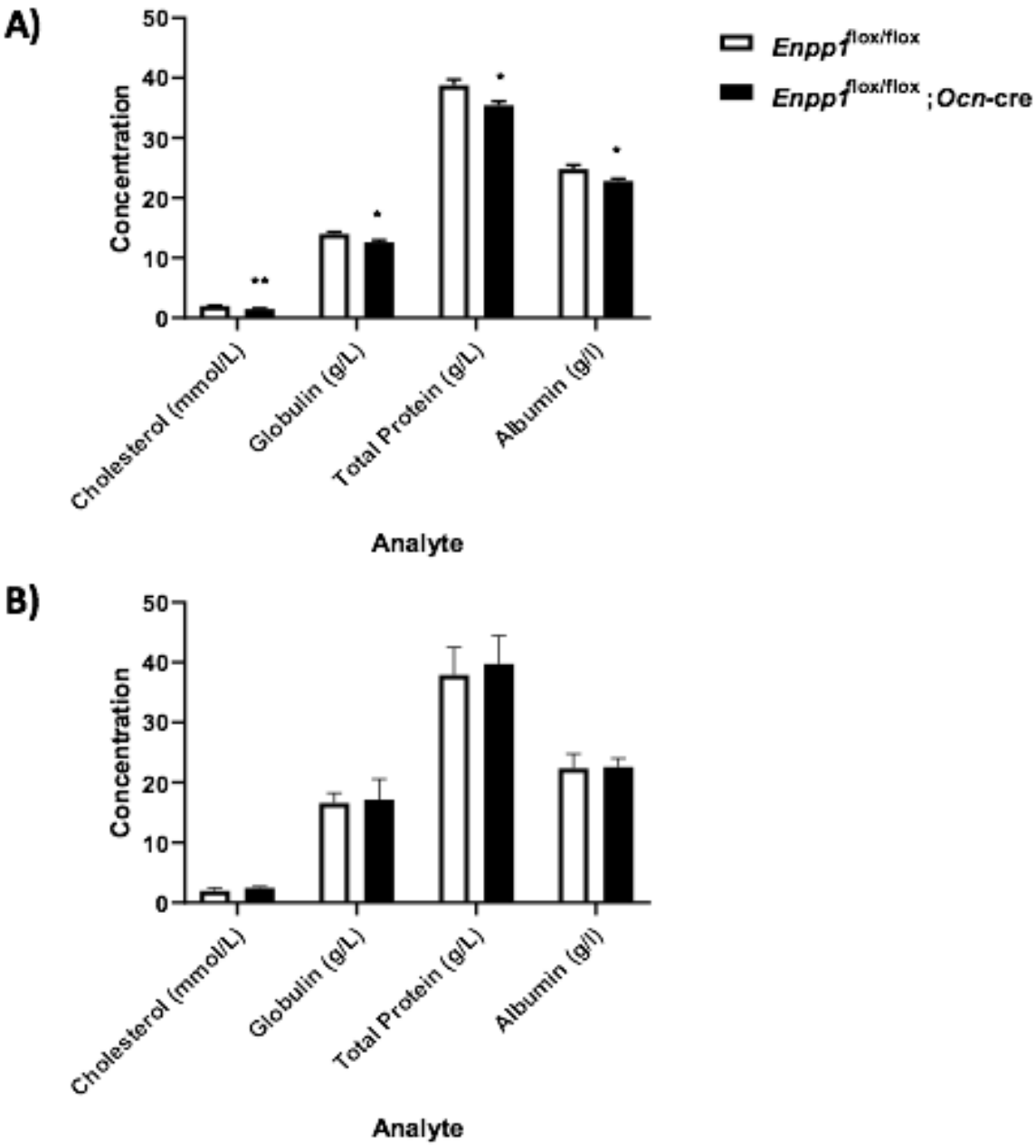

Figure 7.3. Serum analyte analysis from female mice.

Serum analysis from (A) female and (B) make *Enpp1*$^{flox/flox}$*;Ocn*-cre and *Enpp1*$^{flox/flox}$ mice was performed by Colin Wood. Cholesterol, globulin, total protein and albumin were analysed. Data are presented as average values presented with their standard errors of the mean (SEM) (n=6). Significance denoted by *P<0.05, **P<0.01.

The development of insulin resistance, viewed as a pre-requisite for T2DM, occurs when insulin is produced at a higher level than normal for a prolonged time (Cefalu, 2001, Reaven, 2004). This causes a reduction in the sensitivity of tissues to insulin and can occur years in advance of glucose intolerance and pancreatic β-cell dysfunction (Cerf, 2013). Following the discovery of undercarboxylated- and uncarboxylated-OCN, which stimulates insulin secretion, pancreatic β-cell proliferation and promotes insulin sensitivity in peripheral organs in mice, attention has been focused on determining whether these mechanisms exist in humans also.

It has been shown that polymorphisms in human *BGLAP* (OCN) are associated with T2DM and obesity (Xu et al., 2010, Korostishevsky et al., 2012). Murine studies have also shown that it is the under-carboxylated form of OCN that influences glucose metabolism (Ferron et al., 2010a, DiGirolamo et al., 2012, Huesa et al., 2014, Faienza et al., 2015, Chapurlat and Confavreux, 2016). However, the majority of clinical studies use total levels of OCN as the clinical readout (Lee et al., 2007, Reinehr and Roth, 2010, Sarkar and Choudhury, 2013, Chin et al., 2014, Wang et al., 2014b). As such, the current understanding of OCN in the human context is limited due to the lack of information about undercarboxylated- and uncarboxylated-OCN concentrations.

As determined in chapter 5 and 6, the control-fed *Enpp1*$^{flox/flox}$*;Ocn*-cre mice present with significantly increased serum concentrations of uncarboxylated-OCN, which reflects findings of the global *Enpp1*$^{-/-}$ mouse (Huesa et al., 2014). As such, an OCN-dependent mechanism of *Enpp1* regulating energy metabolism may exist. This is notable since the *Enpp1*$^{-/-}$ mice maintain this favourably altered bioactive OCN level following chronic high-fat diet feeding (Huesa et al., 2014). However, the high-fat diet fed *Enpp1*$^{flox/flox}$*;Ocn*-cre mice do not afford the metabolic protection and have unaltered OCN levels, bioactive or otherwise (chapter 6).

In conclusion, this thesis identifies for the first time that osteoblast-specific NPP1 ablation engenders increased bone mass and bone mineral density. This indicates the critical role of osteoblast-derived NPP1 in regulating bone mineralisation. This thesis also reports that osteoblast-specific NPP1 ablation is, unexpectedly, metabolically detrimental and drives obesity and insulin resistance following high-fat diet feeding. The work presented in this thesis suggests many further avenues for investigation. For example, does the liver have a crucial role in

generating and maintaining physiological systemic levels of PP_i? As such, is the liver-generated NPP1 responsible for regulating ectopic mineralisation? Could osteoblast-specific NPP1 be targeted with inhibitors to improve bone conditions whereby bone mass and bone mineralisation decrease (*e.g*. osteoporosis)? Why does the osteoblast-specific ablated mouse lack metabolic protection, yet the global *Enpp1*$^{-/-}$ maintains this following high-fat diet feeding? What other cell-specific contributions of NPP1 are there regarding metabolic phenotypes? Our understanding of the complex relationship of matrix mineralisation regulators, such as NPP1, and their role in energy metabolism will undoubtedly increase in the years to come. It is of great importance that the scientific community continue to delineate the mechanisms that underpin these systemic endocrine roles to enable better diagnosis, management and treatment of patients with metabolic diseases including T2DM and bone mineralisation related disorders.

7.2. Direction for future research

One area that has not been considered in this thesis is the role of osteoblast-specific NPP1 ablation on tooth development. The tooth consists of the crown, neck and root. Within these distinct regions are corresponding specialised tissues, including enamel (the mineralised portion), dentin, the pulp (soft tissue containing blood and nerve supply) and cementum (bone-like tissue covering tooth root) (Li et al., 2017a).

It has been shown that OCN is expressed in the later stages of odontoblast cytodifferentiation during tooth development (Zweifler et al., 2015). OCN has also been detected in odontoblasts and their processes within the ECM at the maturation stage of enamel formation (Bronckers et al., 1994, Papagerakis et al., 2002). The teeth consist of a dentin matrix, which is quite similar (although not identical) to the bone ECM and can be mineralised (Satoyoshi et al., 2001, Petridis et al., 2018). The odontoblasts have been demonstrated to synthesise and deposit OCN into the mineralising dentin (Bronckers et al., 1985, Bronckers et al., 1998). As such, the mouse model here is well suited to study the osteoblast-specific contributions of NPP1 regarding tooth mineralisation. It has been demonstrated that NPP1 and PP_i are critical in physiological tooth development (Beertsen et al., 1999, Rutherford et al., 2006, Foster et al., 2012). However, to date, the osteoblast-specific contributions of NPP1 in tooth mineralisation have not been investigated.

Cementum is important for anchoring the insertion of periodontal ligament fibres to the tooth root (Diekwisch, 2001). Cementum is a mineralised tissue layer, which covers the tooth root (Bosshardt, 2005, Foster et al., 2007). This comprises of two layers including acellular and cellular cementum (Foster et al., 2012). The cellular cementum is thicker, and bone-like, occupying the apical portion of the root (Foster et al., 2012) and has roles in the post-eruption adjustment of tooth occlusion (Diekwisch, 2001, Bosshardt, 2005, Foster et al., 2007). The present understanding of the developmental regulation of the acellular cementum is poorly comprehended, which restricts efforts for regeneration. Work by Foster *et al* has identified that the *Alpl*$^{-/-}$ mice exhibit excess PP_i and concomitantly inhibited cementum formation (Foster et al., 2012). This results in root detachment, a phenomenon consistent with premature tooth loss in the human condition of hypophosphatasia (Bloch-Zupan, 2016). This group also analysed the global *Enpp1*$^{-/-}$ mouse, demonstrating decreased PP_i and increased cementum apposition and thickness compared to controls. However, the knowledge of cell-specific contributions to this mineralisation regulation

remains restricted. It would be of great interest to assess the dental phenotype of the osteoblast-specific *Enpp1* mice to aid in the identification of clinical targets for tooth loss. This could be initially conducted by completing a μ-CT analysis.

NPP1 is detectable in cementoblasts following acellular cementum formation, and at low levels around cellular cementum, and likely plays a crucial role in generating PP_i to regulate bio-mineralisation of the mandible (Zweifler et al., 2015). It has been shown that *Enpp1*$^{-/-}$ demonstrate a rapidly forming cementum, reflecting tooth development in a low PP_i environment (Nociti et al., 2002, Zweifler et al., 2015). However, the cell-specific roles of NPP1 in tooth mineralisation remain undetermined. Identifying this may aid in explaining differences in NPP1's precise function in cementogenesis. A deeper understanding of the role of NPP1 in this context will aid in providing insights into tooth root developments and identification of therapeutic interventions to promote cementum regeneration and functionality of teeth. This is particularly timely and relevant, giving the increasing body of evidence recognising that the acellular cementum is potently influenced by PP_i (and P_i) concentrations.

Although this project was able to provide a comprehensive analysis of the bone phenotype for the *Enpp1*$^{flox/flox}$*;Ocn*-cre mouse, there are various aspects which could be built upon to strengthen the data. Suggestions for additional research that could overcome these issues are suggested below.

The use of μ-CT has provided a useful resource to study the architecture of bone and assess the bone mineral density. However, as discussed in chapter 3, the analysis in this thesis focused on specific regions of the bone, at the distal portion of the femur and the proximal portion of the tibia. Although this allowed me to confirm a significant difference in bone mineral density between groups, this may not be reflective of bone mineral density alterations throughout the bone. Efforts were made to corroborate this data, by completing a histological assessment of juvenile bones using a Bioquant OSTEO software and determining osteoid width. However, these methods to visualise and asses the micro-architecture of bone are not well suited to studying events such as microdamage or assessing total tissue mineral density.

One suitable further technique to support the findings of increased bone mineral density would be the use of Raman spectroscopy, which has been used by several basic studies to evaluate bone quality and bone mineral density (Tarnowski et al., 2002, Chappard et al., 2011, Morris and Mandair, 2011, Fu et al., 2012). This technique involves the inelastic scattering of monochromatic laser light, providing vibrational information of chemical bonds and symmetry of molecules. This can be utilised to determine the components of bone and bone mineral. This data may have supported a hypermineralisation phenotype.

One underappreciated area in this thesis is the role of sexual dimorphism with regard to bone, and it's potential wider effects on systems biology in mice. In recent years, there is increasing evidence emerging to demonstrate complex and multiple levels of sexual divergence in bone. One example of this is that the regulation of the bone vascular network is sexually dimorphic. Here, Goring *et al* assessed the phenotype of mice conditional disruption of VEGF in osteocalcin-expressing cells (osteoblasts). This study demonstrate that VEGF, which is critical for bone growth and repair, and it's signaling exerts a divergent effect on bone properties from between sexes at multiple levels (morphological, cellular and whole bone level). This sophisticated phenotyping included detailed imaging methodology such as synchrotron computed tomography and scanning electron microscopy to reveal significant increases in unmineralized osteoid, enlarged blood vessel canals and increase osteocyte lacunae size in cortical bone of osteoblast-specific VEGF conditional male knockout mice, but not in female mice. Sexual differences in the skeleton are evident in puberty, adulthood and old age, whereby significant quantities of literature demonstrate the importance of sex steroids as key regulators of bone health and mechanical function. It is critical that future studies assess the contribution of sex steroids regarding bone phenotype in order to reveal underlying sex-specific genetic regulators of bone mineralisation. This thesis would likely have benefited from more in-depth assessment of sexual dimorphism regarding the bone phenotype. Given that male mice were selected for metabolic studies, the possibility to assess sexual dimorphism within different feeding conditions is not possible within this study, although also would be warranted. This may have offered greater insight into whether sex-specific changes of bone led to alterations in hormonal signaling (e.g. secreted osteocalcin levels) and cellular signaling (e.g. NPP1 activity), and whether this linked to functional outputs such as resistance to obesity and/or insulin resistance. This work is warranted in future mouse model investigations of bone and metabolic phenotype.

Seahorse metabolic analysis of primary osteoblasts isolated from the osteoblast-specific NPP1 ablated mouse revealed a reduced glycolytic function and capacity compared to controls. These data indicate that the osteoblast-specific NPP1 ablated mouse osteoblasts have compromised mitochondrial function. Recently, a transgenic mitochondrially localised 3XHA epitope tag (MITO-Tag) mouse has been developed (Bayraktar et al., 2019), which allows for rapid, cell-type-specific immune-isolation of mitochondria from tissues of interest. This would allow for the isolation of mitochondrial specifically from osteoblasts, and analysis of the mitochondrial behaviour and metabolite usage. This would permit a comprehensive study of mitochondrial physiology, and would greatly aid the understanding of the metabolic changes in osteoblasts. Such findings may help identify whether these changes are associated with alterations in metabolic demand due to increased mineralisation activity, which is observed in the osteoblast-specific NPP1 ablated mouse.

Furthermore, it would have been insightful to test potential explanatory mechanisms which exist *in vivo* buy using more easily available and rapid tools *in vitro*. For example, to robustly examine the cell signaling mechanisms resultant of osteoblast-specific NPP1 ablation, it would have been useful to utalise knock-down experiments. More quickly and easily available wild-type animals may have been used to isolate both primary osteoblasts from calvaria and primary osteoblasts from long bones (e.g. from the femur). Using specific silencing RNA's (shRNA), a specific knockdown of NPP1 activity in the cell type may be achieved. This could provide a large number of cells such that appropriate technical and biological replicate samples may be utilised, and such that genetic, protein, lipid and metabolite changes may be investigated. This would involve use of more sophisticated, and large dataset, methodology such as proteomics, metabolomics, lipidomics and microarray analysis. This could identify significantly altered downstream effects of NPP1 knockout, and would identify any potential confounding differences between osteoblasts isolated from the calvaria versus osteoblasts isolated from the long bones. Such work would undeniably have been insightful, but was unfortunately unattainable due to financial constraints at the time of study.

Given the changes observed in the concentrations of uncarboxylated-OCN in the *Enpp1*$^{flox/flox}$*;Ocn*-cre mice, it would be of great interest to generate an *Enpp1* and *Ocn* double knockout mouse. As the global *Enpp1*$^{-/-}$ mice present with significantly increased undercarboxylated-OCN and uncarboxylated OCN, insulin sensitivity and resistance to obesity following high-fat diet feeding, this work is imperative. The double knockout could be used to conduct metabolic analysis to

determine whether insulin sensitivity and metabolic protection is an OCN-dependent or OCN--independent mechanism. It would be interesting to extend this analysis, and generate an *Enpp1*$^{flox/flox}$*;Ocn*-cre mouse on an *Ocn* knockout background, to determine whether the differences in metabolic protection between the global and conditional NPP1 knockouts are truly due to the action of OCN.

One further metabolic analysis area of interest identified in this project involves the brown adipose tissue. The high-fat diet fed *Enpp1*$^{flox/flox}$*;Ocn*-cre mice presented with significantly increased brown adipose tissue mass compared to *Enpp1*$^{flox/flox}$ controls. This could suggest an increase in the number of brown fat mitochondria, and as such, the brown fat may contribute to metabolic change due to changes in non-shivering thermogenesis. The activation of brown fat, or so-called 'beiging' of white fat, is a hot topic of study and a potential mechanism for regulating obesity and insulin resistance. Despite the notable increase in BAT of 22% in the *Enpp1*$^{flox/flox}$*;Ocn*-cre mice, I did not observe differences in the expression of BAT enriched genes (*e.g. Ucp1* and *Ucp2*), suggesting that canonical thermogenesis through *Ucp1* is not a mechanism involved in the metabolic phenotype determined in this thesis. It would be interesting to conduct these experiments at conditions outside of the thermoneutrality window. Indeed, the experiments described within this thesis were conducted at standard ambient temperatures of 23°C. This is reported as a mild cold stress for mice. To test the BAT thermogenesis of these mice, they could be challenged with cold temperature to stimulate the *Ucp1,* by placing in a cold exposure (8°C for 98 hours, then to 4°C for up to 5 weeks). Subsequently, glucose tolerance and insulin tolerance testing, followed by necroscopy to assess body weight, fat and muscle mass could be conducted to assess metabolic phenotype. The analysis of BAT mitochondrial activity could also be assessed by targeted qPCR and western blot analysis for genes involved in BAT fat oxidation (*e.g. Ucp3, Cpt1b*). Furthermore, *in vitro* metabolic profiling of primary isolated brown adipocytes could be conducted using seahorse technology.

T2DM is a complicated disease with multiple aetiologies and progressively develops over several years. The identification and assessment of therapeutic agents or targeted interventions to delay progression from pre-diabetic to diabetic state, therefore, take many years and tremendous financial resource and effort to identify. It is critical to better understand the pathogenesis of T2DM by use of appropriate animal models. The mouse model provides a variety of genotypes

and susceptibilities to be studied, relatively quickly and with reduced expense compared to large animal counterparts (King, 2012, King and Bowe, 2016b). However, for a more translational study of animal to human, an appropriate animal model should mirror the pathophysiology and natural history of T2DM. Alternately, the animal model would be suitable if it develops complications of T2DM with an aetiology reflecting that of humans. One example of a suited animal model for T2DM is the feline model (Henson and O'Brien, 2006). Cats, particularly domestic cats, share the same environment as humans and are subject to physical inactivity and obesity (Henson and O'Brien, 2006). Cats have litters, which can facilitate the study of genetic linkage. Similarly, the natural lifespan of a cat, being less than primates and more than mice, allows a study of the onset, progression, treatment and prevention over a more achievable timeframe compared to monkeys or humans (Gurda et al., 2017). Additionally, feline diabetes mellitus typically occurs in middle age, associated with declining insulin secretion and loss of pancreatic β-cell mass, reflecting human disease (O'Brien et al., 1986, Henson and O'Brien, 2006). Furthermore, feline diabetes can be induced by partial (50%) pancreatectomy followed by the addition of dexamethasone and growth hormone (Hoenig et al., 2000, Henson and O'Brien, 2006). CRISPR-Cas9 is a third-generation engineered nuclease which is capable of causing double-strand DNA breaks, eliciting the non-homologous end-joining and homologous recombination repair systems (Sander and Joung, 2014). The utilisation of the CRISPR/Cas9 system to generate cell-specific NPP1 knockout in cats may allow for a greater comprehension of the relationship of NPP1 and T2DM within a pathophysiological context more similar to humans than other animal models (*e.g*. mice).

At present, it is recognised that there is no ideal animal model consistent with clinical presentation and pathology of human T2DM (Rees and Alcolado, 2005), although improvements to animal models are occurring. There is an unmet need to establish genetically modified miniature pig diabetes models to comprehensively study pathogenesis and prevention of T2DM and its downstream consequences. It is recognised that the miniature pig is a highly suitable candidate for investigating metabolic-related human disease (King, 2012). Notable features of the pig that make it a suitable research model include similar anatomy, physiology and biochemical metabolism to humans (Meurens et al., 2012, Roura et al., 2016). More specifically, pigs are omnivores, demonstrating similar dietary needs, nutritional balance and digestion compared to humans (Guilloteau et al., 2010). Indeed, pigs represent the animal model closest to humans (excluding non-primates) (Meurens et al., 2012). The development of an osteoblast-specific NPP1 knockout pig, followed by high-fat diet challenge and metabolic profiling would aid in

demonstrating the translational aspects of the work presented in this thesis. The utilisation of the pig model in this way would aid in bridging the gap between animal and human studies in the field of bone and metabolism.

The experiments suggested in this section would aid in demonstrating the complex and cell-specific contributions of NPP1 in the regulation of skeletal formation and energy metabolism. Uncovering the mechanisms through which NPP1 elicits its action in energy metabolism is likely to aid in the identification and development of novel therapeutic and intervention strategies against T2DM.

1993. The Effect of Intensive Treatment of Diabetes on the Development and Progression of Long-Term Complications in Insulin-Dependent Diabetes Mellitus. *New England Journal of Medicine,* 329**,** 977-986.

1998. Effect of intensive blood-glucose control with metformin on complications in overweight patients with type 2 diabetes (UKPDS 34). *The Lancet,* 352**,** 854-865.

ABATE, N., CARULLI, L., CABO-CHAN, A., JR., CHANDALIA, M., SNELL, P. G. & GRUNDY, S. M. 2003. Genetic Polymorphism PC-1 K121Q and Ethnic Susceptibility to Insulin Resistance. *The Journal of Clinical Endocrinology & Metabolism,* 88**,** 5927-5934.

ABU-AMER, Y., ROSS, F. P., SCHLESINGER, P., TONDRAVI, M. M. & TEITELBAUM, S. L. 1997. Substrate Recognition by Osteoclast Precursors Induces C-src/Microtubule Association. *The Journal of Cell Biology,* 137**,** 247.

ACHARYA, K. D., GAO, X., BLESS, E. P., CHEN, J. & TETEL, M. J. 2019a. Estradiol and high fat diet associate with changes in gut microbiota in female ob/ob mice. *Scientific Reports,* 9**,** 20192.

ACHARYA, K. D., GAO, X., BLESS, E. P., CHEN, J. & TETEL, M. J. 2019b. Estradiol modulates gut microbiota in female ob/ob mice fed a high fat diet. *bioRxiv***,** 612283.

ADDISON, W. N., AZARI, F., SORENSEN, E. S., KAARTINEN, M. T. & MCKEE, M. D. 2007. Pyrophosphate inhibits mineralization of osteoblast cultures by binding to mineral, up-regulating osteopontin, and inhibiting alkaline phosphatase activity. *J Biol Chem,* 282**,** 15872-83.

ADEBAYO, O. O., KO, F. C., WAN, P. T., GOLDRING, S. R., GOLDRING, M. B., WRIGHT, T. M. & VAN DER MEULEN, M. C. H. 2017. Role of subchondral bone properties and changes in development of load-induced osteoarthritis in mice. *Osteoarthritis Cartilage,* 25**,** 2108-2118.

AHIMA, R. S. & FLIER, J. S. 2000. Adipose Tissue as an Endocrine Organ. *Trends in Endocrinology & Metabolism,* 11**,** 327-332.

AKKIRAJU, H. & NOHE, A. 2015. Role of Chondrocytes in Cartilage Formation, Progression of Osteoarthritis and Cartilage Regeneration. *Journal of developmental biology,* 3**,** 177-192.

AKUNE, T., OHBA, S., KAMEKURA, S., YAMAGUCHI, M., CHUNG, U.-I., KUBOTA, N., TERAUCHI, Y., HARADA, Y., AZUMA, Y., NAKAMURA, K., KADOWAKI, T. & KAWAGUCHI, H. 2004. PPAR γ insufficiency enhances osteogenesis through osteoblast formation from bone marrow progenitors. *The Journal of Clinical Investigation,* 113**,** 846-855.

AL-GOBLAN, A. S., AL-ALFI, M. A. & KHAN, M. Z. 2014. Mechanism linking diabetes mellitus and obesity. *Diabetes, metabolic syndrome and obesity : targets and therapy,* 7**,** 587-591.

ALBRIGHT, R. A., STABACH, P., CAO, W., KAVANAGH, D., MULLEN, I., BRADDOCK, A. A., COVO, M. S., TEHAN, M., YANG, G., CHENG, Z., BOUCHARD, K., YU, Z.-X., THORN, S., WANG, X., FOLTA-STOGNIEW, E. J., NEGRETE, A., SINUSAS, A. J., SHILOACH, J., ZUBAL, G., MADRI, J. A., DE LA CRUZ, E. M. & BRADDOCK, D. T. 2015. ENPP1-Fc prevents mortality and vascular calcifications in rodent model of generalized arterial calcification of infancy. *Nature Communications,* 6**,** 10006.

ALI, S. Y. 1976. Analysis of matrix vesicles and their role in the calcification of epiphyseal cartilage. *Fed Proc,* 35**,** 135-42.

ALLEN, M. R. & BURR, D. B. 2014. Chapter 4 - Bone Modeling and Remodeling. *In:* BURR, D. B. & ALLEN, M. R. (eds.) *Basic and Applied Bone Biology.* San Diego: Academic Press.

ALQUIER, T. & POITOUT, V. 2018. Considerations and guidelines for mouse metabolic phenotyping in diabetes research. *Diabetologia,* 61**,** 526-538.

ALTAF, F. M., HERING, T. M., KAZMI, N. H., YOO, J. U. & JOHNSTONE, B. 2006. Ascorbate-enhanced chondrogenesis of ATDC5 cells. *Eur Cell Mater,* 12**,** 64-9; discussion 69-70.

AMBROSI, T. H., SCIALDONE, A., GRAJA, A., GOHLKE, S., JANK, A. M., BOCIAN, C., WOELK, L., FAN, H., LOGAN, D. W., SCHURMANN, A., SARAIVA, L. R. & SCHULZ, T. J. 2017. Adipocyte Accumulation in the Bone Marrow during Obesity and Aging Impairs Stem Cell-Based Hematopoietic and Bone Regeneration. *Cell Stem Cell,* 20**,** 771-784.e6.

ANDERSON, H. C. 1967. ELECTRON MICROSCOPIC STUDIES OF INDUCED CARTILAGE DEVELOPMENT AND CALCIFICATION. *The Journal of Cell Biology,* 35**,** 81.

ANDERSON, H. C. 1969. Vesicles associated with calcification in the matrix of epiphyseal cartilage. *J Cell Biol,* 41**,** 59-72.

ANDERSON, H. C. 1984. Mineralization by matrix vesicles. *Scan Electron Microsc***,** 953-64.

ANDERSON, H. C. 1995. Molecular biology of matrix vesicles. *Clin Orthop Relat Res***,** 266-80.

ANDERSON, H. C., GARIMELLA, R. & TAGUE, S. E. 2005a. The role of matrix vesicles in growth plate development and biomineralization. *Front Biosci,* 10**,** 822-37.

ANDERSON, H. C., HARMEY, D., CAMACHO, N. P., GARIMELLA, R., SIPE, J. B., TAGUE, S., BI, X., JOHNSON, K., TERKELTAUB, R. & MILLAN, J. L. 2005b. Sustained osteomalacia of long bones despite major improvement in other hypophosphatasia-related mineral deficits in tissue nonspecific alkaline phosphatase/nucleotide pyrophosphatase phosphodiesterase 1 double-deficient mice. *Am J Pathol,* 166**,** 1711-20.

ANDERSON, H. C., SIPE, J. B., HESSLE, L., DHANYAMRAJU, R., ATTI, E., CAMACHO, N. P., MILLAN, J. L. & DHAMYAMRAJU, R. 2004. Impaired calcification around matrix vesicles of growth plate and bone in alkaline phosphatase-deficient mice. *Am J Pathol,* 164**,** 841-7.

ANDOH, K., JIN-HUA, P., TERASHIMA, K., NAKAMURA, H. & SANO, K. 1999. Genomic structure and promoter analysis of the ecto-phosphodiesterase I gene (PDNP3) expressed in glial cells1Sequence data from this article have been deposited with the GSDB, DDBJ, EMBL, and NCBI Data Libraries under accession no. AF119714.1. *Biochimica et Biophysica Acta (BBA) - Gene Structure and Expression,* 1446**,** 213-224.

ANON 2001. Osteoporosis prevention, diagnosis, and therapy. *Jama,* 285**,** 785-95.

ARKILL, K. P. & WINLOVE, C. P. 2008. Solute transport in the deep and calcified zones of articular cartilage. *Osteoarthritis Cartilage,* 16**,** 708-14.

ASHCROFT, F. M. & RORSMAN, P. 2012. Diabetes mellitus and the beta cell: the last ten years. *Cell,* 148**,** 1160-71.

ASSALI, A. R., GANOR, A., BEIGEL, Y., SHAFER, Z., HERSHCOVICI, T. & FAINARU, M. 2001. Insulin resistance in obesity: body-weight or energy balance? *J Endocrinol,* 171**,** 293-8.

AUGAT, P. & SCHORLEMMER, S. 2006. The role of cortical bone and its microstructure in bone strength. *Age Ageing,* 35 Suppl 2**,** ii27-ii31.

AYALA, J. E., SAMUEL, V. T., MORTON, G. J., OBICI, S., CRONIGER, C. M., SHULMAN, G. I., WASSERMAN, D. H., MCGUINNESS, O. P. & CONSORTIUM, N. I. H. M. M. P. C. 2010. Standard operating procedures for describing and performing metabolic tests of glucose homeostasis in mice. *Disease models & mechanisms,* 3**,** 525-534.

BABIJ, P., ROUDIER, M., GRAVES, T., HAN, C.-Y. E., CHHOA, M., LI, C.-M., JUAN, T., MORONY, S., GRISANTI, M., LI, X., YU, L., DWYER, D., LLOYD, D. J., BASS, M. B., RICHARDS, W. G., EBELING, C., AMATO, J. & CARLSON, G. 2009. New Variants in the Enpp1 and Ptpn6 Genes Cause Low BMD, Crystal-Related Arthropathy, and Vascular Calcification. *Journal of Bone and Mineral Research,* 24**,** 1552-1564.

BACCI, S., DE COSMO, S., PRUDENTE, S. & TRISCHITTA, V. 2007. ENPP1 gene, insulin resistance and related clinical outcomes. *Curr Opin Clin Nutr Metab Care,* 10**,** 403-9.

BACHNER, D., AHRENS, M., BETAT, N., SCHRODER, D. & GROSS, G. 1999. Developmental expression analysis of murine autotaxin (ATX). *Mech Dev,* 84**,** 121-5.

BAILEY, C. J. 2008. Metformin: effects on micro and macrovascular complications in type 2 diabetes. *Cardiovasc Drugs Ther,* 22**,** 215-24.

BAILEY, C. J. & TURNER, R. C. 1996. Metformin. *New England Journal of Medicine,* 334**,** 574-579.

BALLOCK, R. T. & O'KEEFE, R. J. 2003. Physiology and pathophysiology of the growth plate. *Birth Defects Res C Embryo Today,* 69**,** 123-43.

BANAKH, I., SALI, A., DUBLJEVIC, V., GROBBEN, B., SLEGERS, H. & GODING, J. W. 2002. Structural basis of allotypes of ecto-nucleotide pyrophosphatase/phosphodiesterase (plasma cell membrane glycoprotein PC-1) in the mouse and rat, and analysis of allele-specific xenogeneic antibodies. *Eur J Immunogenet,* 29**,** 307-13.

BAR-SHAVIT, Z. 2007. The osteoclast: a multinucleated, hematopoietic-origin, bone-resorbing osteoimmune cell. *J Cell Biochem,* 102**,** 1130-9.

BARADARAN, A. 2012. Lipoprotein(a), type 2 diabetes and nephropathy; the mystery continues. *J Nephropathol,* 1**,** 126-9.

BARBER, G. N. 2014. STING-dependent cytosolic DNA sensing pathways. *Trends Immunol,* 35**,** 88-93.

BARRAGAN-ADJEMIAN, C., NICOLELLA, D., DUSEVICH, V., DALLAS, M. R., EICK, J. D. & BONEWALD, L. F. 2006. Mechanism by which MLO-A5 late osteoblasts/early osteocytes mineralize in culture: similarities with mineralization of lamellar bone. *Calcified tissue international,* 79**,** 340-353.

BASHIRI, A., TAVALLAEE, G., LI, L. & NG, D. S. 2013. Emerging role of cellular cholesterol in the pathogenesis of nonalcoholic fatty liver disease. *Current Opinion in Lipidology,* 24**,** 275-276.

BASILLAIS, A., BENSAMOUN, S., CHAPPARD, C., BRUNET-IMBAULT, B., LEMINEUR, G., ILHARREBORDE, B., HO BA THO, M. C. & BENHAMOU, C. L. 2007. Three-dimensional characterization of cortical bone microstructure by microcomputed tomography: validation with ultrasonic and microscopic measurements. *J Orthop Sci,* 12**,** 141-8.

BAYRAKTAR, E. C., BAUDRIER, L., ÖZERDEM, C., LEWIS, C. A., CHAN, S. H., KUNCHOK, T., ABU-REMAILEH, M., CANGELOSI, A. L., SABATINI, D. M., BIRSOY, K. & CHEN, W. W. 2019. MITO-Tag Mice enable rapid isolation and multimodal profiling of mitochondria from specific cell types in vivo. *Proceedings of the National Academy of Sciences,* 116**,** 303.

BAYRAKTAR, H. H., MORGAN, E. F., NIEBUR, G. L., MORRIS, G. E., WONG, E. K. & KEAVENY, T. M. 2004. Comparison of the elastic and yield properties of human femoral trabecular and cortical bone tissue. *Journal of Biomechanics,* 37**,** 27-35.

BECK, G. R., JR., ZERLER, B. & MORAN, E. 2000. Phosphate is a specific signal for induction of osteopontin gene expression. *Proc Natl Acad Sci U S A,* 97**,** 8352-7.

BECK, L., LEROY, C., BECK-CORMIER, S., FORAND, A., SALAUN, C., PARIS, N., BERNIER, A., URENA-TORRES, P., PRIE, D., OLLERO, M., COULOMBEL, L. & FRIEDLANDER, G. 2010. The phosphate transporter PiT1 (Slc20a1) revealed as a new essential gene for mouse liver development. *PLoS One,* 5**,** e9148.

BEERTSEN, W., VANDENBOS, T. & EVERTS, V. 1999. Root development in mice lacking functional tissue non-specific alkaline phosphatase gene: inhibition of acellular cementum formation. *J Dent Res,* 78**,** 1221-9.

BELKINA, A. C. & DENIS, G. V. 2010. Obesity genes and insulin resistance. *Curr Opin Endocrinol Diabetes Obes,* 17**,** 472-7.

BELLI, S. I., VAN DRIEL, I. R. & GODING, J. W. 1993. Identification and characterization of a soluble form of the plasma cell membrane glycoprotein PC-1 (5'-nucleotide phosphodiesterase). *Eur J Biochem,* 217**,** 421-8.

BHATTI, J. S., BHATTI, G. K., MASTANA, S. S., RALHAN, S., JOSHI, A. & TEWARI, R. 2010. ENPP1/PC-1 K121Q polymorphism and genetic susceptibility to type 2 diabetes in North Indians. *Molecular and Cellular Biochemistry,* 345**,** 249-257.

BIGELOW, C. L. & TAVASSOLI, M. 1984. Studies on conversion of yellow marrow to red marrow by using ectopic bone marrow implants. *Experimental hematology,* 12**,** 581-585.

BISHOP, N. 2015. Clinical management of hypophosphatasia. *Clinical cases in mineral and bone metabolism : the official journal of the Italian Society of Osteoporosis, Mineral Metabolism, and Skeletal Diseases,* 12**,** 170-173.

BLAIR, H. C., TEITELBAUM, S. L., GHISELLI, R. & GLUCK, S. 1989. Osteoclastic bone resorption by a polarized vacuolar proton pump. *Science,* 245**,** 855.

BLOCH-ZUPAN, A. 2016. Hypophosphatasia: diagnosis and clinical signs – a dental surgeon perspective. *International Journal of Paediatric Dentistry,* 26**,** 426-438.

BOERSMA, B., OTTEN, B. J., STOELINGA, G. B. & WIT, J. M. 1996. Catch-up growth after prolonged hypothyroidism. *Eur J Pediatr,* 155**,** 362-7.

BOHME, K., CONSCIENCE-EGLI, M., TSCHAN, T., WINTERHALTER, K. H. & BRUCKNER, P. 1992. Induction of proliferation or hypertrophy of chondrocytes in serum-free culture: the role of insulin-like growth factor-I, insulin, or thyroxine. *J Cell Biol,* 116**,** 1035-42.

BOLLEN, M., GIJSBERS, R., CEULEMANS, H., STALMANS, W. & STEFAN, C. 2000. Nucleotide pyrophosphatases/phosphodiesterases on the move. *Crit Rev Biochem Mol Biol,* 35**,** 393-432.

BONET, M. L., OLIVER, P. & PALOU, A. 2013. Pharmacological and nutritional agents promoting browning of white adipose tissue. *Biochimica et Biophysica Acta (BBA) - Molecular and Cell Biology of Lipids,* 1831**,** 969-985.

BONEWALD, L. F. 2011. The amazing osteocyte. *J Bone Miner Res,* 26**,** 229-38.

BONNET, N., BOURGOIN, L., BIVER, E., DOUNI, E. & FERRARI, S. 2019. RANKL inhibition improves muscle strength and insulin sensitivity and restores bone mass. *J Clin Invest,* 129**,** 3214-3223.

BONUCCI, E. 1967. Fine structure of early cartilage calcification. *Journal of Ultrastructure Research,* 20**,** 33-50.

BOOTH, S. L., CENTI, A., SMITH, S. R. & GUNDBERG, C. 2013. The role of osteocalcin in human glucose metabolism: marker or mediator? *Nature reviews. Endocrinology,* 9**,** 43-55.

BORISOV, B. K. & MAREI, A. N. 1974. Weight parameters of adult human skeleton. *Health Phys,* 27**,** 224-9.

BORLE, A. B., NICHOLS, N. & NICHOLS, G., JR. 1960. Metabolic studies of bone in vitro. I. Normal bone. *J Biol Chem,* 235**,** 1206-10.

BOSSHARDT, D. D. 2005. Are cementoblasts a subpopulation of osteoblasts or a unique phenotype? *J Dent Res,* 84**,** 390-406.

BOTOLIN, S. & MCCABE, L. R. 2007. Bone Loss and Increased Bone Adiposity in Spontaneous and Pharmacologically Induced Diabetic Mice. *Endocrinology,* 148**,** 198-205.

BOUILLON, R., CARMELIET, G., VERLINDEN, L., VAN ETTEN, E., VERSTUYF, A., LUDERER, H. F., LIEBEN, L., MATHIEU, C. & DEMAY, M. 2008. Vitamin D and human health: lessons from vitamin D receptor null mice. *Endocr Rev,* 29**,** 726-76.

BOURGINE, A., BECK, L., BECK-CORMIER, S., COUASNAY, G., PERRÉ, M., MASSON, M., KHOSHNIAT, S., WEISS, P. & GUICHEUX, J. 2011. Involvement of PiT1 and PiT2 in the response to phosphate in osteoblasts in vitro. *Bone,* 48**,** S106-S107.

BOYAN, B. D., SCHWARTZ, Z., SWAIN, L. D. & KHARE, A. 1989. Role of lipids in calcification of cartilage. *Anat Rec,* 224**,** 211-9.

BREDELLA, M. A., GILL, C. M., KEATING, L. K., TORRIANI, M., ANDERSON, E. J., PUNYANITYA, M., WILSON, K. E., KELLY, T. L. & MILLER, K. K. 2013. Assessment of Abdominal Fat Compartments Using DXA in Premenopausal Women From Anorexia Nervosa to Morbid Obesity. *Obesity,* 21**,** 2458-2464.

BREDELLA, M. A., TORRIANI, M., GHOMI, R. H., THOMAS, B. J., BRICK, D. J., GERWECK, A. V., ROSEN, C. J., KLIBANSKI, A. & MILLER, K. K. 2011. Vertebral Bone Marrow Fat Is Positively

Associated With Visceral Fat and Inversely Associated With IGF-1 in Obese Women. *Obesity,* 19**,** 49-53.

BRONCKERS, A. L., FARACH-CARSON, M. C., VAN WAVEREN, E. & BUTLER, W. T. 1994. Immunolocalization of osteopontin, osteocalcin, and dentin sialoprotein during dental root formation and early cementogenesis in the rat. *J Bone Miner Res,* 9**,** 833-41.

BRONCKERS, A. L., GAY, S., DIMUZIO, M. T. & BUTLER, W. T. 1985. Immunolocalization of gamma-carboxyglutamic acid containing proteins in developing rat bones. *Coll Relat Res,* 5**,** 273-81.

BRONCKERS, A. L., PRICE, P. A., SCHRIJVERS, A., BERVOETS, T. J. & KARSENTY, G. 1998. Studies of osteocalcin function in dentin formation in rodent teeth. *Eur J Oral Sci,* 106**,** 795-807.

BROWN, E. M. 1982. PTH secretion in vivo and in vitro. Regulation by calcium and other secretagogues. *Miner Electrolyte Metab,* 8**,** 130-50.

BROWN, E. M. & HEBERT, S. C. 1997. Calcium-receptor-regulated parathyroid and renal function. *Bone,* 20**,** 303-9.

BRUNO, G., RUNZO, C., CAVALLO-PERIN, P., MERLETTI, F., RIVETTI, M., PINACH, S., NOVELLI, G., TROVATI, M., CERUTTI, F. & PAGANO, G. 2005. Incidence of Type 1 and Type 2 Diabetes in Adults Aged 30–49 Years. *Diabetes Care,* 28**,** 2613.

BRYZGALOVA, G., GAO, H., AHREN, B., ZIERATH, J. R., GALUSKA, D., STEILER, T. L., DAHLMAN-WRIGHT, K., NILSSON, S., GUSTAFSSON, J. A., EFENDIC, S. & KHAN, A. 2006. Evidence that oestrogen receptor-alpha plays an important role in the regulation of glucose homeostasis in mice: insulin sensitivity in the liver. *Diabetologia,* 49**,** 588-97.

BÜHRING, H.-J., SEIFFERT, M., GIESERT, C., MARXER, A., KANZ, L., VALENT, P. & SANO, K. 2001. The basophil activation marker defined by antibody 97A6 is identical to the ectonucleotide pyrophosphatase/phosphodiesterase 3. *Blood,* 97**,** 3303.

BUHRING, H. J., SIMMONS, P. J., PUDNEY, M., MULLER, R., JARROSSAY, D., VAN AGTHOVEN, A., WILLHEIM, M., BRUGGER, W., VALENT, P. & KANZ, L. 1999. The monoclonal antibody 97A6 defines a novel surface antigen expressed on human basophils and their multipotent and unipotent progenitors. *Blood,* 94**,** 2343-56.

BUHRING, H. J., STREBLE, A. & VALENT, P. 2004. The basophil-specific ectoenzyme E-NPP3 (CD203c) as a marker for cell activation and allergy diagnosis. *Int Arch Allergy Immunol,* 133**,** 317-29.

BURGER, E. H., BOONEKAMP, P. M. & NIJWEIDE, P. J. 1986. Osteoblast and osteoclast precursors in primary cultures of calvarial bone cells. *The Anatomical Record,* 214**,** 32-40.

BURGER, E. H. & KLEIN-NULEND, J. 1999. Mechanotransduction in bone--role of the lacuno-canalicular network. *Faseb j,* 13 Suppl**,** S101-12.

BURR, D. B. 2002. Targeted and nontargeted remodeling. *Bone,* 30**,** 2-4.

BUTLER, A. E., JANSON, J., BONNER-WEIR, S., RITZEL, R., RIZZA, R. A. & BUTLER, P. C. 2003. Beta-cell deficit and increased beta-cell apoptosis in humans with type 2 diabetes. *Diabetes,* 52**,** 102-10.

CAETANO-LOPES, J., CANHAO, H. & FONSECA, J. E. 2007. Osteoblasts and bone formation. *Acta Reumatol Port,* 32**,** 103-10.

CAMP, C. L., STUART, M. J. & KRYCH, A. J. 2014. Current concepts of articular cartilage restoration techniques in the knee. *Sports health,* 6**,** 265-273.

CANCELA, L., HSIEH, C. L., FRANCKE, U. & PRICE, P. A. 1990. Molecular structure, chromosome assignment, and promoter organization of the human matrix Gla protein gene. *J Biol Chem,* 265**,** 15040-8.

CANNON, B. & NEDERGAARD, J. 1985. The biochemistry of an inefficient tissue: brown adipose tissue. *Essays Biochem,* 20**,** 110-64.

CANNON, B. & NEDERGAARD, J. 2010. Metabolic consequences of the presence or absence of the thermogenic capacity of brown adipose tissue in mice (and probably in humans). *Int J Obes (Lond),* 34 Suppl 1**,** S7-16.

CAO, J. J., SUN, L. & GAO, H. 2010. Diet-induced obesity alters bone remodeling leading to decreased femoral trabecular bone mass in mice. *Ann N Y Acad Sci,* 1192**,** 292-7.

CAPLAN, A. I. 1991. Mesenchymal stem cells. *J Orthop Res,* 9**,** 641-50.

CARDOSO, L., FRITTON, S. P., GAILANI, G., BENALLA, M. & COWIN, S. C. 2013. Advances in assessment of bone porosity, permeability and interstitial fluid flow. *Journal of Biomechanics,* 46**,** 253-265.

CARPENTIER, A. C., BLONDIN, D. P., VIRTANEN, K. A., RICHARD, D., HAMAN, F. & TURCOTTE, É. E. 2018. Brown Adipose Tissue Energy Metabolism in Humans. *Frontiers in Endocrinology,* 9.

CASES, S., SMITH, S. J., ZHENG, Y. W., MYERS, H. M., LEAR, S. R., SANDE, E., NOVAK, S., COLLINS, C., WELCH, C. B., LUSIS, A. J., ERICKSON, S. K. & FARESE, R. V., JR. 1998. Identification of a gene encoding an acyl CoA:diacylglycerol acyltransferase, a key enzyme in triacylglycerol synthesis. *Proc Natl Acad Sci U S A,* 95**,** 13018-23.

CASWELL, A. M. & RUSSELL, R. G. 1988. Evidence that ecto-nucleoside-triphosphate pyrophosphatase serves in the generation of extracellular inorganic pyrophosphate in human bone and articular cartilage. *Biochim Biophys Acta,* 966**,** 310-7.

CAWTHORN, WILLIAM P., SCHELLER, ERICA L., LEARMAN, BRIAN S., PARLEE, SEBASTIAN D., SIMON, BECKY R., MORI, H., NING, X., BREE, ADAM J., SCHELL, B., BROOME, DAVID T., SOLIMAN, SANDRA S., DELPROPOSTO, JENIFER L., LUMENG, CAREY N., MITRA, A., PANDIT, SANDEEP V., GALLAGHER, KATHERINE A., MILLER, JOSHUA D., KRISHNAN, V., HUI, SUSANTA K., BREDELLA, MIRIAM A., FAZELI, POUNEH K., KLIBANSKI, A., HOROWITZ, MARK C., ROSEN, CLIFFORD J. & MACDOUGALD, ORMOND A. 2014. Bone Marrow Adipose Tissue Is an Endocrine Organ that Contributes to Increased Circulating Adiponectin during Caloric Restriction. *Cell Metabolism,* 20**,** 368-375.

CEFALU, W. T. 2001. Insulin resistance: cellular and clinical concepts. *Exp Biol Med (Maywood),* 226**,** 13-26.

CERF, M. E. 2013. Beta cell dysfunction and insulin resistance. *Frontiers in endocrinology,* 4**,** 37-37.

CHAN, J. C. N., MALIK, V., JIA, W., KADOWAKI, T., YAJNIK, C. S., YOON, K.-H. & HU, F. B. 2009. Diabetes in Asia: Epidemiology, Risk Factors, and Pathophysiology. *JAMA,* 301**,** 2129-2140.

CHANDE, S., HO, B., FETENE, J. & BERGWITZ, C. 2019. Transgenic mouse model for conditional expression of influenza hemagglutinin-tagged human SLC20A1/PIT1. *PLoS One,* 14**,** e0223052.

CHAPPARD, D., BASLE, M. F., LEGRAND, E. & AUDRAN, M. 2011. New laboratory tools in the assessment of bone quality. *Osteoporos Int,* 22**,** 2225-40.

CHAPURLAT, R. D. & CONFAVREUX, C. B. 2016. Novel biological markers of bone: from bone metabolism to bone physiology. *Rheumatology,* 55**,** 1714-1725.

CHARLES, J. F. & ALIPRANTIS, A. O. 2014. Osteoclasts: more than 'bone eaters'. *Trends Mol Med,* 20**,** 449-59.

CHENG, Y., WU, J., HERTERVIG, E., LINDGREN, S., DUAN, D., NILSSON, A. & DUAN, R. D. 2007. Identification of aberrant forms of alkaline sphingomyelinase (NPP7) associated with human liver tumorigenesis. *British journal of cancer,* 97**,** 1441-1448.

CHENTOUFI, J., HOTT, M., LAMBLIN, D., BUC-CARON, M. H., MARIE, P. J. & KELLERMANN, O. 1993. Kinetics of in vitro mineralization by an osteogenic clonal cell line (C1) derived from mouse teratocarcinoma. *Differentiation,* 53**,** 181-9.

CHIN, K.-Y., IMA-NIRWANA, S., MOHAMED, I. N., AHMAD, F., RAMLI, E. S. M., AMINUDDIN, A. & NGAH, W. Z. W. 2014. Serum osteocalcin is significantly related to indices of obesity and lipid profile in Malaysian men. *International journal of medical sciences,* 11**,** 151-157.

CHITRAJU, C., MEJHERT, N., HAAS, J. T., DIAZ-RAMIREZ, L. G., GRUETER, C. A., IMBRIGLIO, J. E., PINTO, S., KOLIWAD, S. K., WALTHER, T. C. & FARESE, R. V., JR. 2017. Triglyceride Synthesis by DGAT1 Protects Adipocytes from Lipid-Induced ER Stress during Lipolysis. *Cell metabolism,* 26**,** 407-418.e3.

CHOI, B.-W., SONG, K.-J. & CHANG, H. 2011. Ossification of the posterior longitudinal ligament: a review of literature. *Asian spine journal,* 5**,** 267-276.

CHONDRONIKOLA, M., VOLPI, E., BØRSHEIM, E., PORTER, C., ANNAMALAI, P., ENERBÄCK, S., LIDELL, M. E., SARAF, M. K., LABBE, S. M., HURREN, N. M., YFANTI, C., CHAO, T., ANDERSEN, C. R., CESANI, F., HAWKINS, H. & SIDOSSIS, L. S. 2014. Brown Adipose Tissue Improves Whole-Body Glucose Homeostasis and Insulin Sensitivity in Humans. *Diabetes,* 63**,** 4089.

CHUNG, C. H., GOLUB, E. E., FORBES, E., TOKUOKA, T. & SHAPIRO, I. M. 1992. Mechanism of action of beta-glycerophosphate on bone cell mineralization. *Calcif Tissue Int,* 51**,** 305-11.

CLAPPER, J. R., HENDRICKS, M. D., GU, G., WITTMER, C., DOLMAN, C. S., HERICH, J., ATHANACIO, J., VILLESCAZ, C., GHOSH, S. S., HEILIG, J. S., LOWE, C. & ROTH, J. D. 2013. Diet-induced mouse model of fatty liver disease and nonalcoholic steatohepatitis reflecting clinical disease progression and methods of assessment. *Am J Physiol Gastrointest Liver Physiol,* 305**,** G483-95.

CLARKE, B. 2008. Normal bone anatomy and physiology. *Clin J Am Soc Nephrol,* 3 Suppl 3**,** S131-9.

CLARKIN, C. E., EMERY, R. J., PITSILLIDES, A. A. & WHEELER-JONES, C. P. D. 2008. Evaluation of VEGF-mediated signaling in primary human cells reveals a paracrine action for VEGF in osteoblast-mediated crosstalk to endothelial cells. *Journal of Cellular Physiology,* 214**,** 537-544.

CLEMENS, T. L. & KARSENTY, G. 2011. The osteoblast: An insulin target cell controlling glucose homeostasis. *Journal of Bone and Mineral Research,* 26**,** 677-680.

CLEMENTS, R. S., JR. & REYNERTSON, R. 1977. Myoinositol metabolism in diabetes mellitus. Effect of insulin treatment. *Diabetes,* 26**,** 215-21.

COHN, D. V. & FORSCHER, B. K. 1962. Aerobic metabolism of glucose by bone. *J Biol Chem,* 237**,** 615-8.

COLLET, C., SCHILTZ, C., GEOFFROY, V., MAROTEAUX, L., LAUNAY, J. M. & DE VERNEJOUL, M. C. 2007. The serotonin 5-HT2B receptor controls bone mass via osteoblast recruitment and proliferation. *The FASEB Journal,* 22**,** 418-427.

COLLINS, M. T. & BOEHM, M. 2011. It ANKH Necessarily So. *The Journal of Clinical Endocrinology & Metabolism,* 96**,** 72-74.

COLNOT, C., LU, C., HU, D. & HELMS, J. A. 2004. Distinguishing the contributions of the perichondrium, cartilage, and vascular endothelium to skeletal development. *Developmental Biology,* 269**,** 55-69.

COPP, D. H. & SHIM, S. S. 1963. The homeostatic function of bone as a mineral reservoir. *Oral Surg Oral Med Oral Pathol,* 16**,** 738-44.

COWIN, S. C. 1984. Mechanical modeling of the stress adaptation process in bone. *Calcif Tissue Int,* 36 Suppl 1**,** S98-103.

COWIN, S. C., MOSS-SALENTIJN, L. & MOSS, M. L. 1991. Candidates for the mechanosensory system in bone. *J Biomech Eng,* 113**,** 191-7.

CROCKETT, J. C., ROGERS, M. J., COXON, F. P., HOCKING, L. J. & HELFRICH, M. H. 2011. Bone remodelling at a glance. *Journal of Cell Science,* 124**,** 991.

CUI, L., HOUSTON, D. A., FARQUHARSON, C. & MACRAE, V. E. 2016. Characterisation of matrix vesicles in skeletal and soft tissue mineralisation. *Bone,* 87**,** 147-58.

CUP, Q., WANG, G.-J. & BALIAN, G. 2000. Pluripotential Marrow Cells Produce Adipocytes when Transplanted into Steroid-Treated Mice. *Connective Tissue Research,* 41**,** 45-56.

CYPESS, A. M. & KAHN, C. R. 2010. Brown fat as a therapy for obesity and diabetes. *Curr Opin Endocrinol Diabetes Obes,* 17**,** 143-9.

CYPESS, A. M., LEHMAN, S., WILLIAMS, G., TAL, I., RODMAN, D., GOLDFINE, A. B., KUO, F. C., PALMER, E. L., TSENG, Y.-H., DORIA, A., KOLODNY, G. M. & KAHN, C. R. 2009. Identification and importance of brown adipose tissue in adult humans. *The New England journal of medicine,* 360**,** 1509-1517.

DALLAS, S. L., PRIDEAUX, M. & BONEWALD, L. F. 2013. The osteocyte: an endocrine cell ... and more. *Endocr Rev,* 34**,** 658-90.

DATTA, N. S. & ABOU-SAMRA, A. B. 2009. PTH and PTHrP signaling in osteoblasts. *Cell Signal,* 21**,** 1245-54.

DAYEH, T., TUOMI, T., ALMGREN, P., PERFILYEV, A., JANSSON, P. A., DE MELLO, V. D., PIHLAJAMAKI, J., VAAG, A., GROOP, L., NILSSON, E. & LING, C. 2016. DNA methylation of loci within ABCG1 and PHOSPHO1 in blood DNA is associated with future type 2 diabetes risk. *Epigenetics,* 11**,** 482-8.

DEFRONZO, R. A. & BECKLES, A. D. 1979. Glucose intolerance following chronic metabolic acidosis in man. *American Journal of Physiology-Endocrinology and Metabolism,* 236**,** E328.

DEFRONZO, R. A. & FERRANNINI, E. 1991. Insulin Resistance: A Multifaceted Syndrome Responsible for NIDDM, Obesity, Hypertension, Dyslipidemia, and Atherosclerotic Cardiovascular Disease. *Diabetes Care,* 14**,** 173.

DEISSLER, H., LOTTSPEICH, F. & RAJEWSKY, M. F. 1995. Affinity purification and cDNA cloning of rat neural differentiation and tumor cell surface antigen gp130RB13-6 reveals relationship to human and murine PC-1. *J Biol Chem,* 270**,** 9849-55.

DEL GUERRA, S., LUPI, R., MARSELLI, L., MASINI, M., BUGLIANI, M., SBRANA, S., TORRI, S., POLLERA, M., BOGGI, U., MOSCA, F., DEL PRATO, S. & MARCHETTI, P. 2005. Functional and Molecular Defects of Pancreatic Islets in Human Type 2 Diabetes. *Diabetes,* 54**,** 727.

DELEZIE, J. & HANDSCHIN, C. 2018. Endocrine Crosstalk Between Skeletal Muscle and the Brain. *Frontiers in neurology,* 9**,** 698-698.

DENG, D. & YAN, N. 2016. GLUT, SGLT, and SWEET: Structural and mechanistic investigations of the glucose transporters. *Protein Sci,* 25**,** 546-58.

DESMARCHELIER, C., DAHLHOFF, C., KELLER, S., SAILER, M., JAHREIS, G. & DANIEL, H. 2012. C57Bl/6 N mice on a western diet display reduced intestinal and hepatic cholesterol levels despite a plasma hypercholesterolemia. *BMC genomics,* 13**,** 84-84.

DESPRÉS, J.-P. & LEMIEUX, I. 2006. Abdominal obesity and metabolic syndrome. *Nature,* 444**,** 881-887.

DESPRES, J. P. 2006. Is visceral obesity the cause of the metabolic syndrome? *Ann Med,* 38**,** 52-63.

DEVLIN, M. J., CLOUTIER, A. M., THOMAS, N. A., PANUS, D. A., LOTINUN, S., PINZ, I., BARON, R., ROSEN, C. J. & BOUXSEIN, M. L. 2010. Caloric restriction leads to high marrow adiposity and low bone mass in growing mice. *Journal of Bone and Mineral Research,* 25**,** 2078-2088.

DI PAOLA, R., CAPORARELLO, N., MARUCCI, A., DIMATTEO, C., IADICICCO, C., DEL GUERRA, S., PRUDENTE, S., SUDANO, D., MIELE, C., PARRINO, C., PIRO, S., BEGUINOT, F., MARCHETTI, P., TRISCHITTA, V. & FRITTITTA, L. 2011. ENPP1 affects insulin action and secretion: evidences from in vitro studies. *PLoS One,* 6**,** e19462.

DIAZ-HERNANDEZ, M., HERNANDEZ, F., MIRAS-PORTUGAL, M. T. & AVILA, J. 2015. TNAP Plays a Key Role in Neural Differentiation as well as in Neurodegenerative Disorders. *Subcell Biochem,* 76**,** 375-85.

DIEKWISCH, T. G. 2001. The developmental biology of cementum. *Int J Dev Biol,* 45**,** 695-706.

DIGIROLAMO, D. J., CLEMENS, T. L. & KOUSTENI, S. 2012. The skeleton as an endocrine organ. *Nat Rev Rheumatol,* 8**,** 674-83.

DILLON, S., STAINES, K. A., MILLÁN, J. L. & FARQUHARSON, C. 2019. How To Build a Bone: PHOSPHO1, Biomineralization, and Beyond. *JBMR Plus,* 3**,** e10202.

DING, M. 2010. Microarchitectural adaptations in aging and osteoarthrotic subchondral bone issues. *Acta Orthop Suppl,* 81**,** 1-53.

DION, N., FORTIN, A. & STE-MARIE, L.-G. 2011. Methods in Bone Histomorphometry for Animal Models.

DONG, H., MADDUX, B. A., ALTOMONTE, J., MESECK, M., ACCILI, D., TERKELTAUB, R., JOHNSON, K., YOUNGREN, J. F. & GOLDFINE, I. D. 2005. Increased Hepatic Levels of the Insulin Receptor Inhibitor, PC-1/NPP1, Induce Insulin Resistance and Glucose Intolerance. *Diabetes,* 54**,** 367.

DONGIOVANNI, P., VALENTI, L., RAMETTA, R., DALY, A. K., NOBILI, V., MOZZI, E., LEATHART, J. B., PIETROBATTISTA, A., BURT, A. D., MAGGIONI, M., FRACANZANI, A. L., LATTUADA, E., ZAPPA, M. A., ROVIARO, G., MARCHESINI, G., DAY, C. P. & FARGION, S. 2010. Genetic variants regulating insulin receptor signalling are associated with the severity of liver damage in patients with non-alcoholic fatty liver disease. *Gut,* 59**,** 267-73.

DOUCETTE, C., HOROWITZ, M., BERRY, R., MACDOUGALD, O., ANUNCIADO-KOZA, R., KOZA, R. & ROSEN, C. 2015. A High Fat Diet Increases Bone Marrow Adipose Tissue (MAT) But Does Not Alter Trabecular or Cortical Bone Mass in C57BL/6J Mice. *Journal of Cellular Physiology,* 230.

DROLET, R., RICHARD, C., SNIDERMAN, A. D., MAILLOUX, J., FORTIER, M., HUOT, C., RHEAUME, C. & TCHERNOF, A. 2008. Hypertrophy and hyperplasia of abdominal adipose tissues in women. *Int J Obes (Lond),* 32**,** 283-91.

DU, J., ZHANG, M., LU, J., ZHANG, X., XIONG, Q., XU, Y., BAO, Y. & JIA, W. 2016. Osteocalcin improves nonalcoholic fatty liver disease in mice through activation of Nrf2 and inhibition of JNK. *Endocrine,* 53**,** 701-9.

DUAN, R. D., BERGMAN, T., XU, N., WU, J., CHENG, Y., DUAN, J., NELANDER, S., PALMBERG, C. & NILSSON, A. 2003. Identification of human intestinal alkaline sphingomyelinase as a novel ecto-enzyme related to the nucleotide phosphodiesterase family. *J Biol Chem,* 278**,** 38528-36.

DUCY, P., AMLING, M., TAKEDA, S., PRIEMEL, M., SCHILLING, A. F., BEIL, F. T., SHEN, J., VINSON, C., RUEGER, J. M. & KARSENTY, G. 2000. Leptin Inhibits Bone Formation through a Hypothalamic Relay: A Central Control of Bone Mass. *Cell,* 100**,** 197-207.

DUCY, P., DESBOIS, C., BOYCE, B., PINERO, G., STORY, B., DUNSTAN, C., SMITH, E., BONADIO, J., GOLDSTEIN, S., GUNDBERG, C., BRADLEY, A. & KARSENTY, G. 1996. Increased bone formation in osteocalcin-deficient mice. *Nature,* 382**,** 448-52.

DUCY, P., ZHANG, R., GEOFFROY, V., RIDALL, A. L. & KARSENTY, G. 1997. Osf2/Cbfa1: A Transcriptional Activator of Osteoblast Differentiation. *Cell,* 89**,** 747-754.

DUMAS, M.-E., BARTON, R. H., TOYE, A., CLOAREC, O., BLANCHER, C., ROTHWELL, A., FEARNSIDE, J., TATOUD, R., BLANC, V., LINDON, J. C., MITCHELL, S. C., HOLMES, E., MCCARTHY, M. I., SCOTT, J., GAUGUIER, D. & NICHOLSON, J. K. 2006. Metabolic profiling reveals a contribution of gut microbiota to fatty liver phenotype in insulin-resistant mice. *Proceedings of the National Academy of Sciences,* 103**,** 12511.

DWEK, J. R. 2010. The periosteum: what is it, where is it, and what mimics it in its absence? *Skeletal radiology,* 39**,** 319-323.

DYSON, E. D. & WHITEHOUSE, W. J. 1968. Composition of trabecular bone in children and its relation to radiation dosimetry. *Nature,* 217**,** 576-8.

EISINGER, K., KRAUTBAUER, S., HEBEL, T., SCHMITZ, G., ASLANIDIS, C., LIEBISCH, G. & BUECHLER, C. 2014. Lipidomic analysis of the liver from high-fat diet induced obese mice identifies changes in multiple lipid classes. *Exp Mol Pathol,* 97**,** 37-43.

EMSLIE-SMITH, A. M., BOYLE, D. I. R., EVANS, J. M. M., SULLIVAN, F., MORRIS, A. D. & FOR THE, D. M. C. 2001. Contraindications to metformin therapy in patients with Type 2 diabetes—a population-based study of adherence to prescribing guidelines. *Diabetic Medicine,* 18**,** 483-488.

ERIKSEN, E. F., AXELROD, D. W. & MELSEN, F. 1994. *Bone Histomorphometry*, Raven Press.

ERSHOW, A. G. 2009. Environmental influences on development of type 2 diabetes and obesity: challenges in personalizing prevention and management. *J Diabetes Sci Technol,* 3**,** 727-34.

ESEN, E. & LONG, F. 2014. Aerobic glycolysis in osteoblasts. *Current osteoporosis reports,* 12**,** 433-438.

ESHTIAGHI, R., ESTEGHAMATI, A. & NAKHJAVANI, M. 2010. Menopause is an independent predictor of metabolic syndrome in Iranian women. *Maturitas,* 65**,** 262-266.

FAIENZA, M. F., LUCE, V., VENTURA, A., COLAIANNI, G., COLUCCI, S., CAVALLO, L., GRANO, M. & BRUNETTI, G. 2015. Skeleton and glucose metabolism: a bone-pancreas loop. *International journal of endocrinology,* 2015**,** 758148-758148.

FANG, H., HUANG, L., WELCH, I., NORLEY, C., HOLDSWORTH, D. W., BEIER, F. & CAI, D. 2018. Early Changes of Articular Cartilage and Subchondral Bone in The DMM Mouse Model of Osteoarthritis. *Scientific Reports,* 8**,** 2855.

FANTNER, G. E., HASSENKAM, T., KINDT, J. H., WEAVER, J. C., BIRKEDAL, H., PECHENIK, L., CUTRONI, J. A., CIDADE, G. A. G., STUCKY, G. D., MORSE, D. E. & HANSMA, P. K. 2005. Sacrificial bonds and hidden length dissipate energy as mineralized fibrils separate during bone fracture. *Nature Materials,* 4**,** 612-616.

FARQUHARSON, C., BERRY, J. L., MAWER, E. B., SEAWRIGHT, E. & WHITEHEAD, C. C. 1995. Regulators of chondrocyte differentiation in tibial dyschondroplasia: An in vivo and in vitro study. *Bone,* 17**,** 279-286.

FAUST, I. M., JOHNSON, P. R., STERN, J. S. & HIRSCH, J. 1978. Diet-induced adipocyte number increase in adult rats: a new model of obesity. *Am J Physiol,* 235**,** E279-86.

FAZELI, P. K., HOROWITZ, M. C., MACDOUGALD, O. A., SCHELLER, E. L., RODEHEFFER, M. S., ROSEN, C. J. & KLIBANSKI, A. 2013. Marrow fat and bone--new perspectives. *The Journal of clinical endocrinology and metabolism,* 98**,** 935-945.

FEDDE, K. N., BLAIR, L., SILVERSTEIN, J., COBURN, S. P., RYAN, L. M., WEINSTEIN, R. S., WAYMIRE, K., NARISAWA, S., MILLAN, J. L., MACGREGOR, G. R. & WHYTE, M. P. 1999a. Alkaline phosphatase knock-out mice recapitulate the metabolic and skeletal defects of infantile hypophosphatasia. *J Bone Miner Res,* 14**,** 2015-26.

FEDDE, K. N., BLAIR, L., SILVERSTEIN, J., COBURN, S. P., RYAN, L. M., WEINSTEIN, R. S., WAYMIRE, K., NARISAWA, S., MILLÁN, J. L., MACGREGOR, G. R. & WHYTE, M. P. 1999b. Alkaline Phosphatase Knock-Out Mice Recapitulate the Metabolic and Skeletal Defects of Infantile Hypophosphatasia. *Journal of Bone and Mineral Research,* 14**,** 2015-2026.

FENG, X. & MCDONALD, J. M. 2011. Disorders of bone remodeling. *Annual review of pathology,* 6**,** 121-145.

FERNÁNDEZ-VERDEJO, R., MARLATT, K. L., RAVUSSIN, E. & GALGANI, J. E. 2019. Contribution of brown adipose tissue to human energy metabolism. *Molecular Aspects of Medicine,* 68**,** 82-89.

FERREIRA, C., ZIEGLER, S. & GAHL, W. A. 1993. Generalized Arterial Calcification of Infancy. *In:* ADAM, M. P., ARDINGER, H. H., PAGON, R. A., WALLACE, S. E., BEAN, L. J. H., STEPHENS, K. & AMEMIYA, A. (eds.) *GeneReviews((R)).* Seattle (WA): University of Washington, Seattle

FERRON, M., WEI, J., YOSHIZAWA, T., DEL FATTORE, A., DEPINHO, R. A., TETI, A., DUCY, P. & KARSENTY, G. 2010a. Insulin signaling in osteoblasts integrates bone remodeling and energy metabolism. *Cell,* 142**,** 296-308.

FERRON, M., WEI, J., YOSHIZAWA, T., DUCY, P. & KARSENTY, G. 2010b. An ELISA-based method to quantify osteocalcin carboxylation in mice. *Biochemical and biophysical research communications,* 397**,** 691-696.

FESTING, M. H., SPEER, M. Y., YANG, H.-Y. & GIACHELLI, C. M. 2009. Generation of mouse conditional and null alleles of the type III sodium-dependent phosphate cotransporter PiT-1. *Genesis (New York, N.Y. : 2000),* 47**,** 858-863.

FLEISCH, H. & BISAZ, S. 1962. Mechanism of Calcification: Inhibitory Role of Pyrophosphate. *Nature,* 195**,** 911-911.

FLORENCIO-SILVA, R., SASSO, G. R. D. S., SASSO-CERRI, E., SIM, #XF5, ES, M. J., CERRI, P. S., #XE9 & RGIO 2015a. Biology of Bone Tissue: Structure, Function, and Factors That Influence Bone Cells. *BioMed Research International,* 2015**,** 17.

FLORENCIO-SILVA, R., SASSO, G. R. D. S., SASSO-CERRI, E., SIMÕES, M. J. & CERRI, P. S. 2015b. Biology of Bone Tissue: Structure, Function, and Factors That Influence Bone Cells. *BioMed research international,* 2015**,** 421746-421746.

FLOREZ, J. C. 2008. Newly identified loci highlight beta cell dysfunction as a key cause of type 2 diabetes: where are the insulin resistance genes? *Diabetologia,* 51**,** 1100-10.

FLOREZ, J. C. 2016. Leveraging Genetics to Advance Type 2 Diabetes Prevention. *PLoS medicine,* 13**,** e1002102-e1002102.

FONSECA-ALANIZ, M. H., TAKADA, J., ALONSO-VALE, M. I. C. & LIMA, F. B. 2007. O tecido adiposo como órgão endócrino: da teoria à prática. *Jornal de Pediatria,* 83**,** S192-S203.

FORD, J. L., ROBINSON, D. E. & SCAMMELL, B. E. 2004. Endochondral ossification in fracture callus during long bone repair: the localisation of 'cavity-lining cells' within the cartilage. *J Orthop Res,* 22**,** 368-75.

FOROUZANDEH, F., SALAZAR, G., PATRUSHEV, N., XIONG, S., HILENSKI, L., FEI, B. & ALEXANDER, R. W. 2014. Metformin beyond diabetes: pleiotropic benefits of metformin in attenuation of atherosclerosis. *J Am Heart Assoc,* 3**,** e001202.

FOSTER, B. L., NAGATOMO, K. J., NOCITI, F. H., JR., FONG, H., DUNN, D., TRAN, A. B., WANG, W., NARISAWA, S., MILLAN, J. L. & SOMERMAN, M. J. 2012. Central role of pyrophosphate in acellular cementum formation. *PLoS One,* 7**,** e38393.

FOSTER, B. L., POPOWICS, T. E., FONG, H. K. & SOMERMAN, M. J. 2007. Advances in defining regulators of cementum development and periodontal regeneration. *Curr Top Dev Biol,* 78**,** 47-126.

FRANCESCHI, R. T. & IYER, B. S. 1992. Relationship between collagen synthesis and expression of the osteoblast phenotype in MC3T3-E1 cells. *J Bone Miner Res,* 7**,** 235-46.

FRANCESCHI, R. T., IYER, B. S. & CUI, Y. 1994. Effects of ascorbic acid on collagen matrix formation and osteoblast differentiation in murine MC3T3-E1 cells. *J Bone Miner Res,* 9**,** 843-54.

FRANZ-ODENDAAL, T. A., HALL, B. K. & WITTEN, P. E. 2006. Buried alive: how osteoblasts become osteocytes. *Dev Dyn,* 235**,** 176-90.

FRITSCH, A. & HELLMICH, C. 2007. 'Universal' microstructural patterns in cortical and trabecular, extracellular and extravascular bone materials: micromechanics-based prediction of anisotropic elasticity. *J Theor Biol,* 244**,** 597-620.

FRITTITTA, L., BARATTA, R., SPAMPINATO, D., DI PAOLA, R., PIZZUTI, A., VIGNERI, R. & TRISCHITTA, V. 2001. The Q121 PC-1 variant and obesity have additive and independent effects in causing insulin resistance. *J Clin Endocrinol Metab,* 86**,** 5888-91.

FRITTITTA, L., SPAMPINATO, D., SOLINI, A., NOSADINI, R., GOLDFINE, I. D., VIGNERI, R. & TRISCHITTA, V. 1998. Elevated PC-1 content in cultured skin fibroblasts correlates with

decreased in vivo and in vitro insulin action in nondiabetic subjects: evidence that PC-1 may be an intrinsic factor in impaired insulin receptor signaling. *Diabetes,* 47**,** 1095-100.

FROST, H. M. 1987. Bone "mass" and the "mechanostat": a proposal. *Anat Rec,* 219**,** 1-9.

FROST, H. M. 1990. Skeletal structural adaptations to mechanical usage (SATMU): 2. Redefining Wolff's law: the remodeling problem. *Anat Rec,* 226**,** 414-22.

FROST, H. M. 1994. Wolff's Law and bone's structural adaptations to mechanical usage: an overview for clinicians. *Angle Orthod,* 64**,** 175-88.

FU, X., CHEN, J., WU, D., DU, Z., LEI, Q., CAI, Z. & SCHULTZE-MOSGAU, S. 2012. Effects of ovariectomy on rat mandibular cortical bone: a study using Raman spectroscopy and multivariate analysis. *Anal Chem,* 84**,** 3318-23.

FUKUSHIMA, N., ISHII, I., CONTOS, J. J., WEINER, J. A. & CHUN, J. 2001. Lysophospholipid receptors. *Annu Rev Pharmacol Toxicol,* 41**,** 507-34.

FULZELE, K., RIDDLE, R. C., DIGIROLAMO, D. J., CAO, X., WAN, C., CHEN, D., FAUGERE, M. C., AJA, S., HUSSAIN, M. A., BRUNING, J. C. & CLEMENS, T. L. 2010. Insulin receptor signaling in osteoblasts regulates postnatal bone acquisition and body composition. *Cell,* 142**,** 309-19.

FUNAKOSHI, I., KATO, H., HORIE, K., YANO, T., HORI, Y., KOBAYASHI, H., INOUE, T., SUZUKI, H., FUKUI, S., TSUKAHARA, M., KAJII, T. & YAMASHINA, I. 1992. Molecular cloning of cDNAs for human fibroblast nucleotide pyrophosphatase. *Archives of Biochemistry and Biophysics,* 295**,** 180-187.

FUSS, B., BABA, H., PHAN, T., TUOHY, V. K. & MACKLIN, W. B. 1997. Phosphodiesterase I, a novel adhesion molecule and/or cytokine involved in oligodendrocyte function. *J Neurosci,* 17**,** 9095-103.

GARG, A. 2011. Clinical review#: Lipodystrophies: genetic and acquired body fat disorders. *J Clin Endocrinol Metab,* 96**,** 3313-25.

GAWRONSKA-KOZAK, B., STASZKIEWICZ, J., GIMBLE, J. M. & KIRK-BALLARD, H. 2014. Recruitment of fat cell precursors during high fat diet in C57BL/6J mice is fat depot specific. *Obesity (Silver Spring, Md.),* 22**,** 1091-1102.

GENGE, B. R., WU, L. N. & WUTHIER, R. E. 1989. Identification of phospholipid-dependent calcium-binding proteins as constituents of matrix vesicles. *J Biol Chem,* 264**,** 10917-21.

GENGE, B. R., WU, L. N. & WUTHIER, R. E. 2007. Kinetic analysis of mineral formation during in vitro modeling of matrix vesicle mineralization: effect of annexin A5, phosphatidylserine, and type II collagen. *Anal Biochem,* 367**,** 159-66.

GERBER, H. P., VU, T. H., RYAN, A. M., KOWALSKI, J., WERB, Z. & FERRARA, N. 1999. VEGF couples hypertrophic cartilage remodeling, ossification and angiogenesis during endochondral bone formation. *Nat Med,* 5**,** 623-8.

GHESHLAGHI, F. 2012. Toxic renal injury at a glance. *J Renal Inj Prev,* 1**,** 15-6.

GHIASI, M. S., CHEN, J., VAZIRI, A., RODRIGUEZ, E. K. & NAZARIAN, A. 2017. Bone fracture healing in mechanobiological modeling: A review of principles and methods. *Bone reports,* 6**,** 87-100.

GIJSBERS, R., CEULEMANS, H., STALMANS, W. & BOLLEN, M. 2001. Structural and catalytic similarities between nucleotide pyrophosphatases/phosphodiesterases and alkaline phosphatases. *J Biol Chem,* 276**,** 1361-8.

GLATZ, A. C., PAWEL, B. R., HSU, D. T., WEINBERG, P. & CHRISANT, M. R. 2006. Idiopathic infantile arterial calcification: two case reports, a review of the literature and a role for cardiac transplantation. *Pediatr Transplant,* 10**,** 225-33.

GODING, J. W., GROBBEN, B. & SLEGERS, H. 2003. Physiological and pathophysiological functions of the ecto-nucleotide pyrophosphatase/phosphodiesterase family. *Biochim Biophys Acta,* 1638**,** 1-19.

GOLDFINE, I. D., MADDUX, B. A., YOUNGREN, J. F., REAVEN, G., ACCILI, D., TRISCHITTA, V., VIGNERI, R. & FRITTITTA, L. 2008. The role of membrane glycoprotein plasma cell antigen

1/ectonucleotide pyrophosphatase phosphodiesterase 1 in the pathogenesis of insulin resistance and related abnormalities. *Endocr Rev,* 29**,** 62-75.

GOLDRING, S. R. 2009. Role of bone in osteoarthritis pathogenesis. *Med Clin North Am,* 93**,** 25-35, xv.

GONCIULEA, A. & DE BEUR, S. J. 2015. The dynamic skeleton. *Rev Endocr Metab Disord,* 16**,** 79-91.

GONG, J. K., ARNOLD, J. S. & COHN, S. H. 1964. COMPOSITION OF TRABECULAR AND CORTICAL BONE. *Anat Rec,* 149**,** 325-31.

GORALSKI, K. B., MCCARTHY, T. C., HANNIMAN, E. A., ZABEL, B. A., BUTCHER, E. C., PARLEE, S. D., MURUGANANDAN, S. & SINAL, C. J. 2007. Chemerin, a novel adipokine that regulates adipogenesis and adipocyte metabolism. *J Biol Chem,* 282**,** 28175-88.

GRENIER-LAROUCHE, T., CARREAU, A.-M. & CARPENTIER, A. C. 2017. Early Metabolic Improvement After Bariatric Surgery: The First Steps Toward Remission of Type 2 Diabetes. *Canadian Journal of Diabetes,* 41**,** 418-425.

GRUPE, A., ALLEMAN, J., GOLDFINE, I. D., SADICK, M. & STEWART, T. A. 1995. Inhibition of insulin receptor phosphorylation by PC-1 is not mediated by the hydrolysis of adenosine triphosphate or the generation of adenosine. *J Biol Chem,* 270**,** 22085-8.

GU, P.-Y., YU, F., JIN, S., YANG, Q., SU, J., CHEN, Y., ZHAO, L. & HU, S.-L. 2017. Analysis of serum undercarboxylated osteocalcin level in rats with type 2 diabetes mellitus and the correlation with cognitive impairment. *Experimental and therapeutic medicine,* 14**,** 2603-2607.

GUILLOTEAU, P., ZABIELSKI, R., HAMMON, H. M. & METGES, C. C. 2010. Nutritional programming of gastrointestinal tract development. Is the pig a good model for man? *Nutr Res Rev,* 23**,** 4-22.

GUNTUR, A. R., LE, P. T., FARBER, C. R. & ROSEN, C. J. 2014. Bioenergetics during calvarial osteoblast differentiation reflect strain differences in bone mass. *Endocrinology,* 155**,** 1589-95.

GUNTUR, A. R. & ROSEN, C. J. 2012. Bone as an endocrine organ. *Endocrine practice : official journal of the American College of Endocrinology and the American Association of Clinical Endocrinologists,* 18**,** 758-762.

GUO, X., LI, H., XU, H., WOO, S., DONG, H., LU, F., LANGE, A. J. & WU, C. 2012. Glycolysis in the control of blood glucose homeostasis. *Acta Pharmaceutica Sinica B,* 2**,** 358-367.

GURDA, B. L., BRADBURY, A. M. & VITE, C. H. 2017. Canine and Feline Models of Human Genetic Diseases and Their Contributions to Advancing Clinical Therapies . *The Yale journal of biology and medicine,* 90**,** 417-431.

GUREVITCH, O., SLAVIN, S. & FELDMAN, A. G. 2007. Conversion of red bone marrow into yellow – Cause and mechanisms. *Medical Hypotheses,* 69**,** 531-536.

GURLEY, K. A., CHEN, H., GUENTHER, C., NGUYEN, E. T., ROUNTREE, R. B., SCHOOR, M. & KINGSLEY, D. M. 2006a. Mineral formation in joints caused by complete or joint-specific loss of ANK function. *J Bone Miner Res,* 21**,** 1238-47.

GURLEY, K. A., REIMER, R. J. & KINGSLEY, D. M. 2006b. Biochemical and genetic analysis of ANK in arthritis and bone disease. *American journal of human genetics,* 79**,** 1017-1029.

HAKIM, F. T., CRANLEY, R., BROWN, K. S., EANES, E. D., HARNE, L. & OPPENHEIM, J. J. 1984a. Hereditary joint disorder in progressive ankylosis (ank/ank) mice I. association of calcium hydroxyapatite deposition with inflammatory arthropathy. *Arthritis & Rheumatism,* 27**,** 1411-1420.

HAKIM, F. T., CRANLEY, R., BROWN, K. S., EANES, E. D., HARNE, L. & OPPENHEIM, J. J. 1984b. Hereditary joint disorder in progressive ankylosis (ank/ank) mice. I. Association of calcium hydroxyapatite deposition with inflammatory arthropathy. *Arthritis Rheum,* 27**,** 1411-20.

HALE, J. E., FRASER, J. D. & PRICE, P. A. 1988. The identification of matrix Gla protein in cartilage. *J Biol Chem,* 263**,** 5820-4.

HALL, B. K. & MIYAKE, T. 1992. The membranous skeleton: the role of cell condensations in vertebrate skeletogenesis. *Anat Embryol (Berl),* 186**,** 107-24.

HANSON, R. W. & GARBER, A. J. 1972. Phosphoenolpyruvate carboxykinase. I. Its role in gluconeogenesis. *Am J Clin Nutr,* 25**,** 1010-21.

HARAHAP, A. R. & GODING, J. W. 1988. Distribution of the murine plasma cell antigen PC-1 in non-lymphoid tissues. *J Immunol,* 141**,** 2317-20.

HARDOUIN, P., RHARASS, T. & LUCAS, S. 2016. Bone Marrow Adipose Tissue: To Be or Not To Be a Typical Adipose Tissue? *Front Endocrinol (Lausanne),* 7**,** 85.

HARIRI, N. & THIBAULT, L. 2010. High-fat diet-induced obesity in animal models. *Nutrition Research Reviews,* 23**,** 270-299.

HARMEY, D., HESSLE, L., NARISAWA, S., JOHNSON, K. A., TERKELTAUB, R. & MILLÁN, J. L. 2004. Concerted Regulation of Inorganic Pyrophosphate and Osteopontin by Akp2, Enpp1, and Ank: An Integrated Model of the Pathogenesis of Mineralization Disorders. *The American Journal of Pathology,* 164**,** 1199-1209.

HART, N. H., NIMPHIUS, S., RANTALAINEN, T., IRELAND, A., SIAFARIKAS, A. & NEWTON, R. U. 2017. Mechanical basis of bone strength: influence of bone material, bone structure and muscle action. *Journal of musculoskeletal & neuronal interactions,* 17**,** 114-139.

HAUSCHKA, P. V., LIAN, J. B., COLE, D. E. & GUNDBERG, C. M. 1989. Osteocalcin and matrix Gla protein: vitamin K-dependent proteins in bone. *Physiological Reviews,* 69**,** 990-1047.

HEINE, P. A., TAYLOR, J. A., IWAMOTO, G. A., LUBAHN, D. B. & COOKE, P. S. 2000. Increased adipose tissue in male and female estrogen receptor-alpha knockout mice. *Proc Natl Acad Sci U S A,* 97**,** 12729-34.

HELDMAIER, G. & BUCHBERGER, A. 1985. Sources of heat during nonshivering thermogenesis in Djungarian hamsters: a dominant role of brown adipose tissue during cold adaptation. *J Comp Physiol B,* 156**,** 237-45.

HENRIKSEN, K., NEUTZSKY-WULFF, A. V., BONEWALD, L. F. & KARSDAL, M. A. 2009. Local communication on and within bone controls bone remodeling. *Bone,* 44**,** 1026-33.

HENSON, M. S. & O'BRIEN, T. D. 2006. Feline models of type 2 diabetes mellitus. *Ilar j,* 47**,** 234-42.

HENZ, S. L., FURSTENAU, C. R., CHIARELLI, R. A. & SARKIS, J. J. 2007. Kinetic and biochemical characterization of an ecto-nucleotide pyrophosphatase/phosphodiesterase (EC 3.1.4.1) in cells cultured from submandibular salivary glands of rats. *Arch Oral Biol,* 52**,** 916-23.

HEROLD, S., KUMAR, P., JUNG, K., GRAF, I., MENKHOFF, H., SCHULZ, X., BÄHR, M. & HEIN, K. 2016. CatWalk gait analysis in a rat model of multiple sclerosis. *BMC neuroscience,* 17**,** 78-78.

HESSLE, L., JOHNSON, K. A., ANDERSON, H. C., NARISAWA, S., SALI, A., GODING, J. W., TERKELTAUB, R. & MILLÁN, J. L. 2002. Tissue-nonspecific alkaline phosphatase and plasma cell membrane glycoprotein-1 are central antagonistic regulators of bone mineralization. *Proceedings of the National Academy of Sciences,* 99**,** 9445.

HILL, J. O. & COMMERFORD, R. 1996. Physical activity, fat balance, and energy balance. *Int J Sport Nutr,* 6**,** 80-92.

HILL, J. O., WYATT, H. R. & PETERS, J. C. 2012. Energy balance and obesity. *Circulation,* 126**,** 126-132.

HO, A. M., JOHNSON, M. D. & KINGSLEY, D. M. 2000. Role of the mouse ank gene in control of tissue calcification and arthritis. *Science,* 289**,** 265-70.

HOENIG, M., HALL, G., FERGUSON, D., JORDAN, K., HENSON, M., JOHNSON, K. & O'BRIEN, T. 2000. A Feline Model of Experimentally Induced Islet Amyloidosis. *The American Journal of Pathology,* 157**,** 2143-2150.

HOLMAN, N., YOUNG, B. & GADSBY, R. 2015. Current prevalence of Type 1 and Type 2 diabetes in adults and children in the UK. *Diabetic Medicine,* 32**,** 1119-1120.

HONG, D., CHEN, H. X., YU, H. Q., LIANG, Y., WANG, C., LIAN, Q. Q., DENG, H. T. & GE, R. S. 2010. Morphological and proteomic analysis of early stage of osteoblast differentiation in osteoblastic progenitor cells. *Exp Cell Res,* 316**,** 2291-300.

HOSODA, N., I HOSHINO, S., KANDA, Y. & KATADA, T. 1999. *Inhibition of phosphodiesterase/pyrophosphatase activity of PC-1 by its association with glycosaminoglycans*.

HOSODA, Y., YOSHIMURA, Y. & HIGAKI, S. 1981. A new breed of mouse showing multiple osteochondral lesions--twy mouse. *Ryumachi,* 21 Suppl**,** 157-64.

HOUSTON, B., STEWART, A. J. & FARQUHARSON, C. 2004. PHOSPHO1-A novel phosphatase specifically expressed at sites of mineralisation in bone and cartilage. *Bone,* 34**,** 629-37.

HOUSTON, D. A., MYERS, K., MACRAE, V. E., STAINES, K. A. & FARQUHARSON, C. 2016. The Expression of PHOSPHO1, nSMase2 and TNAP is Coordinately Regulated by Continuous PTH Exposure in Mineralising Osteoblast Cultures. *Calcif Tissue Int,* 99**,** 510-524.

HU, F. B. 2011. Globalization of Diabetes. *Diabetes Care,* 34**,** 1249.

HUANG, N.-J., LIN, Y.-C., LIN, C.-Y., PISHESHA, N., LEWIS, C. A., FREINKMAN, E., FARQUHARSON, C., MILLÁN, J. L. & LODISH, H. 2018. Enhanced phosphocholine metabolism is essential for terminal erythropoiesis. *Blood,* 131**,** 2955.

HUANG, R., ROSENBACH, M., VAUGHN, R., PROVVEDINI, D., REBBE, N., HICKMAN, S., GODING, J. & TERKELTAUB, R. 1994. Expression of the murine plasma cell nucleotide pyrophosphohydrolase PC-1 is shared by human liver, bone, and cartilage cells. Regulation of PC-1 expression in osteosarcoma cells by transforming growth factor-beta. *The Journal of Clinical Investigation,* 94**,** 560-567.

HUESA, C., HOUSTON, D., KIFFER-MOREIRA, T., YADAV, M. M., MILLAN, J. L. & FARQUHARSON, C. 2015a. The Functional co-operativity of Tissue-Nonspecific Alkaline Phosphatase (TNAP) and PHOSPHO1 during initiation of Skeletal Mineralization. *Biochemistry and biophysics reports,* 4**,** 196-201.

HUESA, C., STAINES, K. A., MILLÁN, J. L. & MACRAE, V. E. 2015b. Effects of etidronate on the Enpp1^{-}/$^{-}$ mouse model of generalized arterial calcification of infancy. *International journal of molecular medicine,* 36**,** 159-165.

HUESA, C., YADAV, M. C., FINNILA, M. A., GOODYEAR, S. R., ROBINS, S. P., TANNER, K. E., ASPDEN, R. M., MILLAN, J. L. & FARQUHARSON, C. 2011. PHOSPHO1 is essential for mechanically competent mineralization and the avoidance of spontaneous fractures. *Bone,* 48**,** 1066-74.

HUESA, C., ZHU, D., GLOVER, J. D., FERRON, M., KARSENTY, G., MILNE, E. M., MILLAN, J. L., AHMED, S. F., FARQUHARSON, C., MORTON, N. M. & MACRAE, V. E. 2014. Deficiency of the bone mineralization inhibitor NPP1 protects mice against obesity and diabetes. *Disease models & mechanisms,* 7**,** 1341-1350.

HULMES, D. J., WESS, T. J., PROCKOP, D. J. & FRATZL, P. 1995. Radial packing, order, and disorder in collagen fibrils. *Biophys J,* 68**,** 1661-70.

HUNZIKER, E. B., SCHENK, R. K. & CRUZ-ORIVE, L. M. 1987. Quantitation of chondrocyte performance in growth-plate cartilage during longitudinal bone growth. *J Bone Joint Surg Am,* 69**,** 162-73.

IDELEVICH, A., KERSCHNITZKI, M., SHAHAR, R. & MONSONEGO-ORNAN, E. 2011. 1,25(OH)2D3 alters growth plate maturation and bone architecture in young rats with normal renal function. *PloS one,* 6**,** e20772-e20772.

IVASKA, K. K., HENTUNEN, T. A., VAARANIEMI, J., YLIPAHKALA, H., PETTERSSON, K. & VAANANEN, H. K. 2004. Release of intact and fragmented osteocalcin molecules from bone matrix during bone resorption in vitro. *J Biol Chem,* 279**,** 18361-9.

IVASKA, K. K., KAKONEN, S. M., GERDHEM, P., OBRANT, K. J., PETTERSSON, K. & VAANANEN, H. K. 2005. Urinary osteocalcin as a marker of bone metabolism. *Clin Chem,* 51**,** 618-28.

JAMES, A. M., COLLINS, Y., LOGAN, A. & MURPHY, M. P. 2012. Mitochondrial oxidative stress and the metabolic syndrome. *Trends Endocrinol Metab,* 23**,** 429-34.

JANSEN, R. S., DUIJST, S., MAHAKENA, S., SOMMER, D., SZERI, F., VARADI, A., PLOMP, A., BERGEN, A. A., OUDE ELFERINK, R. P., BORST, P. & VAN DE WETERING, K. 2014. ABCC6-mediated ATP secretion by the liver is the main source of the mineralization inhibitor inorganic pyrophosphate in the systemic circulation-brief report. *Arterioscler Thromb Vasc Biol,* 34**,** 1985-9.

JANSEN, S., PERRAKIS, A., ULENS, C., WINKLER, C., ANDRIES, M., JOOSTEN, ROBBIE P., VAN ACKER, M., LUYTEN, FRANK P., MOOLENAAR, WOUTER H. & BOLLEN, M. 2012. Structure of NPP1, an Ectonucleotide Pyrophosphatase/Phosphodiesterase Involved in Tissue Calcification. *Structure,* 20**,** 1948-1959.

JANSSEN, I., FORTIER, A., HUDSON, R. & ROSS, R. 2002. Effects of an energy-restrictive diet with or without exercise on abdominal fat, intermuscular fat, and metabolic risk factors in obese women. *Diabetes Care,* 25**,** 431-8.

JAVAHERI, B., CARRIERO, A., STAINES, K. A., CHANG, Y. M., HOUSTON, D. A., OLDKNOW, K. J., MILLAN, J. L., KAZERUNI, B. N., SALMON, P., SHEFELBINE, S., FARQUHARSON, C. & PITSILLIDES, A. A. 2015. Phospho1 deficiency transiently modifies bone architecture yet produces consistent modification in osteocyte differentiation and vascular porosity with ageing. *Bone,* 81**,** 277-291.

JENSEN, E. D., GOPALAKRISHNAN, R. & WESTENDORF, J. J. 2010. Regulation of gene expression in osteoblasts. *Biofactors,* 36**,** 25-32.

JIANG, Q. & UITTO, J. 2012. Restricting dietary magnesium accelerates ectopic connective tissue mineralization in a mouse model of pseudoxanthoma elasticum (Abcc6−/−). *Experimental Dermatology,* 21**,** 694-699.

JIN, Y., CONG, Q., GVOZDENOVIC-JEREMIC, J., HU, J., ZHANG, Y., TERKELTAUB, R. & YANG, Y. 2018. Enpp1 inhibits ectopic joint calcification and maintains articular chondrocytes by repressing hedgehog signaling. *Development,* 145.

JO, J., GAVRILOVA, O., PACK, S., JOU, W., MULLEN, S., SUMNER, A. E., CUSHMAN, S. W. & PERIWAL, V. 2009. Hypertrophy and/or Hyperplasia: Dynamics of Adipose Tissue Growth. *PLoS computational biology,* 5**,** e1000324-e1000324.

JOHNSON, K., GODING, J., VAN ETTEN, D., SALI, A., HU, S. I., FARLEY, D., KRUG, H., HESSLE, L., MILLAN, J. L. & TERKELTAUB, R. 2003. Linked deficiencies in extracellular PP(i) and osteopontin mediate pathologic calcification associated with defective PC-1 and ANK expression. *J Bone Miner Res,* 18**,** 994-1004.

JOHNSON, K., POLEWSKI, M., VAN ETTEN, D. & TERKELTAUB, R. 2005. Chondrogenesis Mediated by PPi Depletion Promotes Spontaneous Aortic Calcification in NPP1−/− Mice. *Arteriosclerosis, Thrombosis, and Vascular Biology,* 25**,** 686-691.

JUPPNER, H., ABOU-SAMRA, A. B., FREEMAN, M., KONG, X. F., SCHIPANI, E., RICHARDS, J., KOLAKOWSKI, L. F., JR., HOCK, J., POTTS, J. T., JR., KRONENBERG, H. M. & ET AL. 1991. A G protein-linked receptor for parathyroid hormone and parathyroid hormone-related peptide. *Science,* 254**,** 1024-6.

JUSTESEN, J., STENDERUP, K., EBBESEN, E. N., MOSEKILDE, L., STEINICHE, T. & KASSEM, M. 2001. Adipocyte tissue volume in bone marrow is increased with aging and in patients with osteoporosis. *Biogerontology,* 2**,** 165-71.

KAFFE, E., KATSIFA, A., XYLOURGIDIS, N., NINOU, I., ZANNIKOU, M., HAROKOPOS, V., FOKA, P., DIMITRIADIS, A., EVANGELOU, K., MOULAS, A. N., GEORGOPOULOU, U., GORGOULIS, V. G., DALEKOS, G. N. & AIDINIS, V. 2017. Hepatocyte autotaxin expression promotes liver fibrosis and cancer. *Hepatology,* 65**,** 1369-1383.

KAMIKUBO, Y., OKUMURA, Y. & LOSKUTOFF, D. J. 2002. Identification of the disulfide bonds in the recombinant somatomedin B domain of human vitronectin. *J Biol Chem,* 277**,** 27109-19.

KANCZLER, J. & OREFFO, R. 2008. *Osteogenesis and angiogenesis: The potential for engineering bone*.

KARLSSON, F. H., TREMAROLI, V., NOOKAEW, I., BERGSTROM, G., BEHRE, C. J., FAGERBERG, B., NIELSEN, J. & BACKHED, F. 2013. Gut metagenome in European women with normal, impaired and diabetic glucose control. *Nature,* 498**,** 99-103.

KARSENTY, G., FERRON, M., KARSENTY, G. & FERRON, M. 2012. The contribution of bone to whole-organism physiology. *Nature,* 481**,** 314-320.

KARSENTY, G., KRONENBERG, H. M. & SETTEMBRE, C. 2009. Genetic control of bone formation. *Annu Rev Cell Dev Biol,* 25**,** 629-48.

KARSENTY, G. & OLSON, E. N. 2016. Bone and Muscle Endocrine Functions: Unexpected Paradigms of Inter-organ Communication. *Cell,* 164**,** 1248-1256.

KARSENTY, G. & WAGNER, E. F. 2002. Reaching a genetic and molecular understanding of skeletal development. *Dev Cell,* 2**,** 389-406.

KASHIWAGI, A., FEIN, M. J. & SHIMADA, M. 2011. A high fat diet-induced impaired glucose metabolism in mice with targeted deletion of calpain in osteoblasts. *Biochem Biophys Res Commun,* 409**,** 235-40.

KASPERK, C., HELMBOLDT, A., BORCSOK, I., HEUTHE, S., CLOOS, O., NIETHARD, F. & ZIEGLER, R. 1997. Skeletal site-dependent expression of the androgen receptor in human osteoblastic cell populations. *Calcif Tissue Int,* 61**,** 464-73.

KAUFFENSTEIN, G., YEGUTKIN, G. G., KHIATI, S., POMOZI, V., LE SAUX, O., LEFTHERIOTIS, G., LENAERS, G., HENRION, D. & MARTIN, L. 2018. Alteration of Extracellular Nucleotide Metabolism in Pseudoxanthoma Elasticum. *Journal of Investigative Dermatology,* 138**,** 1862-1870.

KAWAZOE, Y., SHIBA, T., NAKAMURA, R., MIZUNO, A., TSUTSUMI, K., UEMATSU, T., YAMAOKA, M., SHINDOH, M. & KOHGO, T. 2004. Induction of Calcification in MC3T3-E1 Cells by Inorganic Polyphosphate. *Journal of dental research,* 83**,** 613-8.

KELLY, S. J., DARDINGER, D. E. & BUTLER, L. G. 1975. Hydrolysis of phosphonate esters catalyzed by 5'-nucleotide phosphodiesterase. *Biochemistry,* 14**,** 4983-8.

KENKRE, J. S. & BASSETT, J. 2018. The bone remodelling cycle. *Ann Clin Biochem,* 55**,** 308-327.

KERSHAW, E. E. & FLIER, J. S. 2004. Adipose tissue as an endocrine organ. *J Clin Endocrinol Metab,* 89**,** 2548-56.

KERSTEN, S., SEYDOUX, J., PETERS, J. M., GONZALEZ, F. J., DESVERGNE, B. & WAHLI, W. 1999. Peroxisome proliferator-activated receptor alpha mediates the adaptive response to fasting. *J Clin Invest,* 103**,** 1489-98.

KHERA, R., MURAD, M. H., CHANDAR, A. K., DULAI, P. S., WANG, Z., PROKOP, L. J., LOOMBA, R., CAMILLERI, M. & SINGH, S. 2016. Association of Pharmacological Treatments for Obesity With Weight Loss and Adverse Events: A Systematic Review and Meta-analysis. *JAMA,* 315**,** 2424-2434.

KHOSLA, S., MELTON, L. J., ATKINSON, E. J. & FALLON, W. M. O. 2001. Relationship of serum sex steroid levels to longitudinal changes in bone density in young versus elderly men. *Journal of Clinical Endocrinology and Metabolism,* 86**,** 3555-3561.

KHOSLA, S., OURSLER, M. J. & MONROE, D. G. 2012. Estrogen and the skeleton. *Trends Endocrinol Metab,* 23**,** 576-81.

KIECHL, S., WITTMANN, J., GIACCARI, A., KNOFLACH, M., WILLEIT, P., BOZEC, A., MOSCHEN, A. R., MUSCOGIURI, G., SORICE, G. P., KIREVA, T., SUMMERER, M., WIRTZ, S., LUTHER, J., MIELENZ, D., BILLMEIER, U., EGGER, G., MAYR, A., OBERHOLLENZER, F., KRONENBERG, F., ORTHOFER, M., PENNINGER, J. M., MEIGS, J. B., BONORA, E., TILG, H., WILLEIT, J. & SCHETT, G. 2013. Blockade of receptor activator of nuclear factor-κB (RANKL) signaling improves hepatic insulin resistance and prevents development of diabetes mellitus. *Nature Medicine,* 19**,** 358.

KILLION, C. H., MITCHELL, E. H., DUKE, C. G. & SERRA, R. 2017. Mechanical loading regulates organization of the actin cytoskeleton and column formation in postnatal growth plate. *Molecular biology of the cell,* 28**,** 1862-1870.

KIM, H. J., MINASHIMA, T., MCCARTHY, E. F., WINKLES, J. A. & KIRSCH, T. 2010. Progressive ankylosis protein (ANK) in osteoblasts and osteoclasts controls bone formation and bone remodeling. *Journal of Bone and Mineral Research,* 25**,** 1771-1783.

KIM, Y. J., LEE, M. H., WOZNEY, J. M., CHO, J. Y. & RYOO, H. M. 2004. Bone morphogenetic protein-2-induced alkaline phosphatase expression is stimulated by Dlx5 and repressed by Msx2. *J Biol Chem,* 279**,** 50773-80.

KING, A. & BOWE, J. 2016a. Animal models for diabetes: Understanding the pathogenesis and finding new treatments. *Biochemical Pharmacology,* 99**,** 1-10.

KING, A. & BOWE, J. 2016b. Animal models for diabetes: Understanding the pathogenesis and finding new treatments. *Biochem Pharmacol,* 99**,** 1-10.

KING, A. J. F. 2012. The use of animal models in diabetes research. *British journal of pharmacology,* 166**,** 877-894.

KIRPICHNIKOV, D., MCFARLANE, S. I. & SOWERS, J. R. 2002. Metformin: an update. *Ann Intern Med,* 137**,** 25-33.

KLANGJAREONCHAI, T., NIMITPHONG, H., SAETUNG, S., BHIROMMUANG, N., SAMITTARUCKSA, R., CHANPRASERTYOTHIN, S., SUDATIP, R. & ONGPHIPHADHANAKUL, B. 2014. Circulating sclerostin and irisin are related and interact with gender to influence adiposity in adults with prediabetes. *Int J Endocrinol,* 2014**,** 261545.

KNOWLER, W. C., BARRETT-CONNOR, E., FOWLER, S. E., HAMMAN, R. F., LACHIN, J. M., WALKER, E. A. & NATHAN, D. M. 2002. Reduction in the incidence of type 2 diabetes with lifestyle intervention or metformin. *N Engl J Med,* 346**,** 393-403.

KODAMA, H.-A., AMAGAI, Y., SUDO, H., KASAI, S. & YAMAMOTO, S. 1981. Establishment of a clonal osteogenic cell line from newborn mouse calvaria. *Japanese Journal of Oral Biology,* 23**,** 899-901.

KODE, A., MOSIALOU, I., SILVA, B. C., JOSHI, S., FERRON, M., RACHED, M. T. & KOUSTENI, S. 2012. FoxO1 protein cooperates with ATF4 protein in osteoblasts to control glucose homeostasis. *J Biol Chem,* 287**,** 8757-68.

KOHLI, R. & FELDSTEIN, A. E. 2011. NASH animal models: are we there yet? *J Hepatol,* 55**,** 941-3.

KOMORI, T. 2010. Regulation of osteoblast differentiation by Runx2. *Adv Exp Med Biol,* 658**,** 43-9.

KOROSTISHEVSKY, M., MALKIN, I., TROFIMOV, S., PEI, Y., DENG, H.-W. & LIVSHITS, G. 2012. Significant association between body composition phenotypes and the osteocalcin genomic region in normative human population. *Bone,* 51**,** 688-694.

KRINGS, A., RAHMAN, S., HUANG, S., LU, Y., CZERNIK, P. J. & LECKA-CZERNIK, B. 2012. Bone marrow fat has brown adipose tissue characteristics, which are attenuated with aging and diabetes. *Bone,* 50**,** 546-52.

KRONENBERG, H. M. 2003a. Developmental regulation of the growth plate. *Nature,* 423**,** 332-6.

KRONENBERG, H. M. 2003b. Developmental regulation of the growth plate. *Nature,* 423**,** 332.

LAI, Y.-S., CHEN, W.-C., KUO, T.-C., HO, C.-T., KUO, C.-H., TSENG, Y. J., LU, K.-H., LIN, S.-H., PANYOD, S. & SHEEN, L.-Y. 2015. Mass-Spectrometry-Based Serum Metabolomics of a C57BL/6J Mouse Model of High-Fat-Diet-Induced Non-alcoholic Fatty Liver Disease Development. *Journal of Agricultural and Food Chemistry,* 63**,** 7873-7884.

LAJEUNESSE, D., MASSICOTTE, F., PELLETIER, J. P. & MARTEL-PELLETIER, J. 2003. Subchondral bone sclerosis in osteoarthritis: not just an innocent bystander. *Mod Rheumatol,* 13**,** 7-14.

LANDIS, W. J. & SILVER, F. H. 2009. Mineral deposition in the extracellular matrices of vertebrate tissues: identification of possible apatite nucleation sites on type I collagen. *Cells, tissues, organs,* 189**,** 20-24.

LANYON, L. E. 1993. Osteocytes, strain detection, bone modeling and remodeling. *Calcif Tissue Int,* 53 Suppl 1**,** S102-6; discussion S106-7.

LEAN, M. E. J., LESLIE, W. S., BARNES, A. C., BROSNAHAN, N., THOM, G., MCCOMBIE, L., PETERS, C., ZHYZHNEUSKAYA, S., AL-MRABEH, A., HOLLINGSWORTH, K. G., RODRIGUES, A. M., REHACKOVA, L., ADAMSON, A. J., SNIEHOTTA, F. F., MATHERS, J. C., ROSS, H. M., MCILVENNA, Y., STEFANETTI, R., TRENELL, M., WELSH, P., KEAN, S., FORD, I., MCCONNACHIE, A., SATTAR, N. & TAYLOR, R. 2018. Primary care-led weight management for remission of type 2 diabetes (DiRECT): an open-label, cluster-randomised trial. *The Lancet,* 391**,** 541-551.

LECKA-CZERNIK, B. 2010. Bone loss in diabetes: use of antidiabetic thiazolidinediones and secondary osteoporosis. *Curr Osteoporos Rep,* 8**,** 178-84.

LEE, N. K., SOWA, H., HINOI, E., FERRON, M., AHN, J. D., CONFAVREUX, C., DACQUIN, R., MEE, P. J., MCKEE, M. D., JUNG, D. Y., ZHANG, Z., KIM, J. K., MAUVAIS-JARVIS, F., DUCY, P. & KARSENTY, G. 2007. Endocrine regulation of energy metabolism by the skeleton. *Cell,* 130**,** 456-69.

LEE, P., GREENFIELD, J. R., HO, K. K. Y. & FULHAM, M. J. 2010. A critical appraisal of the prevalence and metabolic significance of brown adipose tissue in adult humans. *American Journal of Physiology-Endocrinology and Metabolism,* 299**,** E601-E606.

LEE, R. H., KIM, B., CHOI, I., KIM, H., CHOI, H. S., SUH, K., BAE, Y. C. & JUNG, J. S. 2004. Characterization and expression analysis of mesenchymal stem cells from human bone marrow and adipose tissue. *Cell Physiol Biochem,* 14**,** 311-24.

LEE, S.-Y. & MÜLLER, C. E. 2017. Nucleotide pyrophosphatase/phosphodiesterase 1 (NPP1) and its inhibitors. *MedChemComm,* 8**,** 823-840.

LEE, S. Y., LEVESQUE, S. A., SEVIGNY, J. & MULLER, C. E. 2012. A highly sensitive capillary electrophoresis method using p-nitrophenyl 5'-thymidine monophosphate as a substrate for the monitoring of nucleotide pyrophosphatase/phosphodiesterase activities. *J Chromatogr B Analyt Technol Biomed Life Sci,* 911**,** 162-9.

LEE, W. C., GUNTUR, A. R., LONG, F. & ROSEN, C. J. 2017. Energy Metabolism of the Osteoblast: Implications for Osteoporosis. *Endocr Rev,* 38**,** 255-266.

LEITÃO, C. B., NABINGER, G. B., KRAHE, A. L., BOLSON, P. B., GERCHMAN, F., FRIEDMAN, R., GROSS, J. L. & CANANI, L. H. 2008. The role of K121Q ENPP1 polymorphism in diabetes mellitus and its complications. *Brazilian Journal of Medical and Biological Research,* 41**,** 229-234.

LI, J., PARADA, C. & CHAI, Y. 2017a. Cellular and molecular mechanisms of tooth root development. *Development (Cambridge, England),* 144**,** 374-384.

LI, L., YIN, Q., KUSS, P., MALIGA, Z., MILLAN, J. L., WU, H. & MITCHISON, T. J. 2014a. Hydrolysis of 2'3'-cGAMP by ENPP1 and design of nonhydrolyzable analogs. *Nat Chem Biol,* 10**,** 1043-8.

LI, M., AMIZUKA, N., ODA, K., TOKUNAGA, K., ITO, T., TAKEUCHI, K., TAKAGI, R. & MAEDA, T. 2004. Histochemical evidence of the initial chondrogenesis and osteogenesis in the periosteum of a rib fractured model: Implications of osteocyte involvement in periosteal chondrogenesis. *Microscopy Research and Technique,* 64**,** 330-342.

LI, Q., GUO, H., CHOU, D. W., BERNDT, A., SUNDBERG, J. P. & UITTO, J. 2013. Mutant Enpp1asj mice as a model for generalized arterial calcification of infancy. *Disease models & mechanisms,* 6**,** 1227-1235.

LI, Q., JIANG, Q. & UITTO, J. 2014b. Ectopic mineralization disorders of the extracellular matrix of connective tissue: molecular genetics and pathomechanisms of aberrant calcification. *Matrix biology : journal of the International Society for Matrix Biology,* 33**,** 23-28.

LI, X., YANG, H.-Y. & GIACHELLI CECILIA, M. 2006. Role of the Sodium-Dependent Phosphate Cotransporter, Pit-1, in Vascular Smooth Muscle Cell Calcification. *Circulation Research,* 98**,** 905-912.

LI, Y., GE, C., LONG, J. P., BEGUN, D. L., RODRIGUEZ, J. A., GOLDSTEIN, S. A. & FRANCESCHI, R. T. 2012. Biomechanical stimulation of osteoblast gene expression requires phosphorylation of the RUNX2 transcription factor. *J Bone Miner Res,* 27**,** 1263-74.

LI, Z., LIU, S.-Y., XU, L., XU, S.-Y. & NI, G.-X. 2017b. Effects of treadmill running with different intensity on rat subchondral bone. *Scientific Reports,* 7**,** 1977.

LINDSTROM, P. 2007. The physiology of obese-hyperglycemic mice [ob/ob mice]. *ScientificWorldJournal,* 7**,** 666-85.

LITWAK, S. A., WILSON, J. L., CHEN, W., GARCIA-RUDAZ, C., KHAKSARI, M., COWLEY, M. A. & ENRIORI, P. J. 2014. Estradiol Prevents Fat Accumulation and Overcomes Leptin Resistance in Female High-Fat Diet Mice. *Endocrinology,* 155**,** 4447-4460.

LIU, F., MALAVAL, L. & AUBIN, J. E. 1997. The Mature Osteoblast Phenotype Is Characterized by Extensive Plasticity. *Experimental Cell Research,* 232**,** 97-105.

LIU, J., NAM, H. K., CAMPBELL, C., GASQUE, K. C. D. S., MILLÁN, J. L. & HATCH, N. E. 2014. Tissue-nonspecific alkaline phosphatase deficiency causes abnormal craniofacial bone development in the Alpl(-/-) mouse model of infantile hypophosphatasia. *Bone,* 67**,** 81-94.

LIU, L.-F., SHEN, W.-J., UENO, M., PATEL, S. & KRAEMER, F. B. 2011. Characterization of age-related gene expression profiling in bone marrow and epididymal adipocytes. *BMC Genomics,* 12**,** 212.

LIU, Q., SILOTO, R. M., LEHNER, R., STONE, S. J. & WESELAKE, R. J. 2012. Acyl-CoA:diacylglycerol acyltransferase: molecular biology, biochemistry and biotechnology. *Prog Lipid Res,* 51**,** 350-77.

LIVAK, K. J. & SCHMITTGEN, T. D. 2001. Analysis of relative gene expression data using real-time quantitative PCR and the 2(-Delta Delta C(T)) Method. *Methods,* 25**,** 402-8.

LOUTIT, J. F. & NISBET, N. W. 1982. The origin of osteoclasts. *Immunobiology,* 161**,** 193-203.

MACHADO, M. V., MICHELOTTI, G. A., XIE, G., ALMEIDA PEREIRA, T., BOURSIER, J., BOHNIC, B., GUY, C. D. & DIEHL, A. M. 2015. Mouse models of diet-induced nonalcoholic steatohepatitis reproduce the heterogeneity of the human disease. *PloS one,* 10**,** e0127991-e0127991.

MACKENZIE, N. C. W., ZHU, D., MILNE, E. M., VAN 'T HOF, R., MARTIN, A., QUARLES, D. L., MILLÁN, J. L., FARQUHARSON, C. & MACRAE, V. E. 2012. Altered Bone Development and an Increase in FGF-23 Expression in Enpp1−/− Mice. *PLOS ONE,* 7**,** e32177.

MACKIE, E. J., AHMED, Y. A., TATARCZUCH, L., CHEN, K. S. & MIRAMS, M. 2008. Endochondral ossification: How cartilage is converted into bone in the developing skeleton. *The International Journal of Biochemistry & Cell Biology,* 40**,** 46-62.

MACKIE, E. J., TATARCZUCH, L. & MIRAMS, M. 2011. The skeleton: a multi-functional complex organ: the growth plate chondrocyte and endochondral ossification. *J Endocrinol,* 211**,** 109-21.

MADDUX, B. A., CHANG, Y.-N., ACCILI, D., MCGUINNESS, O. P., YOUNGREN, J. F. & GOLDFINE, I. D. 2006a. Overexpression of the insulin receptor inhibitor PC-1/ENPP1 induces insulin resistance and hyperglycemia. *American Journal of Physiology-Endocrinology and Metabolism,* 290**,** E746-E749.

MADDUX, B. A., CHANG, Y. N., ACCILI, D., MCGUINNESS, O. P., YOUNGREN, J. F. & GOLDFINE, I. D. 2006b. Overexpression of the insulin receptor inhibitor PC-1/ENPP1 induces insulin resistance and hyperglycemia. *Am J Physiol Endocrinol Metab,* 290**,** E746-9.

MADDUX, B. A. & GOLDFINE, I. D. 2000. Membrane glycoprotein PC-1 inhibition of insulin receptor function occurs via direct interaction with the receptor alpha-subunit. *Diabetes,* 49**,** 13-9.

MADDUX, B. A., SBRACCIA, P., KUMAKURA, S., SASSON, S., YOUNGREN, J., FISHER, A., SPENCER, S., GRUPE, A., HENZEL, W., STEWART, T. A. & ET AL. 1995. Membrane glycoprotein PC-1 and insulin resistance in non-insulin-dependent diabetes mellitus. *Nature,* 373**,** 448-51.

MALKIN, I., ERMAKOV, S., KOBYLIANSKY, E. & LIVSHITS, G. 2006. Strong association between polymorphisms in ANKH locus and skeletal size traits. *Human Genetics,* 120**,** 42-51.

MANIATIS, A., TAVASSOLI, M. & CROSBY, W. H. 1971. Factors Affecting the Conversion of Yellow to Red Marrow. *Blood,* 37**,** 581.

MANOLAGAS, S. C. 2000. Birth and Death of Bone Cells: Basic Regulatory Mechanisms and Implications for the Pathogenesis and Treatment of Osteoporosis*. *Endocrine Reviews,* 21**,** 115-137.

MANOLAGAS, S. C. & WEINSTEIN, R. S. 1999. New Developments in the Pathogenesis and Treatment of Steroid-Induced Osteoporosis. *Journal of Bone and Mineral Research,* 14**,** 1061-1066.

MATHER, K. J., VERMA, S. & ANDERSON, T. J. 2001. Improved endothelial function with metformin in type 2 diabetes mellitus. *Journal of the American College of Cardiology,* 37**,** 1344.

MATIC, M., BRYZGALOVA, G., GAO, H., ANTONSON, P., HUMIRE, P., OMOTO, Y., PORTWOOD, N., PRAMFALK, C., EFENDIC, S., BERGGREN, P.-O., GUSTAFSSON, J.-Å. & DAHLMAN-WRIGHT, K. 2013. Estrogen signalling and the metabolic syndrome: targeting the hepatic estrogen receptor alpha action. *PloS one,* 8**,** e57458-e57458.

MATTHIAS, A., OHLSON, K. B., FREDRIKSSON, J. M., JACOBSSON, A., NEDERGAARD, J. & CANNON, B. 2000. Thermogenic responses in brown fat cells are fully UCP1-dependent. UCP2 or UCP3 do not substitute for UCP1 in adrenergically or fatty scid-induced thermogenesis. *J Biol Chem,* 275**,** 25073-81.

MCATEER, J. B., PRUDENTE, S., BACCI, S., LYON, H. N., HIRSCHHORN, J. N., TRISCHITTA, V. & FLOREZ, J. C. 2008. The ENPP1 K121Q Polymorphism Is Associated With Type 2 Diabetes in European Populations. *Diabetes,* 57**,** 1125.

MCCARTHY, M. I. 2010. Genomics, type 2 diabetes, and obesity. *N Engl J Med,* 363**,** 2339-50.

MEERSON, N. R., DELAUTIER, D., DURAND-SCHNEIDER, A. M., MOREAU, A., SCHILSKY, M. L., STERNLIEB, I., FELDMANN, G. & MAURICE, M. 1998. Identification of B10, an alkaline phosphodiesterase of the apical plasma membrane of hepatocytes and biliary cells, in rat serum: increased levels following bile duct ligation and during the development of cholangiocarcinoma. *Hepatology,* 27**,** 563-8.

MEUNIER, P., AARON, J., EDOUARD, C. & VIGNON, G. 1971. Osteoporosis and the replacement of cell populations of the marrow by adipose tissue. A quantitative study of 84 iliac bone biopsies. *Clin Orthop Relat Res,* 80**,** 147-54.

MEURENS, F., SUMMERFIELD, A., NAUWYNCK, H., SAIF, L. & GERDTS, V. 2012. The pig: a model for human infectious diseases. *Trends in Microbiology,* 20**,** 50-57.

MEYER, J. L. 1984. Can biological calcification occur in the presence of pyrophosphate? *Arch Biochem Biophys,* 231**,** 1-8.

MICLAU, T., LU, C., THOMPSON, Z., CHOI, P., PUTTLITZ, C., MARCUCIO, R. & HELMS, J. A. 2007. Effects of delayed stabilization on fracture healing. *J Orthop Res,* 25**,** 1552-8.

MILLÁN, J. L. 2013. The role of phosphatases in the initiation of skeletal mineralization. *Calcified tissue international,* 93**,** 299-306.

MILLER, G. J., GERSTENFELD, L. C. & MORGAN, E. F. 2015. Mechanical microenvironments and protein expression associated with formation of different skeletal tissues during bone healing. *Biomech Model Mechanobiol,* 14**,** 1239-53.

MILLS, G. B. & MOOLENAAR, W. H. 2003. The emerging role of lysophosphatidic acid in cancer. *Nature Reviews Cancer,* 3**,** 582-591.

MILLWARD, C. A., DESANTIS, D., HSIEH, C. W., HEANEY, J. D., PISANO, S., OLSWANG, Y., RESHEF, L., BEIDELSCHIES, M., PUCHOWICZ, M. & CRONIGER, C. M. 2010. Phosphoenolpyruvate carboxykinase (Pck1) helps regulate the triglyceride/fatty acid cycle and development of insulin resistance in mice. *J Lipid Res,* 51**,** 1452-63.

MINAIRE, P., NEUNIER, P., EDOUARD, C., BERNARD, J., COURPRON, P. & BOURRET, J. 1974. Quantitative histological data on disuse osteoporosis: comparison with biological data. *Calcif Tissue Res,* 17**,** 57-73.

MIRALLES-LINARES, F., PUERTA-FERNANDEZ, S., BERNAL-LOPEZ, M. R., TINAHONES, F. J., ANDRADE, R. J. & GOMEZ-HUELGAS, R. 2012. Metformin-Induced Hepatotoxicity. *Diabetes Care,* 35**,** e21.

MITTON-FITZGERALD, E., GOHR, C. M., BETTENDORF, B. & ROSENTHAL, A. K. 2016. The Role of ANK in Calcium Pyrophosphate Deposition Disease. *Current rheumatology reports,* 18**,** 25-25.

MOHAN, S. & BAYLINK, D. J. 1996. Insulin-like growth factor system components and the coupling of bone formation to resorption. *Horm Res,* 45 Suppl 1**,** 59-62.

MOOLENAAR, W. H. 1995. Lysophosphatidic acid, a multifunctional phospholipid messenger. *J Biol Chem,* 270**,** 12949-52.

MOORE, S. G. & DAWSON, K. L. 1990. Red and yellow marrow in the femur: age-related changes in appearance at MR imaging. *Radiology,* 175**,** 219-223.

MORCOS, M. W., AL-JALLAD, H., LI, J., FARQUHARSON, C., MILLAN, J. L., HAMDY, R. C. & MURSHED, M. 2018. PHOSPHO1 is essential for normal bone fracture healing: An Animal Study. *Bone Joint Res,* 7**,** 397-405.

MOREIRA, C. A., DEMPSTER, D. W. & BARON, R. 2000. Anatomy and Ultrastructure of Bone - Histogenesis, Growth and Remodeling. *In:* FEINGOLD, K. R., ANAWALT, B., BOYCE, A., CHROUSOS, G., DUNGAN, K., GROSSMAN, A., HERSHMAN, J. M., KALTSAS, G., KOCH, C., KOPP, P., KORBONITS, M., MCLACHLAN, R., MORLEY, J. E., NEW, M., PERREAULT, L., PURNELL, J., REBAR, R., SINGER, F., TRENCE, D. L., VINIK, A. & WILSON, D. P. (eds.) *Endotext.* South Dartmouth (MA): MDText.com, Inc.

MORGAN, E. F., BARNES, G. L. & EINHORN, T. A. 2008. CHAPTER 1 - The Bone Organ System: Form and Function. *In:* MARCUS, R., FELDMAN, D., NELSON, D. A. & ROSEN, C. J. (eds.) *Osteoporosis (Third Edition).* San Diego: Academic Press.

MORGAN, S. L. 2001. Calcium and Vitamin D in Osteoporosis. *Rheumatic Disease Clinics of North America,* 27**,** 101-130.

MORNET, E. 2000. Hypophosphatasia: The mutations in the tissue-nonspecific alkaline phosphatase gene. *Human Mutation,* 15**,** 309-315.

MORRIS, M. D. & MANDAIR, G. S. 2011. Raman assessment of bone quality. *Clin Orthop Relat Res,* 469**,** 2160-9.

MOTYL, K. J., GUNTUR, A. R., CARVALHO, A. L. & ROSEN, C. J. 2017. Energy Metabolism of Bone. *Toxicol Pathol,* 45**,** 887-893.

MUECKLER, M. & THORENS, B. 2013. The SLC2 (GLUT) family of membrane transporters. *Mol Aspects Med,* 34**,** 121-38.

MÜLLER, C. E. & JACOBSON, K. A. 2011. Recent developments in adenosine receptor ligands and their potential as novel drugs. *Biochimica et Biophysica Acta (BBA) - Biomembranes,* 1808**,** 1290-1308.

MUMM, S., JONES, J., FINNEGAN, P. & WHYTE, M. P. 2001. Hypophosphatasia: molecular diagnosis of Rathbun's original case. *J Bone Miner Res,* 16**,** 1724-7.

MUNOZ, M. T., MORANDE, G., GARCIA-CENTENERA, J. A., HERVAS, F., POZO, J. & ARGENTE, J. 2002. The effects of estrogen administration on bone mineral density in adolescents with anorexia nervosa. *Eur J Endocrinol,* 146**,** 45-50.

MURSHED, M., HARMEY, D., MILLAN, J. L., MCKEE, M. D. & KARSENTY, G. 2005. Unique coexpression in osteoblasts of broadly expressed genes accounts for the spatial restriction of ECM mineralization to bone. *Genes Dev,* 19**,** 1093-104.

MURSHED, M., SCHINKE, T., MCKEE, M. D. & KARSENTY, G. 2004. Extracellular matrix mineralization is regulated locally; different roles of two gla-containing proteins. *The Journal of cell biology,* 165**,** 625-630.

MURUGANANDAN, S., ROMAN, A. A. & SINAL, C. J. 2009. Adipocyte differentiation of bone marrow-derived mesenchymal stem cells: cross talk with the osteoblastogenic program. *Cell Mol Life Sci,* 66**,** 236-53.

MURUGANANDAN, S. & SINAL, C. J. 2014. The impact of bone marrow adipocytes on osteoblast and osteoclast differentiation. *IUBMB Life,* 66**,** 147-155.

MUSSO, G., GAMBINO, R. & CASSADER, M. 2013. Cholesterol metabolism and the pathogenesis of non-alcoholic steatohepatitis. *Progress in Lipid Research,* 52**,** 175-191.

MUZIK, O., MANGNER, T. J., LEONARD, W. R., KUMAR, A., JANISSE, J. & GRANNEMAN, J. G. 2013. 15O PET measurement of blood flow and oxygen consumption in cold-activated human brown fat. *J Nucl Med,* 54**,** 523-31.

NAGY, C. & EINWALLNER, E. 2018. Study of In Vivo Glucose Metabolism in High-fat Diet-fed Mice Using Oral Glucose Tolerance Test (OGTT) and Insulin Tolerance Test (ITT). *J Vis Exp*.

NAKAJIMA, T., SHIBATA, M., NISHIO, M., NAGATA, S., ALEV, C., SAKURAI, H., TOGUCHIDA, J. & IKEYA, M. 2018. Modeling human somite development and fibrodysplasia ossificans progressiva with induced pluripotent stem cells. *Development,* 145.

NALLA, R. K., KRUZIC, J. J., KINNEY, J. H. & RITCHIE, R. O. 2004. Effect of aging on the toughness of human cortical bone: evaluation by R-curves. *Bone,* 35**,** 1240-1246.

NAM, M., CHOI, M.-S., JUNG, S., JUNG, Y., CHOI, J.-Y., RYU, D. H. & HWANG, G.-S. 2015. Lipidomic Profiling of Liver Tissue from Obesity-Prone and Obesity-Resistant Mice Fed a High Fat Diet. *Scientific Reports,* 5**,** 16984.

NAMASIVAYAM, V., LEE, S. Y. & MULLER, C. E. 2017. The promiscuous ectonucleotidase NPP1: molecular insights into substrate binding and hydrolysis. *Biochim Biophys Acta Gen Subj,* 1861**,** 603-614.

NARAYANASWAMI, V. & DWOSKIN, L. P. 2017. Obesity: Current and potential pharmacotherapeutics and targets. *Pharmacology & Therapeutics,* 170**,** 116-147.

NARISAWA, S., FROHLANDER, N. & MILLAN, J. L. 1997. Inactivation of two mouse alkaline phosphatase genes and establishment of a model of infantile hypophosphatasia. *Dev Dyn,* 208**,** 432-46.

NARISAWA, S., HARMEY, D., YADAV, M. C., O'NEILL, W. C., HOYLAERTS, M. F. & MILLÁN, J. L. 2007. Novel Inhibitors of Alkaline Phosphatase Suppress Vascular Smooth Muscle Cell Calcification. *Journal of Bone and Mineral Research,* 22**,** 1700-1710.

NARITA, M., GOJI, J., NAKAMURA, H. & SANO, K. 1994. Molecular cloning, expression, and localization of a brain-specific phosphodiesterase I/nucleotide pyrophosphatase (PD-I alpha) from rat brain. *J Biol Chem,* 269**,** 28235-42.

NASRI, H., BEHRADMANESH, S., MAGHSOUDI, A. R., AHMADI, A., NASRI, P. & RAFIEIAN-KOPAEI, M. 2014. Efficacy of supplementary vitamin D on improvement of glycemic parameters in patients with type 2 diabetes mellitus; a randomized double blind clinical trial. *J Renal Inj Prev,* 3**,** 31-4.

NATALI, A. & FERRANNINI, E. 2006. Effects of metformin and thiazolidinediones on suppression of hepatic glucose production and stimulation of glucose uptake in type 2 diabetes: a systematic review. *Diabetologia,* 49**,** 434-41.

NAVALE, A. M. & PARANJAPE, A. N. 2016. Glucose transporters: physiological and pathological roles. *Biophys Rev,* 8**,** 5-9.

NEDERGAARD, J., BENGTSSON, T. & CANNON, B. 2010. Three years with adult human brown adipose tissue. *Ann N Y Acad Sci,* 1212**,** E20-36.

NEDERGAARD, J. & CANNON, B. 2010. The Changed Metabolic World with Human Brown Adipose Tissue: Therapeutic Visions. *Cell Metabolism,* 11**,** 268-272.

NESBITT, S. A. & HORTON, M. A. 1997. Trafficking of Matrix Collagens Through Bone-Resorbing Osteoclasts. *Science,* 276**,** 266.

NEVE, A., CORRADO, A. & CANTATORE, F. P. 2013. Osteocalcin: Skeletal and extra-skeletal effects. *Journal of Cellular Physiology,* 228**,** 1149-1153.

NICHOLLS, D. G. & LOCKE, R. M. 1984. Thermogenic mechanisms in brown fat. *Physiological Reviews,* 64**,** 1-64.

NILSSON, A. 1969. *The presence of sphingomyelin- and ceramide-cleaving enzymes in the small intestinal tract*.

NILSSON, O., MARINO, R., DE LUCA, F., PHILLIP, M. & BARON, J. 2005. Endocrine regulation of the growth plate. *Horm Res,* 64**,** 157-65.

NISHIO, M., YONESHIRO, T., NAKAHARA, M., SUZUKI, S., SAEKI, K., HASEGAWA, M., KAWAI, Y., AKUTSU, H., UMEZAWA, A., YASUDA, K., TOBE, K., YUO, A., KUBOTA, K., SAITO, M. & SAEKI, K. 2012. Production of Functional Classical Brown Adipocytes from Human Pluripotent Stem Cells using Specific Hemopoietin Cocktail without Gene Transfer. *Cell Metabolism,* 16**,** 394-406.

NITSCHKE, Y., BAUJAT, G., BOTSCHEN, U., WITTKAMPF, T., DU MOULIN, M., STELLA, J., LE MERRER, M., GUEST, G., LAMBOT, K., TAZAROURTE-PINTURIER, M. F., CHASSAING, N., ROCHE, O., FEENSTRA, I., LOECHNER, K., DESHPANDE, C., GARBER, S. J., CHIKARMANE, R., STEINMANN, B., SHAHINYAN, T., MARTORELL, L., DAVIES, J., SMITH, W. E., KAHLER, S. G., MCCULLOCH, M., WRAIGE, E., LOIDI, L., HOHNE, W., MARTIN, L., HADJ-RABIA, S., TERKELTAUB, R. & RUTSCH, F. 2012. Generalized arterial calcification of infancy and pseudoxanthoma elasticum can be caused by mutations in either ENPP1 or ABCC6. *Am J Hum Genet,* 90**,** 25-39.

NITSCHKE, Y. & RUTSCH, F. 2012. Generalized arterial calcification of infancy and pseudoxanthoma elasticum: two sides of the same coin. *Frontiers in Genetics,* 3.

NITSCHKE, Y. & RUTSCH, F. 2017. Inherited Arterial Calcification Syndromes: Etiologies and Treatment Concepts. *Current Osteoporosis Reports,* 15**,** 255-270.

NOCITI, F. H., BERRY, J. E., FOSTER, B. L., GURLEY, K. A., KINGSLEY, D. M., TAKATA, T., MIYAUCHI, M. & SOMERMAN, M. J. 2002. Cementum: A Phosphate-sensitive Tissue. *Journal of Dental Research,* 81**,** 817-821.

NUDELMAN, F., LAUSCH, A. J., SOMMERDIJK, N. A. J. M. & SONE, E. D. 2013. In vitro models of collagen biomineralization. *Journal of Structural Biology,* 183**,** 258-269.

NUDELMAN, F., PIETERSE, K., GEORGE, A., BOMANS, P. H. H., FRIEDRICH, H., BRYLKA, L. J., HILBERS, P. A. J., DE WITH, G. & SOMMERDIJK, N. A. J. M. 2010. The role of collagen in bone apatite formation in the presence of hydroxyapatite nucleation inhibitors. *Nature materials,* 9**,** 1004-1009.

NUNEZ, J. A., GORING, A., JAVAHERI, B., RAZI, H., GOMEZ-NICOLA, D., PITSILLIDES, A. A., THURNER, P. J., GOMEZ-NICOLA, D., SCHNEIDER, P. & CLARKIN, C. E. 2018. Regional diversity in the murine cortical vascular network is revealed by synchrotron X-ray tomography and is amplified with age. *Eur Cell Mater,* 35**,** 281-299.

NUTTALL, M. E. & GIMBLE, J. M. 2000. Is there a therapeutic opportunity to either prevent or treat osteopenic disorders by inhibiting marrow adipogenesis? *Bone,* 27**,** 177-184.

O'BRIEN, T. D., HAYDEN, D. W., JOHNSON, K. H. & FLETCHER, T. F. 1986. Immunohistochemical morphometry of pancreatic endocrine cells in diabetic, normoglycaemic glucose-intolerant and normal cats. *Journal of Comparative Pathology,* 96**,** 357-369.

ODGREN, P. R., WITWICKA, H. & REYES-GUTIERREZ, P. 2016. The cast of clasts: catabolism and vascular invasion during bone growth, repair, and disease by osteoclasts, chondroclasts, and septoclasts. *Connective tissue research,* 57**,** 161-174.

OFTADEH, R., PEREZ-VILORIA, M., VILLA-CAMACHO, J. C., VAZIRI, A. & NAZARIAN, A. 2015. Biomechanics and mechanobiology of trabecular bone: a review. *J Biomech Eng,* 137.

OGURTSOVA, K., DA ROCHA FERNANDES, J. D., HUANG, Y., LINNENKAMP, U., GUARIGUATA, L., CHO, N. H., CAVAN, D., SHAW, J. E. & MAKAROFF, L. E. 2017. IDF Diabetes Atlas: Global estimates for the prevalence of diabetes for 2015 and 2040. *Diabetes Research and Clinical Practice,* 128**,** 40-50.

OHKUBO, Y., KISHIKAWA, H., ARAKI, E., MIYATA, T., ISAMI, S., MOTOYOSHI, S., KOJIMA, Y., FURUYOSHI, N. & SHICHIRI, M. 1995. Intensive insulin therapy prevents the progression of diabetic microvascular complications in Japanese patients with non-insulin-dependent diabetes mellitus: a randomized prospective 6-year study. *Diabetes Research and Clinical Practice,* 28**,** 103-117.

OIKAWA, H., TOMATSU, S., HAUPT, B., MONTAÑO, A. M., SHIMADA, T. & SLY, W. S. 2014. Enzyme replacement therapy on hypophosphatasia mouse model. *Journal of Inherited Metabolic Disease,* 37**,** 309-317.

OKAWA, A., GOTO, S. & MORIYA, H. 1999. Calcitonin Simultaneously Regulates Both Periosteal Hyperostosis and Trabecular Osteopenia in the Spinal Hyperostotic Mouse (twy/twy) In Vivo. *Calcified Tissue International,* 64**,** 239-247.

OKAWA, A., NAKAMURA, I., GOTO, S., MORIYA, H., NAKAMURA, Y. & IKEGAWA, S. 1998a. Mutation in Npps in a mouse model of ossification of the posterior longitudinal ligament of the spine. *Nat Genet,* 19**,** 271-3.

OKAWA, A., NAKAMURA, I., GOTO, S., MORIYA, H., NAKAMURA, Y. & IKEGAWA, S. 1998b. Mutation in Npps in a mouse model of ossification of the posterior longitudinal ligament of the spine. *Nature Genetics,* 19**,** 271.

OLDKNOW, K. J., MILLAN, J. L., MACRAE, V. E., KARSENTY, G., FERRON, M., BALL, D., BUNGER, L., HUESA, C., RAJOANAH, S., YADAV, M. C., MORTON, N. M. & FARQUHARSON, C. 2014. PHOSPHO1: Recognition of roles beyond skeletal mineralization. *Osteoporosis international,* 25**,** S171-S172.

OMOTOLA, O., LEGAN, S., SLADE, E., ADEKUNLE, A. & PENDERGAST, J. S. 2019. Estradiol regulates daily rhythms underlying diet-induced obesity in female mice. *American Journal of Physiology-Endocrinology and Metabolism,* 317**,** E1172-E1181.

ORGEL, J. P., IRVING, T. C., MILLER, A. & WESS, T. J. 2006. Microfibrillar structure of type I collagen in situ. *Proc Natl Acad Sci U S A,* 103**,** 9001-5.

ORNOY, A., GIRON, S., ANER, R., GOLDSTEIN, M., BOYAN, B. D. & SCHWARTZ, Z. 1994. Gender dependent effects of testosterone and 17 beta-estradiol on bone growth and modelling in young mice. *Bone Miner,* 24**,** 43-58.

ORRISS, I. R., ARNETT, T. R. & RUSSELL, R. G. G. 2016. Pyrophosphate: a key inhibitor of mineralisation. *Current Opinion in Pharmacology,* 28**,** 57-68.

ORTUÑO, M. J., SUSPERREGUI, A. R. G., ARTIGAS, N., ROSA, J. L. & VENTURA, F. 2013. Osterix induces Col1a1 gene expression through binding to Sp1 sites in the bone enhancer and proximal promoter regions. *Bone,* 52**,** 548-556.

OURY, F., SUMARA, G., SUMARA, O., FERRON, M., CHANG, H., SMITH, C. E., HERMO, L., SUAREZ, S., ROTH, B. L., DUCY, P. & KARSENTY, G. 2011. Endocrine regulation of male fertility by the skeleton. *Cell,* 144**,** 796-809.

PAJVANI, U. B., DU, X., COMBS, T. P., BERG, A. H., RAJALA, M. W., SCHULTHESS, T., ENGEL, J., BROWNLEE, M. & SCHERER, P. E. 2003. Structure-function studies of the adipocyte-secreted hormone Acrp30/adiponectin. Implications fpr metabolic regulation and bioactivity. *J Biol Chem,* 278**,** 9073-85.

PALACIO-MANCHENO, P. E., LARRIERA, A. I., DOTY, S. B., CARDOSO, L. & FRITTON, S. P. 2014. 3D assessment of cortical bone porosity and tissue mineral density using high-resolution μCT: effects of resolution and threshold method. *Journal of bone and mineral research : the official journal of the American Society for Bone and Mineral Research,* 29**,** 142-150.

PALMER, G., MANEN, D., BONJOUR, J.-P. & CAVERZASIO, J. 2001. Species-specific mechanisms control the activity of the Pit1/PIT1 phosphate transporter gene promoter in mouse and human. *Gene,* 279**,** 49-62.

PALUCH, E. K., NELSON, C. M., BIAIS, N., FABRY, B., MOELLER, J., PRUITT, B. L., WOLLNIK, C., KUDRYASHEVA, G., REHFELDT, F. & FEDERLE, W. 2015. Mechanotransduction: use the force(s). *BMC Biology,* 13**,** 47.

PAN, W., CHANDALIA, M. & ABATE, N. 2012. New Insights into the Role of ENPP1 in Insulin Resistance. *Journal of metabonomics & metabolites,* 1**,** 10.4172/2325-9736.1000e103.

PAN, W., CIOCIOLA, E., SARAF, M., TUMURBAATAR, B., TUVDENDORJ, D., PRASAD, S., CHANDALIA, M. & ABATE, N. 2011. Metabolic consequences of ENPP1 overexpression in adipose tissue. *American journal of physiology. Endocrinology and metabolism,* 301**,** E901-E911.

PAN, X. R., LI, G. W., HU, Y. H., WANG, J. X., YANG, W. Y., AN, Z. X., HU, Z. X., LIN, J., XIAO, J. Z., CAO, H. B., LIU, P. A., JIANG, X. G., JIANG, Y. Y., WANG, J. P., ZHENG, H., ZHANG, H., BENNETT, P. H. & HOWARD, B. V. 1997. Effects of diet and exercise in preventing NIDDM in people with impaired glucose tolerance. The Da Qing IGT and Diabetes Study. *Diabetes Care,* 20**,** 537-44.

PAPAGERAKIS, P., BERDAL, A., MESBAH, M., PEUCHMAUR, M., MALAVAL, L., NYDEGGER, J., SIMMER, J. & MACDOUGALL, M. 2002. Investigation of osteocalcin, osteonectin, and dentin sialophosphoprotein in developing human teeth. *Bone,* 30**,** 377-85.

PARFITT, A. M. 1976. The actions of parathyroid hormone on bone: relation to bone remodeling and turnover, calcium homeostasis, and metabolic bone disease. Part I of IV parts: mechanisms of calcium transfer between blood and bone and their cellular basis: morphological and kinetic approaches to bone turnover. *Metabolism,* 25**,** 809-44.

PARFITT, A. M. 2002. Targeted and nontargeted bone remodeling: relationship to basic multicellular unit origination and progression. *Bone,* 30**,** 5-7.

PARFITT, A. M., DREZNER, M. K., GLORIEUX, F. H., KANIS, J. A., MALLUCHE, H., MEUNIER, P. J., OTT, S. M. & RECKER, R. R. 1987. Bone histomorphometry: Standardization of nomenclature, symbols, and units: Report of the asbmr histomorphometry nomenclature committee. *Journal of Bone and Mineral Research,* 2**,** 595-610.

PATEL, J. J., BOURNE, L. E., DAVIES, B. K., ARNETT, T. R., MACRAE, V. E., WHEELER-JONES, C. P. D. & ORRISS, I. R. 2019. Differing calcification processes in cultured vascular smooth muscle cells and osteoblasts. *Experimental Cell Research,* 380**,** 100-113.

PATSCH, J. M., KIEFER, F. W., VARGA, P., PAIL, P., RAUNER, M., STUPPHANN, D., RESCH, H., MOSER, D., ZYSSET, P. K., STULNIG, T. M. & PIETSCHMANN, P. 2011. Increased bone resorption and impaired bone microarchitecture in short-term and extended high-fat diet-induced obesity. *Metabolism,* 60**,** 243-9.

PEAD, M. J., SUSWILLO, R., SKERRY, T. M., VEDI, S. & LANYON, L. E. 1988. Increased 3H-uridine levels in osteocytes following a single short period of dynamic bone loading in vivo. *Calcif Tissue Int,* 43**,** 92-6.

PECK, W. A., BIRGE, S. J. & FEDAK, S. A. 1964. Bone Cells: Biochemical and Biological Studies after Enzymatic Isolation. *Science,* 146**,** 1476.

PETRIDIS, X., BEEMS, B. P., TOMSON, P. L., SCHEVEN, B., GIEPMANS, B. N. G., KUIPERS, J., VAN DER SLUIS, L. W. M. & HARMSEN, M. C. 2018. Effect of Dentin Matrix Components on the Mineralization of Human Mesenchymal Stromal Cells. *Tissue Engineering Part A,* 25**,** 1104-1115.

PICHARDO, J. C., TRINDADE, A. A., BRINDLE, J. M. & BOLCH, W. E. 2007. Method for estimating skeletal spongiosa volume and active marrow mass in the adult male and adult female. *J Nucl Med,* 48**,** 1880-8.

PLELI, T., MARTIN, D., KRONENBERGER, B., BRUNNER, F., KÖBERLE, V., GRAMMATIKOS, G., FARNIK, H., MARTINEZ, Y., FINKELMEIER, F., LABOCHA, S., FERREIRÓS, N., ZEUZEM, S.,

PIIPER, A. & WAIDMANN, O. 2014. Serum autotaxin is a parameter for the severity of liver cirrhosis and overall survival in patients with liver cirrhosis--a prospective cohort study. *PloS one,* 9**,** e103532-e103532.

PLOURDE, C.-É., GRENIER-LAROUCHE, T., CARON-DORVAL, D., BIRON, S., MARCEAU, S., LEBEL, S., BIERTHO, L., TCHERNOF, A., RICHARD, D. & CARPENTIER, A. C. 2014. Biliopancreatic diversion with duodenal switch improves insulin sensitivity and secretion through caloric restriction. *Obesity,* 22**,** 1838-1846.

POLONSKY, K. S. 2012. The Past 200 Years in Diabetes. *New England Journal of Medicine,* 367**,** 1332-1340.

POMOZI, V., JULIAN, C. B., ZOLL, J., PHAM, K., KUO, S., TŐKÉSI, N., MARTIN, L., VÁRADI, A. & LE SAUX, O. 2019. Dietary Pyrophosphate Modulates Calcification in a Mouse Model of Pseudoxanthoma Elasticum: Implication for Treatment of Patients. *Journal of Investigative Dermatology,* 139**,** 1082-1088.

POOLE, K. E. & REEVE, J. 2005. Parathyroid hormone - a bone anabolic and catabolic agent. *Curr Opin Pharmacol,* 5**,** 612-7.

PRICE, P. A., URIST, M. R. & OTAWARA, Y. 1983. Matrix Gla protein, a new γ-carboxyglutamic acid-containing protein which is associated with the organic matrix of bone. *Biochemical and Biophysical Research Communications,* 117**,** 765-771.

PROCKOP, D. J. 1997. Marrow Stromal Cells as Stem Cells for Nonhematopoietic Tissues. *Science,* 276**,** 71.

PROVOT, S. & SCHIPANI, E. 2005. Molecular mechanisms of endochondral bone development. *Biochemical and Biophysical Research Communications,* 328**,** 658-665.

PRUDENTE, S., MORINI, E. & TRISCHITTA, V. 2009. Insulin signaling regulating genes: effect on T2DM and cardiovascular risk. *Nat Rev Endocrinol,* 5**,** 682-93.

PURI, P., BAILLIE, R. A., WIEST, M. M., MIRSHAHI, F., CHOUDHURY, J., CHEUNG, O., SARGEANT, C., CONTOS, M. J. & SANYAL, A. J. 2007. A lipidomic analysis of nonalcoholic fatty liver disease. *Hepatology,* 46**,** 1081-1090.

QIU, S., FYHRIE, D. P., PALNITKAR, S. & RAO, D. S. 2003. Histomorphometric assessment of Haversian canal and osteocyte lacunae in different-sized osteons in human rib. *Anat Rec A Discov Mol Cell Evol Biol,* 272**,** 520-5.

QUARLES, L. D., YOHAY, D. A., LEVER, L. W., CATON, R. & WENSTRUP, R. J. 1992. Distinct proliferative and differentiated stages of murine MC3T3-E1 cells in culture: an in vitro model of osteoblast development. *J Bone Miner Res,* 7**,** 683-92.

RADIN, E. L., PAUL, I. L. & TOLKOFF, M. J. 1970. Subchondral bone changes in patients with early degenerative joint disease. *Arthritis Rheum,* 13**,** 400-5.

RADIN, E. L. & ROSE, R. M. 1986. Role of subchondral bone in the initiation and progression of cartilage damage. *Clin Orthop Relat Res***,** 34-40.

RAISZ, L. G. 1988. Hormonal regulation of bone growth and remodelling. *Ciba Found Symp,* 136**,** 226-38.

RALEVIC, V. & BURNSTOCK, G. 1998. Receptors for purines and pyrimidines. *Pharmacol Rev,* 50**,** 413-92.

RAMACHANDRAN, A., SNEHALATHA, C., MARY, S., MUKESH, B., BHASKAR, A. D. & VIJAY, V. 2006. The Indian Diabetes Prevention Programme shows that lifestyle modification and metformin prevent type 2 diabetes in Asian Indian subjects with impaired glucose tolerance (IDPP-1). *Diabetologia,* 49**,** 289-97.

RAMSAY, D. S. & WOODS, S. C. 2014. Clarifying the roles of homeostasis and allostasis in physiological regulation. *Psychological Reviews,* 121**,** 225-247.

RASHDAN, N. A., RUTSCH, F., KEMPF, H., VÁRADI, A., LEFTHÉRIOTIS, G. & MACRAE, V. E. 2016. New perspectives on rare connective tissue calcifying diseases. *Current Opinion in Pharmacology,* 28**,** 14-23.

RATHBUN, J. C. 1948. "HYPOPHOSPHATASIA": A New Developmental Anomaly. *American Journal of Diseases of Children,* 75**,** 822-831.

RAVUSSIN, E. & KOZAK, L. P. 2009. Have we entered the brown adipose tissue renaissance? *Obes Rev,* 10**,** 265-8.

REAVEN, G. 2004. The metabolic syndrome or the insulin resistance syndrome? Different names, different concepts, and different goals. *Endocrinol Metab Clin North Am,* 33**,** 283-303.

REAVEN, G. M. 1988. Role of Insulin Resistance in Human Disease. *Diabetes,* 37**,** 1595.

REES, D. A. & ALCOLADO, J. C. 2005. Animal models of diabetes mellitus. *Diabet Med,* 22**,** 359-70.

REGAN, J. N., LIM, J., SHI, Y., JOENG, K. S., ARBEIT, J. M., SHOHET, R. V. & LONG, F. 2014. Up-regulation of glycolytic metabolism is required for HIF1alpha-driven bone formation. *Proc Natl Acad Sci U S A,* 111**,** 8673-8.

REILLY, S. M. & SALTIEL, A. R. 2017. Adapting to obesity with adipose tissue inflammation. *Nat Rev Endocrinol,* 13**,** 633-643.

REINEHR, T. & ROTH, C. L. 2010. A new link between skeleton, obesity and insulin resistance: relationships between osteocalcin, leptin and insulin resistance in obese children before and after weight loss. *International Journal of Obesity,* 34**,** 852-858.

RHO, J.-Y., KUHN-SPEARING, L. & ZIOUPOS, P. 1998. Mechanical properties and the hierarchical structure of bone. *Medical Engineering & Physics,* 20**,** 92-102.

RHO, J. Y., TSUI, T. Y. & PHARR, G. M. 1997. Elastic properties of human cortical and trabecular lamellar bone measured by nanoindentation. *Biomaterials,* 18**,** 1325-30.

RICHARD, D., CARPENTIER, A. C., DORÉ, G., OUELLET, V. & PICARD, F. 2010. Determinants of brown adipocyte development and thermogenesis. *International Journal of Obesity,* 34**,** S59-S66.

RICHARD, D. & PICARD, F. 2011. Brown fat biology and thermogenesis. *Front Biosci (Landmark Ed),* 16**,** 1233-60.

RIDDLE, R. C. & CLEMENS, T. L. 2017. Bone Cell Bioenergetics and Skeletal Energy Homeostasis. *Physiological reviews,* 97**,** 667-698.

RINELLA, M. E., ELIAS, M. S., SMOLAK, R. R., FU, T., BORENSZTAJN, J. & GREEN, R. M. 2008. Mechanisms of hepatic steatosis in mice fed a lipogenic methionine choline-deficient diet. *J Lipid Res,* 49**,** 1068-76.

ROACH, H. I. 1990. Long-term organ culture of embryonic chick femora: A system for investigating bone and cartilage formation at an intermediate level of organization. *Journal of Bone and Mineral Research,* 5**,** 85-100.

ROBERTS, F., ZHU, D., FARQUHARSON, C. & MACRAE, V. 2019a. *ENPP1 in the Regulation of Mineralization and Beyond*.

ROBERTS, F., ZHU, D., FARQUHARSON, C. & MACRAE, V. E. 2019b. ENPP1 in the Regulation of Mineralization and Beyond. *Trends in Biochemical Sciences*.

ROBERTS, S., NARISAWA, S., HARMEY, D., MILLAN, J. L. & FARQUHARSON, C. 2007a. Functional involvement of PHOSPHO1 in matrix vesicle-mediated skeletal mineralization. *J Bone Miner Res,* 22**,** 617-27.

ROBERTS, S., NARISAWA, S., HARMEY, D., MILLÁN, J. L. & FARQUHARSON, C. 2007b. Functional Involvement of PHOSPHO1 in Matrix Vesicle–Mediated Skeletal Mineralization. *Journal of Bone and Mineral Research,* 22**,** 617-627.

ROBLING, A. G. & TURNER, C. H. 2009. Mechanical signaling for bone modeling and remodeling. *Critical reviews in eukaryotic gene expression,* 19**,** 319-338.

ROBSON, S. C., WU, Y., SUN, X., KNOSALLA, C., DWYER, K. & ENJYOJI, K. 2005. Ectonucleotidases of CD39 family modulate vascular inflammation and thrombosis in transplantation. *Semin Thromb Hemost,* 31**,** 217-33.

RODRIGUEZ, J. P., ASTUDILLO, P., RIOS, S. & PINO, A. M. 2008. Involvement of adipogenic potential of human bone marrow mesenchymal stem cells (MSCs) in osteoporosis. *Curr Stem Cell Res Ther,* 3**,** 208-18.

ROGLIC, G. 2016. WHO Global report on diabetes: A summary. *Int J Non-Commun Dis,* 1.

ROMANELLI, F., CORBO, A., SALEHI, M., YADAV, M. C., SALMAN, S., PETROSIAN, D., RASHIDBAIGI, O. J., CHAIT, J., KURUVILLA, J., PLUMMER, M., RADICHEV, I., MARGULIES, K. B., GERDES, A. M., PINKERTON, A. B., MILLAN, J. L., SAVINOV, A. Y. & SAVINOVA, O. V. 2017. Overexpression of tissue-nonspecific alkaline phosphatase (TNAP) in endothelial cells accelerates coronary artery disease in a mouse model of familial hypercholesterolemia. *PLoS One,* 12**,** e0186426.

ROSEN, C. J. & BOUXSEIN, M. L. 2006. Mechanisms of Disease: is osteoporosis the obesity of bone? *Nature Clinical Practice Rheumatology,* 2**,** 35-43.

ROSS, R., DAGNONE, D., JONES, P. J., SMITH, H., PADDAGS, A., HUDSON, R. & JANSSEN, I. 2000. Reduction in obesity and related comorbid conditions after diet-induced weight loss or exercise-induced weight loss in men. A randomized, controlled trial. *Ann Intern Med,* 133**,** 92-103.

ROURA, E., KOOPMANS, S. J., LALLES, J. P., LE HUEROU-LURON, I., DE JAGER, N., SCHUURMAN, T. & VAL-LAILLET, D. 2016. Critical review evaluating the pig as a model for human nutritional physiology. *Nutr Res Rev,* 29**,** 60-90.

RUTHERFORD, R. B., FOSTER, B. L., BAMMLER, T., BEYER, R. P., SATO, S. & SOMERMAN, M. J. 2006. Extracellular Phosphate Alters Cementoblast Gene Expression. *Journal of Dental Research,* 85**,** 505-509.

RUTKOVSKIY, A., STENSLOKKEN, K. O. & VAAGE, I. J. 2016. Osteoblast Differentiation at a Glance. *Med Sci Monit Basic Res,* 22**,** 95-106.

RUTKOWSKI, J. M., STERN, J. H. & SCHERER, P. E. 2015. The cell biology of fat expansion. *The Journal of Cell Biology,* 208**,** 501.

RUTSCH, F., RUF, N., VAINGANKAR, S., TOLIAT, M. R., SUK, A., HOHNE, W., SCHAUER, G., LEHMANN, M., ROSCIOLI, T., SCHNABEL, D., EPPLEN, J. T., KNISELY, A., SUPERTI-FURGA, A., MCGILL, J., FILIPPONE, M., SINAIKO, A. R., VALLANCE, H., HINRICHS, B., SMITH, W., FERRE, M., TERKELTAUB, R. & NURNBERG, P. 2003. Mutations in ENPP1 are associated with 'idiopathic' infantile arterial calcification. *Nat Genet,* 34**,** 379-81.

RUTSCH, F., VAINGANKAR, S., JOHNSON, K., GOLDFINE, I., MADDUX, B., SCHAUERTE, P., KALHOFF, H., SANO, K., BOISVERT, W. A., SUPERTI-FURGA, A. & TERKELTAUB, R. 2001. PC-1 nucleoside triphosphate pyrophosphohydrolase deficiency in idiopathic infantile arterial calcification. *The American journal of pathology,* 158**,** 543-554.

SAFTIG, P., HUNZIKER, E., WEHMEYER, O., JONES, S., BOYDE, A., ROMMERSKIRCH, W., MORITZ, J. D., SCHU, P. & VON FIGURA, K. 1998. Impaired osteoclastic bone resorption leads to osteopetrosis in cathepsin-K-deficient mice. *Proc Natl Acad Sci U S A,* 95**,** 13453-8.

SAHAI, A., MALLADI, P., MELIN-ALDANA, H., GREEN, R. M. & WHITINGTON, P. F. 2004. Upregulation of osteopontin expression is involved in the development of nonalcoholic steatohepatitis in a dietary murine model. *Am J Physiol Gastrointest Liver Physiol,* 287**,** G264-73.

SAIDAK, Z., LE HENAFF, C., AZZI, S., MARTY, C., DA NASCIMENTO, S., SONNET, P. & MARIE, P. J. 2015. Wnt/beta-catenin signaling mediates osteoblast differentiation triggered by peptide-induced alpha5beta1 integrin priming in mesenchymal skeletal cells. *J Biol Chem,* 290**,** 6903-12.

SAITO, D., YONEI-TAMURA, S., TAKAHASHI, Y. & TAMURA, K. 2006. Level-specific role of paraxial mesoderm in regulation of Tbx5/Tbx4 expression and limb initiation. *Dev Biol,* 292**,** 79-89.

SAKAGAMI, H., AOKI, J., NATORI, Y., NISHIKAWA, K., KAKEHI, Y., NATORI, Y. & ARAI, H. 2005. Biochemical and molecular characterization of a novel choline-specific glycerophosphodiester phosphodiesterase belonging to the nucleotide pyrophosphatase/phosphodiesterase family. *J Biol Chem,* 280**,** 23084-93.

SAKAMOTO, M., HOSODA, Y., KOJIMAHARA, K., YAMAZAKI, T. & YOSHIMURA, Y. 1994. Arthritis and ankylosis in twy mice with hereditary multiple osteochondral lesions: With special reference to calcium deposition. *Pathology International,* 44**,** 420-427.

SALMON, D. M. & HEMS, D. A. 1973. Plasma lipoproteins and the synthesis and turnover of plasma triglyceride in normal and genetically obese mice. *The Biochemical journal,* 136**,** 551-563.

SALO, J., LEHENKARI, P., MULARI, M., METSIKKÖ, K. & VÄÄNÄNEN, H. K. 1997. Removal of Osteoclast Bone Resorption Products by Transcytosis. *Science,* 276**,** 270.

SANDER, J. D. & JOUNG, J. K. 2014. CRISPR-Cas systems for editing, regulating and targeting genomes. *Nature Biotechnology,* 32**,** 347-355.

SANDOVAL, D., COTA, D. & SEELEY, R. J. 2008. The integrative role of CNS fuel-sensing mechanisms in energy balance and glucose regulation. *Annu Rev Physiol,* 70**,** 513-35.

SARKAR, P. D. & CHOUDHURY, A. B. 2013. Relationships between serum osteocalcin levels versus blood glucose, insulin resistance and markers of systemic inflammation in central Indian type 2 diabetic patients. *Eur Rev Med Pharmacol Sci,* 17**,** 1631-5.

SATOYOSHI, M., KAWATA, A., KOIZUMI, T., INOUE, K., ITOHARA, S., TERANAKA, T. & MIKUNI-TAKAGAKI, Y. 2001. Matrix metalloproteinase-2 in dentin matrix mineralization. *J Endod,* 27**,** 462-6.

SAVARI, F., MARD, S. A., BADAVI, M., REZAIE, A. & GHARIB-NASERI, M. K. 2019. A new method to induce nonalcoholic steatohepatitis (NASH) in mice. *BMC Gastroenterology,* 19**,** 125.

SAVINOV, A. Y., SALEHI, M., YADAV, M. C., RADICHEV, I., MILLAN, J. L. & SAVINOVA, O. V. 2015. Transgenic Overexpression of Tissue-Nonspecific Alkaline Phosphatase (TNAP) in Vascular Endothelium Results in Generalized Arterial Calcification. *J Am Heart Assoc,* 4.

SAYOLS-BAIXERAS, S., SUBIRANA, I., LLUIS-GANELLA, C., CIVEIRA, F., ROQUER, J., DO, A. N., ABSHER, D., CENARRO, A., MUNOZ, D., SORIANO-TARRAGA, C., JIMENEZ-CONDE, J., ORDOVAS, J. M., SENTI, M., ASLIBEKYAN, S., MARRUGAT, J., ARNETT, D. K. & ELOSUA, R. 2016. Identification and validation of seven new loci showing differential DNA methylation related to serum lipid profile: an epigenome-wide approach. The REGICOR study. *Hum Mol Genet,* 25**,** 4556-4565.

SCHEEN, A. J. & PAQUOT, N. 2013. Metformin revisited: A critical review of the benefit–risk balance in at-risk patients with type 2 diabetes. *Diabetes & Metabolism,* 39**,** 179-190.

SCHELLER, E. L., DOUCETTE, C. R., LEARMAN, B. S., CAWTHORN, W. P., KHANDAKER, S., SCHELL, B., WU, B., DING, S. Y., BREDELLA, M. A., FAZELI, P. K., KHOURY, B., JEPSEN, K. J., PILCH, P. F., KLIBANSKI, A., ROSEN, C. J. & MACDOUGALD, O. A. 2015. Region-specific variation in the properties of skeletal adipocytes reveals regulated and constitutive marrow adipose tissues. *Nat Commun,* 6**,** 7808.

SCHELLER, E. L. & ROSEN, C. J. 2014. What's the matter with MAT? Marrow adipose tissue, metabolism, and skeletal health. *Ann N Y Acad Sci,* 1311**,** 14-30.

SCHELLER, E. L., TROIANO, N., VANHOUTAN, J. N., BOUXSEIN, M. A., FRETZ, J. A., XI, Y., NELSON, T., KATZ, G., BERRY, R., CHURCH, C. D., DOUCETTE, C. R., RODEHEFFER, M. S., MACDOUGALD, O. A., ROSEN, C. J. & HOROWITZ, M. C. 2014. Use of osmium tetroxide staining with microcomputerized tomography to visualize and quantify bone marrow adipose tissue in vivo. *Methods in enzymology,* 537**,** 123-139.

SCHINDELER, A., MCDONALD, M. M., BOKKO, P. & LITTLE, D. G. 2008. Bone remodeling during fracture repair: The cellular picture. *Semin Cell Dev Biol,* 19**,** 459-66.

SCHOFIELD, R. 1978. The relationship between the spleen colony-forming cell and the haemopoietic stem cell. *Blood Cells,* 4**,** 7-25.

SEEMAN, E. 2001. Clinical review 137: sexual dimorphism in skeletal size, density, and strength. *Journal of Clinical Endocrinology and Metabolism,* 86**,** 4576-4584.

SEEMAN, E. 2009. Bone modeling and remodeling. *Crit Rev Eukaryot Gene Expr,* 19**,** 219-33.

SEFEROVIC, M. D., BEAMISH, C. A., MOSSER, R. E., TOWNSEND, S. E., PAPPAN, K., POITOUT, V., AAGAARD, K. M. & GANNON, M. 2018. Increases in bioactive lipids accompany early metabolic changes associated with beta-cell expansion in response to short-term high-fat diet. *Am J Physiol Endocrinol Metab,* 315**,** E1251-e1263.

SELIGER, W. G. 1970. Tissue fluid movement in compact bone. *Anat Rec,* 166**,** 247-55.

SENA, C. M., MATAFOME, P., LOURO, T., NUNES, E., FERNANDES, R. & SEIÇA, R. M. 2011. Metformin restores endothelial function in aorta of diabetic rats. *British journal of pharmacology,* 163**,** 424-437.

SHAN, C., GHOSH, A., GUO, X.-Z., WANG, S.-M., HOU, Y.-F., LI, S.-T. & LIU, J.-M. 2019. Roles for osteocalcin in brain signalling: implications in cognition- and motor-related disorders. *Molecular Brain,* 12**,** 23.

SHAPIRO, F. 1997. Variable conformation of GAP junctions linking bone cells: a transmission electron microscopic study of linear, stacked linear, curvilinear, oval, and annular junctions. *Calcif Tissue Int,* 61**,** 285-93.

SHEN, G. 2005. The role of type X collagen in facilitating and regulating endochondral ossification of articular cartilage. *Orthod Craniofac Res,* 8**,** 11-7.

SHEN, S. W., REAVEN, G. M. & FARQUHAR, J. W. 1970. Comparison of impedance to insulin-mediated glucose uptake in normal subjects and in subjects with latent diabetes. *The Journal of clinical investigation,* 49**,** 2151-2160.

SHU, Y., SHEARDOWN, S. A., BROWN, C., OWEN, R. P., ZHANG, S., CASTRO, R. A., IANCULESCU, A. G., YUE, L., LO, J. C., BURCHARD, E. G., BRETT, C. M. & GIACOMINI, K. M. 2007. Effect of genetic variation in the organic cation transporter 1 (OCT1) on metformin action. *J Clin Invest,* 117**,** 1422-31.

SINAIKO, A. R. & CAPRIO, S. 2012. Insulin resistance. *The Journal of pediatrics,* 161**,** 11-15.

SINGH, I. 1978. The architecture of cancellous bone. *Journal of anatomy,* 127**,** 305-310.

SKERRY, T. M. 2008. The response of bone to mechanical loading and disuse: fundamental principles and influences on osteoblast/osteocyte homeostasis. *Arch Biochem Biophys,* 473**,** 117-23.

SMITH, M. R. W., KAWCAK, C. E. & MCILWRAITH, C. W. 2016. Science in brief: Report on the Havemeyer Foundation workshop on subchondral bone problems in the equine athlete. *Equine Veterinary Journal,* 48**,** 6-8.

SMITH, R. E. & HOCK, R. J. 1963. Brown Fat: Thermogenic Effector of Arousal in Hibernators. *Science,* 140**,** 199.

SOFFE, Z., RADLEY-CRABB, H. G., MCMAHON, C., GROUNDS, M. D. & SHAVLAKADZE, T. 2016. Effects of loaded voluntary wheel exercise on performance and muscle hypertrophy in young and old male C57Bl/6J mice. *Scandinavian Journal of Medicine & Science in Sports,* 26**,** 172-188.

SOMMER, B., BICKEL, M., HOFSTETTER, W. & WETTERWALD, A. 1996. Expression of matrix proteins during the development of mineralized tissues. *Bone,* 19**,** 371-80.

SOMMERFELDT, D. W. & RUBIN, C. T. 2001. Biology of bone and how it orchestrates the form and function of the skeleton. *Eur Spine J,* 10 Suppl 2**,** S86-95.

SOPHIA FOX, A. J., BEDI, A. & RODEO, S. A. 2009. The basic science of articular cartilage: structure, composition, and function. *Sports health,* 1**,** 461-468.

SPALDING, K. L., ARNER, E., WESTERMARK, P. O., BERNARD, S., BUCHHOLZ, B. A., BERGMANN, O., BLOMQVIST, L., HOFFSTEDT, J., NASLUND, E., BRITTON, T., CONCHA, H., HASSAN, M., RYDEN, M., FRISEN, J. & ARNER, P. 2008. Dynamics of fat cell turnover in humans. *Nature,* 453**,** 783-7.

SQUIER, C. A., GHONEIM, S. & KREMENAK, C. R. 1990. Ultrastructure of the periosteum from membrane bone. *Journal of anatomy,* 171**,** 233-239.

STAINES, K. A., JAVAHERI, B., HOHENSTEIN, P., FLEMING, R., IKPEGBU, E., UNGER, E., HOPKINSON, M., BUTTLE, D. J., PITSILLIDES, A. A. & FARQUHARSON, C. 2017. Hypomorphic conditional deletion of E11/Podoplanin reveals a role in osteocyte dendrite elongation. *Journal of cellular physiology,* 232**,** 3006-3019.

STAINES, K. A., MACKENZIE, N. C. W., CLARKIN, C. E., ZELENCHUK, L., ROWE, P. S., MACRAE, V. E. & FARQUHARSON, C. 2012a. MEPE is a novel regulator of growth plate cartilage mineralization. *Bone,* 51**,** 418-430.

STAINES, K. A., MACRAE, V. E. & FARQUHARSON, C. 2012b. The importance of the SIBLING family of proteins on skeletal mineralisation and bone remodelling. *J Endocrinol,* 214**,** 241-55.

STEFAN, C., JANSEN, S. & BOLLEN, M. 2005. NPP-type ectophosphodiesterases: unity in diversity. *Trends in Biochemical Sciences,* 30**,** 542-550.

STEIN, G. S., LIAN, J. B., WIJNEN, A. J. V., STEIN, J. L., MONTECINO, M., JAVED, A., ZAIDI, S. K., YOUNG, D. W., CHOI, J.-Y. & POCKWINSE, S. M. 2004. Runx2 control of organization, assembly and activity of the regulatory machinery for skeletal gene expression. *Oncogene,* 23**,** 4315-4329.

STEITZ, S. A., SPEER, M. Y., CURINGA, G., YANG, H. Y., HAYNES, P., AEBERSOLD, R., SCHINKE, T., KARSENTY, G. & GIACHELLI, C. M. 2001. Smooth muscle cell phenotypic transition associated with calcification: upregulation of Cbfa1 and downregulation of smooth muscle lineage markers. *Circ Res,* 89**,** 1147-54.

STEPHENSON, K., KENNEDY, L., HARGROVE, L., DEMIEVILLE, J., THOMSON, J., ALPINI, G. & FRANCIS, H. 2018. Updates on Dietary Models of Nonalcoholic Fatty Liver Disease: Current Studies and Insights. *Gene expression,* 18**,** 5-17.

STERN, A. R., STERN, M. M., VAN DYKE, M. E., JAHN, K., PRIDEAUX, M. & BONEWALD, L. F. 2012. Isolation and culture of primary osteocytes from the long bones of skeletally mature and aged mice. *Biotechniques,* 52**,** 361-73.

STEWART, A. J., LEONG, D. T. K. & FARQUHARSON, C. 2017. PLA2 and ENPP6 may act in concert to generate phosphocholine from the matrix vesicle membrane during skeletal mineralization. *The FASEB Journal,* 32**,** 20-25.

STEWART, A. J., ROBERTS, S. J., SEAWRIGHT, E., DAVEY, M. G., FLEMING, R. H. & FARQUHARSON, C. 2006. The presence of PHOSPHO1 in matrix vesicles and its developmental expression prior to skeletal mineralization. *Bone,* 39**,** 1000-1007.

STEWART, H. L. & KAWCAK, C. E. 2018. The Importance of Subchondral Bone in the Pathophysiology of Osteoarthritis. *Frontiers in veterinary science,* 5**,** 178-178.

STOKES, I. A., MENTE, P. L., IATRIDIS, J. C., FARNUM, C. E. & ARONSSON, D. D. 2002. Enlargement of growth plate chondrocytes modulated by sustained mechanical loading. *J Bone Joint Surg Am,* 84**,** 1842-8.

STOLERMAN, E. S., MANNING, A. K., MCATEER, J. B., DUPUIS, J., FOX, C. S., CUPPLES, L. A., MEIGS, J. B. & FLOREZ, J. C. 2008. Haplotype Structure of the ENPP1 Gene and Nominal Association of the K121Q Missense Single Nucleotide Polymorphism With Glycemic Traits in the Framingham Heart Study. *Diabetes,* 57**,** 1971-1977.

STOUT, R. W. 1990. Insulin and Atheroma: 20-Yr Perspective. *Diabetes Care,* 13**,** 631.

STRACKE, M. L., KRUTZSCH, H. C., UNSWORTH, E. J., ARESTAD, A., CIOCE, V., SCHIFFMANN, E. & LIOTTA, L. A. 1992. Identification, purification, and partial sequence analysis of autotaxin, a novel motility-stimulating protein. *J Biol Chem,* 267**,** 2524-9.

STYNER, M., PAGNOTTI, G. M., GALIOR, K., WU, X., THOMPSON, W. R., UZER, G., SEN, B., XIE, Z., HOROWITZ, M. C., STYNER, M. A., RUBIN, C. & RUBIN, J. 2015. Exercise Regulation of Marrow Fat in the Setting of PPARγ Agonist Treatment in Female C57BL/6 Mice. *Endocrinology,* 156**,** 2753-2761.

STYNER, M., THOMPSON, W. R., GALIOR, K., UZER, G., WU, X., KADARI, S., CASE, N., XIE, Z., SEN, B., ROMAINE, A., PAGNOTTI, G. M., RUBIN, C. T., STYNER, M. A., HOROWITZ, M. C. &

RUBIN, J. 2014. Bone marrow fat accumulation accelerated by high fat diet is suppressed by exercise. *Bone,* 64**,** 39-46.

SUCHACKI, K. J., ROBERTS, F., LOVDEL, A., FARQUHARSON, C., MORTON, N. M., MACRAE, V. E. & CAWTHORN, W. P. 2017. Skeletal energy homeostasis: a paradigm of endocrine discovery. *J Endocrinol,* 234**,** R67-r79.

SUDO, H., KODAMA, H. A., AMAGAI, Y., YAMAMOTO, S. & KASAI, S. 1983. In vitro differentiation and calcification in a new clonal osteogenic cell line derived from newborn mouse calvaria. *The Journal of cell biology,* 96**,** 191-198.

SURWIT, R. S., WANG, S., PETRO, A. E., SANCHIS, D., RAIMBAULT, S., RICQUIER, D. & COLLINS, S. 1998. Diet-induced changes in uncoupling proteins in obesity-prone and obesity-resistant strains of mice. *Proceedings of the National Academy of Sciences,* 95**,** 4061.

SWEET, H. O. & GREEN, M. C. 1981. Progressive ankylosis, a new skeletal mutation in the mouse. *J Hered,* 72**,** 87-93.

TAKAHASHI, Y., SOEJIMA, Y. & FUKUSATO, T. 2012. Animal models of nonalcoholic fatty liver disease/nonalcoholic steatohepatitis. *World journal of gastroenterology,* 18**,** 2300-2308.

TAKIZAWA, H., BOETTCHER, S. & MANZ, M. G. 2012. Demand-adapted regulation of early hematopoiesis in infection and inflammation. *Blood,* 119**,** 2991-3002.

TALWAR, R. M., WONG, B. S., SVOBODA, K. & HARPER, R. P. 2006. Effects of estrogen on chondrocyte proliferation and collagen synthesis in skeletally mature articular cartilage. *J Oral Maxillofac Surg,* 64**,** 600-9.

TANDON, N., ANJANA, R., MOHAN, V., KAUR, T., AFSHIN, A., ONG, K., MUKHOPADHYAY, S., THOMAS, N., BHATIA, E., KRISHNAN, A., MATHUR, P., DHALIWAL, R. S., SHUKLA, D., BHANSALI, A., DORAIRAJ, P., PATURI, V. R., YAJNIK, C., KUMAR, G. A., VARGHESE, C. & DANDONA, L. 2018. The increasing burden of diabetes and variations among the states of India: the Global Burden of Disease Study 1990-2016. *LANCET GLOBAL HEALTH,* 6.

TARNOWSKI, C. P., IGNELZI, M. A., JR. & MORRIS, M. D. 2002. Mineralization of developing mouse calvaria as revealed by Raman microspectroscopy. *J Bone Miner Res,* 17**,** 1118-26.

TAYLOR, S. E. B., SHAH, M. & ORRISS, I. R. 2014. Generation of rodent and human osteoblasts. *BoneKEy reports,* 3**,** 585-585.

TEITELBAUM, S. L. 2000. Bone resorption by osteoclasts. *Science,* 289**,** 1504-8.

TEITELBAUM, S. L. 2011. The osteoclast and its unique cytoskeleton. *Ann N Y Acad Sci,* 1240**,** 14-7.

TENCEROVA, M., FIGEAC, F., DITZEL, N., TAIPALEENMAKI, H., NIELSEN, T. K. & KASSEM, M. 2018. High-Fat Diet-Induced Obesity Promotes Expansion of Bone Marrow Adipose Tissue and Impairs Skeletal Stem Cell Functions in Mice. *J Bone Miner Res,* 33**,** 1154-1165.

TERKELTAUB, R. 2006. Physiologic and pathologic functions of the NPP nucleotide pyrophosphatase/phosphodiesterase family focusing on NPP1 in calcification. *Purinergic signalling,* 2**,** 371-377.

TERKELTAUB, R. A. 2001. Inorganic pyrophosphate generation and disposition in pathophysiology. *American Journal of Physiology-Cell Physiology,* 281**,** C1-C11.

THEUWISSEN, E., SMIT, E. & VERMEER, C. 2012. The Role of Vitamin K in Soft-Tissue Calcification. *Advances in Nutrition,* 3**,** 166-173.

THOMAS, A., STEVENS, A. P., KLEIN, M. S., HELLERBRAND, C., DETTMER, K., GRONWALD, W., OEFNER, P. J. & REINDERS, J. 2012. Early changes in the liver-soluble proteome from mice fed a nonalcoholic steatohepatitis inducing diet. *PROTEOMICS,* 12**,** 1437-1451.

THRAILKILL, K., BUNN, R. C., LUMPKIN, C., JR., WAHL, E., COCKRELL, G., MORRIS, L., KAHN, C. R., FOWLKES, J. & NYMAN, J. S. 2014. Loss of insulin receptor in osteoprogenitor cells impairs structural strength of bone. *J Diabetes Res,* 2014**,** 703589.

TIIKKAINEN, M., HÄKKINEN, A.-M., KORSHENINNIKOVA, E., NYMAN, T., MÄKIMATTILA, S. & YKI-JÄRVINEN, H. 2004. Effects of Rosiglitazone and Metformin on Liver Fat Content, Hepatic

Insulin Resistance, Insulin Clearance, and Gene Expression in Adipose Tissue in Patients With Type 2 Diabetes. *Diabetes,* 53**,** 2169.

TILG, H. & HOTAMISLIGIL, G. S. 2006. Nonalcoholic fatty liver disease: Cytokine-adipokine interplay and regulation of insulin resistance. *Gastroenterology,* 131**,** 934-45.

TING, W.-J., HUANG, C.-Y., JIANG, C.-H., LIN, Y.-M., CHUNG, L.-C., SHEN, C.-Y., PAI, P., LIN, K.-H., VISWANADHA, V. P. & LIAO, S.-C. 2017. Treatment with 17β-Estradiol Reduced Body Weight and the Risk of Cardiovascular Disease in a High-Fat Diet-Induced Animal Model of Obesity. *International journal of molecular sciences,* 18**,** 629.

TOKUMURA, A., MAJIMA, E., KARIYA, Y., TOMINAGA, K., KOGURE, K., YASUDA, K. & FUKUZAWA, K. 2002. Identification of human plasma lysophospholipase D, a lysophosphatidic acid-producing enzyme, as autotaxin, a multifunctional phosphodiesterase. *J Biol Chem,* 277**,** 39436-42.

TOLEDO, F. G., MENSHIKOVA, E. V., AZUMA, K., RADIKOVA, Z., KELLEY, C. A., RITOV, V. B. & KELLEY, D. E. 2008. Mitochondrial capacity in skeletal muscle is not stimulated by weight loss despite increases in insulin action and decreases in intramyocellular lipid content. *Diabetes,* 57**,** 987-94.

TONG, X., GU, J., SONG, R., WANG, D., SUN, Z., SUI, C., ZHANG, C., LIU, X., BIAN, J. & LIU, Z. 2018. Osteoprotegerin inhibit osteoclast differentiation and bone resorption by enhancing autophagy via AMPK/mTOR/p70S6K signaling pathway in vitro. *J Cell Biochem*.

TRAUB, W., ARAD, T. & WEINER, S. 1989. Three-dimensional ordered distribution of crystals in turkey tendon collagen fibers. *Proc Natl Acad Sci U S A,* 86**,** 9822-6.

TRAUB, W., ARAD, T. & WEINER, S. 1992. Origin of Mineral Crystal Growth in Collagen Fibrils. *Matrix,* 12**,** 251-255.

TRAYHURN, P. 2018. Brown Adipose Tissue—A Therapeutic Target in Obesity? *Frontiers in Physiology,* 9.

TSAI, S. H., KINOSHITA, M., KUSU, T., KAYAMA, H., OKUMURA, R., IKEDA, K., SHIMADA, Y., TAKEDA, A., YOSHIKAWA, S., OBATA-NINOMIYA, K., KURASHIMA, Y., SATO, S., UMEMOTO, E., KIYONO, H., KARASUYAMA, H. & TAKEDA, K. 2015. The ectoenzyme E-NPP3 negatively regulates ATP-dependent chronic allergic responses by basophils and mast cells. *Immunity,* 42**,** 279-293.

TSENG, Y. H., CYPESS, A. M. & KAHN, C. R. 2010. Cellular bioenergetics as a target for obesity therapy. *Nat Rev Drug Discov,* 9**,** 465-82.

TU, L. N., SHOWALTER, M. R., CAJKA, T., FAN, S., PILLAI, V. V., FIEHN, O. & SELVARAJ, V. 2017. Metabolomic characteristics of cholesterol-induced non-obese nonalcoholic fatty liver disease in mice. *Sci Rep,* 7**,** 6120.

TUOMILEHTO, J., LINDSTRÖM, J., ERIKSSON, J. G., VALLE, T. T., HÄMÄLÄINEN, H., ILANNE-PARIKKA, P., KEINÄNEN-KIUKAANNIEMI, S., LAAKSO, M., LOUHERANTA, A., RASTAS, M., SALMINEN, V., AUNOLA, S., CEPAITIS, Z., MOLTCHANOV, V., HAKUMÄKI, M., MANNELIN, M., MARTIKKALA, V., SUNDVALL, J. & UUSITUPA, M. 2001a. Prevention of Type 2 Diabetes Mellitus by Changes in Lifestyle among Subjects with Impaired Glucose Tolerance. *New England Journal of Medicine,* 344**,** 1343-1350.

TUOMILEHTO, J., LINDSTROM, J., ERIKSSON, J. G., VALLE, T. T., HAMALAINEN, H., ILANNE-PARIKKA, P., KEINANEN-KIUKAANNIEMI, S., LAAKSO, M., LOUHERANTA, A., RASTAS, M., SALMINEN, V. & UUSITUPA, M. 2001b. Prevention of type 2 diabetes mellitus by changes in lifestyle among subjects with impaired glucose tolerance. *N Engl J Med,* 344**,** 1343-50.

UDAGAWA, N., TAKAHASHI, N., YASUDA, H., MIZUNO, A., ITOH, K., UENO, Y., SHINKI, T., GILLESPIE, M. T., MARTIN, T. J., HIGASHIO, K. & SUDA, T. 2000. Osteoprotegerin produced by osteoblasts is an important regulator in osteoclast development and function. *Endocrinology,* 141**,** 3478-84.

UMEZU-GOTO, M., KISHI, Y., TAIRA, A., HAMA, K., DOHMAE, N., TAKIO, K., YAMORI, T., MILLS, G. B., INOUE, K., AOKI, J. & ARAI, H. 2002. Autotaxin has lysophospholipase D activity leading to tumor cell growth and motility by lysophosphatidic acid production. *The Journal of cell biology,* 158**,** 227-233.

VAANANEN, H. K. & HARKONEN, P. L. 1996. Estrogen and bone metabolism. *Maturitas,* 23 Suppl**,** S65-9.

VAANANEN, H. K., ZHAO, H., MULARI, M., HALLEEN, J. M., VAANANEN, H. K., ZHAO, H., MULARI, M. & HALLEEN, J. M. 2000. The cell biology of osteoclast function. *Journal of Cell Science,* 113**,** 377-381.

VELÁZQUEZ, K. T., ENOS, R. T., BADER, J. E., SOUGIANNIS, A. T., CARSON, M. S., CHATZISTAMOU, I., CARSON, J. A., NAGARKATTI, P. S., NAGARKATTI, M. & MURPHY, E. A. 2019. Prolonged high-fat-diet feeding promotes non-alcoholic fatty liver disease and alters gut microbiota in mice. *World journal of hepatology,* 11**,** 619-637.

VILLEMURE, I. & STOKES, I. A. F. 2009. Growth plate mechanics and mechanobiology. A survey of present understanding. *Journal of biomechanics,* 42**,** 1793-1803.

VITALE, C., MERCURO, G., CORNOLDI, A., FINI, M., VOLTERRANI, M. & ROSANO, G. M. C. 2005. Metformin improves endothelial function in patients with metabolic syndrome. *Journal of Internal Medicine,* 258**,** 250-256.

VORHOFF, T., ZIMMERMANN, H., PELLETIER, J., SEVIGNY, J. & BRAUN, N. 2005. Cloning and characterization of the ecto-nucleotidase NTPDase3 from rat brain: Predicted secondary structure and relation to other members of the E-NTPDase family and actin. *Purinergic Signal,* 1**,** 259-70.

WANG, B., CHANDRASEKERA, P. C. & PIPPIN, J. J. 2014a. Leptin- and leptin receptor-deficient rodent models: relevance for human type 2 diabetes. *Curr Diabetes Rev,* 10**,** 131-45.

WANG, D., CHRISTENSEN, K., CHAWLA, K., XIAO, G., KREBSBACH, P. H. & FRANCESCHI, R. T. 1999a. Isolation and characterization of MC3T3-E1 preosteoblast subclones with distinct in vitro and in vivo differentiation/mineralization potential. *J Bone Miner Res,* 14**,** 893-903.

WANG, D., CHRISTENSEN, K., CHAWLA, K., XIAO, G., KREBSBACH, P. H. & FRANCESCHI, R. T. 1999b. Isolation and Characterization of MC3T3-E1 Preosteoblast Subclones with Distinct In Vitro and In Vivo Differentiation/Mineralization Potential. *Journal of Bone and Mineral Research,* 14**,** 893-903.

WANG, D.-S., JONKER, J. W., KATO, Y., KUSUHARA, H., SCHINKEL, A. H. & SUGIYAMA, Y. 2002. Involvement of Organic Cation Transporter 1 in Hepatic and Intestinal Distribution of Metformin. *Journal of Pharmacology and Experimental Therapeutics,* 302**,** 510.

WANG, J.-W., TANG, Q.-Y., RUAN, H.-J. & CAI, W. 2014b. Relation Between Serum Osteocalcin Levels and Body Composition in Obese Children. *Journal of Pediatric Gastroenterology and Nutrition,* 58**,** 729-732.

WAYMIRE, K. G., MAHUREN, J. D., JAJE, J. M., GUILARTE, T. R., COBURN, S. P. & MACGREGOR, G. R. 1995. Mice lacking tissue non-specific alkaline phosphatase die from seizures due to defective metabolism of vitamin B-6. *Nat Genet,* 11**,** 45-51.

WEI, J., HANNA, T., SUDA, N., KARSENTY, G. & DUCY, P. 2014. Osteocalcin promotes β-cell proliferation during development and adulthood through Gprc6a. *Diabetes,* 63**,** 1021-1031.

WEI, J. & KARSENTY, G. 2015a. An overview of the metabolic functions of osteocalcin. *Curr Osteoporos Rep,* 13**,** 180-5.

WEI, J. & KARSENTY, G. 2015b. An overview of the metabolic functions of osteocalcin. *Reviews in endocrine & metabolic disorders,* 16**,** 93-98.

WEIGENSBERG, M. J. & GORAN, M. I. 2009. Type 2 diabetes in children and adolescents. *Lancet,* 373**,** 1743-4.

WEISE, M., DE-LEVI, S., BARNES, K. M., GAFNI, R. I., ABAD, V. & BARON, J. 2001. Effects of estrogen on growth plate senescence and epiphyseal fusion. *Proc Natl Acad Sci U S A,* 98**,** 6871-6.

WELSH, G. I., GRIFFITHS, M. R., WEBSTER, K. J., PAGE, M. J. & TAVARE, J. M. 2004. Proteome analysis of adipogenesis. *Proteomics,* 4**,** 1042-51.

WELTMAN, M. D., FARRELL, G. C. & LIDDLE, C. 1996. Increased hepatocyte CYP2E1 expression in a rat nutritional model of hepatic steatosis with inflammation. *Gastroenterology,* 111**,** 1645-53.

WENNBERG, C., HESSLE, L., LUNDBERG, P., MAURO, S., NARISAWA, S., LERNER, U. H. & MILLAN, J. L. 2000. Functional characterization of osteoblasts and osteoclasts from alkaline phosphatase knockout mice. *J Bone Miner Res,* 15**,** 1879-88.

WHITE, P. J. & MARETTE, A. 2014. Potential role of omega-3-derived resolution mediators in metabolic inflammation. *Immunol Cell Biol,* 92**,** 324-30.

WHITE, Z., TERRILL, J., WHITE, R. B., MCMAHON, C., SHEARD, P., GROUNDS, M. D. & SHAVLAKADZE, T. 2016. Voluntary resistance wheel exercise from mid-life prevents sarcopenia and increases markers of mitochondrial function and autophagy in muscles of old male and female C57BL/6J mice. *Skeletal Muscle,* 6**,** 45.

WHYTE, M. P., MAHUREN, J. D., FEDDE, K. N., COLE, F. S., MCCABE, E. R. & COBURN, S. P. 1988. Perinatal hypophosphatasia: tissue levels of vitamin B6 are unremarkable despite markedly increased circulating concentrations of pyridoxal-5'-phosphate. Evidence for an ectoenzyme role for tissue-nonspecific alkaline phosphatase. *J Clin Invest,* 81**,** 1234-9.

WHYTE, M. P., ZHANG, F., WENKERT, D., MCALISTER, W. H., MACK, K. E., BENIGNO, M. C., COBURN, S. P., WAGY, S., GRIFFIN, D. M., ERICSON, K. L. & MUMM, S. 2015. Hypophosphatasia: Validation and expansion of the clinical nosology for children from 25years experience with 173 pediatric patients. *Bone,* 75**,** 229-239.

WILSON, A., LAURENTI, E., OSER, G., VAN DER WATH, R. C., BLANCO-BOSE, W., JAWORSKI, M., OFFNER, S., DUNANT, C. F., ESHKIND, L., BOCKAMP, E., LIO, P., MACDONALD, H. R. & TRUMPP, A. 2008. Hematopoietic stem cells reversibly switch from dormancy to self-renewal during homeostasis and repair. *Cell,* 135**,** 1118-29.

WINZELL, M. S. & AHRÉN, B. 2004. The High-Fat Diet–Fed Mouse. *Diabetes,* 53**,** S215.

WIREN, K., KEENAN, E., ZHANG, X., RAMSEY, B. & ORWOLL, E. 1999. Homologous Androgen Receptor Up-Regulation in Osteoblastic Cells May Be Associated with Enhanced Functional Androgen Responsiveness*. *Endocrinology,* 140**,** 3114-3124.

WIREN, K. M., ZHANG, X., CHANG, C., KEENAN, E. & ORWOLL, E. S. 1997. Transcriptional Up-Regulation of the Human Androgen Receptor by Androgen in Bone Cells*. *Endocrinology,* 138**,** 2291-2300.

WIT, J. M. & CAMACHO-HUBNER, C. 2011. Endocrine regulation of longitudinal bone growth. *Endocr Dev,* 21**,** 30-41.

WOHL, G. R., LOEHRKE, L., WATKINS, B. A. & ZERNICKE, R. F. 1998. Effects of high-fat diet on mature bone mineral content, structure, and mechanical properties. *Calcif Tissue Int,* 63**,** 74-9.

WRONSKI, T. J., MOREY-HOLTON, E. & JEE, W. S. S. 1981. Skeletal alterations in rats during space flight. *Advances in Space Research,* 1**,** 135-140.

WU, J., HANSEN, G. H., NILSSON, A. & DUAN, R. D. 2005. Functional studies of human intestinal alkaline sphingomyelinase by deglycosylation and mutagenesis. *Biochem J,* 386**,** 153-60.

WU, L. N., GENGE, B. R. & WUTHIER, R. E. 2008. Analysis and molecular modeling of the formation, structure, and activity of the phosphatidylserine-calcium-phosphate complex associated with biomineralization. *J Biol Chem,* 283**,** 3827-38.

WU, Y., DING, Y., TANAKA, Y. & ZHANG, W. 2014. Risk factors contributing to type 2 diabetes and recent advances in the treatment and prevention. *International journal of medical sciences,* 11**,** 1185-1200.

WUTHIER, R. E. & LIPSCOMB, G. F. 2011. Matrix vesicles: structure, composition, formation and function in calcification. *Front Biosci (Landmark Ed),* 16**,** 2812-902.

XU, H., XIAO, W., LUO, D., LIU, Y.-M., ZOU, L. & KUANG, H.-B. 2010. Association analysis of genetic polymorphisms and potential interaction of the osteocalcin (BGP) and ER-α genes with body mass index (BMI) in premenopausal Chinese women. *Acta Pharmacologica Sinica,* 31**,** 455-460.

XU, Y., HAN, J., DONG, J., FAN, X., CAI, Y., LI, J., WANG, T., ZHOU, J. & SHANG, J. 2019. Metabolomics Characterizes the Effects and Mechanisms of Quercetin in Nonalcoholic Fatty Liver Disease Development. *International journal of molecular sciences,* 20**,** 1220.

YADAV, M. C., SIMAO, A. M., NARISAWA, S., HUESA, C., MCKEE, M. D., FARQUHARSON, C. & MILLAN, J. L. 2011a. Loss of skeletal mineralization by the simultaneous ablation of PHOSPHO1 and alkaline phosphatase function: a unified model of the mechanisms of initiation of skeletal calcification. *J Bone Miner Res,* 26**,** 286-97.

YADAV, M. C., SIMÃO, A. M. S., NARISAWA, S., HUESA, C., MCKEE, M. D., FARQUHARSON, C. & MILLÁN, J. L. 2011b. Loss of skeletal mineralization by the simultaneous ablation of PHOSPHO1 and alkaline phosphatase function: a unified model of the mechanisms of initiation of skeletal calcification. *Journal of bone and mineral research : the official journal of the American Society for Bone and Mineral Research,* 26**,** 286-297.

YAMADA, M. & OZAWA, H. 1978. Ultrastructural and cytochemical studies on the matrix vesicle calcification in the teeth of the killifish, Oryzias latipes. *Arch Histol Jpn,* 41**,** 309-23.

YANG, G., BADEANLOU, L., BIELAWSKI, J., ROBERTS, A. J., HANNUN, Y. A. & SAMAD, F. 2009. Central role of ceramide biosynthesis in body weight regulation, energy metabolism, and the metabolic syndrome. *American Journal of Physiology-Endocrinology and Metabolism,* 297**,** E211-E224.

YANG, J., ZHANG, X., WANG, W. & LIU, J. 2010. Insulin stimulates osteoblast proliferation and differentiation through ERK and PI3K in MG-63 cells. *Cell Biochem Funct,* 28**,** 334-41.

YANG, L., TSANG, K. Y., TANG, H. C., CHAN, D. & CHEAH, K. S. 2014. Hypertrophic chondrocytes can become osteoblasts and osteocytes in endochondral bone formation. *Proc Natl Acad Sci U S A,* 111**,** 12097-102.

YANO, T., FUNAKOSHI, I. & YAMASHINA, I. 1985. Purification and Properties of Nucleotide Pyrophosphatase from Human Placenta1. *The Journal of Biochemistry,* 98**,** 1097-1107.

YELLOWLEY, C. E., LI, Z., ZHOU, Z., JACOBS, C. R. & DONAHUE, H. J. 2000. Functional gap junctions between osteocytic and osteoblastic cells. *J Bone Miner Res,* 15**,** 209-17.

YEN, C. L., STONE, S. J., KOLIWAD, S., HARRIS, C. & FARESE, R. V., JR. 2008. Thematic review series: glycerolipids. DGAT enzymes and triacylglycerol biosynthesis. *J Lipid Res,* 49**,** 2283-301.

YEPURU, M., ESWARAKA, J., KEARBEY, J. D., BARRETT, C. M., RAGHOW, S., VEVERKA, K. A., MILLER, D. D., DALTON, J. T. & NARAYANAN, R. 2010. Estrogen receptor-{beta}-selective ligands alleviate high-fat diet- and ovariectomy-induced obesity in mice. *The Journal of biological chemistry,* 285**,** 31292-31303.

YIU, A. J., CALLAGHAN, D., SULTANA, R. & BANDYOPADHYAY, B. C. 2015. Vascular Calcification and Stone Disease: A New Look towards the Mechanism. *Journal of cardiovascular development and disease,* 2**,** 141-164.

YOSHIKAWA, Y., KODE, A., XU, L., MOSIALOU, I., SILVA, B. C., FERRON, M., CLEMENS, T. L., ECONOMIDES, A. N. & KOUSTENI, S. 2011. Genetic evidence points to an osteocalcin-independent influence of osteoblasts on energy metabolism. *J Bone Miner Res,* 26**,** 2012-25.

YOSHIKO, Y., CANDELIERE, G. A., MAEDA, N. & AUBIN, J. E. 2007. Osteoblast autonomous Pi regulation via Pit1 plays a role in bone mineralization. *Molecular and cellular biology,* 27**,** 4465-4474.

YOUNG, D. R., RICHARDSON, D. W., MARKEL, M. D. & NUNAMAKER, D. M. 1991. Mechanical and morphometric analysis of the third carpal bone of Thoroughbreds. *Am J Vet Res,* 52**,** 402-9.

YOUNG, M. F. 2003. Bone matrix proteins: their function, regulation, and relationship to osteoporosis. *Osteoporos Int,* 14 Suppl 3**,** S35-42.

ZAKARIA, E. & SHAFRIR, E. 1967. Yellow Bone Marrow as Adipose Tissue. *Proceedings of the Society for Experimental Biology and Medicine,* 124**,** 1265-1268.

ZEMA, M. J. 2012. Colesevelam hydrochloride: evidence for its use in the treatment of hypercholesterolemia and type 2 diabetes mellitus with insights into mechanism of action. *Core Evid,* 7**,** 61-75.

ZHANG, M., XUAN, S., BOUXSEIN, M. L., VON STECHOW, D., AKENO, N., FAUGERE, M. C., MALLUCHE, H., ZHAO, G., ROSEN, C. J., EFSTRATIADIS, A. & CLEMENS, T. L. 2002. Osteoblast-specific knockout of the insulin-like growth factor (IGF) receptor gene reveals an essential role of IGF signaling in bone matrix mineralization. *J Biol Chem,* 277**,** 44005-12.

ZHANG, Q., RIDDLE, R. C. & CLEMENS, T. L. 2015. Bone and the regulation of global energy balance. *Journal of internal medicine,* 277**,** 681-689.

ZHAO, J., KINGMAN, J., SUNDBERG, J. P., UITTO, J. & LI, Q. 2017. Plasma PPi Deficiency Is the Major, but Not the Exclusive, Cause of Ectopic Mineralization in an Abcc6(-/-) Mouse Model of PXE. *J Invest Dermatol,* 137**,** 2336-2343.

ZHONG, Z., ZYLSTRA-DIEGEL, C. R., SCHUMACHER, C. A., BAKER, J. J., CARPENTER, A. C., RAO, S., YAO, W., GUAN, M., HELMS, J. A., LANE, N. E., LANG, R. A. & WILLIAMS, B. O. 2012. Wntless functions in mature osteoblasts to regulate bone mass. *Proc Natl Acad Sci U S A,* 109**,** E2197-204.

ZHOU, H. H., CHIN, C. N., WU, M., NI, W., QUAN, S., LIU, F., DALLAS-YANG, Q., ELLSWORTH, K., HO, T., ZHANG, A., NATASHA, T., LI, J., CHAPMAN, K., STROHL, W., LI, C., WANG, I. M., BERGER, J., AN, Z., ZHANG, B. B. & JIANG, G. 2009. Suppression of PC-1/ENPP-1 expression improves insulin sensitivity in vitro and in vivo. *Eur J Pharmacol,* 616**,** 346-52.

ZHOU, X., CUI, Y., ZHOU, X. & HAN, J. 2012. *Phosphate/Pyrophosphate and MV-related Proteins in Mineralisation: Discoveries from Mouse Models.*

ZHU, K. & PRINCE, R. L. 2015. Lifestyle and osteoporosis. *Curr Osteoporos Rep,* 13**,** 52-9.

ZIMMERMANN, E. A., SCHAIBLE, E., BALE, H., BARTH, H. D., TANG, S. Y., REICHERT, P., BUSSE, B., ALLISTON, T., AGER, J. W., 3RD & RITCHIE, R. O. 2011. Age-related changes in the plasticity and toughness of human cortical bone at multiple length scales. *Proceedings of the National Academy of Sciences of the United States of America,* 108**,** 14416-14421.

ZIMMERMANN, H. 2001. Ectonucleotidases: Some recent developments and a note on nomenclature. *Drug Development Research,* 52**,** 44-56.

ZIMMERMANN, H., ZEBISCH, M. & STRÄTER, N. 2012. Cellular function and molecular structure of ecto-nucleotidases. *Purinergic Signalling,* 8**,** 437-502.

ZOCH, M. L., CLEMENS, T. L. & RIDDLE, R. C. 2016. New insights into the biology of osteocalcin. *Bone,* 82**,** 42-49.

ZWEIFLER, L. E., PATEL, M. K., NOCITI, F. H., WIMER, H. F., MILLÁN, J. L., SOMERMAN, M. J. & FOSTER, B. L. 2015. Counter-regulatory phosphatases TNAP and NPP1 temporally regulate tooth root cementogenesis. *International Journal of Oral Science,* 7**,** 27-41.

Appendix I. PCR primers.

Gene	Primer Name	Primer Sequence (5' to 3')	From	Source
Ank	Forward	GCC CAT TGT CAA CCT CTT CGT	Sigma	(Kim *et al.,* 2012)
	Reverse	GAA TGG CCA CTG CCT CTG TAG		
Atgl	Forward	GGC CAT GAT GGT GCC CTA T	PrimerBank	Dr Karla Suchacki
	Reverse	CAC TCC AAC AAG CGG ATG AT		
β-actin	Forward	AGT TCG CCA TGG ATG ACG AT	Sigma	Dr Dongxing Zhu
	Reverse	TGC CGG AGC CGT TGT C		
Dgat1	Forward	GTG CAC AAG TGG TGC ATC AG	Eurofins	Dr Carmen Huesa
	Reverse	CAG TGG GAT CTG AGC CAT CA		
Dgat2	Forward	ACT CTG CAG GTT GGC ACC AT	Eurofins	Dr Carmen Huesa
	Reverse	GGG TGT CGGC TCA GGA GGA T		
Enpp1	Forward	GCT AAT CAT CAG GAG GTC AAG	Sigma	Dr Dongxing Zhu
	Reverse	CTG GTA GAA TC CGT CA		
Fgf23	Forward	GGA TCT CCA CGG CAA CAT TT	Eurofins	Dr Dongxing Zhu
	Reverse	GTA GTG ATG CTT CTG CGA CAA		
Glut2	Forward	TGT GCT GCT GGA TAA ATT CGC CTG	Eurofins	Dr Carmen Huesa
	Reverse	AAC CAT GAA CCA AGG GAT TGG ACC		
Leptin	Forward	ATTTCACACACGCAGTCGGTAT	PrimerBank	Dr Karla Suchacki
	Reverse	GGTGGAGCCCAGGAATGAAG		
Lpl	Forward	TCT GTA CGG CAC AGT GG	PrimerBank	Dr Karla Suchacki
	Reverse	CCT CTC GAT GAC GAA GC		
Mgp	Forward	GTG GCA ACC CTG TGC TAC	Eurofins	Dr Dongxing Zhu
	Reverse	CAG GCT TGT TGC GTT CC		
Ocn	Forward	sequence not available	PrimerDesign	Primerdesign
	Reverse	sequence not available		
Opn	Forward	GGA TGC TGT GTC CTC TGA AGA	Eurofins	Dr Dongxing Zhu
	Reverse	ATC GTC ATC ATC ATC GTC ATC AT		
Pck1	Forward	CAT ATG CTG ATC CTG GGC ATA AC	PrimerBank	Dr Karla Suchacki
	Reverse	CAA ACT TCA ATC CAG GCA ATG TC		
Phospho1	Forward	GAC AAT GAG CGG GGT GTT TTC	Sigma	Dr Dongxing Zhu
	Reverse	GGG GAT GGT CTC GTA GAC AG		
Pparα	Forward	CCC TGA ACA TCG AGT GTC GA	PrimerBank	Dr Karla Suchacki
	Reverse	AAT AGT TCG CCG AAA GAA GCC		
Pparg	Forward	CTG CCT ATG ACT TCA CAA	Eurofins	Dr Carmen Huesa
	Reverse	CTC TTG TGA ATG GAA TGT CTT CA		
Ppargca1	Forward	CCCTGCCATTGTTAAGACC	PrimerBank	Dr Karla Suchacki
	Reverse	TGCTGCTGTTCCTGTTTTC		
Prkaa2	Forward	GTCAAAGCCGACCCAATGATA	PrimerBank	Dr Karla Suchacki

	Reverse	CGTACACGCAAATAATAGGGGTT		
Runx2	Forward	ACC ATA ACA GTC TTC ACA A	Sigma	Dr Dongxing Zhu
	Reverse	CAG GCG ATC AGA GAA CAA A		
Slc2a1	Forward	TCA ACA CGG CTT CAC TG	PrimerBank	(Flessner et al., 2012)
	Reverse	CAC GAT GCT CAG ATA GGA CAT C		
Slc2a2	Forward	TGT GTC GCT GGA TAA ATT CGC CTG	PrimerBank	(Flessner et al., 2012)
	Reverse	AAC CAT GAA CCA AGG GAT GGA CC		
Slc2a4	Forward	CCA GTA TGT TGC GGA ATG CTA T	PrimerDesign	Dr Karla Suchacki
	Reverse	TTA GGA AGG TGA AGA TGA AGA AG		
Slc2a10	Forward	ACC AAA GGA CAG TCT TTA GCT G	PrimerBank	(Flessner et al., 2012)
	Reverse	ATC TTC CAA CGA GAC GGA TG		
Slc2a12	Forward	GGG TGT CAA CCT TCT CAT CTC	PrimerBank	(Flessner et al., 2012)
	Reverse	CCA AAG AGC ATC CCT TAG TCT C		
Tnap	Forward	GGG ACG AAT CTC AGG GTA CA	Sigma	Dr Dongxing Zhu
	Reverse	AGT AAC TGG GGT CTC TCT CTT T		
Ucp1	Forward	AGG CTT CCA GTA CCA TTA GGT	PrimerBank	Dr Karla Suchacki
	Reverse	CTG AGT GAG GCA AAG CTG ATT T		
Ucp2	Forward	AAT CTC GGG AGG CAC CTT TC	PrimerBank	Dr Karla Suchacki
	Reverse	GAG AAT GGG ACT GGG CAG AG		
18s	Forward	GTA ACC CGT TGA ACC CCA	Eurofins	Dr Dongxing Zhu
	Reverse	CCA TCC AAT CGG TAG TAG		

Appendix II. Buffers and solutions.

Cell Culture buffers

Primary osteoblast and cell line calcification media medium

αMEM with 10% FBS, 0.05mg/mol gentamicin.

Primary osteoblast and cell line calcification media medium

αMEM with 10% FBS, 0.05mg/mol gentamicin, 5Mm β-GP, 50mg/ml ascorbic acid.

Primary osteoblast TNAP inhibition study cell medium

αMEM with 10% FBS, 0.05 mg/mol gentamicin and 30 μM TNAP inhibitor.

Freezing mix for cell lines

60% DMEM/F-12; 20% FBS; 20% DMSO

Gel Electrophoresis

Tris-Acteric Acid-EDTA (TAE)

40 mM Tris, 1 mM EDTA, 0.1 % Acetic Acid

Tris-Boric Acid-EDTA (TBE)

(90 mM Tris, 2 mM EDTA, 90 mM boric acid

Western Blotting

MOPS running buffer

50 mM MOPS pH 7.7, 50 mM Tris, 0.1% SDS, 1mM EDTA

1X Transfer buffer

100 ml 10X transfer buffer, 200 ml 98% Ethanol, 700 ml dH2O

10X Transfer buffer

29.3 mg/ml glycine, 58 mg/ml Tris Base (trismethylamine), 18.8 µl/ml 20% SDS in dH_2O

Tris-Bufferd Saline with Tween 20 (TBST)

10mM Tris HCl pH8.0, 150mM NaCl, 0.1% Tween-20

Blocking Solution

5% (w/v) BSA Faction V in TBST

Fixatives and histological Stains

10% Neutral Buffered Formalin (NBF)

100 ml strong formalin, 900 ml tap water, 4.0 g sodium dihydrogen phosphate, monohydrate ($NaH_2PO_4.H_2O$) and 6.5 g Disodium hydrogen phosphate, anhydrous (Na2HPO4)

4% Paraformaldehyde (PFA)

800 ml 1x PBS 60°C, 40 g paraformaldehyde powder, 1M NaOH added dropwise until the solution cleared, adjust volume to 1L with 1x PBS

Oil-Red-O stock stain

0.5 g Oil-Red-O (CI 26125, Merc Millipore) dissolve in 100 ml isopropanol with gentle heat

Oil-Red-O working solution

Dilute 30 ml stock stain in 20 ml of dH_20, stand and filter

General buffer recipes

PBS

140 mM NaCl, 2.5 mM KCl, 10 mM NaH_2PO_4, 1.8 mM KH_2PO_4

Hanks Buffered Saline Solution (HBSS)

1.26 mM $CaCl_2$, 0.493 mM $MgCl_2$, 0.407 mM $MgSO_4$, 5.33 mM KCl, 0.441 mM KH_2PO_4, 4.17 mM $NaHCO_3$, 137.93 mM NaCl, 0.338 mM Na_2HPO_4, 5.56 mM D- Glucose

Appendix III. Schematics of Animal Use.

Schematic of primary calvaria cell isolation

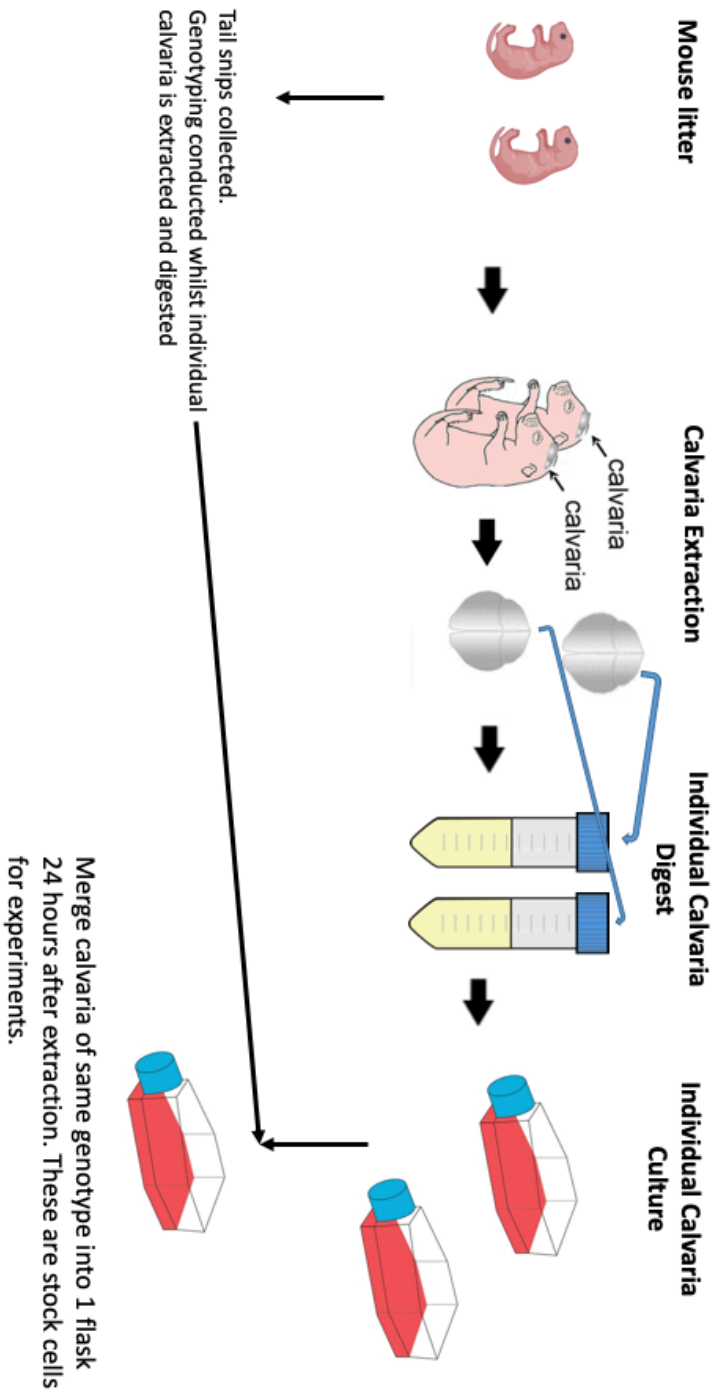

Schematic of mouse use for bone and metabolic phenotyping.